Institut für Biophysik
Fachrichtung Physik
Fakultät Mathematik und Naturwissenschaften
der Technischen Universität Dresden

**TECHNISCHE
UNIVERSITÄT
DRESDEN**

Min-Protein Waves on
Geometrically Structured Artificial Membranes

Doktorarbeit

zur Erlangung des akademischen Grades

Doctor rerum naturalium

(Dr. rer. nat.)

vorgelegt von

Hans Jakob Charles Schweizer

geboren in S-Bad Cannstatt am 11. März 1977

1. Gutachter: Prof. Dr. Petra Schwille

2. Gutachter: Prof. Dr. Karsten Kruse

Die Arbeit wurde eingereicht am: 16. November 2012.
Die Arbeit wurde verteidigt am: 6. Februar 2013.

Contents

Contents

Abstract

Escherichia coli, a rod-like bacterium, divides by binary fission. Cell division into two daughter cells of equal size requires that fission takes place at a midcell position. In *E. coli*, cell division is initiated by assembly of the FtsZ-proteins at the inner membrane to the Z-ring. Topological regulation of the Z-ring is achieved by spatiotemporal pole-to-pole oscillations of Min-proteins. MinC, MinD and MinE bind to and detach from - under hydrolysis of ATP - the membrane in an antagonistic manner leading to an alternating accumulation of MinC and MinD at the cell poles. Averaged over time, the distribution profile of MinD exhibits maximal concentration at the cell poles and a minimum at the cell center. MinC binds to MinD and thus follows its distribution. FtsZ assembly is inhibited by MinC and therefore the Z-ring can only form at a cell position low in MinC — at the cell center.

In the past, the Min-system was also investigated in an *in vitro* approach by reconstitution of Min-proteins into a supported lipid bilayer (SLB). Here, Min-proteins did not self-organize into an oscillatory pattern but into parallel and propagating waves [1]. In this *in vitro* assay, the membrane substrate was infinitely large compared to the wavelength. However, *in vivo*, the cell length is on the same order of magnitude as the respective length scale of the oscillatory pattern of Min-proteins. Therefore, we wished to investigate the effect of lateral confinement and geometric structuring of artificial lipid bilayers on the Min-protein wave propagation.

Lateral confinement of artificial membranes was achieved by microfabrication technology. Glass slides were patterned by a gold coating with microscopic windows of different geometries, and functional SLBs were only formed on uncoated areas. Upon reconstitution, Min-proteins organized into parallel waves on the geometric membrane patches. Confinement of the artificial membranes determined the direction of propagation of Min-protein waves. Min-protein waves could be guided along curved membrane stripes, in rings and even along slalom-geometries. In elongated membrane structures, the protein waves always propagate along the longest axis. Coupling of protein waves across spatially separated membrane patches was observed, dependent on gap size and level of molecular crowding of the aqueous media above the bilayer. This indicates the existence of an inhomogeneous and dynamic protein gradient in the solution above the membrane. Furthermore, reconstitution of Min-protein waves in various three-dimensional artificial membranes was achieved.

In wild-type *E. coli*, Min-protein dynamics resemble that of an oscillation with a characteristic length scale of 5 µm. On supported lipid bilayers, Min-proteins self-organize into waves with a wavelength approximately 10-fold larger than *in vivo*. These discrepancies between the *in vivo* and *in vitro* world were investigated and discussed. *In vitro*, the wavelength could be decreased by a factor of 50% by increase of the molecular crowding in solution and by 33% through temperature increase. The oscillatory pattern is thought to be a consequence of compartmentalization and first attempts to encapsulate the Min-system in closed bilayer compartments are presented.

Kurzfassung

Das stäbchenförmige Bakterium *Escherichia coli* teilt sich in zwei gleich große Tochterzellen. Dies ist nur möglich, wenn sich die Zelle in der Mitte teilt. Bei *E. coli* wird die Zellteilung durch den Zusammenschluss der FtsZ-Proteine an der Membran zum Z-Ring eingeleitet. Topologische Regulierung des Z-Ringes erfolgt durch räumlich-zeitliche Oszillationen von Min-Proteinen zwischen den beiden Zellpolen. MinC, MinD und MinE binden an und lösen sich von der Membran unter Hydrolyse von ATP und in antagonistischer Art und Weise, was zu einer alternierenden Ansammlung von MinC und MinD an den Zellpolen führt. Gemittelt über die Zeit ergibt sich somit ein MinD-Verteilungsprofil, das maximale Konzentration an den Zellpolen und ein Minimum in der Zellmitte aufweist. MinC bindet an MinD und folgt somit seiner Verteilung. Der Zusammenschluss von FtsZ-Proteinen wird durch MinC unterbunden, und somit kann sich der Z-ring nur an einer Position herausbilden, die ein Minimum an MinC aufweist — der Zellmitte.

Das Min-system wurde in der Vergangenheit auch mit einem *in-vitro*-Ansatz untersucht, indem Min-Proteine in künstliche, aufliegende Lipiddoppelschichten (supported lipid bilayers, SLB) rekonstitutiert wurden. Dabei bildeten die Min-Proteine kein oszillierendes Muster aus, sondern organisierten sich vielmehr in parallelen und propagierenden Wellen [1]. In diesen *in-vitro*-Experimenten war das Membransubstrat wesentlich größer als die Wellenlänge der Min-Proteinwellen. *In vivo* hingegen ist die Länge der Zelle in der gleichen Größenordnung wie die charakteristische Länge des Oszillationsmusters der Min-Proteine. Daher war es das Ziel dieser Arbeit, den Einfluß einer beschränkten Fläche und geometrischer Formgebung der künstlichen Lipiddoppelschichten auf die Wellenpropagation der Min-Protein zu untersuchen.

Flächige Beschränkung künstlicher Membranen erfolgte durch Mikrostrukturtechnologie. Deckglässchen wurden mit einer Goldschicht und mikroskopischen Aussparungen unterschiedlicher geometrischer Formen strukturiert. Funktionale SLBs bildeten sich nur auf Glasflächen ohne Goldbeschichtung aus. Nach der Rekonstitution der Min-Proteine, organisierten sich diese auf den Membranstücken in parallele Wellen. Dabei bestimmte die flächige Beschränkung der künstlichen Membranen die Ausbreitungsrichtung der Min-Proteinwellen. Min-Proteinwellen konnten entlang gekrümmter Membranstreifen, in Ring- und sogar in Slalomstrukturen geleitet werden. In geraden, länglichen Strukturen richteten sich die Wellen entlang der längsten Achse aus. Kopplung von Proteinwellen auf räumlich getrennten Membranstücken in Abhängigkeit des Abstandes und des sogenannten *Molecular Crowdings* in der wässrigen Lösung konnte ebenfalls beobachtet werden. Diese Kopplung ist ein Indiz für inhomogene Proteinverteilungen in der Lösung oberhalb der Membran. Desweiteren konnten Min-Proteinwellen auch in diversen dreidimensionalen künstlichen Membranen rekonstitituiert werden.

Im Wildtyp von *E. coli* ähneln die Min-Proteindynamiken der einer Oszillation mit einer charakteristischen Länge von 5 µm. Auf SLBs, bilden Min-Proteine Wellen mit einer Wellenlänge aus, die ca. zehnmal größer ist als *in vivo*. Dieser Unterschied zwischen der *in-vivo*- und der *in-vitro*-Welt wurde untersucht und diskutiert. *In vitro* konnte die Wellenlänge um 50 % durch Erhöhung des *Molecular Crowding* in der Lösung sowie um 33 % durch Temperaturerhöhung verkleinert werden. Das oszillierende Muster könnte dahingegen eine Folge der Kompartimentierung sein. Erste Versuche, das Min-System in geschlossene Membrankompartimente zu rekonstituieren, wurden getestet.

Introduction

> It has, I believe, been often remarked that a hen is only an egg's way of making another egg.
> Samuel Butler, in *Life and Habit*, 1877 [2]

This famous quotation by Samuel Butler was brought into context of cell biology by Wilson in 1925 when he stated, "The individual appears as an evanescent by-product; it is but an incident - almost, we might say, an accident." [3, 4].

The cell can be regarded as a vehicle for the perpetuation of the genetic code. In order to spread, cells have to replicate and cell division is a major step in cellular replication. However, essential aspects of cell division still remain obscure.

Most cells divide into two equally halved cells, thus, they must separate at the center. But how does the cell know where its center is located?

Nature excels through high variety, hence it is difficult to find uniform answers to biological questions that would apply to all organisms. Thus, it has been a successful concept in biology to investigate biologically relevant questions by means of model organisms [5]. A popular model organism representing the bacterial world is *Escherichia coli* (*E. coli*), which was discovered in 1885 by Theodor Escherich and named after him in 1919 [6, 7].

This PhD-thesis is based in the context of the research on the cell division mechanism in *E. coli*. In *E. coli*, cell division is initiated by the protein FtsZ to the membrane and assembly to a Z-ring. In wild type cells, this Z-ring is localized to the cell center [8]. Topological regulation of the Z-ring is controlled by oscillations of the so-called Min-system [9]. Recently, Min-proteins were reconstituted in an artificial membrane system [1, 10]. Here, on flat, supported lipid bilayers, Min-proteins organized into parallel and propagating waves. In these studies, the surface area was infinitely large in respect to the wavelength. The motivation for the present study was to investigate whether lateral confinement of the artificial bilayer would affect Min-protein waves, and if yes, how membrane confinement and boundaries influence wave propagation. Moreover, further aspects of membrane structuring were investigated.

Successful cell division into two equally halved daughter cells does not only require fission at the cell center but also that the plane of division is perpendicular to the long axis of the cell [11]. In the work presented here, I try to show that the mechanism that has been already known to be responsible for the selection of the division at mid-cell position — the Min-system — is also capable of detecting the long axis of the cell, and thus it's plane of division.

Reading guidance

This PhD-thesis is organized in such a way that the relevance increases with each chapter. Therefore, if a fast overview is desired by the reader, I would like to suggest to read the conclusions first (Sec. 10). For more detailed information on the specific outcome, the chapter that presents the results is recommended (Sec. 9).

In general, the thesis tries to give not only a summary of the research study on *Min-protein waves in geometrically structured artificial membranes* but also a general introduction to bacterial cell division and the mechanism of the cell division machinery. In doing so, this PhD-thesis applies

an epistemological approach by following the research history of the discovery of bacterial cell division.

In the first chapter, a basic introduction into bacterial cell structure and life cycle is given. The second chapter tries to elucidates the research history that has led to the discovery of the FtsZ and related proteins. The collectivity of proteins involved in cell division is also denominated *divisome* [12]. Known and speculative regulation mechanisms of cell division are discussed in the third chapter. The forth chapter tracks the research history of the Min-system. Chapter 5 summarizes the current knowledge of molecular structure and action of members of the divisome and the Min-system. Dynamics of the Min-system were also investigated by the means of mathematical descriptions and numerical simulations. Chapter 6 tries accommodate for this with a short overview of past and recent contributions to the mathematical description. Chapter 7 introduces briefly the biological concept applied in this work, namely *synthetic biology*. Chapter 8 represents the material and methods section. Chapter 9 finally presents the data and results achieved during this PhD-thesis. The last chapter discusses the results in context of cell division and tries to give an outlook to possible future work. This dissertation is closed by broaching the potential relevance of the work presented here for other fields in science.

This PhD-thesis is accompanied by a DVD which contains movies of the most important fluorescence micrographs of Min-protein waves on artificial membranes. Furthermore, AutoCAD-drawings of the gold microstructures can be found as well as a collection of MATLAB codes developed and applied in this study (see also the appendix, Sec. 11).

1 Cell structure and cell cycle in *Escherichia Coli*

During cell division, a structural entity is replicated and divided in two copies [13]. This involves the entire cell and not only certain substructures. Therefore, it is useful to obtain a general overview over the cell structure and, in the case of this PhD-thesis, over bacterial cell structures. The cell wall represents the part of the cell which is most involved with the process of cell division. The actual mechanism of FtsZ, member of the division machinery (see Sec. 2), and related proteins act mainly on the cell wall: By closure and septation of two new daughter cells, the process of cell division is accomplished. This closure and septation is achieved by the cell wall. Furthermore, the mechanisms of the Min-system, which is the object of investigation of this PhD-thesis, take place basically on the cell membrane. In this context, we will also see that the geometric form of the cell is defined by the cell wall. Hence, while discussing the structural basis of the bacterial cell, the focus of this chapter will be on the cell wall and the plasma membrane.

1.1 Structure of the bacterial cell

It must be assumed that the main "goal" of all organisms is the proliferation of its genetic material. This already illustrates the central role of the DNA among the different types of cellular structural elements. In addition to the distribution of its genetic information, the DNA also serves as a blueprint for the production of vital proteins for the cell. In multicellular organisms, such as the human body, DNA is subject to proliferation only in few cells (namely sperm cells and ova) whereas in most cells the function of DNA is limited to this blue print job. The vitality and function of cells which are not directly involved in reproduction of the respective organism is however always coupled to the objective of reproduction. We eat, we walk, we think in order to reproduce. The DNA is *the* central structural element of the biological cell across all organisms. In eukaryotes, i.e. all human, animal, plant, fungi cells and even in unicellular eukaryotic organisms, the DNA is encapsulated inside a membrane structure, the nucleus. Prokaryotes, i.e. bacterial cells, lack the nucleus structure and the DNA floats as a coiled structure within the cytosol without any proper boundary to the rest of the inner volume of the cell.

The cell's content is separated from the environment by the plasma membrane. In fact, it is the boundary between inside and outside that defines a cell, not only in biology. The cell wall is a special structure that accompanies the plasma membrane in prokaryotes and plant cells. The cell wall renders rigidity and form to the cell. The world of bacterial cells can be divided into two different classes of cells: Gram-negative and Gram-positive cells (see below) which are defined by the structure of the cell's boundary.

The cytoplasm includes the cytosol with the cytoskeleton and further structural elements which shall not be discussed in detail in this work.

Figure 1.1: Cell envelope of bacterial cells. Left: Gram-positive bacteria are surrounded by an inner membrane (IM) and a thick layer of peptidoglycan exoskeleton. Right: Gram-negative bacteria have three layers, the IM, a single peptidoglycan layer and the outer membrane (OM). Further elements are: covalently attached proteins (CAP), integral membrane proteins (IMP), lipoproteins (LP), lipopolysaccharides (LPS), lipoteichoic acids (LTA), outer membrane proteins (OMP) and wall teichoic acids (WTA). Image is taken from Ref. [16].
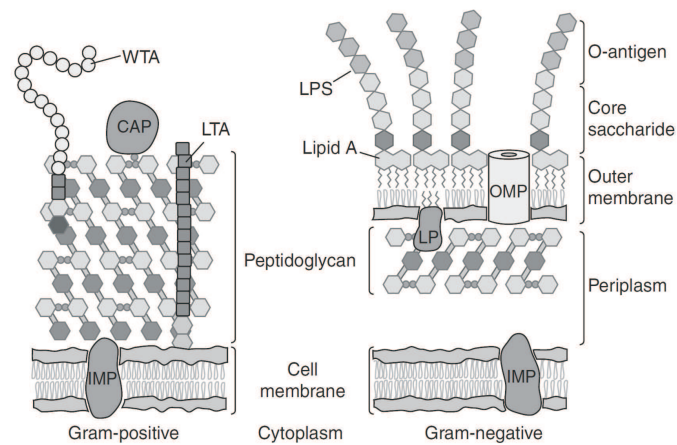
1.1.1 The bacterial genome

The genome of bacteria consists of a single DNA-macromolecule, a circular chromosome with about 1000-5000 genes [14, 15]. In the case of *E. coli*, these sum up to about 4 Mbp [13]. If extended it would be 1 mm long [14]. In contrast to eukaryotes, the bacterial genome is not encapsulated in a cell nucleus with a proper membrane but resides as a coiled structure within the cytosol [14]. In respect to the entire cell volume, it occupies a relatively large space, about one fifth of the cytosolic volume, i.e. about $1\,\mu m^3$ [14, 15].

1.1.2 Cell wall of Gram-negative bacteria

One of the first systematic classifications of bacterial cells was achieved in 1884 by Christian Gram who observed different staining results in different cell types [17]. Upon staining with crystal violet followed by washing with ethanol, *Streptococcus pneumoniae* retained the staining, whereas in *Klebsiella pneumoniae*, the staining could be washed out. Similar behavior was observed in other bacterial organisms, too. Later it was shown that the different staining results are due to different cell envelope structures. Some bacteria have a cell wall that consists of an inner membrane (IM) and a thick cell wall, whereas other bacteria feature a sandwich structure of an inner and outer membrane (OM) with a single-layered, thin cell wall in between as depicted in Fig. 1.1. Cells of the first class with thick cell walls retain the staining upon washing with ethanol and were thus classified as "Gram-positive" whereas cells with two membranes and a thin cell wall lost the staining upon treatment with ethanol, thus classified as "Gram-negative".

E. coli belongs to the family of Gram-negative cells. Therefore, cell structure, growth and cell cycle will be discussed mainly for Gram-negative cells.

Outer membrane (OM)

The OM is a lipid bilayer with a highly anisotropic structure: the lipid composition of the inner leaflet is based only on phospholipids like the IM (see below). However, the lipid composition of the outer leaflet of the OM is mainly built from glycolipids, there are no phospholipids in the outer leaflet (see Fig. 1.1). Most of these glycolipids are lipopolysaccharides (LPS), which are made up of three subunits: lipid A, which resides in the membrane, a core polysaccharide and an O-antigen polysaccharide [16]. The polysaccharides protrude into the extra-cellular space and help the cell to stabilize the cell envelope and protect it against alien influence. The OM hosts two different classes of membrane proteins. Lipoproteins (Lp) are not transmembrane proteins but lipid-associated via a lipid moiety. There are about 100 different OM lipoproteins, most of
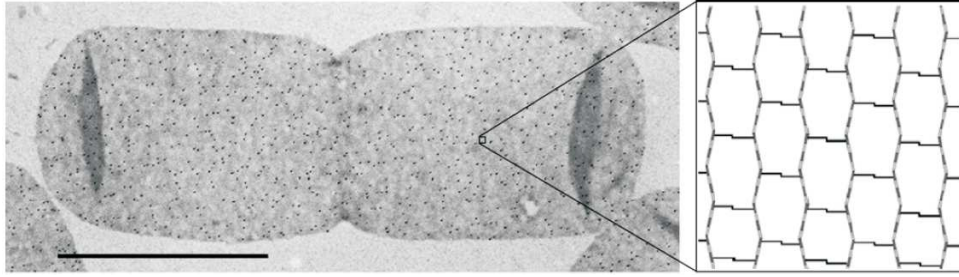
Figure 1.2: Left: Electron micrograph of a sacculus isolated from a dividing *E. coli* cell (left). Murein structural elements are labeled using murein-antibody gold labels, visible as black dots. Scale bar is 1 microm. Right: Sketch of the murein layer structure. Glycan strands (vertical and perpendicular to the cell long axis) are connected by muropeptides (horizontal lines). One hexagonal structure element is called "tessera". The sketch corresponds to an area of 30 nm × 30 nm. Image is taken from Ref. [19].

them with unknown function [16]. The second class of OM proteins are β-barrel proteins which span the entire leaflet. In contrast to OM lipoproteins, outer membrane proteins (Omp) are well studied with OmpF being maybe the best-researched representative [18].

The sacculus

The murein wall represents an extraordinary structure since it consists of a single, giant macro-molecule or polymer, called sacculus [20, 19]. The sacculus can be isolated from other cell structures, including periplasmic and outer membrane, without rupture and imaged in electron microscopy as shown in Fig. 1.2. Its dimension corresponds to the living cell but the thickness of the sacculus shell is only about 6 nm. Despite this thinness, the sacculus is extremely rigid and protects the cell against lysis even in the presence of high osmotic pressure. This is one reason why bacteria can survive in hostile environments like the mammalian guts or salt lakes. However, upon addition of penicillin, the murein layer can be weakened which gives rise to bulges or spheroplasts due to the cell turgor [21]. The knowledge of this effect was important for the discovery of the penicillin-binding proteins (Pbp). Pbp3 (or PbpB), also known as FtsI, is part of the divisome (see Sec. 3.3.3 and 5.1.1).

The sacculus is made of murein (also called peptidoglycan), a polymer consisting of linear and parallel glycan chains interconnected by peptides building a mesh-like structure. The hexagonal subunits of this mesh structure are called "tessera" (Fig. 1.2). The amino sugar chains are built from β-1,4-linked N-acetylglucosamine (GlcNAc) and N-acteylmuramic acid (MurNAc) in alternating order (see Fig. 1.2) [19]. Cross-linking of amino-sugar chains is achieved by more than 50 so-called muropeptides which differ depending on the organism. The muropeptides define the rigidity of the entire sacculus which have a limited flexibility perpendicular to the longitudinal axis of the cell but exhibits high elasticity in direction of the long axis. Presumably, the glycan strands run perpendicular to the cell's long axis whereas the cross-linking muropeptides are oriented parallel to it [19].

The sacculus' elasticity also allows the structure to expand and relax. When isolated from other cell components, the sacculus is found in its relaxed state with tesserae forming pores of about 2 nm in diameter, permeable for proteins of up to 24 kDa. In the living cell, the sacculus is thought to be in its expanded state due to the turgor and permeable for proteins of up to 100 kDa [19]. This permeability is of great relevance for the delivery of proteins from the cytoplasm through the perisplasm (the space between inner and outer membrane) to the OM. The sacculus is anchored to the OM via the so-called Braun' lipoprotein Lpp. A third of the cell's Lpp is covalently bound to the murein structure and embedded in the glycolipid bilayer of
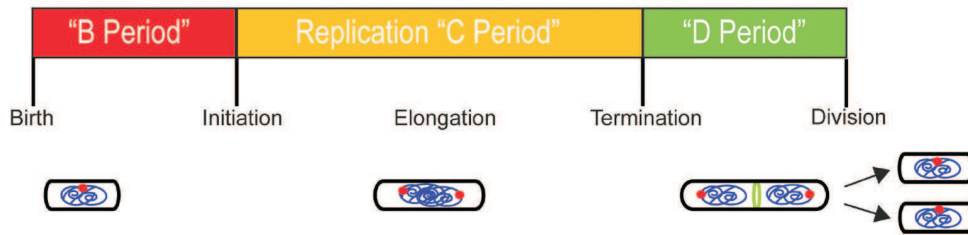
Figure 1.3: Scheme of the bacterial cell cycle. The graph is taken from Ref. [13]

the OM via an N-terminal lipid residue. Lpp is the most abundant protein in *E. coli* with about 500 000 to 1 000 000 molecules per cell [22, 16].

Inner membrane (IM)

The OM's task is mainly to protect the cell, whereas the sacculus gives the cell its shape and rigidity. It is the role of the IM to constitute the boundary between the cytosolic and extracellular space. The IM of Gram-negative, but also of Gram-positive bacteria, is composed like a classical cell membrane out of amphiphatic phospholipids and many embedded proteins. The bilayer has a thickness of about 80 Å and comprises about 70 % of the cell's entire phospholipids which are about 2×10^7 lipid molecules [22]. In *E. coli*, the lipid composition comprises phosphatidyl ethanolamine (PE), phosphatidyl glycerol (PG) and cardiolipin (CA). Fractions might differ depending on the strain, cell culture conditions and growth phase. Documented values are 70 % for PE, 20 % for PG and 5 % for CA [23, 22]. Respective sketches of the molecular structures are given in the Material & Methods chapter (Chapter 8.1.10). Since bacteria have no intracellular organelles, the IM (IM) of the bacterium has to take over all intracellular membrane-associated processes. Consequently, it contains a high quantity of membrane proteins. About 25 % of all cellular proteins can be found in or attached to the IM [22]. For the work presented here, the IM is of high importance since the processes studied in the work of this PhD thesis occur at the IM of *E. coli*.

1.2 The bacterial cell cycle

The cell cycle of prokaryotes is divided in three periods as shown in Fig. 1.3: B, C and D [24, 13]. The B-period marks the phase from birth of a new cell to initiation of DNA replication. DNA replication takes place during the C-period, accompanied by segregation of the sister chromosomes and growth of the cell, which corresponds to an elongation of the cellular structure in the case of rod-like cells. Segregation of nucleoids occurs in parallel to DNA replication. The D-period marks the phase from termination of DNA replication to final division which is equal to the birth of two new cells. In consequence, bacterial cell division is characterized as a binary fission [25]. In fast growing cell cultures, the B-period does not exist, but after division, the newborn cells immediately start with DNA replication again.

In contrast to the eukaryotic cell cycle, which is rather characterized by serial processing, the prokaryotic cell cycle partially shows parallel processes of cell division [13].

In this work, I would like to focus on the division process itself. However, since processes that take place during the C-period gave rise to findings about the fission mechanism, it is useful to look into the DNA-replication and growth processes as well.

(a)   (b)
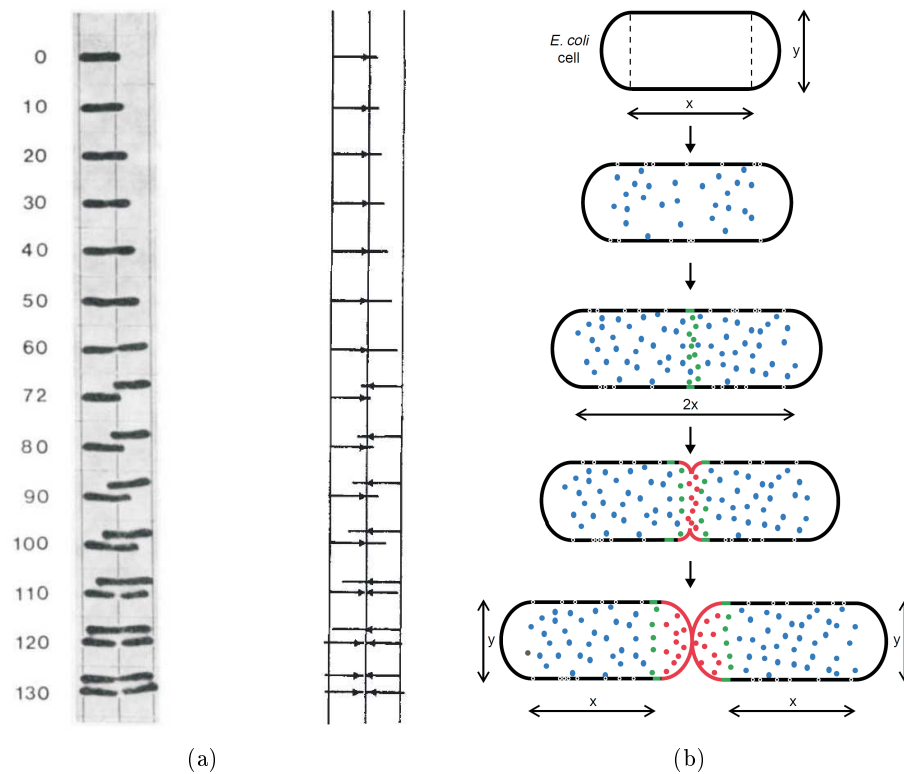
Figure 1.4: Growth and division in *Escherichia coli*. (a) *E. coli* wild type cells double in length prior to division (here, the strain $15T^-$ JG151). When maintained in minimal medium as shown, *E. coli* cells grow only from one cell pole (in this example the right pole of the first cell). The numbers to the left indicate the time in minutes and the graph to the right indicates the schematic growth direction. After fission (after 60 min), two new cell poles are generated and the daughter cells continue growing from the new cell poles, thus in opposite direction. The distance between vertical lines is 1.7 µm which is referred as the minimal length or "unit cell" of *E. coli* [26]. Image is taken from Ref. [26]. (b) During a first growth phase, the cylindrical part of the bacterial cell envelope grows at the entire surface by diffusive incorporation of new cell wall material, murein (blue dots), until the cell has doubled it length followed by preseptal (green dots) and finally septal murein (red dots). Through the entire growth process, the cell diameter is maintained. Graph is taken from Ref. [27].
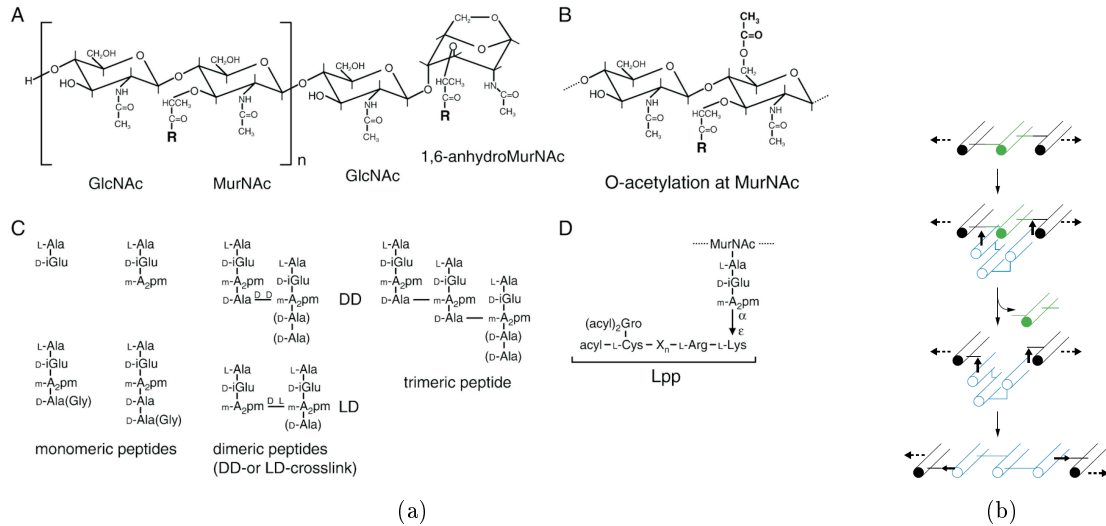
Figure 1.5: Components and possible growth mechanism of the sacculus. (a) Molecules involved in the sacculus structure. β-1,4-linked N-acetylglucosamine (GlcNAc) and N-acteylmuramic acid (MurNAc) (A) muropeptides (C) cross-link the amino sugar chains and Braun' lipoproteins (D) anchor the sacculus to the IM. The illustration is taken from Ref. [19]. (b) The proposed three-for-one model by Höltje et al. [28]. Three new murein strands (murein triplet, in blue) replace one strand (in green) from the stress-bearing sacculus. Image is taken from Ref. [27].

1.2.1 B-period: cell growth

From "birth" to fission into two new daughter cells, *E. coli* cells double in size as shown in Fig. 1.4(a). How does a bacterial cell grow? Chromosomes do not "grow", they are replicated and proteins are just increased in number, but they do not "grow" either. So, cell growth is mainly characterized by the growth of the cell envelope and the cytoskeleton. How does the cell envelope grow? Does it grow equally at each point or are there specific growth regions? The growth of the cell wall is dominated by the growth of the cell wall, i.e. of the sacculus [27]. In consequence, morphogenetic changes of the cell can be studied by the metabolism of the murein layer. Furthermore, the growth of the sacculus is tightly connected to the growth of inner and OM [21].

Sacculus growth occurs in two phases: growth along the cylindrical part of the rod-like cell envelope, followed by a focused synthesis of the murein layer at the central division site for the formation of new polar caps [19]. During the elongation phase, murein synthesis and insertion occurs across the entire cylindrical part, whereas the cell poles remain metabolically silent. In the division phase, two new cell poles emerge from the septal murein. Thus, the cell cycle requires a switch to redirect murein synthesis from the cylindrical cell envelope to the formation of the septum [29]. After formation of the new cell poles, murein synthesis stops at the cell poles and they become metabolically silent again.

The exact molecular mechanism of sacculus growth still remains obscure but most discussed models involve synthesis of new peptidoglycan strands or precursors in the cytosolic volume, transport across the IM and consequent insertion into the existing murein layer. As far as it is known, synthesis of new cell wall material starts in the cytoplasm from the precursors UDP-N-acetylmuramyl-pentapeptide (UDP-MurNAc-pentapeptide) and UDP-N-acetylglucosamine (UDP-GlcNAc) [19, 16]. UDP-MurNAc is linked via pyrophosphate onto the membrane acceptor bactoprenol which results in the Lipid I-complex. The addition of GlcNAc from the precursor UDP-GlcNAc produces a lipid-bound disaccharide-pentapeptide intermediate, Lipid II. Lipid II

is flipped across the cytoplasmic membrane into the periplasmic space. Again, the exact process of this transport mechanism is still unknown but it presumably involves a translocase or flippase. The final steps of incorporation of new murein into the cell wall is achieved by penicillin-binding proteins (Pbp) with a transglycosylase or transpeptidase activity. Lipid II is transferred as peptidoglycan strands into the existing murein layer by a transglycosyl reaction, catalyzed by a Pbp protein [30]. During the incorporation of the murein precursor, the lipid carrier bactoprenol is released from Lipid II. Incorporated peptidoglycan strands are finally cross-linked via pentapeptide side chains. This is catalyzed by Pbp proteins with a transpeptidase activity [28, 31].

Different models are suggested for the incorporation mechanism of new peptidoglycan strands into the existing murein layer. For the work presented here, the three-for-one model by Hoeltje et al. shall be of interest [28]. In this model, a peptidoglycan strand of the sacculus is replaced by a triplet of new peptidoglycan strands (see Fig. 1.5(b)).

Presumably, there exist two penicillin binding protein (Pbp) complexes responsible for the growth of the murein layer. Pbp2 is assumed to be responsible for elongation, since inhibition of Pbp2 by mecillinam stops growth and leads to the formation of spherical cells [32, 19, 33]. The process of cell division also requires a switch from peptidoglycan synthesis for the cylindrical cell part to the formation of the septum and thus new cell poles [29, 31]. Pbp3, also known as FtsI (see Sec. 5.1), is supposed to be involved in the formation of the murein layer of the septum during division. Its inhibition leads to a blocking of the cell division and the formation of filaments [27].

The control of this 2-phase growth is presumably regulated by the actin-like MreB cytoskeleton which contains enzymes for the precursor lipid II synthesis, murein synthesis complexes responsible for cell elongation and murein hydrolase subcomplexes [19]. During elongation, the MreB cytoskeleton might serve as a track or assembly scaffold for the murein synthesis complex. When it comes to cell division by assembly of the Z-ring at the division site, the murein synthesis complex could switch from the MreB-cytoskeleton to the FtsZ-structure of the Z-ring [30, 19].

1.2.2 C-period: Chromosome replication and segregation

DNA-replication

E. coli has one single origin of replication, called *oriC* [34, 35, 36]. At the beginning of the C-phase, *oriC* is located on the membrane at the cell center [14, 15, 13]. The replication of DNA is initiated by binding of the protein DnaA, which forces separation of the DNA strand by inducing curvature to the double helix. The base pair separation is continued in both directions by action of DnaB whose binding is facilitated by DnaC. This allows binding of the DNA polymerase III and further proteins which start to replicate the DNA by proceeding in both directions of the DNA until it reaches the terminus *terC* which is located on the opposite side of the circular chromosome. There, the replication fork is disengaged from the DNA chain by the action of termination proteins. During the replication process, the polymerase stays immobile whereas the DNA purrs through the enzyme [13]. In *E. coli*, the C-period takes about 40 min [37, 38, 39, 40].

Nucleoid segregation

As already stated, the bacterial cell cycle is characterized by parallel or at least overlapping processes instead of distinct serial steps [13]. For example, segregation of the new chromosomes starts right after the replication of the first base pairs, namely the origin *oriC*. As the DNA-polymerase remains immobile, the two freshly synthesized origin points move away from the replication fork in opposite directions to the two poles of the cell and are followed by further replicated DNA material [13]. Since the bacterial genome is of circular nature, the terminus of the DNA takes the opposite direction, from the cell poles of the mother cell to midcell position

[41, 42, 43, 13]. Since the midcell position is the place of division, replicated termini flank the invaginating septum. Termini are located at the new cell poles after cell fission.

1.2.3 D-period: cell division

The D-period marks the phase from termination of DNA replication to final and total division of the sister cells. Although sister chromosomes have already been synthesized and even segregated, the term "division" is usually reserved for the emergence of a new border between the future daughter cells and the spatial separation of the two sisters. As will be shown later, the concept of spatial confinement or compartmentalization is crucial for the development of life (see Sec. 7.5). While investigating the phenomenon of division, the focus in this work should not be laid on the division mechanism itself but rather on its spatial regulation: Where in the cell does division occur? What is the mechanism behind positioning of cell division action?

Division is achieved by building a new cell wall between the two future daughter cells (see Sec. 1.2.1). As long as the cells are not completely separated, this border is referred to as the septum. In the case of *E. coli*, septation is accompanied by a constriction of the cell wall [44, 29]. The septum is initiated by binding of FtsZ-proteins to the IM and assembly to a ring, the so-called Z-ring (abbreviation of FtsZ-ring, see Sec. 2). The function of this Z-ring has not been completely elucidated, but apparently, it serves as scaffold for further proteins that build the septum. The segregation starts with an invagination of the cell wall leading to a constriction at the future division site. The D-period takes about 20 min [37, 38, 39].

In wild type cells of *Escherichia coli*, this division occurs at a midcell position with high precision (see Sec. 3.1). This high precision is crucial in order to obtain two functional cells both containing a complete copy of the bacterial genome. But how does the cell know where its center is?

2 Research history I: FtsZ and the Z-ring

As often in microbiology, deeper understanding of cell mechanisms was motivated and made possible by the appearance of abnormal cell behavior found in cells with a genetic mutation. Apparently, it is the exception from the rule which explains the rule. On the long journey to the discovery of Fts- and Min-proteins, there were basically two abnormal morphologies in cell shape that finally led to a better understanding of the cell division process: long filamentous cells and, interestingly, its complete opposite, minicells of *Escherichia coli*.

Cell division is initiated by the assembly of FtsZ-proteins to the so-called Z-ring which initiates constriction of the bacterial cell. The discovery of these factors on the nano-scale was triggered by the observation of phenotypes on the microscopic level. Under certain conditions, some rod-like bacteria like E. coli loose the ability to divide and in consequence grow to long filaments.

2.1 Inhibition of cell division and filamentous cells

Filamentation of bacterial cells is a morphological phenotype that can be caused by many different means. Some involve only external boundary conditions such as certain cell culture media. Other factors directly affect the genetic configuration of the bacterium. By tracking the research history of filamentation of bacteria, the following sections give an overview of this phenomenon that finally led to the discovery of the division factor FtsZ and the Z-ring. Filamentation can be caused by different means, by genetic mutations or external conditions. This section will differentiate factors which are relevant for the research of cell division from those which are of no significance for the discovery of the divisome.

2.1.1 First observation of filamentation

In 1904, Walker and Murray observed that cells of certain bacterial strains loose the ability to divide but not to grow when a small percentage of certain dyes were present in the culture medium [45]. In consequence, the cells continued growing into long filaments as shown in Fig. 2.1(a). This phenomenon was observed for *Bacillus typhosus*, *Escherichia coli* and *Cholera vibrio* and in combination with several methyl dyes such as Grubler's methyl violet, gentian violet, fuchsin, methyl-green and methylene-blue [45]. When subcultures were regrown in media without the respective dyes, cells started to divide normally again and cell lengths corresponded to the wild type. A similar phenotype of non-dividing and filamentous cells was observed in the following for further bacteria strains and varying treatment methods. In 1906, Wilson, for example, documented filaments for *Escherichia coli* and other bacteria upon growing cultures in media containing urea (see Fig. 2.1(b)) [46].

Strong irradiation of bacterial cells by UV-light normally leads to cell death. In 1933, Gates reported that irradiation of *E. coli* by weak doses of UV-light did not kill the bacteria but inhibited division, and in the following 2-4 hours after UV-treatment cells grew to filaments of up to 150 μm [48]. After this period, cells started to divide normally again. The daughter cells, if not irradiated, divided and grew normally, which excluded the possibility of a genetic mutation as it was the case in previous works by Walker and Wilson. Similar behavior was observed by Lea et

(a) (b) (c)
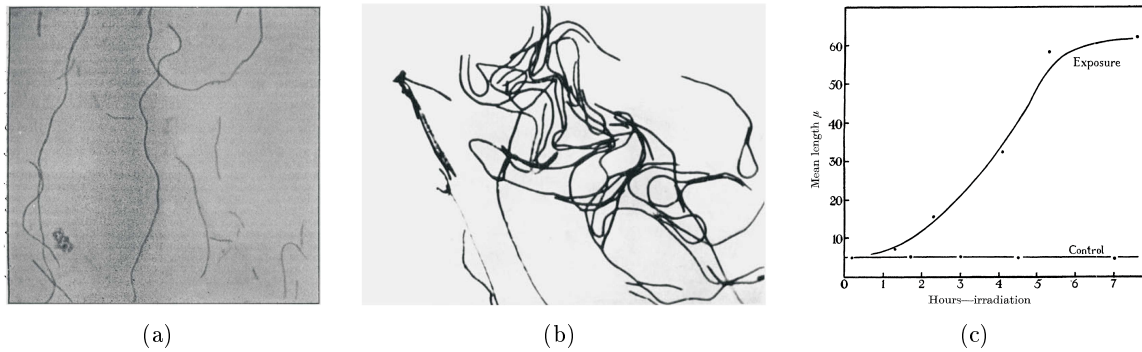
Figure 2.1: Filamentation of bacteria. (a) First documented observation of abnormal appearance of filamentous bacteria cells in 1904. Filaments of *Bacillus typhosus* were grown for 48 h in a broth culture containing 0.2 % of the dye methyl-violet. Image is taken from reference [45]. (b) Filaments of *E. coli* grown in medium containing 3.5 % urea for 18 days. Image is taken from reference [46]. (c) Growth of filamenting *E. coli* in response to γ-irradiation. Image is taken from reference [47]

al. in 1936 upon treatment of *E. coli* with γ-irradiation (see Fig. 2.1(c))[47]. Filament formation can also be motivated by crystal violet, novobiocin, penicillin, or radioactive phosphorus [49]. In all cases, however, inhibition of division was reversible, at least for the daughter generation.

Filament formation upon weak irradiation and various other treatments were found to be non-hereditary. In all cases, normal division took place several hours after irradiation was stopped or after the cells had been transferred into standard medium [45, 46, 48, 47].

2.1.2 Irradiation resistance

On August 6th, 1945, an atomic bomb exploded over Hiroshima with immediate 75 000 casualties, followed by a second explosion two days later in Nagasaki exterminating the life of about 22 000 people at once. With the first nuclear attack, carried out by the USA against Japan, World War II came to an end. The initial motivation for the atomic bomb was the massive explosive power and thus its capability of mechanical destruction through the pressure blast and high temperature. However, soon it became clear that nuclear bombs do not only act lethally through these parameters but that also the emitted radioactivity acts as an additional threat. In consequence, researchers started to investigate the influence of radioactive irradiation on biological matter. Two laboratories in the USA were involved with the Manhattan project. The more famous research center was in Los Alamos, where the first atomic bomb was set off on July 16th, 1945 [50]. A second research center, the Oak Ridge Laboratory in Tennessee, was rather involved inthe background work. In order to study the impact of radioactivity on biological matter, scientists in the Oak Rigde laboratory performed a large series of irradiation experiments on mammal organisms and bacterial cells which finally led to the discovery of the mechanisms of cell division [51, 52, 53, 54, 55]. It appears cynical that the development of weapons of mass destruction helped elucidating the miracles of life.

In 1946, Witkin observed that, when a cell culture of *E. coli* B was exposed to strong UV- or γ-irradiation, a small fraction of cells had survived the irradiation. Interestingly, the daughter cells of these survivors showed an increased resistance to strong UV- and γ-irradiation as well, which indicated that this resilience property could be of genetic nature. It was considered that the observed radiation resistance was not due to a genetic modification upon irradiation but that the cell culture already had contained - before irradiation - a small fraction of genetically mutated cells which were resistant to UV- or γ-irradiation and that this fraction was singled out by irradiation. These cells were denominated as *E. coli* B/r [56]. The same strain also did not

<center>(a)   (b)</center>
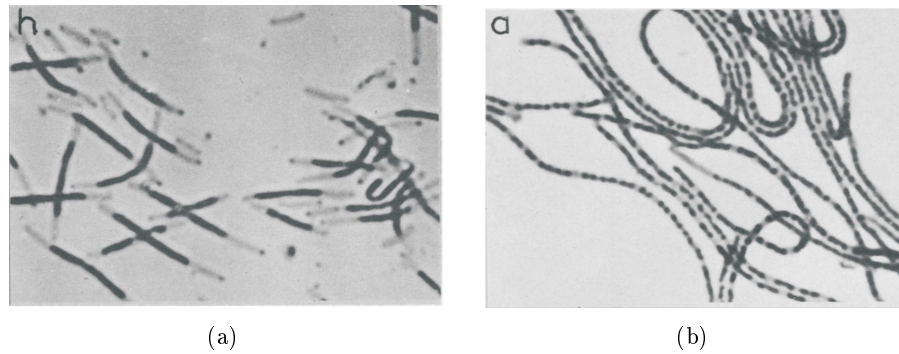
Figure 2.2: Temperature sensitive *E. coli* mutants grown at 40°C. Certain phenotypes, such as septation and DNA segregation, are coupled for certain mutations or are independent for other strains. (a) PAT32: both, septation and DNA segregation are affected by the strain's mutation. (b) PAT84: Inhibition of septation but not of DNA segregation. Images are taken from reference [60].

show the phenomenon of filamentation upon UV-irradiation or other treatments that normally inhibit division, which led to the consideration that the ability to survive strong UV-irradiation or X-rays must be coupled to the absence of the filament formation phenomenon [57].

2.1.3 Filamentation, the *fil* gene and septum formation

In 1963, van de Putte determined a gene possibly responsible for the UV-resistance and filament formation of *E. coli* B strains, hence called *fil* [49]. *fil*$^+$ denominates the wild type and *fil*$^-$ the mutant being resistant to high UV-doses and showing no filament formation for low UV-doses. *E. coli fil*$^-$ also showed higher resilience to other agents that motivate filament formation. In the case of *E. coli fil*$^+$, filament formation could be inhibited by pantoyl-lactone. Pantoyl-lactone is known to initiate cross plate or so-called septum formation in *E. coli*. In consequence, it was assumed that the filament-forming mutants lack the ability to form such cross plates, which was the first hint towards the subsequent discovery of the Z-ring (see Sec. 2.3) [58, 59].

2.1.4 Filamentation, the *lon* gene and temperature sensitivity

A similar relationship between the appearance of filamentation and irradiation survival as for *E. coli* B/r was also observed for *E. coli* K12 (for example strain AB1157). In contrast to *E. coli* B and its mutant *E. coli* B/r, in whose cases the wild type strain shows filamentation upon weak irradiation and is killed by strong irradiation, it is a mutant of *E. coli* K12 (AB1899) that is characterized by cessation of division and a decreased survival rate upon irradiation [61, 59]. These findings led to the conclusion that the genes responsible for UV-resistance and inhibition of filament formation must be the same. This gene was denominated as *lon* for the filament forming mutant and *lon+* for the wild type [55] and was located at a position between the loci *lac* and *gal* responsible for the utilization of lactose and galactose. For the filament forming strain (*lon*), again filament formation could be stopped and normal cell division initiated by addition of pantoyl-lactone but also by incubation of the cells at an elevated temperature (around 42°C).

2.1.5 Temperature sensitivity and the *fts*-gene

In contrast to this temperature-dependent behavior, mutants of the *E. coli* K-12 strain KMBL 49 obtained after treatment with the mutagenic agent N-methyl-N'-nitro-N-nitrosoguanidine showed the inverse behavior: normal cell division at 30°C but filament formation at 42°C [62]. In the case of this temperature-sensitive mutant, filament formation can not be reversed upon addition

(a)   (b)
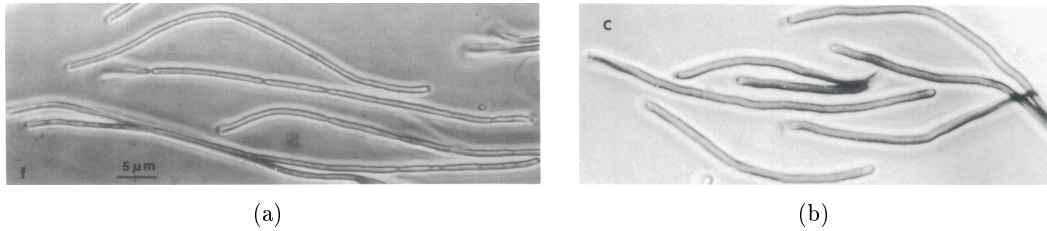
Figure 2.3: Filamentation of different *E. coli* K12 strains with and without constrictions. (a) *ftsA*-strain AX655 ts2158 features constrictions indicating that septation has started but was not completed. (b) Strain PAT84, originally thought to carry a mutation in *ftsA* as well, shows no constrictions indicating this strain carries a mutation which acts early within the septation process. Images are taken from reference [64].

of pantoyl-lactone which led to the conclusion that the genetic loci for filament formation of this strain must be different than that of the previously mentioned *E. coli* strains. The corresponding gene was hence denominated as *fts* for *filamentous growth is thermosensitive* [62].

The phenomenon of temperature sensitivity gained greater attention and was also observed for DNA synthesis and segregation. Several mutants showed temperature sensitivity only for one feature (septation/DNA synthesis) but some also for both (see also Sec. 3.3.4). In 1968, Hirota et al. investigated several temperature sensitive mutants of *E. coli* in order to classify the phenotypes of DNA segregation, cell growth and septation [63]. For example, in the group of non-septa forming strains, the strain PAT32 shows DNA-synthesis without segregation of DNA which results in long filaments with one large DNA entity (Fig. 2.2(a)). Apparently, both, formation of septation and DNA synthesis, were affected by the respective mutation of the strain. In contrast, the strain PAT84 also lacked the ability for septation, but DNA is synthesized and segregated normally (Fig. 2.2(b)). Hirota and his coworkers concluded that the single steps of cell division such as chromosome segregation and septation are not organized as a sequential mechanism but rather as a process of parallel mechanisms that only partially depend on each other (compare with Sec. 1.2). On the other hand, they already assumed a tight relation between the phenomena of filament formation and septum placement. They have also foreseen the central role of the bacterial membrane [63]:

> *Whatever the solution to these alternatives may be, it is clear that the systems by which growth, initiation of DNA synthesis, septation, and cellular division are coordinated lie in the cellular membrane.*

This hypothesis turned out to be true as shown later (see Sec. 5).

2.1.6 *fts*-gene confusion

Some temperature-sensitive *E. coli* mutants show increased lysis at elevated temperatures [65]. Apparently, the responsible mutation of *lts* (*temperature-sensitive lysis*) is located in a genetic region close to the *fts*-mutations responsible for filament formation. In order investigate this issue, Wijsman identified a genetic locus between *murC* and *envA* responsible for filament formation in the three *E. coli* mutants TKF 10, 12, 15 [65]. This paper, which was published in 1972, is especially interesting since it is the first publication to cite a specific gene of the *fts*-family with the name *ftsA*. Actually, it refers to a paper by Normark et al. which in fact does not contain the term *ftsA* [65, 66]. Therefore, Wijsman has to be considered the one who has published the first representative of a long series of *fts*-genes [65].

Subsequently, the *fts*-family started to grow. The laboratory around Hirota identified seven different genes affected by the mutations in strains capable of DNA segregation but with suppressed septation at elevated temperatures [67]. Independently of the work of Wijsman, one gene was also denominated as *ftsA* and the others as *ftsB* through *ftsG*. All mutations were characterized by the phenomenon of inhibited cell division at 42°C but could resume septation when the temperature of the respective cell cultures was lowered again to 30°C. Ricard and Hirota classified them according to this division behavior in dependence of the synthesis of new protein and DNA. This revealed that not all of the *fts*-proteins are essential for cell division. For example, strains carrying mutations in the genes *ftsA* and *ftsE* were able to resume septation without synthesis of new proteins whereas strains with mutations in the other *fts*-genes inhibited cell division when the cell cultures were returned to 30°C. From these findings, Ricard and Hirota concluded that the mutations in the essential *fts*-genes are specific for septation and that filamentation is not a secondary phenomenon upon DNA or protein synthesis [67]. But it is worth pointing out that, in addition to the dispensability of *ftsA* and *ftsE*, not all of the supposedly identified genes survived the further development of research. For example, *ftsC*, *ftsD* and *ftsF* appear only in the paper by the Hirota group and *ftsG* appears only once again in literature [68]. I will present the current list *fts*-genes known to be essential for cell division in Sec. 5.1.

To make confusion complete, the identity of *ftsA* remained ambiguous for some time. Several strains of *E. coli* K12 were already associated with mutations in *ftsA*, including the strain PAT84 by Ricard and Hirota, and thanks to further work by other people, more strains could be isolated that have mutations in *ftsA* as well [67, 64]. Interestingly, the filaments of most of these mutants featured constrictions, indicating that septation has very well been initiated but just not completed. These observations provoked the assumption that different *fts*-genes could act on different steps within the process of septation, and apparently *ftsA* takes action at a later stage (Fig. 2.3(a)). This assumption could be confirmed by later works as shown in Sec. 5.1. However, filaments of the strain PAT84, originally assumed to have the same mutations as the other *ftsA* mutants, did not show such constrictions (Fig. 2.3(a)) [64]. Finally, Lutkenhaus et al. showed that the filament-causing mutation in PAT84 was distinct from *ftsA* and hence denominated as *ftsZ* [69].

In the following years, several more *fts*-genes were identified. At the latest from the finding that increased levels of the protein expressed by *ftsZ*, denominated as FtsZ, augmented the frequency of cell division, it was clear that the *ftsZ* gene and its protein product play a major role in cell division. For this reason, I would like to focus on FtsZ in the following [70, 71].

2.2 FtsZ-protein

In 1985, the genetic sequence of the 1800 bp of the *ftsZ* gene was finally published by Yi and Lutkenhaus [73]. They also discovered a genetic overlap of the 3'-end of *ftsA* with the 5'-end of *envA*. To each gene there is one ore several proteins. In the case of *ftsZ* it is FtsZ. The discovery of the genetic sequence allowed further characterization of the protein FtsZ expressed by *ftsZ* such as the molecular weight [73]. First documented purification of the protein was achieved by RayChaudhuri and Park in 1992 and by Mukherjee et al. in 1993. During this work, it was also discovered that FtsZ contains a binding site for GTP which led to the assumption that FtsZ is a GTPase [74, 75, 76, 77, 78]. The protein's secondary and tertiary structures were first revealed by Löwe and Amos in 1998 by X-ray crystallography with a resolution of 2.8 Å and are shown in Fig. 2.4(b) and 2.4(c) [72]. The amino acid sequence is given in Fig. 2.4(a).

(a)

(b)

(c)
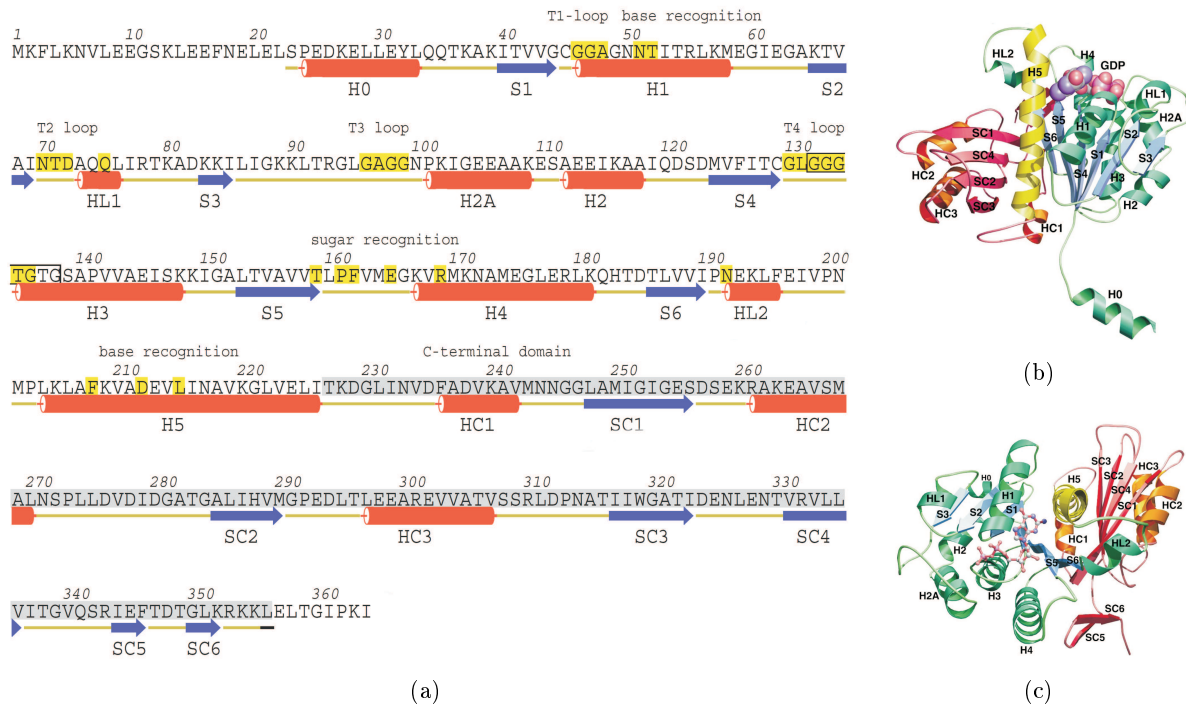
Figure 2.4: Properties of the protein FtsZ. (a)Amino acid sequence of FtsZ. (b) and (c) Protein structures of FtsZ. Blue and green: GTPase domain, red and orange: C-terminal domain in yellow: connecting helix H5. Images are taken from reference [72].
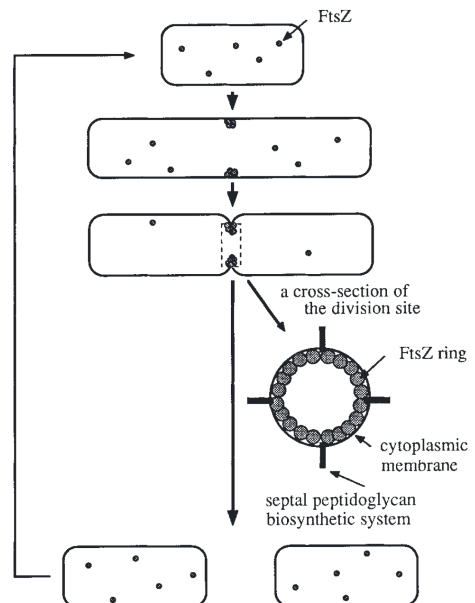
Figure 2.5: Original model of the Z-ring. Image is taken from reference [79].

<center>(a)   (b)   (c)</center>
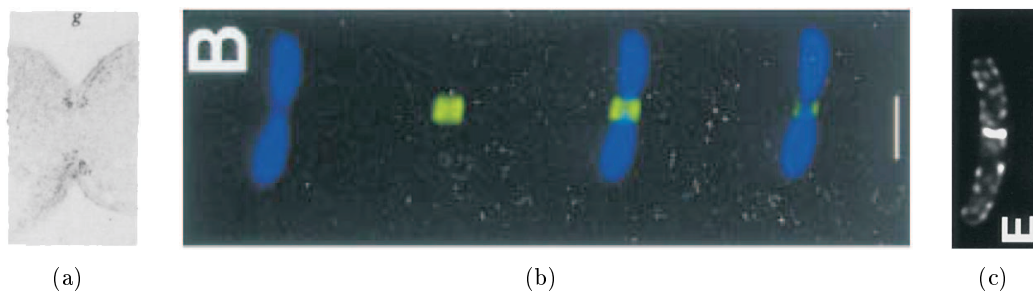
Figure 2.6: Z-ring in *E. coli*. (a) Immunogold-labeling reveal the ring-like structure of FtsZ-assembly. Image is taken from reference [79]. (b) Fluorescence micrograph of GFP-FtsZ at midcell-position in green assembles to a ring in a DNA-free zone (in blue). (c) GFP-FtsA colocalizes with the FtsZ-ring. Scale bars are 1 μm. Both images are taken from reference [80].
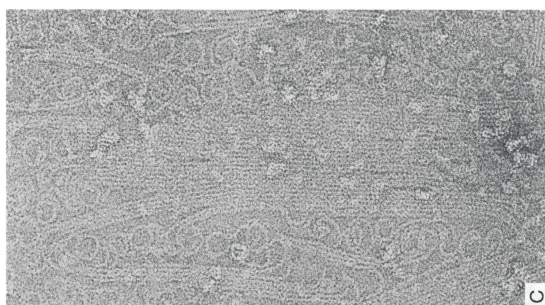
Figure 2.7: Tubulin-like sheets of protofilaments and ring-like structures assembled from FtsZ. Image is taken from Ref. [81]

2.3 Z-ring

In 1991 it was shown by Bi and Lutkenhaus that the constriction of dividing cells is accompanied by aggregation of FtsZ-proteins at a central region of the cell in form of a ring [79]. FtsZ-proteins were marked by immunogold-labeling and the distribution of FtsZ within the cell was observed for dividing and non-dividing cells by electron microscopy. For all longitudinal sections of dividing cells gold labels were always found at the leading edge of the invagination of the cell wall. This indicates a rotationally symmetric distribution of FtsZ-protein in a ring-like structure at the cell center (see Fig. 2.6(a)).

Ring-like assembly at the cell center was also observed for GFP-tagged FtsZ using fluorescence microscopy in living *E. coli* cells [80]. By staining the DNA, it could be shown that the Z-ring assembles in a zone which is free from plasmid material as shown Fig. 2.6(b) which is in agreement with the nucleoid occlusion model as described in Sec. 3.3.4 [80, 82, 83]. *In-vitro*, FtsZ could not only form sheets of protofilaments like its homologue tubulin but also ringlike structures (Fig. 2.7) [81].

These observations led to the first model of the so-called *Z*-ring as shown in Fig. 2.5. Prior to cell division, FtsZ-monomers diffuse through the cytosol. When it comes to cell division, FtsZ-proteins gather at the cell center assemble to a ring, the so-called Z-ring. But how do the FtsZ-proteins "know" that they should assemble at the cell center?

One option would that there is a fixed nucleation site for the assembly of FtsZ-monomers to a functional Z-ring. Such a nucleation site should define the future location of the Z-ring and and lower the concentration threshold for assembly [84]. Furthermore, the nucleation site should also identify the orientation of the future Z-ring in respect to the long axis of the cell. This could be for example achieved by the presence of several nucleation sites within the same plane perpendicular to the long cell axis. Or, if only one nucleation site exists within the cell wall, it should grow bidirectionally in order to form a ring on the cell wall [84].

Alternatively, distribution of FtsZ-proteins and the localization of the Z-ring could be organized not by a static structure such as one or several nucleation sites but rather by a dynamic system that positively or negatively regulates the topology of the Z-ring. As it will be shown in the following sections, the division site selection in *E. coli* is not achieved by a fixed marker at the central region but regulated through a dynamic mechanism, the Min-system.

3 Control of cell division

In order to investigate and understand the mechanism that underlie the precision of cell division, it is worth to look more deeply into some interesting aspects of growth and cell division.

3.1 *E. coli* bacteria divide into equally halved cells

The phenomenon that cells often divide into daughters of equal size had been noted for a long time but was not further investigated. Apparently, a phenomenon that exhibits uniformity attracts less attention to itself than a phenomenon which shows variation (see also Sec. 2).

Such a phenomenon within in the field of cell division exhibiting both uniformity and non-uniformity is for example the interdivision time, the time between two successive divisions. The interdivision time can vary strongly within the same cell culture. This phenomenon was subject to several research works in the 1960s. Schaechter et al., for example, discovered that sister cells have similar interdivision times whereas interdivision times of mother and daughter cells are not correlated in *E. coli* B/r cultures [85]. Along the way, the researchers also estimated the coefficient of variation of the cell sizes of sister cells to be less than to 10%. The fact that sister cells have equal sizes does not mean that all cells within a bacteria culture have the same size since individual mother cells can grow to different length before they divide. Therefore, investigation of the size distribution of daughter cells should be normalized to the size of the mother cell [87]:

$$p = \frac{\text{Size of the daughter cell}}{\text{Size of the mother cell}} \tag{3.1}$$

Marr and his co-workers measured the geometry of 214 cells of an *E. coli* ML30 culture, calculated the relative size value p and plotted its occurrence distribution (see Fig. 3.1(c)) [86]. The distribution was found to follow the Gaussian law, standard deviation was estimated to 0.0192 and the coefficient of variation to 0.0383. At the latest since this work, it can be assumed to be a confirmed hypothesis that - under normal circumstances - cell division in *E. coli* occurs into equally sized halves. Along with this work, Marr and his co-workers could also confirm that *E. coli* only grow in length but not in diameter [86].

The results of Marr et al. were confirmed 16 years later in a more detailed work by Trueba and his co-workers [25]. They took electron micrographs of different *E. coli* cultures and varying media, measured the halves of 10300 (!) dividing cells and calculated the ratio p of the daughter's length in respect to the mother's length as defined by Marr et al. Trueba and his co-workers also determined the aspect ratio of the cell's geometry as the ratio a of length L and diameter $2R$ of the cells:

$$a = \frac{L}{2R} \tag{3.2}$$

Since the diameter remains more or less constant, the aspect ratio a should increase linearly with cell length as shown in Fig. 3.2(b).

Trueba and his co-workers could not only confirm the high precision of division at midcell position for most *E. coli* cultures, but they also found that this precision anti-correlates with
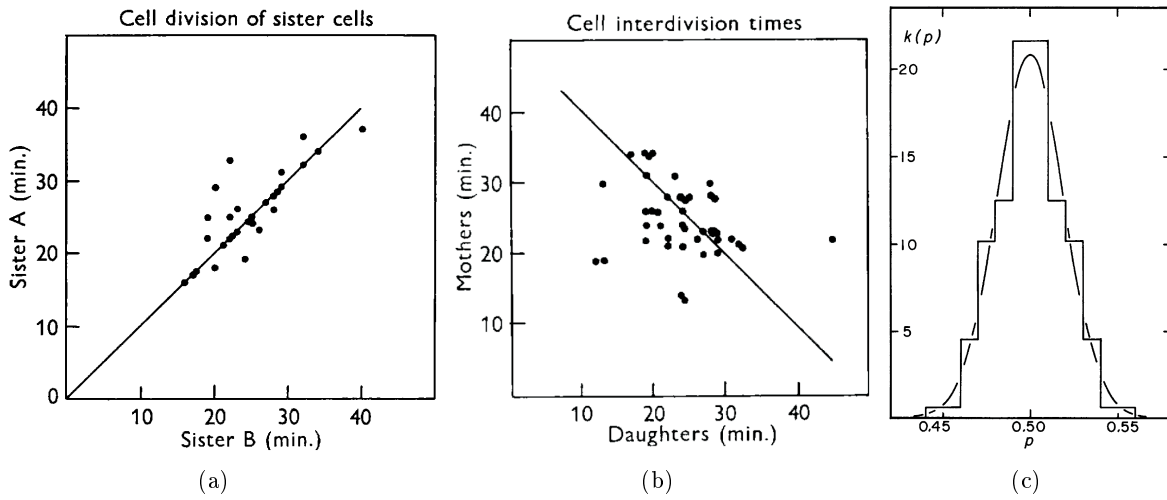
Figure 3.1: Correlation of interdivision times of cells for different relationships. Interdivision times of sister cells are correlated (a) whereas those of mother and daughter cells are not correlated (b). Both graphs are taken from Ref. [85]. Size distribution of daughter cells normalized to the mothers's size shortly after cell division for *E. coli* strain ML30 (c). Graph is taken from Ref. [86].
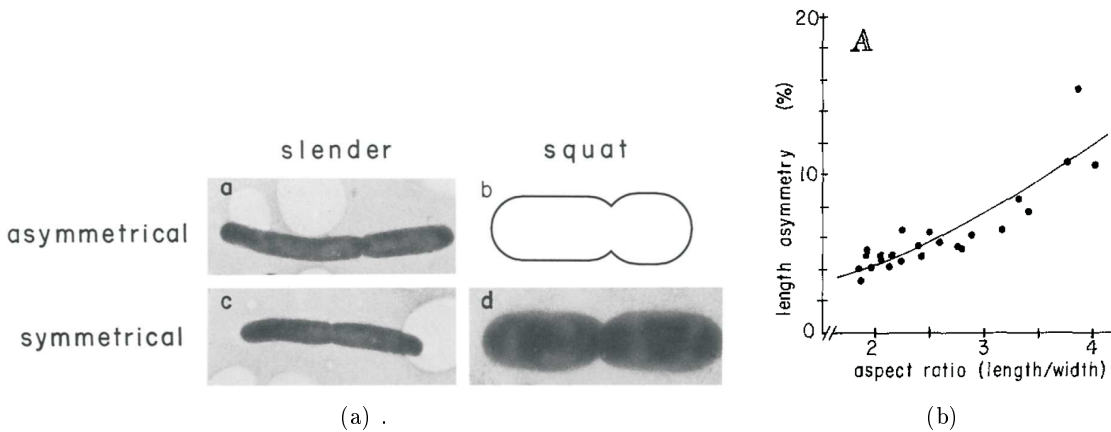
Figure 3.2: The higher the aspect ratio $a = \frac{L}{2R}$ of length and axial radius the more likely are asymmetric cell divisions. (a) Exemplary micrographs of long and thus asymmetric and of short and symmetrically dividing cells. (b) Anti-correlation of cell division asymmetry vs. aspect ratio. Images and graphs are taken from Ref. [25].
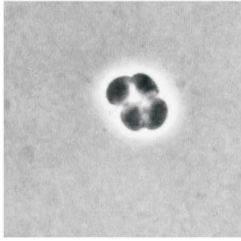
Figure 3.3: Structure of cell cultures is determined by cell migration, cell form and orientation of division planes. Parallel preservation of division planes of rod-like cells results in parallel arrays of cells. In the case of spherical cells and for alternating division planes, cluster-like cell culture structures evolve. Graph is taken from Ref. [93].

the total length, and thus the aspect ratio of the dividing cell: the longer the bacterium, the less precise division occurred at midcell position. With a coefficient of variation of 4.13 %, the highest precision was recorded for a B/R strain in LB medium which also exhibited the shortest cells at the point of division with an aspect ratio a of 1.84. In contrast, the same strain in ala + pro medium grew to very long cells before fission with an aspect ratio a of 3.86. These cells exhibited the highest coefficient of variation (15.35 %) indicating low accuracy of division. This anti-correlation is also plotted in figure 3.2(b).[1]

This precision of division was verified later for a different *E. coli* strain (LMC500) by Taschner et al. They determined a coefficient variation of 4.5 %. In 2008, Guberman et al. revised the results using more refined image processing methods. They determined a standard deviation of 2.9 % for the *E. coli* strain BW25113 [91].

3.2 Orientation of division planes

If cells do not move much and always divide in the same direction, they can either build chains or parallelly aligned cell cultures [94]. Chain-forming cell cultures can be found in cocci and cyanobacteria [95]. In *E. coli*, nearly parallel aligned cell cultures dominate, whereas in spherical *E. coli* cells with alternating division planes, cluster-like cell culture patterns emerge as shown in Fig. 3.3 [93]. It could be further speculated that division plane orientation could influence the mutual orientation of cells and thus the supracellular structure in tissue of higher organisms [27].

3.3 Division site selection

Under normal circumstances, wild type *E. coli* cells divide at the cell center (see Sec. 3.1) and in some rare cases at either of the two cell poles resulting in the septation of so-called minicells (see Sec. 4.1). Apparently, every cell has three potential division sites: at midcell position and at the two cell poles, of which the center is highly preferred [96, 97, 98]. Where does the preference for these three potential division sites come from? And how is the correct division site, the midcell position, selected out of these three?

3.3.1 Relationship between cell center and cell poles

At first sight, the preference of cell division for all three potential division sites, for cell poles as well as for the cell center, seems to be arbitrary, since there is no apparent connection between the cell center and cell poles. However, cell poles and division sites do have a close relationship: After cell fission, division sites become the new cell poles of the new daughter cells. Therefore, in each cell, one cell pole originates from a division site of the mother cell and the other cell

---

[1]Interestingly, the work of Trueba is usually only cited by the statement "*E. coli* divides with high precision" but no values are given [88, 82, 29, 89, 9]. In only few subsequent publications, concrete values for the deviation of cell division from cell center are cited. Moreover, those differ according to the citing author between 1 % and 3 % [90, 91, 92].

<div align="center">(a)   (b)</div>
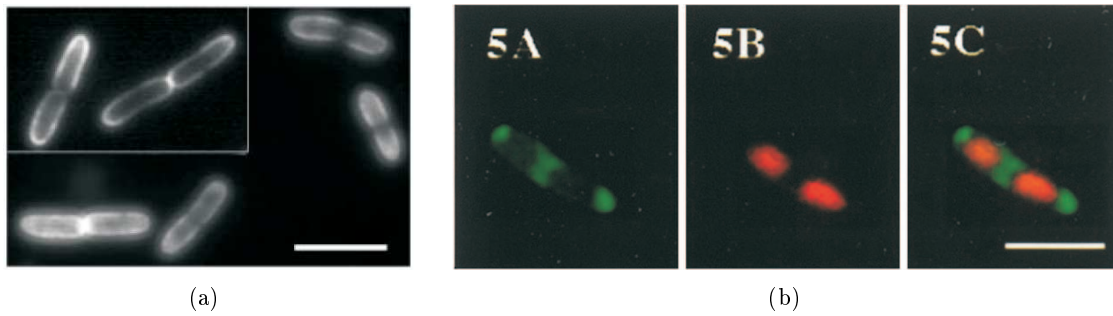
Figure 3.4: Domains of different lipid compositions in *E. coli*. (a) *E. coli pbpB* cells stained with lipophilic dye FM 4-64. Enhanced fluorescence can be either found at the cell pole prior to or after cell division, or at midcell position during the fission process. Scale bar is 5 μm. Image is taken from Ref. [99]. (b) *E. coli* AD90/pDD72 cells stained with the cardiolipin indicator NAO in green and with DAPI (in red) for the DNA. Image is taken from Ref [100].

pole from a division event of an earlier cell ancestor [97]. Consequently, cell poles have different "ages", but the cell is apparently unable to distinguish between the ages of cell poles. If cell division at cell poles is allowed, there is no observable preference for either cell pole [25].

3.3.2 Membrane signaling

Cell division in *E. coli* occurs in wild type cells at a midcell position. For certain mutations, cell division can also take place at the cell poles (see Sec. 3.3.4 and 4.1). As shown before, the responsible protein, FtsZ, localizes at midcell position by attaching to the membrane (see Sec. 2.3 and 5.1.2). Therefore, the most straightforward strategy for a division site selection mechanism would be if the membrane at this position exhibited a specific composition serving as an attracting signal for Z-ring regulating proteins or even comprise binding sites. Alternatively, the membrane at the "forbidden" regions could show a "repulsive" membrane composition. Such a signal could, for example, be represented by a specific lipid composition. In fact, lipid domains were found in *E. coli* at midcell position and at cell poles as shown in Fig. 3.4 [99, 100]. Fishov and Woldringh observed enhanced fluorescence of the lipophilic dye FM 4-64 either at the cell poles prior to or after cell division but also an increased dye concentration at the midcell position during fission. One explanation was that the dye preferentially resided at the division site and fluorescence at the cell poles were remainders of previous division events [99]. Mileykovskaya et al. could show that cell poles and the mid-cell position feature lipid domains enriched in cardiolipin [100]. A recent study indicated that accumulation of cardiolipin could be linked to the membrane curvature [101].

This observation goes along with the concept of a membrane growth zone which was supposed to be located to the midcell position as well (see Sec. 3.3.3). On the other hand, no positively or negatively regulating effect of *E. coli* lipid domains on division proteins such as FtsZ binding or assembly could be found. In contrast, addition of FtsZ in the presence of GTP is able to destabilize DPPG/DLPE domains in monolayers [102]. Membranes, their lipid composition and the emergence of phase separation and domains seem to play a major role in the regulation of cellular processes [103, 104]. However, so far no evidence was found that this concept also applies to division site selection in *E. coli*. The fact that certain lipid domains colocalize with potential division sites at the cell center and the poles might be due to a different causality. As it will be shown later, it is not the presence of lipid domains that motivate cell division at certain positions but rather other division site selection mechanisms which restrict cell division to the central region and in certain cases to the polar caps (Sec. 4). If now the lipid composition is itself

$\qquad$(a)$\qquad\qquad\qquad\qquad$(b)$\qquad\qquad\qquad\qquad$(c) .
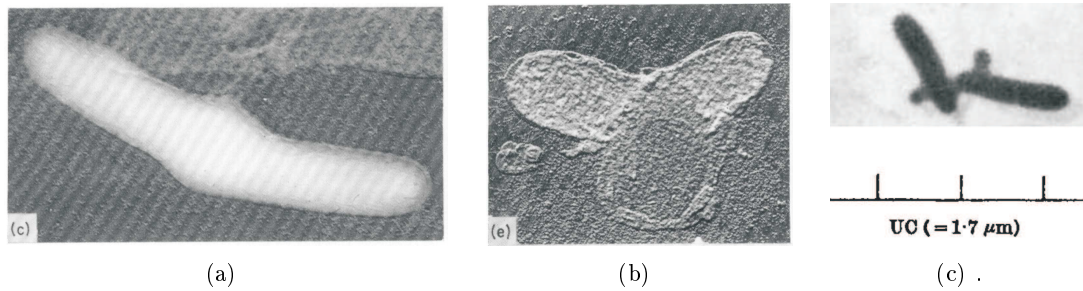
Figure 3.5: Emergence of spheroplasts from *E. coli* cells upon lysis upon addition of penicillin. (a) Fluorescence image of a "bulging" cell. (b) Electron micrograph of a spheroplast emerging from a cell. (c) Spheroplasts formation off the center at a unit cell distance from one pole. Images are taken from Ref. [21, 26]

a consequence of cell division, it certainly coincides with the division site selection but does not initiate it. Division sites are the future polar caps of newborn cells (Sec. 3.3.1). Perhaps polar caps require a certain lipid composition for unknown reasons, and other division site selection mechanisms, ensure that polar caps of newborn cells have this particular lipid composition.

3.3.3 Is there a central growth zone?

Tying in with the previously mentioned difference in membrane composition, it is worth to consider the idea of central and polar growth zones. Jacob et al. suggested that the incorporation of new cell wall material does not occur throughout the entire envelope but only in a central zone [34]. This hypothesis was motivated by the need for a model of segregation of the two copies of the origin *oriC* for DNA replication and thus of the segregation of the replicated chromosome [14]. The hypothetical membrane growth zone in a central region of the cell should take an analogous role to the mitotic spindle in eukaryotes. The idea was that the cell wall grows bidirectionally from a midcell position towards the cell poles and thereby dragging the attachment points of the replicated chromosomes, the two copies of the origin, apart from each other [34, 14].

Several other issues motivated the idea of a central growth zone. During the cell division process, two new cell caps have to be synthesized, therefore it seemed to make sense that a region for cell wall synthesis should exist at the site of the future cell poles which is at the cell center. In consequence, a "central growth zone" was considered as a candidate for a preseptal structure. Furthermore, the observation that cells grown in minimal media elongate only at the cell poles, which originate from the previous division site and hence from a hypothetical growth zone, seemed to justify the model of central growth zones (see also Fig. 1.4(a)) [26]. Last but not least, such a central growth zone could also serve as a marker for a cell division site selection mechanism as already discussed in Sec. 3.3.2.

Penicillin inhibits the synthesis of murein but not hydrolysis of murein and thus the murein layer of the cell wall is degraded. In case that penicillin is added only at a low concentration, the murein layer is weakened but synthesis of murein continues. Consequently, bulges emerge due to the weakened sacculus and the osmotic pressure [21]. However, these bulges can only grow at positions where new murein is synthesized. Therefore, penicillin can be used to indicate the location of murein synthesis. In 1969, Schwarz et al. observed that such bulges, or spheroplasts, are preferentially formed at the cell center (see Fig. 3.5(a) and 3.5(b)) [105, 21]. In filamenting cells, several spheroplasts could be observed, of which one was located at the cell center and the others in a distance that corresponded to the length of a wild type cell as shown in Fig. 3.5(c). This distance was later also observed by Donachie and Begg and termed "unit cell" (see Sec. 1.2.1 and 3.3.5). Similar experiments could be reproduced by several researchers, and other works

relying on radioactive markers supported the idea of a central growth zone [106, 107, 108]. But in fact, most of them were only a proof of enhanced cell wall synthesis activity in the center during cell division. Enhanced synthesis of cell wall material at the cell center is evident, because during cell division, the septum and the new cell poles have to be formed at the division site (see Sec. 1.2.1).

In 1985, Jaffé and D'Ari could, with the help of gold-labeled proteins in the OM, finally show that specific cell wall growth zones do not exist but that growth of the cell envelope takes place throughout the entire cell [109, 110]. A "growth zone" only appears during the division phase of the cell as shown in Fig. 1.4(b) and thus can not be understood as a spatial regulator of cell division but more likely as a consequence of the spatial division control itself [111, 27].

3.3.4 DNA-mediated cell division

Nucleoids are the most important entities that have to be segregated during cytokinesis and their level of segregation defines the required grade of precision for cell fission. In consequence, division should occur according to the spatial distribution of the bacterial chromosomes. In fact, in wild type cells, the division machinery is never assembled over an integral nucleosome and therefore no cell division occurs in such a way that one of the two copies of the bacterial chromosomes would be cut apart [112]. Nucleoid replication and segregation on the one hand and cell division on the other hand are not strictly coupled to each other, but rather coordinated in both a serial and parallel manner [13]. The process of cell division does not affect DNA replication and nucleoid segregation but vice versa, the replication of DNA and segregation of the nucleoids influences cell division [113]. For example, *E. coli* cells with mutations affecting nucleoid replication and segregation often septate in a region close to the polar positions of the cell by pinching off small, DNA-less cell-like structures (see Sec. 4.1) leading to long filamentous cells [114, 115, 116, 63, 117]. The DNA mainly interacts with the process of cell division via two mechanisms which shall be briefly presented here: the SOS-system and the NO-system.

The SOS-system

One known interaction between chromosome replication and division is the SOS mechanism, which is activated when chromosome replication fails or DNA is damaged due to abnormal conditions [118]. In this emergency case, the SOS mechanism makes sure that the division process is halted. One known agent of the SOS-system is *sulA*, also known as *sfiA* [119, 120, 121, 114, 30]. The respective protein SulA binds directly to FtsZ [122, 123, 124] and therefore blocks the assembly of the Z-ring [119]. *In vitro*, it was observed that SulA forms dimers and each subunit of these dimers binds to the T7-loop of FtsZ which is the initial protein of the divisome (see Sec. 2.2 and 5.1) [125]. This interaction of SulA and FtsZ leads to a decrease of FtsZ available for the Z-ring. SulA can even destabilize existing Z-rings due to the turnover of FtsZ assembly and disassembly in the Z-ring [30]. If SulA is depleted, Z-ring assembly is resumed [30]. But the SOS mechanism is not responsible for division site selection or temporal regulation in the standard case [30].

The nucleoid occlusion model

One possibility for DNA-mediated cell division site selection could be that the chromosomes themselves control the cell division machinery. Two principles are conceivable. Chromosomes could positively regulate cell division by motivating it in its (DNA-free) vicinity. Or, following the principle of negative control, cell division could be prevented in DNA-zones. The latter principle became known as the nucleoid occlusion (NO) model and was proposed by Woldringh

Cell division / DNA segregation	Yes	No
Yes		
No		without exemplary image

Figure 3.6: Effect of activation or inhibition of DNA segregation and/or constriction of the cell wall. In all cases, final cell division is suppressed, thus cells grow to long filaments. If both, segregation of DNA and constriction are allowed, DNA separates and cells constrict between both daughter chromosomes (top left). In the case when only constriction is inhibited, DNA still can segregate but cells show no constrictions (top right). If segregation of DNA is suppressed, sister chromosomes are not separated and form a large DNA region in the cell. When constrictions are allowed, these are never found across the chromosomal region but at locations without DNA (bottom left). In consequence, when cell divisions resumes, DNA-less cells are septated. When both, constrictions and segregation are inhibited, cells form filaments with one large DNA region (without exemplary image). Images are taken from Ref. [82]

et al. in 1985 [82, 126, 127, 90, 128, 83]. They observed that the distribution of chromosomes in *E. coli* mutants was inhibited in cell division but allowed constrictions [126]. In filaments with suppressed chromosome replication, only one bacterial chromosome was present and the constrictions were randomly distributed within the filament except for the chromosome region as shown in Fig. 3.6. For cells only inhibited in chromosome replication or segregation but allowing cell division, one daughter cell was always anucleate. In contrast, in filaments with functional chromosome replication but with inhibited cell division, multiple copies of bacterial chromosome could be found in a single filament. In this case, constrictions were always located in the space between the DNA coils. These experiments provided evidence that chromosome positioning has an influence on division site selection. The authors suggested an enzyme-mediated signal that is released by the chromosome during the phase of transcription and translation, inhibiting the activity of the cell division machinery in a close proximity of the chromosome. If this is the case, then the DNA concentration could serve as a barrier or even as a trigger for localization of the divisome action [129]. In fact, complete chromosome segregation is not absolutely necessary for successful midcell assembly of the Z-ring, which represents the first step of the divisome and leads to constriction of the cell at the division site [39, 41, 130]. The Z-ring is built from FtsZ proteins (see Sec. 2.3). In some rare cases, Z-rings can form across chromosomes at positions with a lower DNA concentration, indicating that it is not the mere presence of chromosomes which has an inhibitory effect but rather that there exists a threshold of local DNA concentration for inhibition of Z-ring assembly as pointed out by Errington and other researchers [117, 116, 131, 132, 133, 134, 135, 89, 30]. This can occur, for example, when only about 50 % of the chromosomes are segregated [41, 130].

Woldringh suggested that this inhibiting effect of the DNA-material could act on the synthesis of peptidoglycan of the invaginating cell wall and by this on the cell division [127]. Later, however, it was found that it is not the synthesis of new cell walls that is inhibited in the vicinity of nucleoids but rather the assembly of the cell division machinery. Recently, a gene function, *slmA*, was identified in *E. coli* that acts as a NO factor [112]. Cells lacking *slmA* show the minicelling phenomenon, mutations in both, *slmA* and *min* (see Sec. 4) lead to filamentation with randomly distributed constrictions, even across nucleoids. SlmA proteins bind simultaneously to DNA and FtsZ, preventing proper assembly of the Z-ring in DNA proximity [136]. *In vitro*, it was observed that SlmA affects NO by direct binding of FtsZ [112, 137].

Mutants parC and mukB form cells without nucleoids. In these cells, division occurs at midcell

position with lower precision compared to wild type cells which partially confirmed the occlusion model [117, 90, 30]. But interestingly, septation still took place close to a midcell position, however, with lower accuracy. This indicated that the nucleoid occlusion could not be the only the regulation mechanism for division site selection. Furthermore, the NO model can only explain inhibition of division at regions close to the chromosome. If the NO mechanism was the only factor, divisions would be not only allowed at the center, which is desired, but also at the cell poles. There must be an additional mechanism that restricts cell division to the only useful one of the three potential division sites, to the center [30].

3.3.5 Geometric control

It is also cogitable that certain stages of growth and geometric parameters of the cell wall could control location and time of cell division. In fact, it is not only an assumable option, but monodisperse morphology of different generations within in the same cell culture even suggest the inevitability of a linkage between cell division and cell growth to ensure that cells always divide after they have doubled their masses [13]. It is not the question whether cell growth and division are coupled or not, but rather what the mechanism of this coupling could be.

Experimental evidence of such coupling was provided by the influence of nutrient availability on cell growth and division times. Nutrient availability is one of the major factors for cell growth. Donachie and Begg investigated the growth behavior of *E. coli* cells and reported that cell wall growth can assume different modes, mainly depending on the size of the cell and the medium conditions [26]. They observed *E. coli* cells which were fixed to a support equipped with spatial markers. The markers allowed the identification of growth directions. Cells in minimal medium grew unidirectionally at only one end (see Fig. 1.4(a)). During fission, the mother cell divides and two new cell poles emerge at the former division site, therefore each daughter cell contains one "old" and one "new" cell pole. After fission, both daughter cells start to grow from the "new" cell poles, thus in opposite direction. The size of a newborn cell, thus the minimal length, was found to be about 1.7 µm which was referred as the "unit cell". In contrast to these findings, in rich medium, cells grew from both ends and generation times of cells was about 30 min and thus half of that of cell cultures in minimal medium. However, newborn cells always had a the length of one or multiple unit cells.

Woldringh speculated that a specific surface/volume ratio could be the key parameter [82]. Such a signal would especially address the time point of division. This point of view was challenged in the following, denying initiation of replication by a specific cell size [138, 139, 38, 24, 13]. Presumably, it is not the surface/volume ratio but the absolute cell length that defines the time point for cell division. However, the exact coupling mechanism between cell growth and division still remains unclear. As it will be discussed in the Conclusions (Sec. 10.2.5), cell length could indeed be a trigger for cell division but possibly via another kinetic system that will be discussed in the next sections: the Min-system.

Apparently, there is at least a coupling mechanism between cell size and cell division through action of DnaA. First of all, the ratio of DNA and cell mass is proportional throughout the cell cycle. Under- or overexpression of *dnaA* increases or decreases the mass at initiation of cell division. Therefore, DnaA is thought to be responsible for the coordination of cell size and initiation of DNA replication [140, 141].

3.3.6 Timing of cell division

Next to spatial and geometric issues, temporal regulation of cell division is of equal importance. Schaechter et al. observed that interdivision times of the cell envelope and chromosome segregation are correlated (see Sec. 3.1) [85]. Furthermore, it was reported that, similar to the

equal sizes of daughter cells, the interdivision time of sister cells was similar (Fig. 3.1(a)). In contrast, interdivision times of the mother and daughter generations were estimated to be negatively correlated, though for many samples the correlation was close to zero (not correlated) (see Fig. 3.1(b)).

If cell division and chromosome segregation were not tightly linked in terms of time points, one would find much more cells with double sets of chromosomes and others without. This is the case for only 0.015 % of the cells of a wild type cell culture, thus cell division and chromosome segregation are highly correlated in time [15, 142]. In consequence, chromosome segregation was not only considered as a candidate for spatial regulation of the divisome but also as a temporal trigger of the division event. What is the temporal relationship between both? It is clear that chromosome segregation has to be terminated when cell division has been accomplished. Contradictory results make a clear picture difficult. In some published studies, the formation of the Z-ring, the essential first step of cell division in *E. coli* (see below), starts only when the DNA replication has terminated whereas other works suggest that the Z-ring formation already starts when DNA replication is just halfway through [41, 43]. Independent of the exact timing of both, chromosome segregation could be a potential trigger for cell division and more precisely for Z-ring formation. The replisome is located via *oriC* at a central position in the cell. Therefore, it could be possible that the replication fork masks the potential binding site for the proteins involved in Z-ring anchoring and unmasks it by splitting of the replisome upon initiation of replication [143, 131]. Up to now it is not clear whether the Z-ring is formed by assembly of few FtsZ molecules at a single site on the membrane followed by a bidirectional growth in order to form a ring. Or, whether Z-ring assembly starts at once at several locations on the membrane at midcell position. Latter mechanism would clearly exclude a masking mechanism by the replisome. Additionally, the central location of the replisome at initiation of DNA replication was found to be less precise than previously considered, and the replisome itself as highly mobile [144, 145]. Also, termination of DNA replication does not have an influence on timing and positioning of the Z-ring [146, 132]. Blocking of of the final steps of DNA replication in *terC* mutants does not inhibit assembly and proper localization of the Z-ring [147, 148]. In consequence, temporal control of cell division by chromosome segregation has to be considered to be highly unlikely [30].

A certain minimal concentration of the division factor FtsZ is necessary for assembly of the Z-ring. In wild type cells, there is normally only enough FtsZ available for one single Z-ring [71]. Polymerization of FtsZ in *in vitro* experiments is concentration-dependent as well [149]. For *C. crescentus*, it is known that after division, the cellular FtsZ is either degraded or split between the two daughter cells [150, 151, 152]. The newborn cell starts life with a reduced number of FtsZ molecules and new FtsZ has to be expressed from the cell's DNA blueprint in order to raise the FtsZ concentration above the threshold for Z-ring-assembly again. Thus, it is conceivable that the current FtsZ concentration could serve as a potential temporal trigger in such a way that FtsZ synthesis is synchronized with or even controls cell division [29]. However, it was found that the FtsZ concentration is relatively constant over a long period of time during the cell cycle [153]. Apparently, the final FtsZ level is reached in a newborn cell shortly after cell division. Another possibility would be that minimal variations in concentration could be decisive upon the assembly of the Z-ring but this idea was rejected as well [154]. Lowering the FtsZ level does not change the time of cell division and only a slight increase of cell size by a factor of 1.5 was observed [155]. In contrast, increase of the FtsZ Level increased the number of polar septations and led to enhanced minicelling phenomenon (see also Sec. 4.1) [70]. Rather than the absolute FtsZ concentration, the ratio of FtsZ to other cell division proteins seems to be a crucial parameter (see Sec. 5.1) [156, 157, 29, 129].

Wild type *E. coli* cells divide at the cell center. So far no specific special markers could

be found at this position, a possible central growth zone was shown to be non-existent. Lipid domains were observed at cell poles and at a mid-cell position but were found to have no influence on division site selection. In contrast, DNA apparently influences the localization of the division machinery via the nucleoid occlusion mechanism. Other DNA-mediated systems, such as the SOS-system, that influence the process of cell division, only act in emergency cases. Temporal coordination of the action of the division machinery seems to be linked to other events of the cell. However, obvious suspects such as DNA segregation and FtsZ concentration could not be proven to trigger cell division. So, what is the mechanisms behind the division site selection in *E. coli*?

4 Research history II: Min-proteins and oscillations

As already discussed earlier, essential insights into the laws of biology are revealed when rules are broken (Sec. 2). Often, it is the abnormal phenotype and behavior that gives deeper insight into biological mechanisms. This is surprising at first sight, this is because variation draws more attention than uniformity. The discovery of the principles of division site selection and Z-ring placement is another good example of the mechanism of cognition in modern biology. Abnormality was actually the reason to ask why cells divide with such high accuracy into equally sized daughter cells: some strains of *E. coli* show abnormal division by fission of so-called minicells.

4.1 Discovery of the minicelling phenotype

The most prominent point in research leading to the discovery of the Min-protein machinery was certainly the observation of abnormal division of a certain *E. coli* strain resulting in the septation of small, spherical and anucleus cells, so-called minicells in the 1960s. Minicelling was actually already observed in earlier times and for other organisms, first documented by Gardner in 1930 for *Vibrio cholera* [158]. Similar observations were made for *Spirillum serpens* in 1956, for *Erwinia amylovora* in 1965 and for *Chlamydia psittaci* in 1973 [159, 160, 161].

In the case of *Escherichia coli*, Hoffmann and Frank already reported the fission of one (!) minicell in 1963. But only in 1967, while screening different mutants of *E. coli* for resistance against ionizing but not UV-radiation, Adler and co-workers observed aberrant minicelling in the *E. coli* strain K12 P678-54 [96]. This mutant was obtained after treatment of a log-phase nutrient-broth culture of the mother strain P678 with triethylenemelamine and showed normal cell division and replication but also a large number of septations close to the cell poles (see Fig. 4.1). The septation process itself was observed to be the same as for normal cell division at midcell position. The amount of RNA compared to the amount of protein was similar to that of normal cells but the DNA content was drastically reduced to a few traces. The resulting minicells were not capable of further cell division or replication. It was further stated that this phenotype was not caused by alteration of the external cell culture settings but strictly due to
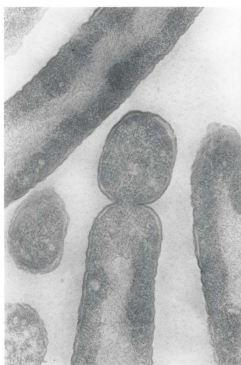
Figure 4.1: Septation of anucleus minicells in the K12 P678-54 strain of *Escherichia coli*. Image is taken from Ref. [96].
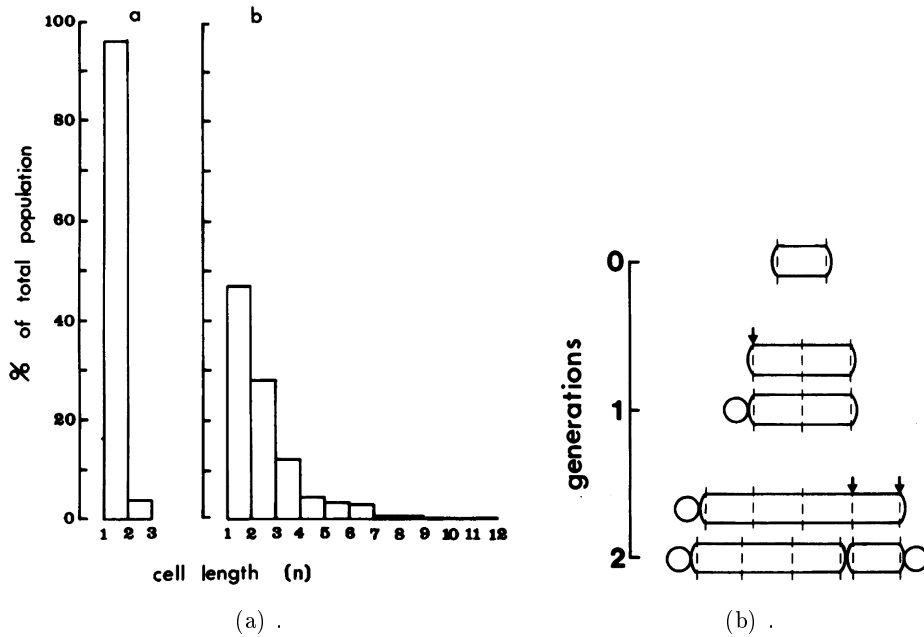
Figure 4.2: "Unit cell" length of *E. coli*. (a) Ocurrence of different cell lengths. Left: wild type *E. coli*, right minicelling mutant. (b) Relationship between the potential division sites and the unit cell length for minicelling mutant. Graphs are taken from Ref. [97]

genetic modification. A genetic analysis revealed that the genome must have changed at the region of the chromosome that controls utilization of lactose and galactose which is close to the *lon*-locus whose mutation is responsible for filamentation (also compare Sec. 2.1.4) [55, 96].

4.2 A name for the minicelling-gene

In the publication by Adler et al. in 1967, the gene responsible for the minicelling phenomenon is still without a name [96]. In 1966, Demerec et al. proposed guidelines for the nomenclature of genes [162]. They recognized the common practice to name genes according to the phenotype that comes with the mutation to the respective gene.[1] Amongst others, they recommended to limit denomination to a minuscule three-letter abbreviation. Different loci that lead to the same phenotype should have the same abbreviation but should be distinguished by an additional single capital letter. According to these guidelines the gene responsible for minicelling was baptized "*min*" and was cited for the first time in a publication by Cohen et al. in the same year [163]. However, this publication is only a short abstract which does not appear in the usual literature databases. First citation of the *min*-gene in an indexed article is found in a genetic linkage map of *E. coli* by Taylor and Trotter [164].

4.3 Min-locus and Min-confusion

Already in the year of discovery, 1967, the Min-gene was localized to a position at 11 min (unit "minute", not the gene abbreviation of "minicelling") on the *E. coli* genome [164]. In 1971, Stallions et al. published two different loci presumably responsible for the minicelling-phenomenon, *minA* and *minB* and they refer to a work by Cohen et al. published during the Cold Spring Harbor Symposia on Quantitative Biology [165, 166, 167]. Another paper published four months later refers to unpublished data [168]. Further follow-up publications were concerned with a more precise localization of the genes on the genome of *E. coli* [169, 170, 171, 172]. *minB* was finally localized at 25.6 min on the *E. coli* genome but the *minA* gene was proved to be non-existent by Davie et al. [171, 173]. The assumption that two genetic loci are involved in the minicelling phenomenon was perhaps motivated by the finding, that suppression of two genetic loci is responsible for similar minicelling phenomenon in *B. subtilis* [174]. At the latest from this finding, it was clear that the regulation of division site selection through the Min-system is determined solely by a single locus, *minB*, and therefore only by few proteins. This distinguishing role of *minB* made it possible to narrow down the mechanisms behind the division site selection mechanism.
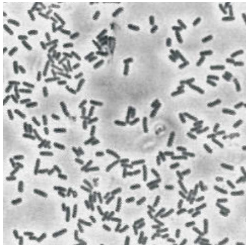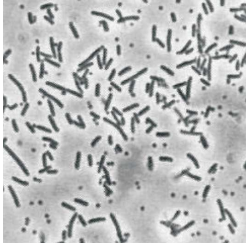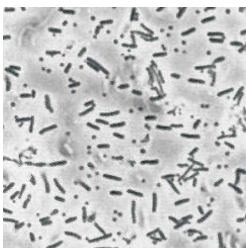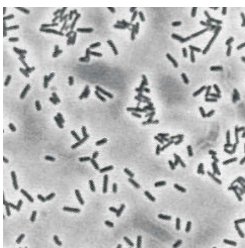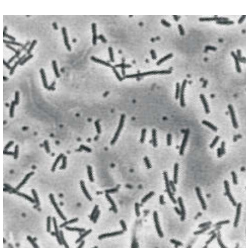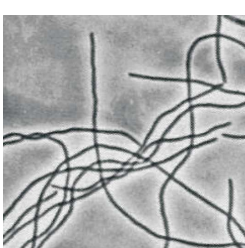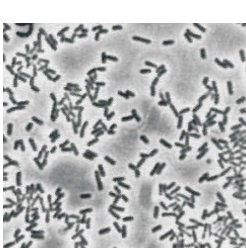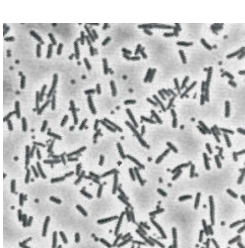
4.4 Discovery of MinC, MinD and MinE

Next landmark in the hunt for the division mechanism in *E. coli* was the identification of the single genes in the *minB* locus and the corresponding proteins. In 1989, de Boer et al. identified three genes in the *minB* locus coding for three proteins, from now on assigned as *minC*, *minD* and *minE* [176, 175]. They deleted the *minB*-locus in the *E. coli*-strain PB103, resulting in the Δ*minB* strain PB114. As expected, deletion of the *minB* locus exhibited the minicelling phenotype as depicted in Tab. 4.1, line 2, column 1. For comparison, the wild type phenomenon of strain PB103 is shown in Tab. 4.1, line 1, column 1. The wild type phenotype could be restored in Δ*minB* by expressing the plasmid λDB170 carrying the genes *minC*, *minD* and *minE* (in combination with isopropyl thiogalactoside (IPTG)), proving that the combination or at least one of the three genes is responsible for proper division at a midcell position (see Tab. 4.1: line 3 column 2). Different combinations of plasmids for individual protein expression by the genes *minC*, *minD* or *minE* finally revealed that all three sister genes are essential for proper division site selection. Plasmids carrying only *minE* yielded minicells (see Tab. 4.1, line 5, column 2) indicating that cell division was allowed everywhere, whereas the integration of the combination *minCD* into the Δ*minB*-strain produced long filaments suggesting that cell division was inhibited (see Tab. 4.1, line 4, column 2). Addition of *minE* to cells carrying only *minCD* restored the wild type phenomenon again [175]. Plasmids with combinations of *minC* and *minE* (*minCE*) or *minD* and *minE* (*minDE*) allowed cell division at all potential division sites and thus yielded minicells as well.

Also, deletion of single genes yielded a similar picture: Deletion of either *minC* or *minD* produced minicells indicating that cell division were allowed at all potential division sites (cell center and cell poles) [175, 177, 178]. In contrast, deletion of *minE* led to filaments suggesting that in these cells division was blocked throughout the entire cell [175, 179].

These findings were completed with a series of overexpression experiments of single genes or combinations: Overexpression of *minCD* blocked cell division and produced long filaments [175].

---

[1]This practice does not seem to be straight-forward and is even contradictory: often a gene is named after the effect that takes place when the respective gene is **not** active. It would be more logical to name a gene after the phenotype that appears when the respective gene is active. For example, a more appropriate name for the minicelling gene could be *cen* since it makes sure that cell division occurs at a *central* position. But this is just a physicist's view.

Bacteria strain / plasmid	without IPTG	with IPTG
PB103 ($minB^+$)	wild type	n.A.
PB114 ($\Delta minB$)	minicells	n.A.
PB114 λDB170($\Delta minB +$ $minCDE$)		wild type
PB114 λDB170($\Delta minB +$ $minCD$)		no septation, long filaments
PB114 λDB170($\Delta minB +$ $minE$)		minicells

Table 4.1: Mutations in min genes and the corresponding phenotypes. Micrographs are taken from Ref. [175].
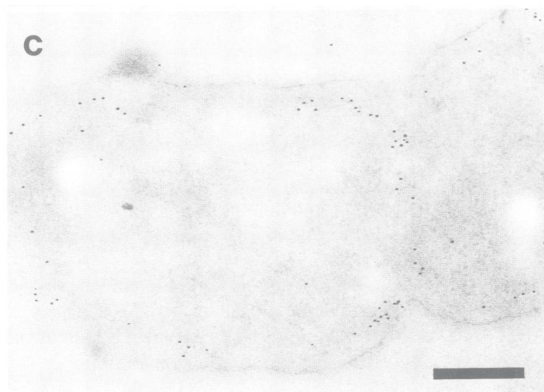
Figure 4.3: Immunogold-staining of MinD in combination with electron microscopy revealed that MinD binds to the inner periphery of the IM. Scale bar is $0.25\,\mu$m. Images is taken from Ref. [182].

Overexpression of *minE* allowed cell division at all three potential division sites leading to the emergence of minicells [176, 175].

Altogether, these results suggested the following picture: without the genes of the entire *minB*-locus (*minCDE*) septation can take place at all potential division sites (cell poles or midcell position), the common action of *minCD* can block septation at all potential division sites, whereas *minE* limits the blocking ability of *minCD* to the cell poles allowing septation at the midcell position (wild type phenotype) [175, 180, 181, 179]. *minC* is obviously responsible for inhibition of cell division.

But how does the Min-system affect cell division? Or more specifically, which part of the bacterial division machinery is the target of Min-activity? And which are the specific tasks of the single factors of the Min-family?

4.5 MinD is an ATPase and a peripheral membrane protein

From the DNA sequence of the respective *minD* gene it was already predicted that the MinD-protein would contain a nucleotide binding site [175]. Mutation of this putative binding site led to minicelling, i.e. the topological control of cell division was lost, which was probably due to inactivation of MinD through the corresponding mutation. The hypothetical nucleotide binding site was further confirmed when de Boer and his fellow researchers could identify other known proteins with a similar amino acid sequence by scanning protein databases. Strikingly, similarity was significant for regions with nucleotide binding sites of the known proteins indicating that MinD might be an ATPase [182].

First localization experiments of Min-proteins were performed by de Boer et al. at the beginning of the 1990s [182]. They used MinD antiserum and colloidal gold-labeled second antibody assays to visualize the distribution of MinD in *E. coli* by immunoelectron microscopy. MinD was observed to attach to the inner membrane as shown in (Fig. 4.3). However, MinD was also found in the soluble fraction after cell breakage indicating that MinD is a peripheral membrane protein. It was already known that the Min-system is responsible for preventing septation at the cell poles and limiting cell division to the cell center. Yet, it was not clear whether the Min-proteins do this via other factors or whether they would themselves act on the respective division machinery. Furthermore, such direct action might imply the localization of Min-proteins either to the cell center in case of a positive regulatory mechanism or to the cell poles in case of a negative regulatory mechanism. However, the authors pointed out that the reported localization experiments by immunogold-staining only allowed to identify MinD as a peripheral membrane protein but no statements about polar or central localization could be made.

The affinity of MinD for the membrane was confirmed later on. Fluorescence microscopy of labeled MinD-proteins showed that MinD attaches homogeneously to the membrane in the
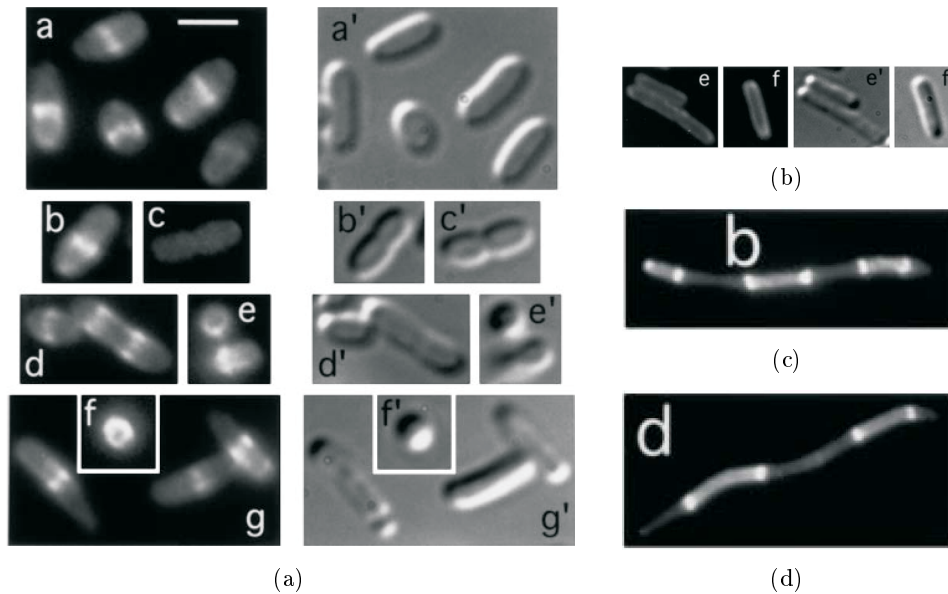
Figure 4.4: Fluorescence and transmitted light micrographs of MinE-GFP in *E. coli* cells. (a) In cells expressing both MinE and MinD, the fluorescence of MinE-GFP accumulates as a visible band at midcell position (scale bar 2 μm). Insets e and f show cross section views which clearly reveal the ring-like structure at midcell position. Rarely was a MinE-ring observed together with a constriction (inset b and b') whereas in constricting cells in most cases MinE-Fluorescence did not show membrane binding but was homogeneously distributed in the cytoplasm (inset c and c'). In the rare case of delayed division, cells could also exhibit two MinE-rings within the same cell (inset d and d'). (b) In mutants lacking MinD, MinE assembles through the entire cytoplasm without any specific membrane affinity or even localization to the cell center. If cell division is inhibited, several MinE-rings can emerge, for example by (c) blocking of Z-ring assembly by SfiA or (d) complete suppression of FtsZ expression. Images are taken from Ref. [179].

absence of MinE [183].

4.6 Interaction of Min-proteins with the Z-ring

Overexpression of MinC and MinD blocks cell division [175]. This inhibition could be overcome again by overexpression of FtsZ [177, 178]. This finding was supported by the observation that overexpression of FtsZ also leads to the minicelling phenomenon just like deletion of the *min*-operon [70]. In addition, some *ftsZ*-mutations are able to suppress MinCD overexpression and thus lead to the production of minicells as well [184]. Altogether, these findings suggested that an interaction between the Min-system and FtsZ affects cell division which was already assumed by Bi and Lutkenhaus in 1990 [184, 119, 177, 185, 186]. Still, attempts made in 1996 failed to proof interactions between the Min-proteins and FtsZ [123]. Back then, it was suggested that MinCD and FtsZ could probably compete for the same membrane binding sites [84]. In 1999, it was proclaimed by Yu et al. that the function of the Min-system could be the topological regulation of the Z-ring [90]. Since it was already clear from previous works that it is the role of MinC to inhibit cell division, it was evident that it is MinC that addresses the Z-ring. Also in 1999, Hu discovered that MinC affects the Z-ring by destabilizing FtsZ-polymers [185].

4.7 MinE-ring

In 1989, de Boer had proposed two different models of how MinE could regulate the topology-specific action of MinCD [175]. In one model, MinE itself was supposed to accumulate at the cell poles as a positive marker for MinCD [181]. The considered alternative suggested a negatively regulated mechanism by MinE-assembly at the cell center and thus blocking this site for MinCD action [180, 123, 187]. To come to the point, the first model could not prevail whereas the second model was later proven to be correct.

In 1997, Raskin and de Boer could show by fluorescent labeling with GFP that MinE localizes at midcell position. Fluorescence microscopy revealed, that MinE, similar to MinD, accumulates on the inner periphery of the IM as shown in Fig. 4.4(a) [179]. Cross-sectional views of *E. coli* cells show a ring-like distribution of the fluorescence signal which could either indicate a thin ring-like or tubular distribution of MinE in the cell (Fig. 4.4(a), insets e/e' and f/f'). However, longitudinal views of the cell show a narrow band of MinE at the cell center which only allowed a ring-like structure of MinE as a valid interpretation of the observations (Fig. 4.4(a), insets a/a', b/b' and g/g').

Mutations in *minC* did not affect the emergence of a MinE-ring. In contrast, in MinD-mutants, no MinE-rings could be observed but MinE was homogeneously distributed throughout the cytosplasm without any visible association to the membrane (Fig. 4.4(b)). This indicated that MinD, although itself not part of the MinE-ring, is required for MinE to assemble into the ring-like structure. In long cells with a delayed division, two MinE-rings emerged at 1/4 and 3/4 positions. When division was completely stopped, several MinE-rings were observed in the resulting filaments, in some rare cases up to 30 rings within one filament. The spatial distribution of these rings were characterized by an equidistant separation which is in agreement with the concept of a unit cell length (Sec. 3.3.5).

The MinE-ring assembly was also observed when the assembly of the Z-ring was inhibited by action of SulA, which is an actor of the SOS system (see Sec. 3.3.4), and even in *ftsZ*-mutants. In certain minicelling mutants, thus in cells with Z-ring assembly at the polar caps, the MinE-ring still appeared at a midcell position. In addition, it was observed that the MinE-ring also disassembles during constriction. Altogether, these results indicated that the MinE-ring was not part of the Z-ring or even the septum but rather a proper structure [179].

Actually, the authors were close to reveal the true mechanism. As it appears, only static micrographs were acquired throughout the study but no timelapses [179]. Min-proteins show a dynamic membrane attachment behavior (see below, Sec. 4.8) on a slow timescale which can be visualized by time scaling of micrograph timelapses but easily eludes human perception in real time. Interestingly, the authors observed that in long filaments, MinE exhibited - next to the distribution of MinE in ring-like structures - a second topological specificity: Apparently, always two MinE-rings formed a pair-like structure with increased accumulation of MinE on the inner membrane between the two rings, separated by a non-fluorescent gap between MinE-ring-pairs resulting in a band-like pattern as shown in Fig. 4.4(c) and 4.4(d). Furthermore, in normally dividing, cells it was observed that always one half of the cell was characterized by a slightly enhanced fluorescence of MinE-GFP. The authors interpreted this with the consideration that MinE could distinguish between the two halves of a cell or even establish a distinct polarization. In fact, this observation of partial distribution of MinE outside the ring-structure in both, filaments and dividing cells, was the simple consequence of static image acquisition of an oscillatory pattern of the MinE-ring.
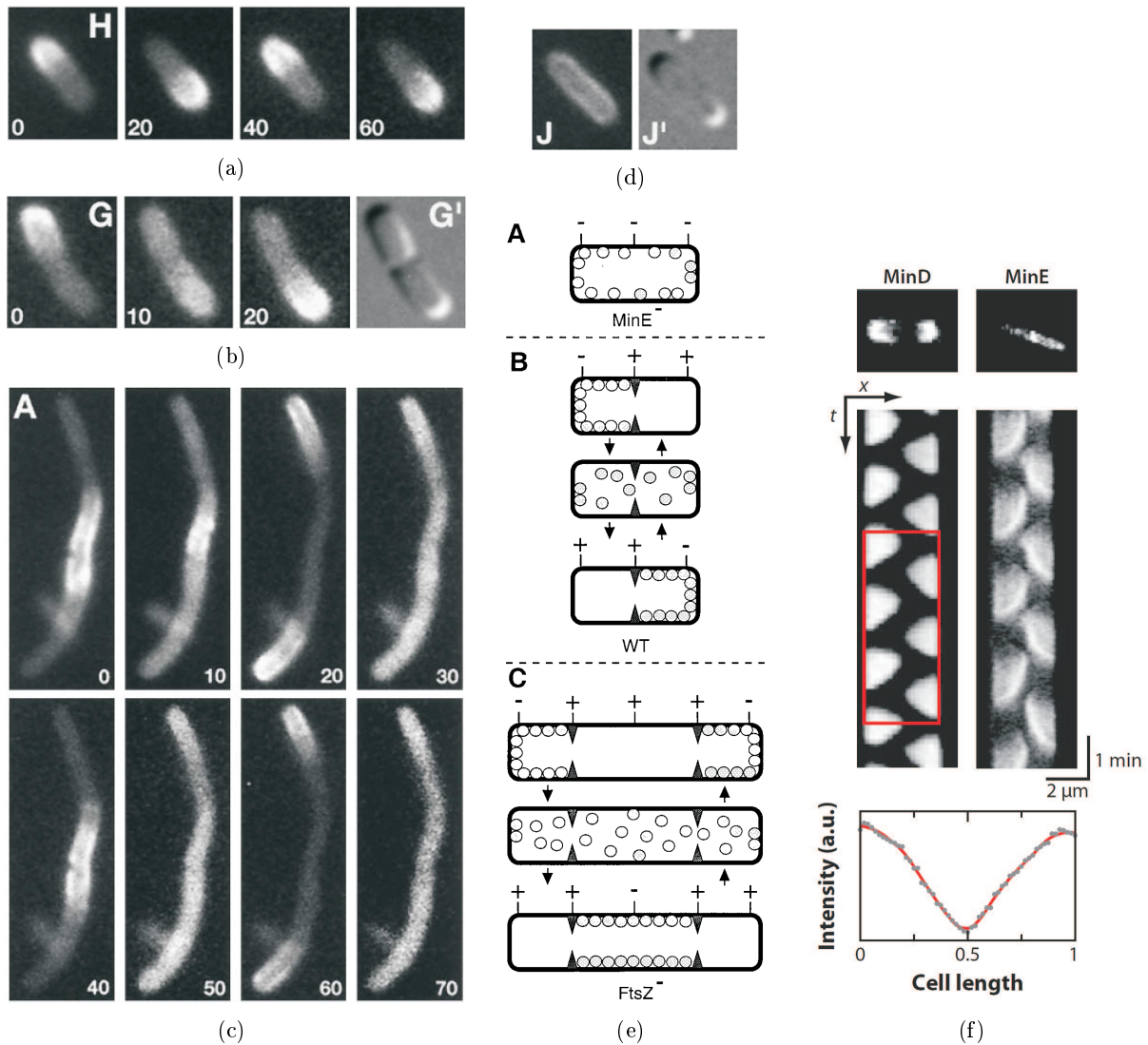
Figure 4.5: Oscillations of MinD in *E. coli*. (a) Cytosolic MinD binds to the membrane at one pole of the cell, then detaches and binds again to the other cell half. The period of the displayed oscillation is about 40s. (b) MinD can also oscillate in constricting cells as long as these are not fully separated by a closing septum. (c) In filamenting cells with inhibited cell division, several oscillations can emerge. In the example here, two oscillations occupy the filamentous cell, with each oscillation in one cell half. Oscillations are mirror inverted. Again, the period of both oscillations is 40s. In follow-up studies also other modes of periodic patterns were observed in filamentous cells. Especially in very long cells, propagating waves instead of oscillations can emerge. (d) Oscillations of MinD require MinE. Without MinE, MinD can still bind to the membrane but no dynamic pattern evolve. (e) Raskin and de Boer suggested the shown depicted for the Min-oscillation (see text). Images are taken from Ref. [188]. (f) Kymographs of MinD and MinE oscillations in *E. coli* and the respective time-averaged MinD-profile exhibiting the characteristic minimum of MinD at midcell. Figure is taken from Ref. [92].

4.8 Min-oscillations

The dynamic nature of the Min-protein system remained unrevealed until 1999 when again Raskin and de Boer observed the spatial and temporal distribution of GFP-tagged MinD in *E. coli* cells [188]. First of all they, could confirm the previously in electron microscopy observed accumulation of MinD to the inner membrane (IM) (see Sec. 4.5).

Previously, it was observed that MinE forms a ring like structure at the cell center, but also shows a slight accumulation in one cell half (Sec. 4.7). For MinD no such ring-like structure was observed but MinD could be found only within in one cell half as well. The fluorescence intensity of fluorescently-labeled MinD in one entire cell half was much stronger and more homogeneously distributed throughout one cell half than the distribution of MinE. This led to the conclusion that MinD binds more broadly to the inner membrane [179]. But in contrast to the work published two years before, now it was observed that the residence of MinD in one cell half alternated between both halves of the cell in an oscillatory manner with an oscillation time of $40 - 120\,\mathrm{s}$ for a full cycle (back and forth) as shown in Fig. 4.5(a) [188]. When switching from one cell half to the other, the fluorescence signal on the IM decreased and increased within the cytoplasm, indicating that the protein detached from the cell envelope during transition and before binding again to the opposite cell pole. Mutations in *minC* did not change this pattern indicating that the oscillatory behavior of MinD does not require MinC. In contrast, mutations in *minE* allowed binding of MinD to the IM but stalled the dynamic pattern of MinD, as one can see in Fig. 4.5(d). In this case, MinD is bound to the entire cell envelope.

As shown earlier, deletion of MinE leads to the formation of filaments [175, 114]. Thus, it was reasoned that the oscillatory behavior should be the consequence of an interaction of MinD and MinE. It was assumed that the MinE-ring disassembles the membrane-bound MinD which then reattaches at the opposite cell pole. This oscillation continues even throughout the division process until the cell is fully constricted and both daughter cells are completely separated (Fig. 4.5(b)). After complete fission each, daughter cell resumes its own MinD oscillation. A further observation was, that decreasing the MinE/MinD-ratio led to an increase of the oscillation period [188].

In filaments twice the size of a normal cell, double oscillations were observed between either cell pole and the cell center with the two oscillations meeting at a midcell position (Fig. 4.5(c)). This observation is in agreement with the 1/4 and 3/4 positions of MinE-rings in double-sized cells observed previously by Raskin and de Boer in 1997 [179]. Segmentation of the non-dividing cells by Min-oscillations supported the idea of a unit length of *E. coli* (see Sec. 3.3.5). Oscillation patterns in even longer cells exhibited a periodicity of $5\,\mathrm{\mu m}$ which can be seen as the "intrinsic" wavelength of the Min-oscillations.[2]

Finally, the authors suggested that oscillations of MinD could be a regulatory mechanism for the cell to find its center. This observation also evoked the idea that the Min-system could not only serve as a tool for defining the central division site of the cell but also as a cellular ruler which triggers cell division in dependence of cell length [188, 191, 92]. Raskin and de Boer proposed a model for the Min-mechanism as shown in Fig. 4.5(e). In cells without MinE (inset A), MinD binds anywhere on the inner membrane without any topological specificity. In wild type cells, MinE "blocks" the central position allowing MinD to bind only in extracellular positions (inset B). However, an explanation of the oscillation mechanism could not be given. Also note, that still back then, binding of MinE to the cell center was assumed to be of static nature which was, in fact, wrong. In filamenting cells, several independent oscillations can emerge with several static MinE-positions which serve as as the pivotal points for the oscillation (inset C).

---

[2]Interestingly, the publication by Raskin did not quantify this wavelength. Later publications cite the article by Raskin with a wavelength of $8\,\mathrm{\mu m}$ [189, 190]. However, an evaluation of the respective figure yields rather a value of $5\,\mathrm{\mu m}$.

The concept of the Min-system as a selection mechanism for cell division was further supported by the finding that two independent oscillations evolve in constricting cells (see Fig. 4.5(b)) [185]. Apparently, as soon as the principal task of the Min-proteins, division site selection, has been accomplished, the oscillation mechanism switches from the mother to the daughter cells, in which the Min system again provides division site selection.

It was already known that MinC is the actual factor for inhibition of Z-ring assembly and that the spatial MinC activity is coupled to MinDE oscillations (see Sec. 4.6). Two models for the spatial distribution of MinC itself were considered: either MinC is distributed throughout the cell but inactive and is activated only upon contact with oscillating MinD. Or, the spatial distribution of MinC is linked to the spatial distribution of MinD.

Within in the same year and by the same group of Raskin, similar oscillations of MinC proteins were observed which proved the second model to be correct [114]. These observations were confirmed shortly after by Hu et al. and also by Rowland et al. who worked on this topic independently from Raskin and de Boer [185, 183]. Altogether, MinC oscillations did not differ much from MinD dynamics. First of all, MinC fluorescence alternated with a similar period between cell poles. Fluorescence of the GFP-label was strongest on the membrane indicating that MinC binds to the cell envelope like MinD. Between accumulation at the cell poles, fluorescence decreased at the cell periphery which indicated that MinC disassociates from the membrane for transition to the opposite pole. MinC oscillations depend on both, MinD and MinE, but not on FtsZ. MinC and MinD oscillations occur synchronously indicating that dynamics of both are coupled. This idea was supported by yeast two-hybrid assays proving direct interaction of MinC with MinD [123, 186, 192]. Altogether, these results together with the fact that MinD can oscillate solely in the presence of MinE but MinC does not show oscillations without MinD, suggested that MinD is piggybacking MinC and therefore facilitates MinC-oscillations.

Previously it was believed, that the MinE-ring represents an immobile structure [179, 114, 185]. But in 2001, oscillatory behavior could also be shown for the MinE-ring and one year later, the simultaneous observation of MinD and MinE oscillations was published [193, 194, 195]. From then on, it was clear that the MinE-ring assembles at the cell center, starts detaching MinD from the membrane close to the central region and progresses towards the adjacent region of peripherally bound MinD, thus towards the cell pole occupied by MinD. Once, all MinD proteins are detached from the inner membrane, MinE detaches from the membrane itself and reassembles at midcell and starts progressively detaching MinD towards the opposite cell pole. MinE-ring dynamics do not depend on FtsZ which makes the entire Min-family independent of FtsZ [194].

In filaments, multiple MinE-rings could be observed which also moved towards the adjacent low density region membrane-bound MinE [193, 194]. For example, in the case when two MinE-rings were visible, they first moved towards the cell poles simultaneously. At the cell poles they detached and reassembled at 1/4 and 3/4 positions as also observed by Raskin et al. in 1997 [179]. Between both rings a new region emerged showing weak MinE-binding on the membrane. Both rings again moved towards the adjacent regions of low surface density of membrane-bound MinE [193, 194]. This region of low density of membrane-bound MinE corresponds to the membrane region binding MinD and MinC.

FtsZ assembles only in membrane areas free of MinC. Thus, due to the oscillatory pattern of the Min-proteins and its inhibitory effect on Z-ring assembly one would expect a corresponding and thus also oscillating response of FtsZ assembly. However, under normal circumstances, the Z-ring is assembled at the cell center and does not show any complementary oscillation behavior. How can a dynamic pattern of an inhibitory system determine the position of a static structure? In 2001, de Boer et al. proposed that it is not the momentary position of the MinC-proteins that defines the assembly site for the Z-ring but the time-averaged pattern. Averaged over time, MinD and thus MinC proteins show an increased residence time on the cell poles and a minimum

(a)

(b)

(c)
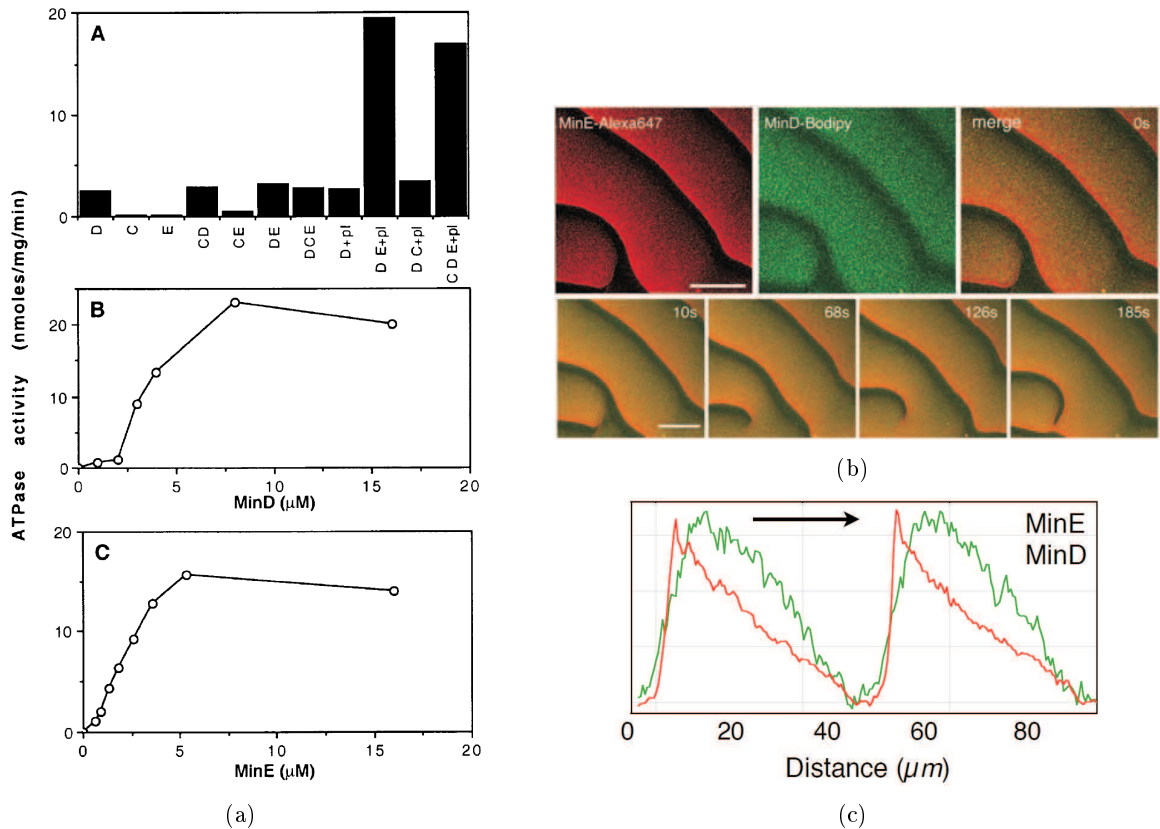
Figure 4.6: Min-dynamics in vitro. (a) Min-protein action in the presence of liposomes. Top: AT-Pase activity of different Min-protein combinations. MinD shows significant ATPase activity only in the presence of phospholipids and MinE. Center: ATPase activity of MinD in dependence of MinD concentration. Bottom: ATPase activity of MinD in dependence of MinE concentration. Graph is taken from Ref. [197].(b) MinD and MinE waves on artificial lipid bilayers obtained by confocal fluorescence laser scanning microscopy. (c) Profiles of the fluorescence intensities reflect the surface density of MinD and MinE on the membrane. Both images and graphs are taken from Ref. [1].

at the cell center [194, 196]. Fig. 4.5(f) shows kymographs of MinD and MinE oscillations and the profile of time-averaged membrane-bound MinD with a minimum at the central position of the cell.

4.9 Min-proteins *in vitro*

The more detailed insight into the Min-system and the regulation of cell division prepared the ground for the understanding that the biochemical mechanism of Z-ring placement by Min-proteins represents a rather simple system which only requires a membrane, the three Min-proteins MinC, MinD and MinE and ATP. Therefore the Min-system excels for *in vitro* studies. Hereby, "simple" refers to the number of agents involved but not to the complexity of the mechanism.

Naturally, *in vivo* studies, i.e. in the cell, entail a high number of components. Often, most of these components are actually not required for the investigation of the phenomenon of interest. In contrast, these unnecessary components often interfere with the observation of the investigated mechanism. Thus, for certain studies, it is useful to remove all unnecessary components and reduce the biological system to the essential factors. This can be for example achieved by the

concept of bottom-up synthetic biology using components from disassembled cells as described in Sec. 7.4.3. Biochemical systems which involve only few factors lend themselves for such an *in vitro* approach. Since the Min-system represents such a cellular mechanism with a low number of agents, an *in vitro* approach is suitable.

First attempts to reconstitute the Min-system in an artificial environment was performed by Hu and Lutkenhaus in 2001. They mixed ATP, Min-proteins and liposomes in order to test the ATPase activity of Min-proteins in dependence of the presence of lipids [197]. As expected, for pure MinD or the combination of MinD and lipids, the ATPase activity was low. Significant activity was only observed if at least MinD, MinE and lipids were present and was about ten fold higher than the base activity of MinD (Fig. 4.6(a) A). ATPase activity was also determined in dependence of MinD and MinE concentration. ATPase activity showed a cooperative behavior in dependence of MinD concentration which suggest cooperative binding of MinD to the membrane (Fig. 4.6(a) B). In an initial regime the ATPase activity of MinD increased linearly with increasing MinE concentration until a plateau was reached at a molar MinE/MinD ratio of about 0.33 (Fig. 4.6(a) C).

This initial work was soon followed by further studies by the same group but also by others, mainly researchers around de Boer [196]. They amended the work by Hu and Lutkenhaus with similar experiments using lipid vesicles and sedimentation protocols. They confirmed that MinD can only bind to the membrane in the presence of ATP but not when the nucleotides are replaced by ADP which could be interpreted in such a way that binding of MinD requires the hydrolysis of ATP. However, MinD could also bind to the membrane in the presence of a non-hydrolyzable analogue of ATP (ATPγS) which suggested that binding of MinD requires ATP but not its hydrolysis. Furthermore, binding of MinC and MinE to membrane-bound MinD was proven in the presence of ATP, but also in the presence of ATPγS, suggesting that also binding of both proteins to MinD does not require ATP hydrolysis [196, 198]. Addition of MinE to vesicles previously decorated with MinD led to unbinding of MinD in the presence of ATP but not in the case of ATPγS. Thus, ATP hydrolysis was found to be necessary for the detachment of MinD from the membrane. In experiments with vesicles previously reconstituted with both, MinD and MinC, addition of MinE induced detachment of MinC (but not of MinD), even in the case of ATPγS. This elucidated three more aspects: MinC detaches from MinD through displacement by MinE, ATP hydrolysis is neither necessary for MinC displacement, nor for binding of MinE to MinD. ATP hydrolysis is only required for the very last step, detachment of MinD from the membrane (together with MinE). Cooperative membrane binding of MinD was confirmed as it was also observed by Hu and Lutkenhaus [197, 196].

Meacci and Kruse have suggested in 2005, that it should be in principle possible to reconstitute the Min-system outside a biological cell [199]. Furthermore, they also reasoned that an enclosed compartment would not be essential for the basic Min-protein dynamics and proposed to use an open geometry instead. Finally in 2008, Loose et al. could not only reconstitute the Min-protein system into an artificial membrane system but also observe and visualize periodic protein binding patterns in fluorescence microscopy. In brief, a supported lipid bilayer was prepared from vesicles composed out of polar lipid extract from *E. coli* on a hydrophilic and transparent support like mica glued onto a microscopy cover slide (Sec. 7.7.1). Alternatively, supported lipid bilayers could also be formed directly on glass slides that have been cleaned extensively ((Sec. 8.1.7). Then, a small amount of MinD was given to the working buffer above the membrane. Upon addition of ATP, MinD bound to the membrane. Next, MinE was added which led to detachment of membrane-bound MinD. After several minutes MinD started to bind again to membrane regions that were free from MinE. Finally, a periodic pattern of proteins binding to the supported lipid bilayer evolved. However, this periodic pattern was not of oscillatory nature as observed *in vivo* but rather a wave-like pattern with parallel and propagating waves as shown in Fig. 4.6(b). The

fluorescence intensity reflects the protein density on the membrane and can be plotted in a profile as shown in Fig. 4.6(c). The front of the wave is characterized by a low concentration of both, MinD and MinE. Towards the rear of the wave, the protein concentration increases towards a peak shortly before the trailing edge of the wave. After this peak, the protein concentration decreases rapidly. For MinE the protein concentration rises initially slower than for MinD, its peak is shifted by few µm and it decrease more sharply at the rear than MinD, which can be seen as a sharp MinE-edge in the micrographs (Fig. 4.6(c)).

The approach of reconstitution of proteins into supported lipid bilayers goes beyond classical *in vitro* studies and allows a more systematic manipulation of biochemical processes to the point of mimicking of biological phenomena in an artificial environment which is why such an approach is rather positioned in the field of synthetic biology (see also Sec. 7.4). The investigation of Min-proteins in synthetic biology triggered a veritable cascade of new insights into the mechanism of the Min-system as explicated in Sec. 5.2.5. Furthermore, in far future it might be even possible to mimic a complete cell-division-like process in an artificial system.

5 The current picture of Fts- and Min-action in cell division

5.1 The *fts*-family, further essential division proteins and the septation pathway

As already pointed out, the division of *E. coli* cells does not only require FtsZ but an entire armada of fission proteins. Some are essential for cell division and a subset of these is essential for assembly of the Z-ring. For *E. coli* K-12, mutations at different loci lead to blocking of cell division indicating that several genes are responsible for proper cell septation. Since filament formation occurs for most of these mutations at elevated temperatures of around 42°C, they are attributed to the *fts*-family (Sec. 2.1.5). It is clear that all these genes must have different functions within the process of cell septation, and therefore it was obvious that the different *fts*-genes were responsible for different consecutive steps of the septation process.

5.1.1 The divisome family

Up today there are 10 genes known to be essential for *E. coli* to septate successfully: *ftsA*, *ftsI*, *ftsK*, *ftsL*, *ftsB*, *ftsN*, *ftsQ*, *ftsW*, *ftsZ*, *zipA* and *amiC* [201, 69, 84, 29, 12, 202, 30, 203, 8]. *ftsA* and/or *zipA* and of course *ftsZ* are essential for the assembly of the Z-ring itself, whereas the others contribute to later steps in the septation process. The function of all these members of the divisome is not fully understood. Most of them recruit their respective interaction partners to the division site, assist in the formation and stabilization of the Z-ring and remove replicated DNA from the division site. Presumably, some proteins are also responsible for redirection of cell wall growth from the cylindrical region to the septum. Action of the respective proteins has to be carefully coordinated by the cell or by proteins themselves. The state of knowledge suggests a combination of serial and parallel processing.

The action pathway was mainly investigated by morphological effects such as filamentation and constrictions at division sites and combinations of different mutations in the *fts*-and zip genes [64, 88, 204, 84].

Begg and Donachie created double mutants of different combinations of mutations of *rodA* or *pbpA* and mutations of *ftsZ, FtsQ, FtsI* and *ftsA* [88]. Genes *rodA* or *pbpA* are responsible for growth in cylindrical shape, hence their mutation leads to a rather spherical growth resulting in cocci when in addition cell division is inhibited (see Fig. 5.1(a)). Neither the cocci mutant nor the filament mutants affect the ability of cell growth itself. Therefore, if the cocci phenotype is combined with the inhibition of cell septation, the individual daughter cells still grow isotropically but connected with each other like a pearl necklace. The combination of the mutation in cylindrical cell growth with certain mutations in cell septation made individual daughter cells visible in long filaments. So, constrictions were not only observed for *ftsA* but also for *ftsQ* and *ftsI* but not for *ftsZ*. This indicates that the mutation in *ftsZ* inhibits cell septation at a very early stage so that no sign of septation at all can be observed. In contrast to that, constrictions in long filaments can be observed for mutations in *ftsQ, FtsI* and *ftsA* of the double mutants, i.e.
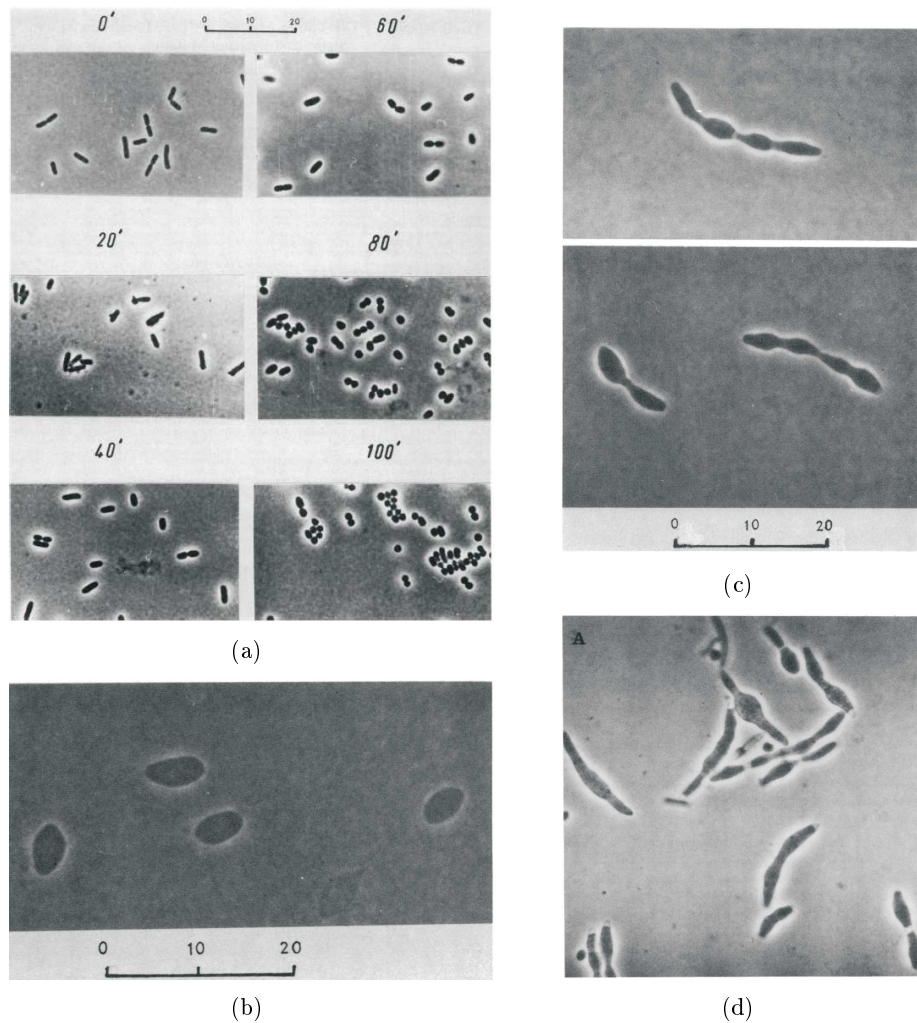
Figure 5.1: Mutations of different *fts*-genes and the resulting phenotypes. Growth morphology and the appearance of constrictions helped putting order into the septation pathway of the divisome. (a) Cocci formation due to mutation in *rodA* or *pbpA*: cells grow isotropically instead in length (images taken at different time intervals). (b) Unconstricted cells from double mutations in cylindrical growth and in *ftsZ*. (c) Constricted cells from double mutations in cylindrical growth and in *ftsA*. (d) Constricted cells from double mutations in cylindrical growth and in *ftsI*. Images are taken from reference [88].
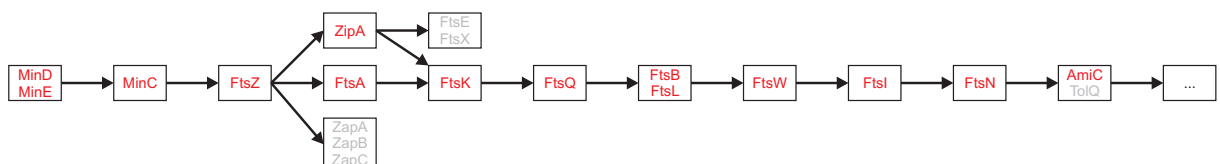
Figure 5.2: Presumable pathway of divisome protein action and assembly of the Z- and septal ring with all essential division proteins (in red) including Min-proteins and some non-essential proteins (in gray). According to Ref. [84, 29, 12, 8] and upon personal communication with Paola Bisichia.

Protein	FtsZ	FtsA	ZipA	ZapA*	FtsK	FtsQ	FtsB	FtsL	FtsW	FtsI	FtsN	AmiC
Nucleotide size in base pairs	1152	1263	987	330	3990	831	312	366	1245	1767	960	1254
Number of amino acids	383	420	328	109	1329	276	103	121	414	588	319	417
Protein Molecular weight in kD	40.324	45.33	36.475	12.594	146.66	31.434	11.622	13.627	45.987	63.877	35.793	45.634
Number of molecules per cell (Estimates)	5000–20 000	200	?	?	?	20 – 40	25	?	?	50-200	3000–6000	?
Function/ Action	Assembles to the Z-ring	Stabilizing and anchoring of the Z-ring to the inner membrane	Supporting Z-ring assembly	Z-ring assembly by cross-linking FtsZ oligomers and sta-bilizing longi-tudinal inter-actions of FtsZ monomers	Chromosome dimer resolution via XerCD; removal of DNA away from the septum	Formation of the FtsQBL-complex			Redirection of PG synthesis, from cylin-drical elonga-tion to septum forma-tion in the septum (as-sumed function)	Murein syn-thesis, cross-linking of PG wall for-mation (as-sumed function)	Coordi-nation of cell division and cell wall for-mation (as-sumed function)	Separation of repli-cated daughter cells through degrada-tion of murein cross links

Table 5.1: Essential and important non-essential (marked by an asterisk) members of the divisome in the order of their action in the septation pathway. Nucleotide size, number of amino acids and protein weight are taken from EcoCyc, the Encyclopedia of *Escherichia coli* K-12 Genes and Metabolism [200].

some steps of cell septation have apparently been accomplished and these genes act presumably after *ftsZ*.

Thus, FtsZ was found to be the very first protein that is recruited to the future division site, followed by the other members of the divisome [64, 88, 204, 205, 78].

Another method to identify the action pathway of the Fts proteins are colocalization studies. For example, Ma et al. could visualize colocalization of the FtsZ-ring with a FtsA-ring using GFP-tagged FtsZ and FtsA, indicating that the Z-ring recruits FtsA molecules [80]. Not all of these genes are as well conserved as *ftsZ* which suggests that evolution has adapted the divisome to an optimal configuration for each organism individually [30].

In the following I would like to give an overview over the genes and proteins essential for the septation process.

FtsZ is the most conserved bacterial protein [134]. It can be also found in plant chloroplasts and in the mitochondria of some lower eukaryot8es which underlines the importance of this protein for cell biology in general [206]. The protein has a molecular weight of 40 294 Daltons [73]. The amino acid sequence is given in Fig. 2.4(a) and protein secondary and tertiary structures are shown in Fig. 2.4(b) and 2.4(c) [72]. The secondary structure of FtsZ is similar to α- and β-tubulin and is considered as an ancestral homologue of tubulin [207, 208, 209]. FtsZ consists out of two domains, the GTP-binding domain and the carboxyl-terminal, separated by a central helix [30]. The GTPase covers the residues 23-227 and contains six parallel β-sheets (S1-S6), surrounded by five α-helices (H1-H4 and HL1) (Fig. 2.4(b) and 2.4(c)). Six sequence regions bind GTP: T1 to T4 and the sugar and base recognition sequence (Fig. 2.4(a)). The c-terminal covers the residues 228-356 and consists of four β-sheets (SC1-SC3 parallel, SC4 antiparallel to the others) which are accompanied by two α-helices (HC2 and HC3). Both domains, GTPase and carboxyl-terminal are connected via 23-residue long α-helix (H5). FtsZ molecules can be found in relatively large quantities in *E. coli*, however, numbers differ between 5 000 and 20 000 molecules per cell depending on the strain, cell culture conditions and measurement methods [210, 156, 211]. Accordingly, the average cellular concentration is in the range of 3-15 µM. The concentration of FtsZ is rate-limiting for cell-division [71, 70]. Apparently, there is sufficient FtsZ only for one Z-ring. However, this view is questioned within the community of researchers since multiple Z-rings can appear in *slmA*-mutants without increasing the total amount of FtsZ [212]. Mutation in *ftsZ* leads to filamentation without constrictions, suggesting that it acts early in the septation pathway [88]. In fact, blocking of FtsZ action leads to inactivation all other eight septation proteins, therefore it has to be considered that FtsZ is the very first protein that assembles and acts at the division site. FtsZ is also a target of SulA. When DNA is damaged, cell division is transiently inhibited [119, 121].

FtsA is the second most conserved division protein in bacteria and was identified in 1985 by Tormo to contribute to the formation of the septum [213]. Like FtsZ, FtsA is a cytoplasmic protein but 50 % of it is found in the plasmic membrane [214]. Next to FtsZ, it is the only essential division protein that resides within the cytoplasm. All other essential septation proteins are membrane proteins (ZapA, ZapB and ZapC can also be found in the cytoplasm but are not considered as essential division proteins [212]). FtsA is a member of the ATPase superfamily that also includes for example actin [215, 216]. FtsA is the second protein which is localized to the septum since blocking of FtsZ localization also leads to an inhibited localization of FtsA to the division site suggesting a direct interaction between FtsA and FtsZ [78, 80]. In contrast, mutation in *ftsA* leads to filamentation accompanied by a constriction, suggesting that it acts later with respect to FtsZ [64, 217, 218]. Since its inactivation leads also to the inactivation of all other *fts*-proteins and ZipA, this protein

seems to act directly after FtsZ and localizes early to the Z-ring [219, 80, 220]. FtsA binds to FtsZ directly via the C-terminal of FtsZ [220, 221, 222, 80, 223, 224]. FtsA is not required for the formation of the Z-ring itself but it is thought that FtsA, in collaboration with or alternatively to ZipA (see below), stabilizes the Z-ring by anchoring it to the inner membrane by its conserved amphiphatic helix [221, 220, 225, 226]. FtsA can be found in much smaller amounts than FtsZ, it is assumed that each cell contains about 200 copies of FtsA [227, 156]. The ratio of FtsA to FtsZ is essential for proper cell division [156, 228] though estimates of this ratio differ between 1:5 and 1:100 [156, 228, 93, 29, 219, 229]. Independent of the knowledge of the exact ratio, it is known that in wild type cells the entire FtsZ ressources are sufficient just for one division site (see also the description of FtsZ above). Thus, due to the limited number of FtsA molecules, FtsA can only bind to a subset of FtsZ-proteins within the Z-ring. Increase of the FtsA level leads to an inhibition of division [230]. This division can be overcome by a proportional increase of FtsZ [156, 228]. Excess of both, FtsZ and FtsA, leads to the formation of minicells. FtsA localizes to midcell position simultaneously with FtsZ. FtsA recruits FtsK and in consequence FtsQ, FtsI and FtsN (see below) [231, 225, 232].

ZipA: The acronym of the *Zip*-protein family stands for "Z-interacting protein". In contrast to FtsZ and FtsA, ZipA is an integral membrane protein with an N-terminal transmembrane and a cytosolic C-terminal globular domain separated by a flexible linker [233, 234]. ZipA requires FtsZ for its action and is recruited to the Z-ring via direct interaction with the C-terminal of FtsZ [233, 235, 236, 237, 223]. Similar to FtsA, ZipA takes an anchoring role of the Z-ring to the inner membrane by strengthening lateral associations between FtsZ protofilaments [238]. Z-rings can also assemble without FtsA if at least ZipA is present, therefore ZipA seems to be not dependent of FtsA but rather acts in parallel [239, 225]. However, no Z-ring can assemble if both, FtsA and ZipA, are missing [226, 225]. Both FtsA and ZipA, are required to recruit the next protein downstream in the septation pathway: FtsK [225]. Furthermore, ZipA is required for recruitment of FtsQ, FtsL and FtsN [240].

FtsK is a multi-spanning membrane protein as well and it excels by being the largest protein in *E. coli* with 13299 aa [29, 30]. It is recruited to the Z-ring, too. It requires FtsZ, ZipA and FtsA and itself recruits FtsQ, FtsI, FtsL and FtsN [241, 242, 243, 43, 231, 225, 232]. FtsK serves for different tasks, next to cell division, FtsK is also responsible for the coordination of fission and chromosome segregation [29, 30, 244]. The N-terminal of FtsK is involved in the division process and has 4 transmembrane sequences which are responsible for localization to Z-ring [241, 245, 242, 243]. In contrast, the C-terminal is required for successful DNA translocation and consists out of three domains: α, β and γ [242, 246, 247, 248, 249, 250]. Deletion of the C-terminal in FtsK leads to abnormal chromosome positioning and bisection by the closing septum. In the current model, FtsK prevents interference of the septum and chromosomes by active transport of DNA away from the septum. The $\alpha\beta$-domain contains a nucleotide binding motif which belongs to the AAA-family of ATPases and has an ATP-dependent DNA translocase activity [241, 248, 251]. The translocase can displace DNA with a step size of 2 bp per ATP [252].

FtsQ is another rare representative of the *fts*-family, only about 20–40 copies can be found on average in a single cell [253, 253, 156, 12]. The structure of FtsQ is similar to that of FtsL and FtsB (see below): all three are bitopic proteins consisting of a short N-terminal cytoplasmic region, a single transmembrane segment and a large periplasmic domain [254, 255, 256, 257, 258]. The periplasmic domain is responsible for recruitment to the division site [259, 260]. The cytoplasmic and transmembrane region specifies solely the position within the membrane [257]. FtsQ localization depends on FtsZ , FtsA , ZipA, and FtsK

[260, 261, 240]. FtsQ is required for action of FtsL and FtsB and all three proteins form a common complex, *FtsQLB*, even in the absence of FtsK. Since FtsK is required for the localization of FtsQ to the division site, the protein complex can form without being recruited to the division site [262, 258, 263]. In fact, *FtsQLB*-complexes form in the cytoplasm and are subsequently recruited to the division site [263]. Presumably, FtsQ takes a central role in this complex: several domains of FtsQ are considered to be responsible for interactions with FtsA , FtsI, FtsN and other proteins [264, 265].

FtsL: Similar to FtsQ, FtsL is present only in small amounts in the bacterial cell. Solely 25 copies on average can be found in a single cell [254, 255]. The transmembrane segment and the periplasmic domains are responsible for the localization to the division septum [266]. The cytoplasmic domain is responsible for the recruitment of further proteins of the division machinery. Localization of FtsL itself to the division site depends on FtsZ , FtsA , ZipA, FtsK and FtsQ [262, 261, 240]. FtsL is required for localization of FtsI to the division site [267].

FtsB is required for the recruitment of FtsI and FtsW to the Z ring and depends itself on FtsQ and FtsL with which it forms a protein complex [268]. The N-terminal of FtsB with the periplasmic domain interacts with FtsL, whereas the C-terminal domain is responsible for interaction with FtsQ [269].

FtsW is part of the so-called SEDS-family of polytopic membrane proteins which are involved in cell shape, elongation, division and sporulation [30]. FtsW is essential for the synthesis of the septum [270, 271]. FtsW localization depends on FtsZ, FtsA, FtsQ, and FtsL and is required by FtsI [272, 273, 274]. FtsW interacts directly with FtsN and forms a subcomplex with FtsI [275, 276]. 10 transmembrane segments are predicted for FtsW and the N- and C-terminal are considered to reside in the cytoplasm [277]. Presumably one of its tasks is the recruitment of FtsI to the division site and thus for the redirection of PG synthesis from the cylindrical cell wall to the formation of new cell poles by invaginating cell wall growth [30, 19] (see also Sec. 1.2.1). Furthermore, FtsW acts a flippase for Lipid II by transferring lipid-linked peptidoglycan precursors across the inner membrane [278] (Sec. 1.2.1).

FtsI is also known as *Pbp*3 (penicillin-binding protein 3) [279]. Penicillin-binding proteins belong to the family of acyl serine transferase proteins involved in the final step of murein synthesis [280]. About 50–200 FtsI-molecules can be found in each *E. coli* cell [281, 282, 283, 284]. However, the low degree of concentration is apparently not crucial, since overproduction of FtsI does not affect cell viability [285]. FtsI has a short N-terminal cytoplasmic domain, a single transmembrane helix and large periplasmic C-terminal domain with 537 residues that can be again divided into a non-catalytic and a catalytic subdomain [286, 287]. The noncatalytic part of the periplasmic domain is necessary for the recruitment of FtsN [288]. The catalytic subdomain contains the transpeptidase activity and is responsible for the cross-linking of the peptidoglycan strands of the evolving septum [289, 290, 256, 280]. The transmembrane helix is responsible for the localization of FtsI to the Z-ring [267, 288, 291]. The N-terminal anchors FtsI to the cytosolic plasma membrane. The localization of FtsI to the division site depends on FtsZ , FtsQ, FtsL and FtsW [283, 292, 261, 273]. It is recruited to the division site before the septum is formed, right after the *FtsQLB*-complex [267].

FtsN is a member of the Fts-family that is poorly conserved in the bacterial community [135]. About 3000 to 6000 copies can be found in a single cell [293, 293]. FtsN consists, just like the members of the FtsQLB-complex, out of a short N-terminal cytoplasmic domain, a

single transmembrane spanning segment and a large C-terminal periplasmic domain [294, 293, 257]. The periplasmic C-terminal is responsible and sufficient for the localization to the division site [295]. The cytoplasmic N-terminal and transmembrane domain are only necessary to transport the C-terminal domain to the periplasm, by which the protein binds to the murein layer [257, 296]. It is the last protein that is recruited to the septum depends on FtsZ , FtsA , ZipA, FtsI, and FtsQ [294, 240, 288]. Once located at the division site it assembles in a ring-like structure [294]. Its exact task is still unknown. Despite the late recruitment it can have long-range impact: On one hand, mutations in FtsN leads to cell defects early in the cell division process, on the other hand overexpression of FtsN can compensate mutations in *ftsA* and FtsK [29, 30]. Perhaps it has stabilizing effect on the divisome throughout division process [293, 245, 297]. It is assumed that FtsN spans the periplasm acting as a bridge between the divisome and the cell wall. Through this connection, FtsN could coordinate division and the murein-shaping processes [298]. FtsN is required for action of AmiC [299].

Much less is known about the following proteins which are also essential for cell division but do not belong to the *fts*-family, just like ZipA.

AmiC is localized to the septal ring during septation and is responsible for the degradation of the septum so that the two new daughter cells can separate [299, 300]. AmiC, an N-acetylmuramyl-L-alanine amidase, does so by removal of the murein cross links through cleavage of peptide moiety from N-acetylmuramic acid [301]. In consequence, cell cultures with mutations in *amiC* lack the ability to separate from each other after cell division and thus form chains of cells [301]. AmiC depends on FtsN [299].
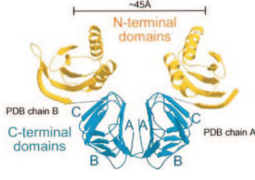
ZapA: The acronym "Zap" stands for "Z-ring associated protein" [302]. ZapA supports Z-ring formation by cross-linking FtsZ -polymers and stabilizing longitudinal interactions between FtsZ -molecules [303, 304]

Further genes that belong to the *fts*-family are *ftsE*, *ftsH*, *ftsJ*, *ftsY*, and *ftsX* but apparently these are less essential for cell division [305, 84].

5.1.2 Z-ring assembly

FtsZ-proteins form filaments, and these protofilaments again assemble in an overlapping manner to the Z-ring. [306]. For *B. subtilis* it was observed that the FtsZ-filaments actually form a spiral-like structure that spans throughout the cell and collapses to the ring structure [307, 308, 30, 309, 13]. In *E. coli*, spiral-like FtsZ structures could be observed in mutants leading to abnormal constrictions [310]. For wild type *E. coli* such helical structures of FtsZ were only documented once [80]. However, in a more recent publication, it was observed that FtsZ exhibits movements throughout the cell in a helical pattern prior Z-ring assembly [311]. Here, the spiral-like dynamic pattern of FtsZ also reorganizes finally into the Z-ring. This latter work also argues against the existence of nucleation site with bidirectional growth as suggested by previous works [310, 117] (see Sec. 2.3).

The assembly of FtsZ-proteins into a ring depends on GTP and there is a substantial delay of about 14-21 min between Z-ring assembly and recruitment of further proteins required for septum formation and constriction. The Z-ring assembly itself proceeds actually very fast, within in 1 min [84, 117, 294, 229] but exists for a relatively long time [12]. FtsZ is considered to be involved in the synthesis of peptidoglycan and thus the delay between Z-ring formation and cell division could be due to the required synthesis of new peptidoglycan for the invaginating cell wall [12, 312]. After the Z-ring has assembled and during its existence, it is not a static structure but

	MinC	MinD	MinE
Secondary and tertiary structure			
Nucleotide size in bp	696	813	267
Number of amino acids	231	270	88
Molecular weight in kDa	24.8	29.6	10.2

Table 5.2: Crystal structures and molecular properties of Min-proteins. Data and structures by Ref. [175, 324]. For MinD, the image is taken from the RCSB PDB (www.pdb.org) of PDB ID 3Q9L [325].

exhibits a high turnover of its FtsZ-subunits. FRAP-experiments (Fluorescence recovery after photobleaching) revealed a turnover halftime of 9 s [313, 314]. The fine structure of the Z-ring remains unclear [30]. For *Caulobacter crescentus* it is known that the Z-ring disassembles and FtsZ-proteins are degraded when the mother cell is fully constricted [150, 151, 152].

5.1.3 Z-ring action

The exact mechanism of action of the Z-ring is not clear up today. In principle, two different models are considered. In the first model, it is assumed that the Z-ring itself could provide the required force for constriction and invagination [315]. Two versions of this concept are assumed and in both the hydrolysis of GTP would play a major role. Either, GTP hydrolysis induces conformational changes of the FtsZ polymers which would execute a pinching force on the membrane [316, 306, 317, 318, 319]. When GTP is bound FtsZ-filaments are straight, whereas GDP-bound FtsZ-filaments are bended. However, structural studies of FtsZ argue against the concept of filament bending through GTP [320]. Alternatively, the depolymerization of the Z-ring, which involves GTP hydrolysis as well, could lead to a constriction of the ring and thus to a constriction of the attached cell wall. The second model suggests that the Z-ring rather serves as a scaffold for further proteins that assemble to the Z-ring to build the septum and execute the constriction force [30, 321, 311, 13]. Independently, which of these tasks are accomplished by the Z-ring, it is clear that the Z-ring is not sole structure required for septation [84].

5.1.4 Septum formation

Little is known about the formation of the septum itself. It is assumed that the septum is formed of an inward growth of the cell wall which requires switching of the peptidoglycan synthesis from lateral growth to septal growth [31]. In contrast to this widely accepted assumption is the observation that invagination also occurs even if the synthesis of new cell wall material is blocked which would argue rather for a reorganization of existing peptidoglycan [322, 323].

5.2 Min-proteins

The *min*-locus of *E. coli* codes for three proteins: MinC, MinD and MinE [176, 175].

5.2.1 MinC

MinC is the actual inhibitor for the capability of FtsZ to assemble to a ring [177, 178]. It is a 24.8 kDa protein consisting out of 231 amino acids [175]. Within the cell it is present as dimers [186]. It has two independent domains involved in interaction with MinD and FtsZ [186]. Interaction with MinD and FtsZ was proven by two-hybrid system [123, 186, 192]. The C-terminal is responsible for dimerization of MinC, binding to MinD, and it can also block lateral interactions of FtsZ-filaments [186, 326, 192, 30, 92]. However, actual inhibition of FtsZ-assembly is probably caused by the N-terminal by reducing the attraction between longitudinal bonds between individual FtsZ -molecules [186, 192]. Existing Z-rings can be disassembled by MinC [327]. However, GTPase activity of FtsZ is not affected by MinC [328].

In order to become active, MinC has to be bound to the membrane and membrane binding of MinC occurs via binding of MinC to MinD. Binding of MinC to MinD was proven by yeast two-hybrid assays yeast [123, 186, 192]. Without MinD MinC has only a low impact on FtsZ-assembly, in the presence of MinD inhibition of FtsZ-assembly is increased 25- to 50-fold [178]. Active MinC can even disassemble existing Z-rings [327]. Four amino acids of MinC, RGSQ, are responsible for the interaction with MinD [154, 329]. MinC and MinE occupy the same binding site on MinD, therefore MinC is displaced when MinD recruits MinE [330, 331, 196, 325].

The crystal structure of MinC was solved by Cordell et al. and is shown in Tab. 5.2 [332].

5.2.2 MinD

MinD has two tasks: first it activates FtsZ-inhibition of MinC by serving as a membrane-bound carrier for MinC. Secondly, trough interaction with MinE it provides the topographic specificity necessary for successful assembly of the Z-ring at a midcell position. Direct interaction of MinC and MinD was first proven by Huang et al .

MinD is slightly larger than MinC with a molecular weight of 29.6 kDa and 270 amino acids [175]. The structure MinD-dimers was solved in 2011 [325]. MinD is an ATPase belonging to the family of ParA-proteins which is characterized by a Walker motif for binding of ATP [182, 333, 334]. Estimates for the number of MinD-molecules range from 2000 to 3000 [195, 182].

Early immune-electron microscopy studies revealed that MinD binds peripherally with the inner membrane [182]. MinD binds to the inner membrane by the so-called membrane-targeting sequence (MTS) which is formed by the amphiphatic, helical c-terminal and exposed upon binding of ATP [331, 335]. MinD does not bind if ADP instead of ATP is present [196]. Probably after binding to the membrane MinD dimerizes [336, 197]. FRET experiments showed an increased energy transfer signal of fluorescently labeled MinD in the presence of lipid vesicles supporting the idea of membrane-dependent dimerization [337, 196, 338]. However, this view was challenged by experiments showing that MinD can apparently also dimerize in the absence of lipids [331]. Dimerization definitely depends on ATP [198]. Presumably, the dependence of the membrane binding capability of MinD on ATP is due to the requirement of ATP for dimerization.

Binding of MinD to the membrane follows a cooperative pattern, i.e. that MinD preferentially binds to membrane regions which already contain MinD [197, 337]. One possible explanation for cooperative membrane attachment could be the membrane-dependent dimerization.

MinD binds MinC via direct interaction which was proven by yeast two-hybrid assay [123, 186, 192]. Through binding MinD recruits MinC to the membrane [114, 185]. Membrane-binding of MinD and recruitment of MinC or MinE only requires binding of ATP but not hydrolysis as it was shown in *in vitro* studies using liposomes and ATPγS instead of ATP. In the presence the non-hydrolyzable form of ATP MinD could bind to the lipid vesicles and consecutively bind MinC and MinE whereas MinE replaced MinC from MinD [196, 198].

Pure MinD - that is MinD that is not bound to the membrane nor has recruited MinE - has

a low ATPase activity. It was shown that the ATPase activity of MinD can be increased by a factor ten in the presence of MinE and liposomes which suggest that both interactions of MinD are necessary: binding to the membrane and recruitment of MinE [182, 197].

5.2.3 MinE

The task of MinE is to prevent the inhibiting influence of MinC on Z-ring assembly at a midcell position and to limit its activity to the cell poles. MinE binds to — and only to — membrane bound MinD, displaces MinC from MinD, stimulates the ATPase activity of MinD and induces detachment of MinD from the membrane. MinE-dimers form a ring-like structure which assembles close to a midcell position processes MinD-detachment towards the cell poles [180, 123, 179, 193, 194]. Through this mechanism the central region of *E. coli* remains mainly free from MinD and therefore from MinC. In consequence, FtsZ can assemble at the membrane to the Z-ring.

MinE is the smallest protein from the Min-family with only 10.2 kDa and 88 amino acids [175]. It consists out of two domains. NMR-studies suggest that the protein is composed as a sandwich structure with 3 α-helices at the N-terminal (aa 1 - 33) and 2 β-sheets at the C-terminal (aa 33-38). Furthermore MinE, similar to MinC and MinD, forms dimers (see Tab. 5.2) [324, 339]. However, MinE is thought to exist as monomers and dimers in the cytoplasm, though only the dimer is capable of binding to MinD, displacing MinC from MinD and detaching MinD from the membrane [181, 340, 324, 339]. Estimates for the number of MinE-monomers per cell differ largely, ranging from 200 to 1400 [180, 195].

Mutations in the N-terminal domain affect the ability of MinE to bind to MinD and its ATPase activity [197, 198]. Therefore the N-terminal is considered to be responsible for MinD-binding and ATPase activation and is thus called "Anti-MinCD" [179, 180, 123, 341, 181, 330]. The C-terminal forms the so-called Topological Specificity Domain (TSD) [187, 324]. Originally it was thought that the MinE-ring is formed by direct interaction of the TSD with a specific binding site on the membrane at midcell position but this hypothesis could not be verified [179]. In fact, the TSD does facilitate the formation of the MinE-ring but rather by regulation of the activity of the Anti-MinCD-domain, furthermore it supports dimerization of MinE-proteins [342, 343]. Mutations of MinE without the TSD fail to dimerize and thus no MinE-ring is formed [324, 181, 195, 340, 180]. However, for certain mutations in *minE* leading to the loss of the MinE-ring, MinD still exhibits oscillations, however, with a longer oscillation period [183, 195]. Contrary to earlier observations the MinE-ring is not static but does also show an oscillatory behavior [114, 185, 193, 194, 195]. Apparently, the oscillating MinE-ring assembles into a helical structure [344]. Upon binding to MinD MinE can displace MinC from the membrane since MinE and MinC share the same binding site on MinD [331, 196, 325]. Since MinD ATPase only becomes active after binding of MinE, this replacement process of MinC is independent of ATP.

Each cell contains about 200 copies of the MinE-protein. The number of MinE proteins is crucial, especially in respect to the number of MinC and MinD proteins. If the concentration of MinE is raised, MinD fails to bind and thus the inhibitory effect of MinC is blocked. In consequence, the Z-ring can assemble at all potential division sites (in wild type *E. coli* at the cell center and at the two cell poles) and therefore lead to the minicelling phenomenon [84].

MinE was assumed to have a cooperative-like membrane-binding behavior, however the nature of this cooperativity was unclear [272, 345]. Cooperativity could be either due to dimerization of MinE-monomers on the membrane itself, or be the consequence of the potential capability of existing MinE-dimers to form protein superstructures or the necessity of two MinE-dimers to activate both monomers in a MinE-dimer complex [272, 196, 337, 338, 346]. Loose finally discovered that binding of MinE-dimers to the membrane is not cooperative but depends only on the number of free MinD-binding sites. Binding of MinD-dimers to the membrane itself

Cell membrane ▭▭ MinD-ATP dimer ▢ MinD-ADP monomer ▲▲ MinC dimer ● MinE dimer ⟳ Z-Ring
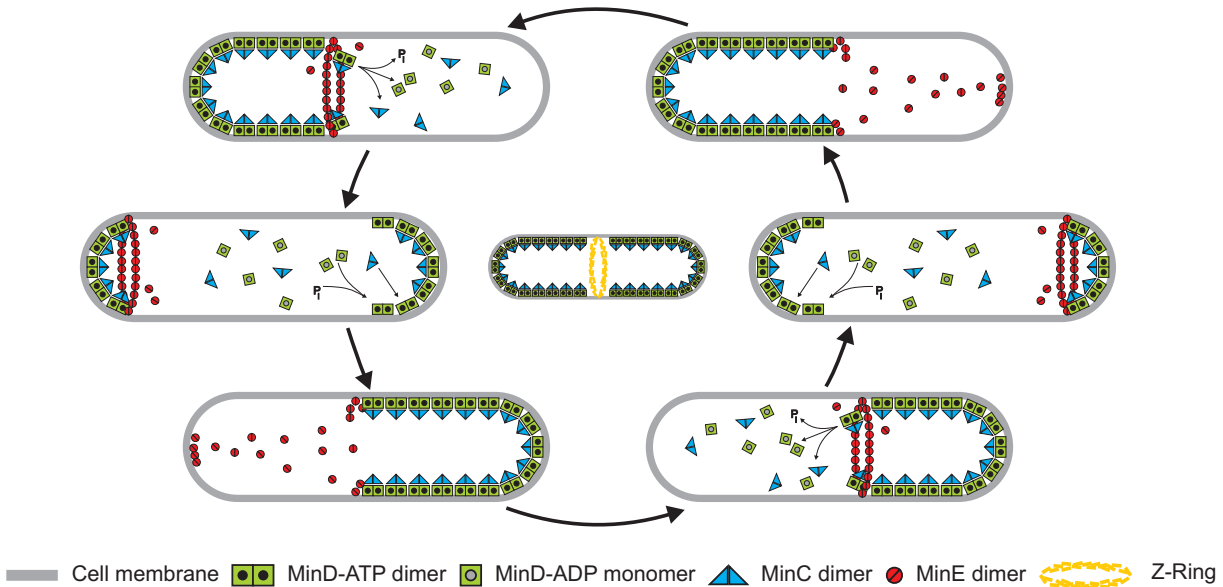
Figure 5.3: Sketch of the Min-oscillations.

however is of cooperative nature [346].

The dynamics of MinE-dimerization itself is still ambigous. One model assumes that only MinE-monomers are active in Min-oscillations whereas MinE-dimers are only found in the MinE-ring and become inactive [338, 196]. Another model considers that MinE is already present as a homo-dimer in the cytoplasm. This hypothesis is supported by the recent *in vitro* studies of Martin Loose with Min-protein waves on supported lipid bilayers [346]. The FRET signal of Cy3- and Cy5-labeled MinE proteins did not change upon binding to the trailing MinE-edge of the Min-protein wave. MinE-monomers could be observed but the monomer/dimer-ratio did not change upon binding of MinE to MinD. These results suggest that MinE-homo-dimers are already present in bulk or in the cytoplasm and bind as dimers to MinD indicating that only MinE dimers are active. In consequence, the accumulation of MinE at the trailing edge of Min-protein waves *in vitro* or to the MinE-ring in vivo cannot be due to dimerization of MinE but must be of other origin. Probably MinE-monomers represent a cold reserve. Interestingly, the formation and localization of the MinE-ring is not affected by DNA [347].

5.2.4 Min-oscillation and regulation of the Z-ring placement

The current knowledge about the essential steps of Min-dynamics is summarized in Fig. 5.3. Upon binding of ATP, MinD-monomers dimerize and thus bind to the membrane, membrane-bound MinD recruits MinC-dimers and consecutively MinE-dimers. MinE displaces MinC and activates MinD ATPase activity. Upon hydrolysis of ATP, the *MinDE*-complex detaches from the membrane and splits up. The MinD-dimers split further into monomers. Within the cell this mechanism gives rise to an oscillatory behavior. MinD covers almost an entire cell membrane half by starting at the cell pole and processing towards the cell center. Hereby, the MinC binding pattern follows MinD. When the MinCD-carpet reaches the central region of the cell, further coverage is stopped by MinE binding to MinD, displacing MinC and detaching MinD and itself. Furthermore, MinE processes displacement of MinC from MinD and detachment of MinD from the membrane from the central region versus the cell pole. While MinE is still busy sweeping membrane-bound MinCD, already detached MinD and MinC start rebinding to the membrane. This is most successful at regions which are basically free of MinE and therefore MinD and thus MinC start binding to the membrane at the opposite cell pole [197, 345, 348]. Synthesis

of Min-proteins is not required for oscillations [188]. The entire cycle takes about $20 - 60\,$s [114, 185, 188]. Frequency is influenced by concentrations of Min-proteins. An increase of the MinD-concentration reduces the frequency which can be again compensated by overexpression of MinE suggesting that is rather the MinE/MinD-ratio that rules the oscillation period than the absolute concentration of Min-proteins. In wild-type cells the ratio of MinE to MinD is about 0.2. If this ratio decreased to a ratio of 0.1, then the oscillation period is increased by a factor of 6 [188]. Mutations in the α-face of the TSD of MinE decreases the frequency, too, and leads to an irregular oscillation pattern without any pronounced MinE-ring feature [195].

Evidence for topographical regulation of Z-ring placement was brought by overexpression experiments. Overexpression of MinC and MinD blocks cell division whereas this effect could overcome again by overexpression of the *ftsZ*-gene which suggested an inhibitory effect of MinC and MinD on the Z-ring assembly [175, 177, 178]. However, regulatory influence of the Min-system on the Z-ring was proven only in 1999 by Yu et al. [90].

The Z-ring is affected by MinC through inhibition of FtsZ polymerization or depolymerization of the Z-ring [328, 192].

If there is already the Min-system for the proper placement of the Z-ring at midcell position, why is there still the nucleoid occlusion system? If both division site selection mechanisms, the Min- and the NO-system are suppressed, division occurs not only at a midcell or polar position but at random locations [90]. In *E. coli* mutants lacking the NO-system, cells still are able to place the Z-ring at a central region, however, with a lower precision [117, 90]. This of course does not clarify, why nature did not evolve a single mechanism which would be sufficient to regulate division site selection.

5.2.5 Molecular mechanism of the Min-protein wave *in vitro*

The detailed actions of Min-proteins in the Min-oscillation remained obscure for a long time until the system was transferred from the in vivo to the *in vitro* world. The first successful reconstitution of the Min-system into an artificial environment and its observation of Min-dynamics was achieved using supported lipid bilayers obtained from polar lipid extract from *E. coli* [1]. Upon addition of MinD, MinE and ATP to the SLB parallel and propagating waves of MinD and MinE binding patterns evolved. The wave-like protein binding pattern is supposed to be the equivalent of Min-oscillations in vivo. An unexpected but welcomed feature of these waves in the artificial environment is that the wavelength is about 10-fold larger than in the cell [188, 1, 349]. This upscaling of protein dynamics made it possible to study structural and dynamical properties of the waves with high precision using fluorescence microscopy. Even single-molecule studies of individual Min-proteins could be executed [10]. Especially wave profiles, sequence of protein binding, duration of membrane binding, protein ratios and so on could be investigated.

From fluorescence intensities and with the help of calibration standards, it was possible to estimate the surface density of Min-proteins on the membrane (see Fig. 5.4 d). At its peak, the MinD-concentration was twice as high as the MinE-concentration at the respective peak [10]. Note that the peaks of the MinD and MinE concentrations are shifted by about ?$\,\mu$m. However, from the concentration profiles of MinD and MinE it was possible to calculate the ratio between MinE and MinD (see Fig. 5.4d, black curve in the inset). As one can see, the MinE/MinD-ratio increases slowly until the very rear of the wave to an almost equimolar ratio of 0.9, i.e. almost every MinD dimer carries a MinE dimer. After the peak the MinE/MinD ratio decreases rapidly again.

Similarly, maximal binding of MinC predates the maximum surface concentration of MinE by about 2.5$\,\mu$m (Fig. 5.4 g) [346]. MinE replaces MinC from MinD. Yet, due to the low surface concentration of MinE at the front of the wave, binding of MinC to MinD is not affected. However, towards the rear of the wave, more and more MinC proteins are displaced from MinD
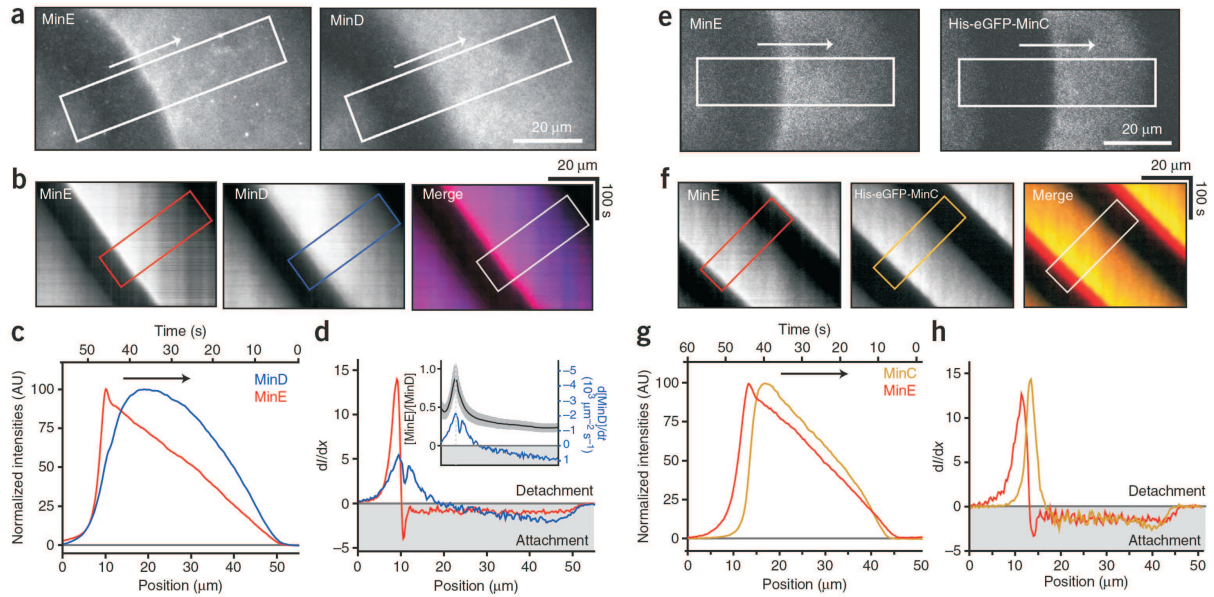
Figure 5.4: Surface density of Min-protein waves. (a) Snapshot of a timelapse TIRF micrograph of Min-Wave. Left: fluorescence signal of dyes tagged to MinE. Right: fluorescence signal of dyes tagged to MinD. Rectangles show the area which is used for the calculation of kymographs. (b) Kymographs of respective timelapses with MinE (left), MinD (center) and the merged channels (right). (c) Surface density profiles of MinD and MinE obtained from kymographs. Note the sudden increase at the rear (position $x = 10\,\mu$m) of the MinE profile. (d) Differentiation of the density after position $\frac{dI}{dx}$ yields the binding kinetics of proteins. Values below zero represent binding to the membrane whereas positive values describe unbinding. Note that the apex of MinD binding is located at the magic position $x = 10\,\mu$m whereas MinE shows a sharp switch from binding to unbinding. Inset: MinD/MinE ratio (black curve) and for comparison binding kinetics (blue curve). (e) Snapshot of a timelapse micrographs of MinE (left) and MinC (right) wave. (f) Kymographs of respective timelapses with MinE (left), MinD (center) and the merged channels (right). (g) Surface density profiles of MinD and MinE obtained from kymographs. (h) Differentiation of the density after position $\frac{dI}{dx}$ yields the binding kinetics of proteins. Images and graphs are taken from Ref. [10].
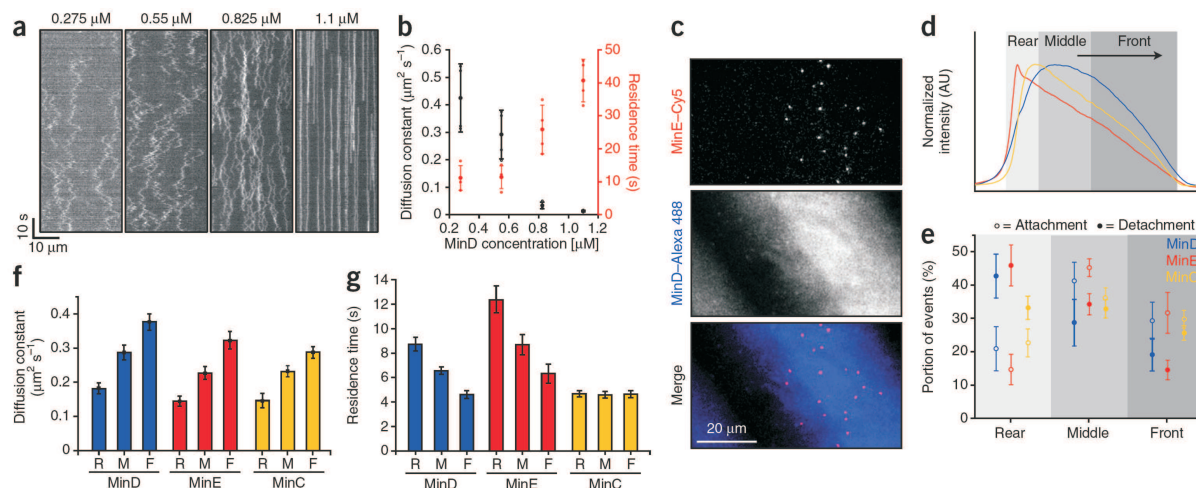
Figure 5.5: Lateral diffusion of single Min-proteins in the artificial membrane observed by TIRF microscopy. (a) Kymographs of membrane-bound and diffusing single MinD proteins for different protein concentrations in bulk. With increasing concentration, MinD proteins diffuse less which can be recognized by the more straight diffusion pathway. (b) Diffusion coefficient (black data) and residence time (red data) of MinD proteins in dependence of bulk MinD concentration. (c) Snapshots of a timelapse Min wave. Top: single, diffusing MinE-proteins, single-molecule imaging made possible by a low labeling degree. Center: corresponding MinD wave (ensemble level). Bottom: merged images. (d) Surface density profiles of MinC, MinD and MinE derived from kymographs obtained from ensemble fluorescence micrographs (see also Fig. 4.4). For further analysis the wave is divided into three sections: front, middle and rear. (e) Membrane attachment and detachment frequency of the different Min-proteins for the three different wave sections. Initially attachment events dominate whereas in the rear of the wave detachment events outnumber attachment events. (f) Diffusion coefficients of all three Min-proteins in the different wave sections front (F), middle (M) and rear (R). Note that the lateral diffusion of membrane-bound proteins decreases towards the rear of the wave. (g) Residence time of all three Min-proteins in the different wave sections. Accordingly to the increasing diffusion time, residence time of MinD increases. Since lateral diffusion also slows down for MinC one would expect an increase of the residence time of MinC. However, the time a single MinC protein is bound to the membrane does not change through the course of the wave since it is displayed by MinE. In contrast, residence time of MinE increases more than that of MinD. Additionally the absolute average residence time of a single MinE is longer than that of MinD. This an explained by persistent binding of MinC, i.e. MinE bound to MinD immediately binds to a neighboring MinD protein after its previous carrier has detached from the membrane. Image is taken from Ref. [10].

before MinD itself is displaced by MinE.

So apparently, at the front of the wave only few MinD proteins are occupied by MinE proteins whereas at the rear of the wave almost every MinD protein is occupied by MinE. But this is only the big picture averaged from an ensemble of molecules. So far it is not clear whether MinD proteins stay on the membrane until the very rear of the wave or whether they are exchanged by MinD from bulk during wave propagation. Same is true for MinE. This issue was addressed by single-molecule experiments combined with total internal reflection fluorescence microscopy (TIRF-M) [350, 351]. In TIRF the excitation light is directed onto the cover slide carrying the specimen under the angle of total reflection. At the interface from the medium with higher (glass) to lower optical density (air or water or biological matter), the excitation light is reflected away from the sample except for a thin evanescent field of few hundred nanometers that penetrates into the space above the optical interface. This thin "light sheet" excites the sample only in a small layer which allows excitation of thin section just above the cover slide and therefore suppress any background fluorescence.

By a low portion of labeled MinD and MinE proteins in combination with TIRF microscopy, it was possible to observe and track the movements of individual Min-proteins on the supported lipid bilayer (see Fig. 5.5 c). It was observed that proteins did not stay on the membrane after binding throughout the entire course of one wave but detached before the wave peak has passed. Furthermore, proteins were not immobile but showed lateral diffusion. For better analysis the wave was divided into three zones: front, middle and rear (Fig. 5.5 d). By this it could be evaluated diffusion of all three proteins, MinC, MinD and MinE slowed down towards the rear of the wave whereas the residence time increased except for MinC (Fig. 5.5 f and g). Interestingly, the residence time of MinE was considerably higher than that of MinD throughout all three wave zones.

This persistent binding of MinE was interpreted such that an individual MinE protein can occupy several MinD proteins consecutively which could be carried out by two mechanisms: transient binding [352, 353] or fast rebinding of MinE without diffusing into the bulk [199, 354].

Loose suggested fast rebinding in order to explain the accumulation of MinE at the rear of the wave: After binding of MinE, MinD detaches but cannot rebind either due to the lack of free space on the membrane or because it will be detached immediately by MinE again. Thus, MinD diffuses into the bulk. MinE, however, after the joint detachment from the membrane with its supporting MinD, rebinds quickly to neighboring MinD without MinE (see Fig. 5.6) [346]. Hu and Lutkenhaus already had investigated the stoichiometry of MinD and MinE interaction in an *in vitro* assay [197]. They measured the ATPase activity of MinD in the presence of liposomes for varying MinE concentrations between 0 and $15\,\mu M$, the MinD concentration was kept constant at $15\,\mu M$. Both concentrations refer to the bulk. As expected, the ATPase activity increased linearly with increasing MinE concentration - but only up to a MinE/MinD-ratio of about 0.33 (Fig. 4.6(a) C). Unfortunately, only one higher concentration was measured at an equimolar ratio for MinE/MinD, the respective ATPase activity is at the same level like for an protein ratio of 0.33. Only on a first sight, this seems to contradict our understanding of the MinD-MinE interaction. Since every MinD-dimer is capable of recruiting one MinE-dimer one would expect that an activity plateau is only reached for an equimolar concentration and not already at much lower protein ratios. Probably fast rebinding could also be an explanation for this observation. After detachment MinD diffuses away from the vesicles into the bulk, whereas MinE remains in the vicinity of the liposomes. Therefore, an equimolar ratio can be reached in the microenvironment, even if the bulk concentration of MinE is much lower than that of MinD.
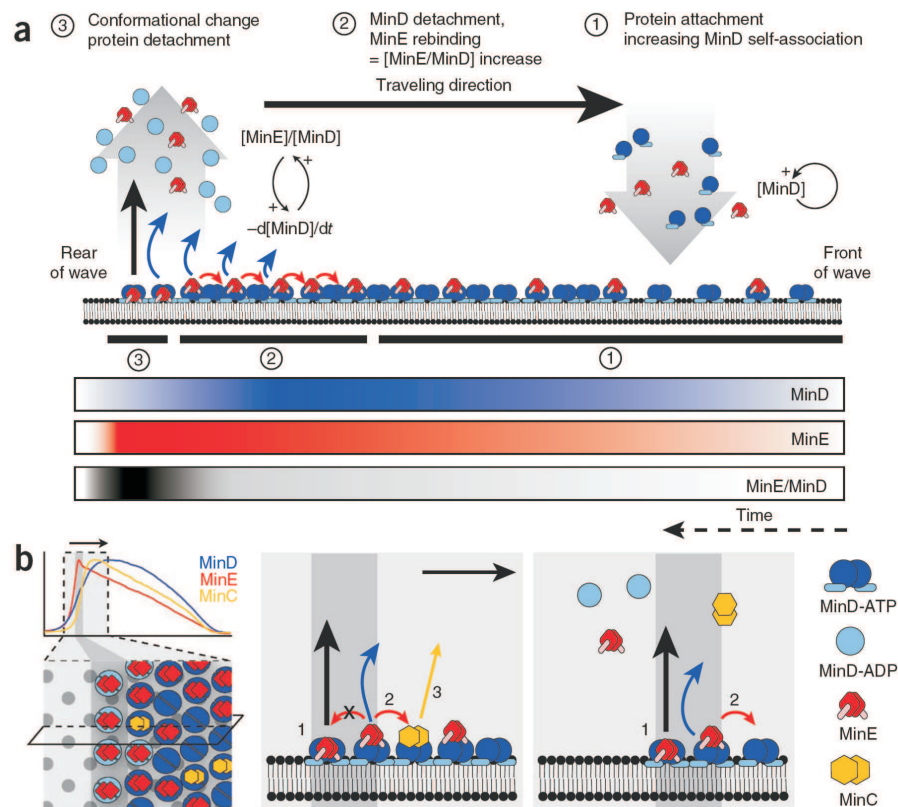
Figure 5.6: Principle of the model of transient binding for Min-protein wave propagation according to Loose [10]. (a) At the front of the wave, binding of MinD-dimers (dark blue) dominates (1). At the central region of the wave, more and more MinE-dimers (red) bind to membrane-bound MinD, inducing hydrolysis of ATP, and thus detachment of MinD from the membrane (2). Consequently, the MinE/MinD-ratio increases. In contrast to detaching MinD, MinE does not diffuse into the bulk but reattaches immediately to another membrane-bound MinD, thus increasing the MinE/MinD-ratio further. When MinE does not find any free membrane-bound MinD, it leaves the membrane as well which leads to a rapid decrease of the MinE surface density (3). Once unbound, MinE presumably keeps its dimer-conformation whereas MinD splits up into monomers (light blue) after ATP hydrolysis and membrane unbinding. (b) Left: Surface density profiles of Min-proteins (top) and detailed top view of the trailing edge (bottom sketch). Center and right: side view of the persistent binding model. Image is taken from Ref. [10].

6 Mathematical models

Mathematical description and investigation through numerical models has gained large application in biology and its contributions to gain further knowledge about biological processes are undoubted [355]. Approaching scientific problems through the use of numerical simulations requires that the number of different components and actors is limited whereas the total number of particles does not impose greater limitations. The latter issue only concerns the pure computing power and this challenge can be met by sufficient CPU and memory power. However, the number of different components determines the complexity of equations that have to established by the researcher. Therefore, it will be easier to model a system with a high number of particles but which, in fact, represents only few different acting components in comparison with a system with a low number of particles but of which each represents a proper agent with individual characteristics and dynamics.

In these terms, the Min-system excels not only for *in vitro* concepts but also for an *in silico* approach. The task of the Min-system is inhibition of cell division at the extremal potential division sites, i.e at the cell poles. This is achieved through inhibition of the Z-ring assembly by MinC. However, the principal mechanism that governs localization of cell division is executed by oscillation of the Min-proteins. These oscillations in turn, only require MinD, MinE, a phospholipid membrane and ATP. This limitation to four components makes the Min-system especially suitable for *in vitro* approaches - and for mathematical modeling [355]. Min-protein oscillations were observed for the first time in 1999 [114, 188]. The discovery of this fascinating dynamic behavior was accompanied by the finding that the self-organization only require these few factors [1]. Therefore, it is no wonder that both approaches, *in vitro* and *in silico* were motivated shortly after and at the same time. The first *in vitro* approach based on the Min-system was published in 2001 by Hu and Lutkenhaus who mixed Min-proteins, ATP and liposomes (see Sec. 4.9) [197]. In the same year, the first two attempts to describe the action of the Min-system in mathematical terms were published by Howard et al. and by Meinhardt and de Boer [356, 272]. These works motivated further studies following different concepts and using different modeling tools.

In the following, a short overview will be given of the most important models. An excellent overview of the established mathematical models on the Min-system can be found in the PhD-thesis of Elisabeth Fischer-Friedrich [357]. Parallel to this PhD-work, a new mathematical model was developed by our collaborators Mike Bonny and Karsten Kruse in order to describe the experimental findings discusses in the present study [358]. Here, only the most essential models which had led to our current mathematical model will be described. These models are listed in

Table 6.1: Overview of the different mathematical descriptions of the Min-system grouped by the categories for the aggregation current model (AC) and cooperative attachment model (CA). Within the two categories, the studies are sorted according to their publication date and by the boundary condition *membrane geometry*. The table summarizes references, boundary conditions, differential equations and parameters. The color coding of the differential equations corresponds to the color coding presented in Eq. 6.5. Within a row a legend is always valid to the left until a new legend appears. In the digital version of this PhD-thesis, the table appears at the end of the PDF-file.

Tab. 6.1 and 6.2.

6.1 Boundary conditions

All models have a common basis made of assumptions that were derived from experimental findings. This common basis includes the main components such as MinD, MinE and the membrane (the role of ATP is considered in some of the models), basic coarse mechanism and interactions of Min-proteins:

- MinD binds to the membrane

- MinD forms aggregates on the membrane (depending on the model either after or upon binding)

- MinE binds to the membrane via MinD (depending on the model, either already in the cytoplasm or directly on the membrane)

- MinE initiates the detachment of MinD from the membrane

Next to this common basis, the various models also consider further experimental findings. Additionally, most models also require considerations which were not proven experimentally at the time of publication but which were of speculative nature. Later on, some of the considerations could be confirmed by experimental studies whereas others were shown to be wrong. The following assumptions made by different models can be taken as valid:

- Transport of Min-proteins in the intracellular volume is purely diffusive

- The bacterial intracellular volume is approximated as a homogeneous solution

- The bacterial membrane is of - in relevance for the Min-system - a homogeneous and isotropic composition. Structural inhomogeneities such as domains might exist but do not affect the Min-system

- Diffusion in the cytoplasm is much faster than on the membrane

- MinC dynamics correspond to MinD dynamics, thus they are not explicitly treated

- Oscillations are fast in respect to cell growth. Thus cell length will be considered as constant during the course of oscillations

ATP and/or ADP do not appear as proper factors in any of the models. In most models, the role of ATP/ADP is completely ignored whereas in one other model the nucleotides serves - like the membrane - for further differentiation of variables (MinD with and without ATP or ADP, see below). Most models also consider conservation of the number of Min-proteins and deny that protein synthesis and degradation has any influence on the phenomenon of Min-protein dynamics. This view is justified by experimental studies of Raskin and de Boer who could observe that Min-oscillations occurred in cells even when the synthesis of Min-proteins was blocked [188].

Table 6.2: Overview of the results for the different mathematical descriptions of the Min-system. Again, studies are sorted by the model type (AC/CA), publication date and membrane geometry. For explanation of the respective figures and graphs, please see the text. In the digital version of this PhD-thesis, the table appears at the end of the PDF-file.

However, the model of Meinhardt and de Boer bases on process of constant and catalytic protein synthesis and degradation in the cytosol and on the membrane [272].

Furthermore, all models use a common methodology by assigning only the Min-proteins as factors whereas the membrane is not considered as a proper agent. However, the membrane interaction with the Min-proteins serves for further subdivision of the Min-factors depending on the membrane-binding state. Consequently, the minimal set of components that are used in all models presented here includes four different variables:

- cytoplasmic MinD

- cytoplasmic MinE

- membrane-bound MinD

- membrane-bound MinE (or MinDE-complexes)

6.2 Benchmarks

For comparison of the results of the mathematical descriptions with biological reality, certain benchmarks have to be established. Most studies on Min-protein models compared the outcome of numerical simulations with *in vivo*-phenomenology. The most obvious phenomenon of Min-protein dynamics is of course the emergence of oscillations as observed *in vivo* (see Sec. 4.8 and Ref. [188, 185, 183]). Furthermore, oscillations of MinD and MinE are not exactly in phase. Distributions of MinD and MinE-proteins are not superposed but a polar MinD-cap is "pushed" by or "pulls" a distribution maximum of MinE. The MinE-maximum is much sharper than that of MinD and is referred to as the MinE-ring which emerges at a midcell position and propagates towards the cell poles (see Sec. 4.7 and Ref. [179, 193, 194, 195]). It was assumed that the oscillation of MinD — averaged over time — produces a minimum at a midcell position (Sec. 4.8, [194, 196, 92]). MinC inhibits the assembly of FtsZ-proteins to the Z-ring which initiates cell-division. Since the MinC-distribution is coupled more or less to the distribution of MinD, a MinD-minimum at a midcell position would be another benchmark for modeling of cellular Min-protein dynamics [114]. Both, variation of the MinE/MinD ratio and the cell length affect the oscillation period [188, 193]. Oscillation period increases with cell length [193]. If inhibited in division, cells grow two filaments and exhibit several oscillations within one cell. In short cells, oscillations do not have a constant period but the temporal behavior follows a stochastic pattern [359]. For a certain mutation of MinE, cells fail to produce a pronounced MinE-ring, however still support oscillations but with a very long oscillation period of up to 10 min [183, 195].

The different publications did not regard all of these issues. Depending on the model, some of these aspects were emphasized or neglected. Bringin all of the questions from all of the presented models together, the following list, which covers the most important benchmarks for comparing mathematical descriptions with biological reality, is made:

- Does the model produce oscillations?

- Are oscillations topological comparable to *in vivo* oscillations?

- Is the oscillation period consistent with that *in vivo*?

- Are oscillations of MinD and MinE shifted in phase?

- Does the time-averaged profile of the MinD-concentration along the cell elongation exhibit a minimum at midcell position?
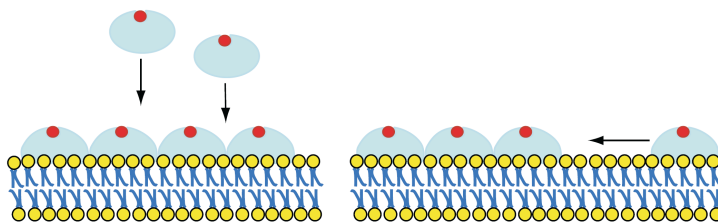
Figure 6.1: Mechanism of the cooperative attachment (CA, left) and of the aggregation current model (AC, left) model. In the CA model proteins attach preferentially to membrane binding sites in the vicinity of already bound proteins. In the aggregation current model, the binding process is not independent of the proximity to other bound proteins. However, once bound to the membrane, proteins tend to aggregate. Image by courtesy of Elisabeth Fischer-Friedrich [357].

- Can a MinE-ring be produced?

- How does the oscillation period depend on MinD and MinE-concentrations?

- How does the oscillation period depend on cell length ?

- Are multiple oscillations produced for filaments?

- Are MinD-oscillations supported also in the absence of a MinE-ring?

The topology of Min-protein oscillations is especially crucial. All models presented here generate stable oscillations of Min-proteins for a certain choice of parameters and initial conditions. In the biological cell, MinD populates the cell poles by growing from the poles to the midcell and then shrinking back to the poles due to detachment by MinE. As it will be shown below, many models fail to reproduce this specific pattern of MinD-caps and growth dynamics. One model produces a ring of MinD-proteins which propagates from midcell to the cell poles. Other models are able to generate polar caps of enhanced MinD-population which even shrink towards the cell poles, however, these polar caps do not grow slowly but appear all of a sudden (Sec. 6.6 and 6.7).

Different membrane geometries were also addressed. Whereas the first models were developed and applied to simulate Min-oscillations in a cell-like geometry, i.e. a rod-like or cylindrical compartment with a closed volume, later models also addressed Min-protein wave propagation in open and flat systems like on supported lipid bilayers (SLB) (see Tab. 6.1). In case of a cell-like geometry, most models consider a protein distribution that is rotationally invariant in respect to the long axis. Thus, the three-dimensional space was reduced to one dimension by projection of the cylinder representing the rod-shape of the cell to the axis of elongation.

6.3 Model classification and methodology

Though all models are based on common assumptions derived from experimental studies, the models differ also in their more detailed considerations of molecular interactions. These considerations address the mechanism of MinD-aggregation on the membrane. *In vivo* and *in vitro* studies, it was observed that MinD aggregates on the membrane [360, 344]. The nature of attraction is not clear yet, however, it could, for example, be due to electrostatic forces [191]. Furthermore, the exact steps and sequence of steps of the aggregation process remain unclear and therefore left room for speculation. Consequently, models can be classified into two different groups according to the assumptions made:

In the **aggregation current** model (AC), aggregation on the membrane is assumed to be a two-step process. MinD is supposed to bind first to the membrane, then diffuses on the membrane, meets other membrane-bound MinD-proteins, and these form — through strong intermolecular interactions — MinD-aggregates [360]. Attractive forces specific for membrane-bound MinD proteins where shown in yeast two-hybrid assays [361]

In the **cooperative attachment** models (CA), MinD-molecules preferentially bind directly to membrane-sites in close proximity to other membrane-bound MinD-molecules. Thus, this can be seen as a single-step process. This hypothesis was motivated by *in vitro* experiments [196].

This differentiation might seem somehow irrelevant, or at least one could think that there must be more fundamental differences between the existing models. However, the process of aggregation of MinD-proteins on the membrane is of great significance since it is thought that it is this aggregation process that breaks the homogeneous state of isotropically distributed Min-proteins and leads to the formation of dynamic instabilities.

The different mathematical approaches can be distinguished not only according to the various models and assumed mechanisms but also by the methodology. The studies can be thus classified in two groups [357]. This classification according to methodology is independent from the modeled mechanism:

Using a **deterministic** approach, the spatial and temporal distribution of particles is described in terms of concentrations. The destiny of a system is determined by the given concentrations, stochastic effects are not considered.

In a **particle**-based approach, the system is described with discrete particles. Protein state changes and translocation of particles is of random nature superimposed with certain boundary conditions and mechanisms.

Here, the presentation of different mathematical approaches will be limited to the deterministic methodology.

6.4 Differential equations

In the deterministic approach, the mathematical description is formulated as a set of — coupled — differential equations. Assuming solely free diffusion in three-dimensional space, the temporal distribution of particles is given as

$$\partial_t c(x, y, z) = \boxed{D \Delta c(x, y, z)} \tag{6.1}$$

In most models, the cell is approximated as a cylinder with the circular ends representing the cell poles (the model by Fischer-Friedrich 2007 tries to account for a more realistic geometry by assuming hemi-spherical caps instead of flat, round ends). In this case, it makes sense to express the Laplace operator in terms of cylindrical coordinates r, ϕ, x (see also Fig. 9.24(a), z is replaced by x). Furthermore all models consider rotational invariance in respect to the x-axis. Consequently, the Laplace operator collapses to the spatial variables r and x. Furthermore, some models assume that the cytosolic diffusion is so fast that the distribution of proteins in the cytosol is homogeneous along the radial axis r. This allows a further reduction to a one-dimensional system and an expression of the differential space operator as $\frac{\partial}{\partial_x}$ or $\frac{\partial^2}{\partial_x^2}$ respectively. For lateral membrane diffusion, the Laplace operator Δ corresponds to a two-dimensional differentiation in x and y.

Equation 6.1 applies only for systems, which are solely affected by diffusion. In the case of further mechanisms and interactions, additional terms have to be taken into account. For the Min-system, these are binding and unbinding events between proteins or to the membrane. Both proteins, MinD and MinE, can assume two states: as free particles diffusing in the cytosol or bound to the membrane. Here, a common notation of observables will be used in order to simplify comparison of the different models. The suggested notation is geared to the description given in the model by Bonny and Kruse [358]. The first state is indicated by a capital letter subscript and the latter by a lower case subscript. The respective distribution of the cytosolic proteins is given as concentration c_D for MinD and c_E for MinE and as c_d and c_e respectively for the membrane-bound states. In some models, bound MinE is only considered in a complex with MinD, thus written as c_{de}.

In the differential equations, the temporal evolution $\frac{\partial c}{\partial t} = \partial_t c$ of these protein concentrations c is related to their spatial distributions at time t. The spatial distribution again is determined by a diffusive part characterized by respective diffusion coefficients (D_D or D_E for cytosolic diffusion and D_d or D_e for membrane diffusion if considered) and by rates of molecular interactions between proteins or between proteins and the membrane. These interactions refer basically to protein binding or membrane attachment. Thus, for most models, these differential equations follow a similar pattern:

Cytosolic MinD

$$\partial_t c_D = \boxed{\text{Cytosolic diffusion of MinD}} - \boxed{\text{Membrane attachment of MinD}} + \boxed{\text{Membrane detachment of MinD}}$$ (6.2)

Cytosolic MinE

$$\partial_t c_E = \boxed{\text{Cytosolic diffusion of MinE}} - \boxed{\text{Membrane attachment of MinE}} + \boxed{\text{Membrane detachment of MinE}}$$ (6.3)

Membrane-bound MinD

$$\partial_t c_d = \boxed{\text{Membrane diffusion of MinD*}} + \boxed{\text{Membrane attachment of MinD}} - \boxed{\text{Membrane detachment of MinD}} - \boxed{\text{Aggregation current*}}$$ (6.4)

Membrane-bound MinE

$$\partial_t c_e = \boxed{\text{Membrane diffusion of MinE*}} + \boxed{\text{Membrane attachment of MinE}} - \boxed{\text{Membrane detachment of MinE}} - \boxed{\text{Aggregation current*}}$$ (6.5)

Terms addressing the same interactions are highlighted in the same color: blue for diffusion, green for MinD-attachment to the membrane, red for recruitment of MinE to MinD, yellow for the detachment of MinD and MinE and gray for all other terms. Colors for MinD- and MinE-attachment were chosen in agreement with the color coding used in other publications [272, 1, 362, 92]. Note that the algebraic sign of each term differs.

The terms indicated by an asterisk apply only for models which consider membrane diffusion or aggregation current. The mathematical description presented by Meinhardt and de Boer also assumes synthesis and decay of proteins [272]. This is regarded by source and sink terms in the differential equations. However, since it is clear nowadays that production and decay of proteins are not essential for Min-protein oscillations, respective terms are omitted in the general pattern of differential equations given in Equations 6.5. Regarding the overall effect, synthesis and degradation of cytosolic and membrane proteins are actually comparable to processes of attachment and detachment (see below in the description of the Meinhardt/de Boer-model).

The attachment and detachment terms are usually composed of an attachment or detachment rate and respective concentrations. For example, in its basic setting, the attachment of MinD to the membrane is expressed as an attachment rate for MinD multiplied with the cytosolic concentration of MinD. Only if cytosolic MinD is available, can MinD attach to the membrane.

Thus, also the MinD attachment rate appears as a negative term in the equation describing the cytosolic distribution of MinD since MinD is transferred from the cytosol to the membrane. In some models, also the concentration of membrane-bound proteins appear in the attachment rate. This is for example the case for cooperative attachment models for which it is thought that membrane-bound proteins enhance the attachment of free proteins.

In some models, bound MinE is described in terms of MinDE-complexes. Consequently, the disappearance of membrane-bound MinD is dependent on the membrane attachment of MinE and disappearance of membrane-bound MinE is described as the detachment of the MinDE-complex. Thus, the equations describing the concentrations of membrane-bound Min-proteins follow a slightly different pattern:

Membrane-bound MinD

$$\partial_t c_{\mathrm{d}} = \boxed{\text{Membrane diffusion of MinD*}} + \boxed{\text{Membrane attachment of MinD}} - \boxed{\text{Membrane attachment of MinE}} \tag{6.6}$$

Membrane-bound MinDE

$$\partial_t c_{\mathrm{de}} = \boxed{\text{Membrane diffusion of MinE*}} + \boxed{\text{Membrane attachment of MinE}} - \boxed{\text{Membrane detachment of MinDE}} \tag{6.7}$$

All models discussed in this section are also summarized in Tab. 6.1 which sorts them in terms of model types (AC/CA) and membrane geometry (cell/SLB). Furthermore, the table lists dimensionality, boundary conditions, specific considerations, differential equations, numerical parameters.

For all models, the variables representing protein distributions and concentrations were adapted to the nomenclature applied by the recent publications of our collaborators Kruse and colleagues [199, 363, 357, 1, 358]. Furthermore, for better comparison, the sequence of the different terms in the differential equations were brought into the same order as in Equations 6.5.

Oscillations in a cell-like geometry are displayed either as a function of the concentration c of membrane-bound Min-proteins vs. time t (*ct*-plots) or as kymographs (*cxt*-concentration plots). From these kymographs, time-averaged profiles of the density of membrane-bound MinD and MinE-proteins can be obtained.

6.5 Results

All published models could induce oscillations of Min-proteins in a cell-like geometry and the maxima of MinD and MinE-oscillation were slightly out of phase as observed *in vivo*. However, the form and characteristics of oscillations differ depending on the specific proposed mathematical description. Further specific results of each model will be given in the next sections. Tab. 6.2 summarizes principal results and respective kymographs, plots etc.

6.6 Aggregation current models (AC)

In order to reflect the concept of aggregation current, a particle flux (J_{d} or j_{d}) of membrane-bound MinD has to be introduced. The model proposed by Meacci and Kruse also assumes a particle flux for MinDE-complexes (j_{de}). AC-models also consider lateral diffusion of Min-proteins on the membrane to be much smaller than the diffusion of cytosolic proteins . However, it is essential for all different AC models that the diffusion of membrane-bound proteins is non-zero.

6.6.1 Cell-like geometry

Kruse 2002 (AC)

The first mathematical description of Min-oscillations based on the concept of the aggregation current model was published by Kruse et al. in 2002 [191]. Here, the flux of MinD-molecules on the membrane was considered to be based on a mechanism of MinD hopping from one membrane site to a neighboring membrane site. This hopping mechanism was influenced by a probability p depending on the proximity of neighboring MinD-molecules. The equation was established for concentrations and parameters without units and scale to cells which makes comparison to *in vivo* observations difficult. All parameters were defined without any units.

Min-protein dynamics were illustrated as plots of MinD and MinE concentrations at the polar positions versus time. These plots reveal oscillations of MinD and MinE that are in phase but with maxima that are slightly shifted in space and time which corresponds well to observations *in vivo*. Unfortunately, no kymographs were established so that a direct comparison with *in vivo* phenomenology remains difficult. A ring-like structure of MinE could only be produced upon an additional modification of the MinE attachment rate (ω_3, see Tab. 6.1). A time-averaged profile of the MinD-concentration plotted versus the longitudinal extension of the cell revealed a minimum of MinD at a midcell-position which corresponds to observations *in vivo*. However, the numerical simulations also produced a minimum of MinE at a midcell position which contradicts observations *in vivo* (see Sec. 4.8).

Furthermore, a phase diagram was established marking phases of stable homogeneous (I), stable oscillatory (II) and stationary nonhomogeneous states (III) in dependence of total MinD and MinE concentrations. For long cells (factor of 1.5 in respect to the standard length), double oscillations could be generated.

In this publication, Kruse also showed the possibility that the Min-system might not only serve as a mechanism for the selection of the central division site, but also as a temporal trigger for the initiation of cell division (see also the Conclusions, Sec. 10).

Meacci 2005 (AC)

The mathematical description of Kruse in 2002 was further developed by Meacci and Kruse in 2005 [199]. Here, the effect of an aggregation current was not described through the stochastic effect of MinD hopping from one membrane binding site to another with a certain probability depending on proximity of neighboring MinD-molecules but by intermolecular attractions parametrized through the constants $k_1, k_2, \bar{k}_1, \bar{k}_2$. Furthermore, an aggregation current was considered not only for MinD-proteins but also for MinDE-complexes.

The mathematical description considered boundary conditions and parameters with a scale and units corresponding to the biological cell. Numerical simulations were carried out for a cylinder of length $L = 2\,\mu m$, however condensed to one dimension.

Oscillations of MinD and MinE were expressed with the help of kymographs whereas, for the distribution of MinD, both pure MinD and MinDE-complexes were regarded. Oscillation of MinE was described solely in terms of MinDE-complexes. Here, MinD does form polar caps which shrink towards the cell pole but there is no period of growth of polar MinD-caps. Furthermore, no MinE-ring is produced but the MinE-distribution follows more or less the MinD-distribution, though with a small shift between MinD- and MinE-maxima. As before, a MinD minimum was found at a midcell-position but also a MinE-minimum. Oscillations periods were basically determined by the detachment rate of MinDE-complexes. Values for the oscillation period covered the range of $40 - 120$ s and were thus in good agreement with observations *in vivo*. In contrast to the previous study, a phase diagram of dynamics in dependence of total MinD and MinE

concentrations revealed only two different states: oscillatory and homogeneous distributions of Min-proteins.

When the virtual cell length was doubled, two oscillations emerged which corresponds to the observation of two or even more oscillations in filaments *in vivo*. Furthermore, as expected from experimental findings, oscillation periods increased for increasing MinD concentrations and for decreasing MinE concentration.

Fischer-Friedrich and Kruse 2007 (AC)

In 2007, Fischer-Friedrich and Kruse extended the previous mathematical descriptions from one to three dimensions [363]. The cell geometry was approximated by a cylinder with two hemispherical caps at both ends representing the cell poles. The mathematical equations correspond to those established by Meacci and Kruse. However, an aggregation current was considered again only for MinD. Numerical simulations produced coupled oscillations of MinD and MinE between these cell poles.

6.6.2 Flat open geometry

6.6.3 Fischer-Friedrich and Kruse 2007 (AC)

It was also Fischer-Friedrich and Kruse who addressed the comportment of Min-protein dynamics on flat and open geometry for the first time [357]. This investigation was motivated by the *in vitro* studies performed by Loose at the same time using supported lipid bilayers for Min-protein reconstitution (see Sec. 4.9) [357, 1]. However, the output of the numerical simulations was not comparable to the *in vitro*-observations. Thus, in consequence, the model of aggregation current was questioned. Alternatively, the model of cooperative attachment was developed.

6.7 Cooperative attachment models (CA)

6.7.1 Cell-like geometry

Meinhardt 2001 (CA)

The model developed by Meinhardt and de Boer also took into account the dynamics of the Z-ring assembly [272]. However, when regarding the differential equations for the distribution of MinD and MinE it is clear that these, and thus also Min-protein dynamics, are independent from FtsZ. Therefore, the FtsZ-protein distribution will be neglected in this section.

Both cytosolic and lateral membrane diffusion were considered. The main difference to the previous models is that the study by Meinhardt and de Boer is the sole publication which considers protein synthesis to be essential for the emergence of an oscillatory pattern. The synthesis of proteins was expressed by a constant and by a catalytic rate. For the catalytic rate, the protein synthesis is additionally enhanced by the respective protein concentration $\left(\rho_{\mathrm{d}} c_{\mathrm{D}} \left(c_{\mathrm{d}}^2 + \sigma_{\mathrm{d}}\right)\right.$ in the term of the differential equation for membrane-bound MinD in Tab. 6.1). Thus, due to this cooperative character, this model is attributed to the class of cooperative attachment models.

In Tab. 6.1, the different terms of the differential equations are highlighted with the same color pattern as presented in Eq. 6.5. The appearance of Min-proteins on the membrane through synthesis can be compared to the appearance of membrane-bound Min-proteins through attachment. Likewise, the decay of membrane-bound proteins in the Meinhard/de Boer-model corresponds to the detachment of membrane-proteins in the other models. In similar manner, the addition of Min-proteins to the cytosol through synthesis has a comparable effect to the detachment of

membrane-bound proteins and the decay of cytosolic proteins corresponds to the removal of cytosolic proteins through detachment. However, the basic difference is that in the other models, the total number of MinD and MinE proteins is conserved. This requires that the addition of proteins to the cytosol has to be equal to the detachment of membrane-bound proteins, and, vice-versa, the removal of cytosolic proteins has to occur at the same rate as the attachment of the proteins to the membrane. In the Meinhardt/de Boer-model all these processes are independent of each other.

However, this (false) assumption generated oscillations that reproduce the *in vivo*-dynamics quite well. Like the model proposed by Meacci and Kruse, the numerical simulations of Meinhard and de Boer produced polar MinD-caps and even a MinE-ring. However, again, MinD-caps shrink towards the cell pole but do not grow as it is observed *in vivo*. Furthermore, the benchmark of a decreasing oscillation period for decreasing MinD- or increasing MinE-concentration was fulfilled by this model by simply decreasing the MinD- or increasing the MinE-synthesis rate in the differential equations. Likewise, increase of the cell length led to longer oscillations periods as observed *in vivo*. Furthermore, the model could also reproduce the phenomenology of multiple oscillations in long cells.

This is a nice example of how completely different assumptions and models produce results that show the same phenomenology. Thus, the pure reproduction of biological phenomena can *indicate* that a certain explanation of biological processes might be correct, however it is not a *proof*.

Howard 2001 (CA)

Howard introduced the concept of reaction-diffusion into the cooperative attachment model[356]. In contrast to other models, this description considered that MinE is already recruited by MinD in the cytoplasm which is in contradiction with *in vitro* observations [360]. Other models assume MinE attachment to the membrane via recruitment of membrane-bound MinD. Here, diffusion of Min-proteins on the membrane was set to zero.

Kymographs of MinD and MinE oscillations exhibited a strong phase shift between MinD and MinE. Furthermore, MinE showed a pronounced profile which could be interpreted as a MinE-ring. However, an even more pronounced profile was also found for MinD. In addition, these MinD-rings propagated from a nearly midcell-position to the cell poles whereas *in vivo*, MinD populates the entire cap of the cell pole forming a tube-like-structure which shrinks towards the cell pole with time.

Corresponding time-averaged distribution profiles revealed a minimum for MinD at midcell but also a midcell maximum for MinE. In fact, this is not only the sole theoretical study that produced a midcell MinE maximum but also the only publication that considered a MinE-maximum to be correct. The phase diagram of attachment behavior in dependence of MinD and MinE-distributions exhibited only two states: oscillations and static, homogeneous protein distributions. With increasing cell length and below standard MinE/MinD-ratio, wavelength and oscillation period increased to a maximal wavelength of 4.2 µm and a maximal oscillation period of 145 s. Furthermore, an increase of the total MinD-concentration yielded an increase of the oscillation period as observed *in vivo*. However, for long cells, the oscillation period increased in an unrealistic manner up to 1000 s for a length of 7 µm. The issue of multiple oscillations was not addressed. Taking into account the (unrealistic) relationship of oscillation period vs. cell length indicates that this model would probably also to produce multiple oscillations in filamentous cells.

Huang 2003 (CA)

For the class of cooperative attachment models, it was Huang et al. who made the transition from one to three dimensions [345]. They also considered effects of MinE-dimerization and introduced a slow exchange rate of ADP to ATP in MinD that is taken into account into the differential equations. Consequently, cytosolic MinD was differentiated into ADP-bound and ATP-bound MinD which required an additional differential equation. As Howard in 2001, Huang et al. set the membrane diffusion of Min-proteins to zero. The differential equations in Tab. 6.1 seem to not follow the pattern presented in Eq. 6.5: In the equation for membrane-bound MinD no negative detachment term appears but the number of membrane-bound MinD is decreased by a term describing MinE-recruitment. This is because the number of pure MinD-molecules bound to the membrane is not reduced directly by detachment but by the association of MinD and MinE to a complex.

Oscillations of MinD nicely exhibited the *in vivo* characteristic of growing and shrinking MinD-caps at the cell poles. The distribution of MinE also reproduced a ring-like feature. Yet, this ring was not localized at a midcell-region as expected but emerged only close to the cell poles.

However, almost all other essential effects observed *in vivo* could be reproduced. A phase diagram of MinD/MinE-concentrations showed that the oscillation period increased for increasing MinD- and for decreasing MinE-concentration. The phase diagram also revealed a minimum for the oscillation period of 33 s which is in agreement with *in vivo* observations [188]. Cell elongation led to longer oscillation periods as well. For very long cells (filaments) multiple oscillations emerged. The reduction of the hydrolysis rate produced oscillations of MinD and MinE without any sharp MinE-profile mimicking the effect of mutation of the of MinE which also leads to Min-protein oscillations in the absence of MinE-rings.

Fischer-Friedrich and Kruse 2008 (CA)

Fischer-Friedrich and Kruse did not only investigate the aggregation current model but also established a new description within the concept of cooperative attachment [357]. This mathematical description is kind of a synthesis of former descriptions by Kruse and co-workers and of the model proposed by Huang. Like almost all other models but in contrast to Huang in 2003, the ATP-exchange was considered to be fast enough to be neglected. Although it was estimated to be slow compared to cytosolic diffusion, membrane diffusion was considered to be as essential as in the aggregation current model for both MinD and MinE. Furthermore, the model of cooperative attachment was further implemented by the introduction of specific attachment rates due to cooperative binding of MinD/MinD and also that of MinE/MinE as already suggested by Huang [345].

The obtained oscillation period was determined to be 67 s and is thus in good agreement with experimental findings. Only kymographs for MinD and MinE were established but no time-averaged profiles of the Min-protein concentrations. The strong advantage of this model was, however, that it could — as the only model at the time of its publication — reproduce the phenomenology of Min-protein dynamics in cell-like shape *and* on a flat and open geometry.

6.7.2 Flat and open geometry

Huang 2003 (Fischer-Friedrich 2008, CA)

According to Fischer-Friedrich and Kruse, the aggregation current model failed to reproduce the phenomena of parallel and propagating waves observed in a flat and open geometry as for example demonstrated on supported lipid bilayers. Thus, Fischer-Friedrich also investigated the model

of cooperative attachment for a flat and open geometry. However, the implementation of the mathematical description developed by Huang in 2003 only produced chaotic waves [345, 357].

Fischer-Friedrich and Kruse 2008 (CA)

Thus, Kruse and Fischer-Friedrich, in collaboration with Loose, developed a new mathematical description that could reproduce cell-like Min-protein oscillations as well as parallel propagating waves in flat and open geometry [357]. This model corresponds to the mathematical description already cited in Sec. 6.7.1. In contrast to all other models, this model could reproduce parallel and propagating waves of MinD and MinE as observed in the *in vitro*-studies performed by Loose on supported lipid bilayers [1]. As observed for Min-protein waves *in vitro*, simulated waves also exhibited a small phase shift between the MinD and MinE-maxima. The basic change in respect to the simulations for cell geometry was the increase of the cytosolic diffusion coefficients. In the biological cell, the diffusion of unbound proteins is decreased by molecular crowding and enhanced viscosity of the cytoplasm. In contrast, in the experimental settings, the cytoplasm was replaced by an aqueous buffer above the supported lipid membrane with lower viscosity and without any molecular crowding. Thus, for simulation of *in vitro* experiments, the diffusion coefficient for cytosolic MinD and MinE were increased from $12.5\,\mu\text{m}^2/\text{s}$ to $60\,\mu\text{m}^2/\text{s}$.

Bonny and Kruse 2012 (CA)

The model by Fischer-Friedrich and Kruse was further developed by taking into account the idea of transient binding of MinE [357, 1, 10]. The mathematical description by Bonny and Kruse will serve to reproduce the *in vitro*-experiments presented in this PhD-thesis. In combination with experimental findings, this model helped to elucidate further details of the Min-mechanism. Together with my collaborators Karsten Kruse, Mike Bonny and Martin Loose, I would like to suggest that this mathematical model as the one which approximates currently the real *in vivo*-processes in the best way.

7 Synthetic biology

The dynamics of Min-proteins shall be investigated further in detail using the ansatz of *synthetic biology*. But what is actually meant by the term *synthetic biology*? This chapter tries to give a short introduction to this new domain of modern biological research with a particular focus on the issues which are relevant for the Min project. Therefore, this chapter elucidates primarily the use of biomembranes within the field of synthetic biology. The following sections are based on a text book chapter which I have written for the monographic publication *Bio and Nano Packaging Techniques for Electron Devices: Advances in Electronic Device Packaging* [364]. Furthermore, at the end of this chapter, I would like to present a strategy how to reach artificial cells supporting the Min system implying a roadmap for the application of lipid bilayers for the reconstitution of proteins.

7.1 Biological cells in analogy to technology

In modern biosciences, the biological cell is perceived as a largely mechanistic system, similar to a factory or a highly integrated technical device, consisting of a set of different interacting machines which are built from parts acting by mechanical, electrical and chemical means (Fig. 7.1). Particularly striking is the comparison to machines in computing and communication. The cell nucleus, containing DNA, which is the central memory of the living organism, can be compared to an information storage unit in a computer. Organelles such as the endoplasmatic reticulum and the Golgi apparatus work as assembly lines, building and packaging proteins ("machines") from the blue print documented in the DNA. The cytoskeleton, in addition to providing stability, serves as a supply chain of signaling biomolecules, similar to a railroad track network. In plant cells, chloroplasts serve as solar panels providing the necessary energy, which is generated by mitochondria in eukaryotic cells working like small engines converting carbon hydrogens ("fuel") without heat production into ATP, the universal biological energy currency. Further functional elements, like membrane proteins in the outer cell membrane, serve as communication and nutrition channels. The comparability becomes even more evident by reversing the perspective: Lazebnik speculated whether a biologist could fix a radio [365]. This is certainly an ironic approach and it shows limitations of comparability, but it states the general validity of comparing biological and man-made technology.

7.2 Biology as an example for engineering

We notice that the biological cell can be understood as a technical system, but as a technical system on the microscopic and nanoscopic level. This makes it an inspiring model for engineering. Not only the realization of machines and electronic systems on the molecular level but also further features distinguish the biological cell as an inspiration for engineering [366]. In contrast to technical systems, the biological cell is capable of self-assembling its parts, adapting to changing environments and conditions. It shows self-repair, automatic replacement of dysfunctional elements, and - most striking from the engineering perspective - it can self-replicate. Engineering a technical device is a challenging task, producing it in mass quantities another challenge.
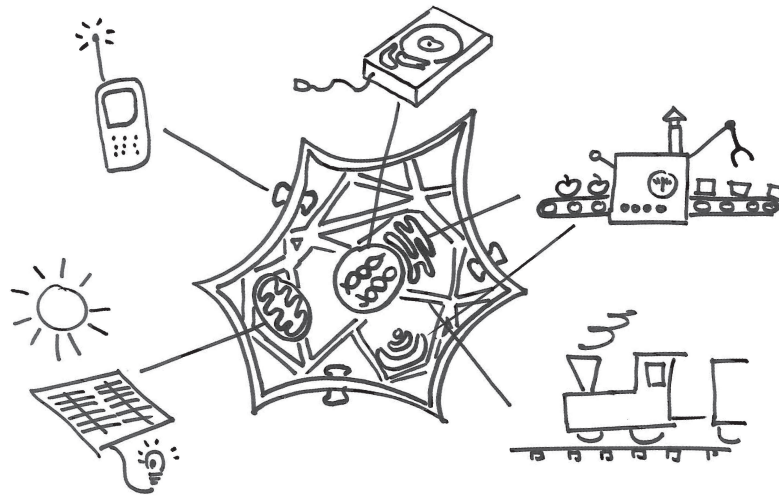
Figure 7.1: The biological cell can be compared to a small factory in which different cell organelles execute the function of technological machines.

Imagine a technical product such as a mobile phone that reproduces itself. The term *cell phone* would get a new meaning. Furthermore, *Green IT* has become an important issue in technology. This is already achieved in biology: if biological machines or entire factories (cells) break down, they are immediately degraded and even recycled.

Furthermore, biological self-assembly is an outstanding example for packaging. The term packaging originates from the semi-conductor industry and describes the technology to assemble functional elements together on a minimal space while maintaining or even increasing the performance of the system. Both, quantitative and qualitative levels of packaging in biological cells are unparalleled in the technological world. A simple yeast cell contains more than 5000 different proteins (functional elements) in a femtoliter volume. 2D- and 3D-packaging are both realized in parallel.

7.3 Why synthetic biology?

The mechanistic understanding of the biological cell as a well-tuned collection of machines certainly provokes question whether it is not only possible to compare nature to human-made technology but also to treat biology like an engineering science in practice. Following this challenge, researchers have started to use biological matter as a construction kit in the past. This recent approach to biology has been denominated - in contrast to "natural" biology: synthetic biology. The main concept of synthetic biology is to treat biological systems as a set of interacting modules that can be separately characterized, standardized, and reconstituted or re-arranged for desired functionality [367]. These modules may range from protein motifs and sub-structures to full reaction cascades and networks. Such a modular approach with standardized elements is characteristic for engineering, and consequently, synthetic biology aims to open biology to engineers of various backgrounds, including information processing, and micro- and nanotechnology. Synthetic biology is perhaps one of the most innovative and challenging disciplines in modern biosciences [368]. Motivations to apply concepts of synthetic biology can have various

motivations [369].

One motivation is the general concept of complexity reduction. If the observation of a phenomenon is too complicated within a real biological cell, the system may be reduced to the minimal function units so that controlled observation is made possible (this will motivation will be also further discussed in Sec. 7.9). This is also the motivation for this work: since the analysis of the Min-system *in vitro* remains complicated, it shall be transferred in artificial and radically reduced system in order to facilitate investigations.

Another motivation is to reduce living matter to its absolutely necessary requirements to better understand the basics of life: What are the essential features and elements that are necessary that cells replicate, grow, evolve? And, how did cells actually evolve and how did the very first cell, in analogy to anthropology, the "Lucy" of cell biology, look like? It is obvious that the very first cells must have been much simpler structures. What are the minimal components of such a protocell? Furthermore, if there is a very first cell, is a also the world before the cell. How did biological structures evolve from non-living matter? Again, in analogy to anthropology, where is the "missing" link between the non-living and living world and what did it look like? Is there at all a true border between living and non-living matter or has "life" simply to be understood as a high level of structural dynamic complexity of molecules [370, 371]?

A third motivation and economically most important is the generation of adapted or new organisms that can be exploited for medical and technical applications. All three motivations - complexity reduction to solve open problems in cell biology, the question of the nature and origin of life, and newly synthesized organisms for technical applications - can be approached by two opposing concepts of synthetic biology: top-down and bottom-up.

7.4 Concepts of synthetic biology

7.4.1 Top-down

The top-down concept follows a very radical principle in order to answer the question what are the minimal requirements for a functioning, e.g. living, cell by successively reducing the cell, by removing non-essential parts and genes, e.g., through gene knock-out as depicted in Fig. 7.2. This is as if one would like to find out how a car works and starts by taking parts away. First the car radio is removed and it becomes clear that the radio is not essential for driving as the basic task of a car. By removing the engine, it is found to be crucial for the functioning of the car. This can even go as far as a complete reduction to the essential biochemical configuration for the basic tasks of life: eat, grow, replicate, and evolve [370]. This huge enterprise is currently best represented by Venter and co-workers, and their goal to reduce the bacterium *Mycoplasma* to its genetic minimum [372, 373]. Such a reduced bacterium could either serve to study the basic needs, tools and mechanisms of life. But it may also serve as a living platform, into which further modules, such as synthetic genes, could be integrated to fulfill novel tasks for technology and health [374].

The concept of top-down is in its work flow closer to "traditional" biotechnology, and thus promises reasonably fast results in generally achieving a modification or streamlining of biological systems and in satisfying the above mentioned three basic motivations, but it relies on existing organisms, and has to deal with their evolutionary obtained mechanisms for protection against genetic modification. Furthermore, it follows rather the principle of try-and-error and therefore provides less insight into very basic molecular interactions of living matter.

Physicist Richard Feynman once phrased the famous quote "What I cannot create, I do not understand" [375]. In strict sense, following this quote, we would only fully understand a biological system if we were able to make it from scratch. This idea is the motivation for the contrary concept of top-down: bottom up.
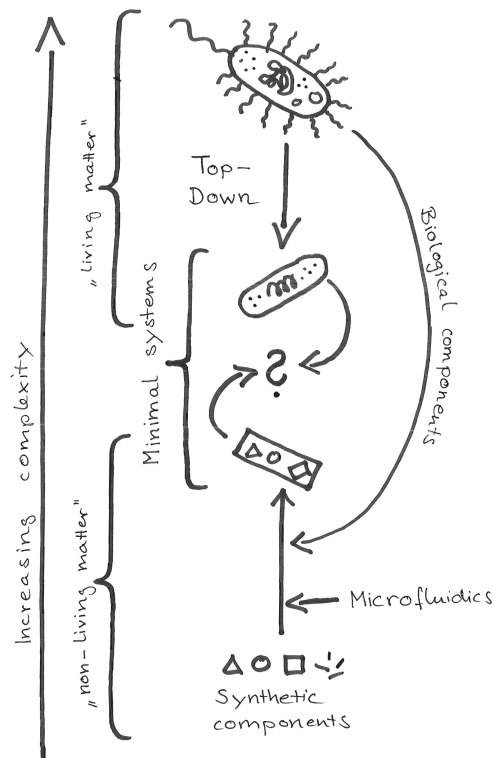
Figure 7.2: Different concepts of synthetic biology. Following the top-down approach, an existing organism (e.g. bacterium) may be reduced with regard to its genetic program, resulting in a minimal configuration of that specific organism. To the converse, in the bottom-up concept, individual parts from synthetic or biological origin are assembled together to build a new entity. End products of both approaches can be denominated as a "minimal system" but they are distinguished by an essential feature: minimal systems obtained by top-down do, without doubt, still belong to the regime of living matter, whereas a possible transition to this regime is still questionable (and not the scope of this article) for the bottom-up approach.

7.4.2 Bottom-up

The alternative route for the understanding of biological systems of bottom-up using elementary building blocks to generate modules that mimic a certain cellular functionality, providing the biochemical environment for cell-like processes [376, 368]. Strictly speaking, this approach is "synthetic biology" in its literal sense. The bottom-up concept is even extended to using simplistic modules not originating from biological sources, such as unnatural organic, or even inorganic material. The goal is to reach the level of complexity and functionality of existing biological cells by self-assembly and self-organization [377]. This is certainly a long way to go. It has been widely adopted by researchers interested in the design of minimal life forms, with no or only indirect practical implications to modern biology and biotechnology [378]. Although there are fascinating reports particularly on RNA-based protocells [379, 380], the progress in this field has been rather slow in the past decades.

7.4.3 The compromise: Biomolecules as a construction kit

More viable is a pragmatic bottom-up approach starting from already existing biological organisms, to dissect them into their elementary functional units, such as lipids, proteins and DNA, characterize each unit individually under defined conditions, and then use this well-characterized library as a modular construction kit for the reconstitution of biological systems or the creation of new structures and functions [376, 368, 382]. In spite of the massive efforts in systems biology, the immense entanglement of regulatory networks in the living cell raises very little hope that looking at the full system may also result in a complete quantitative understanding of the physical principles and (bio-) chemical modules of living systems. Thus, dissecting the cellular interaction network module by module will, although it does not give us a complete view of the

Figure 7.3: Illustrative sketch of the principle of bottom-up synthetic biology based on biomolecules provided by nature. This illustration will appear in Ref. [381].

Figure 7.4: Historic illustration of the setup used by Stanley Miller and Harold Urey to synthesize amino acids from inorganic gases. Image is taken from Ref. [383].
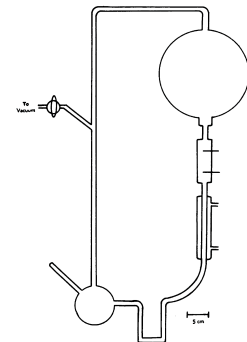
full system, at least help us in understanding the essential principles and functional elements that might have been assembled and combined in ancient forms of living systems. This approach is similar to a construction kit using ready-made components.

7.5 Biomembranes – origin of life?

Today we know more or less how cells are built, we know the components, to some extent we know how cells work. We dissect cells, reassemble biomolecules and are trying to build artificial cells. We also have a fair understanding how life and nature has evolved through its successful career from single cells to multi-cellular organisms. We understand that evolution is driven by the random mutation of the genetic code and subsequent prevailing of the new configuration. Nowadays it has to be assumed that living matter had evolved from non-living matter. Way below the complexity-level of cells we also have a rough understanding how organic molecules and biomolecules can be produced out of inorganic matter. Four billion years ago the earth was dominated by chemistry but not by biology [370]. No life could be found but only hot gases

and saline lakes. Presumably, life had started its successful career in such primordial soups. In 1953 Miller and Urey had shown that it was in principal to synthesize maybe not directly life but at least essential biomolecules such as amino acids by incubation of inorganic gases in an electric field [383]. In between the evolution from inorganic to organic matter on one side and the evolution of modern cells on the other side, there is still a unknown transition, a missing link: How did the first organisms evolve out of organic molecules and what did these "living" entities look like? We can describe and modify "life", but we don't know where it came from and we know little about the very early evolution of life.

It would exceed the scope of this chapter if the complexity of the question of the origin of life should be discussed here in detail. Nevertheless, we would like reason briefly about the nature of the very first cells because this might give us interesting insights also for the concepts of bottom-up synthetic biology.

Considering the hypothesis that living matter has evolved originally from inorganic matter implies that the evolution of life is characterized by a continuous increase of complexity in terms of structure of the evolving matter and dynamics. Regarding the first steps this complexity increase must have been dramatic. Following the the converse argument it has to be considered that the very early cells must have been of extremely simple nature. Furthermore, this raises the question whether there was ever any "qualitative jump" in evolution from non-living matter to living organisms, or whether this transition was not rather continuous. Such a continuous transition between non-life and life would certainly question the clear distinction between both.

The classical definition of life characterizes living entities by its capability of growth, metabolism, replication and evolution [370]. This definition has been proven to apply well in most cases when people tried to categorize the world into a non-living and living matter. However, zooming into micro- and nanoscopic scales of life, this definition becomes diffuse. So, for example, viruses show a life-like behavior but are in fact considered as non-living matter since they rely on a host cell for replication.

Jack Szostak has suggested an alternative definition for life [376]. According to him, life is characterized by the phenomenon of information that replicates within a container that replicates. The nature of the very first container remains a secret, but the postulation of a protocell assumes a cellular structure that is already highly sophisticated, consisting at least a semi-permeable compartment containing self-replicating molecules. Such a simple cellular structure is also superior to any structure that can be found among non-living matter. No crystal, metal oxide or gas cloud comes close to cells in terms of organizational complexity and especially in terms of transformability. A concrete example of the information-in-container hypothesis is given by the model of self-replicating RNA (information) in a self-replicating lipid vesicle (container). It is highly improbable that both, container and content, had evolved in parallel, but it is more likely that the appearance of one catalyzed the other. Therefore, there are two different schools of thought: one hypothesis is that there was first self-replicating RNA, and the other hypothesis states the formation of containers, such as bubbles of lipid films, occurred spontaneously and actually provided the environment so that biochemical reactions could take place at all [384, 385].

Here, we would like to emphasize and outline the important role of lipid containers for the early evolution of cells and explain why compartmentalization, i.e., the existence of boundaries, is the essential requirement for evolvable living systems. In modern cells, this boundary is provide by cell membrane.

For compartmentalization, biomembranes provide the appropriate material and looking at the remarkable transforming potential that biomembranes provide, it is tempting to speculate that life has actually started in a bubble, made of amphiphilic molecules. It is nowadays generally assumed that life had started in the earth's oceans, and biologists actually understand life as an ensemble of fine-tuned biochemical reactions. It is obvious that the probability for such

a biochemical reaction to take place is very low if the associated reaction partners have to find each other in the open sea. Therefore, compartmentalization is a key requirement for life. By including the reaction partners into a tiny compartment this probability is increased tremendously. Furthermore, a small reaction chamber guarantees that the reaction product is not diluted immediately into the open space but is preserved for further use.

And finally, compartmentalization is the prerequisite for evolution of distinct species. Consider two compartments with the same reaction partners encapsulated. One would expect that the same reactions would occur. But one compartment shall be modified, for example by UV-radiation, which alters the molecule composition which produces then a different reaction product. If there would be no boundary between the two sets of reaction partners, reaction products would mix. But if both populations are separated by boundaries, different species will eventually evolve.
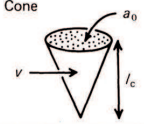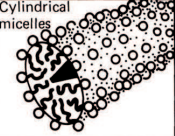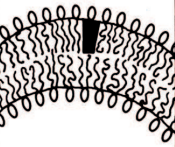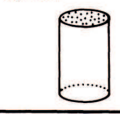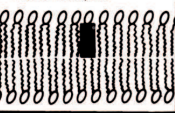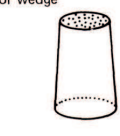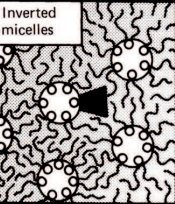
Pure lipid bilayers already offer a highly complex selective permeability, water and other small molecules can penetrate the lipid bilayer but not larger molecules or ions. Thus, compartments made from lipid bilayers can easily adapt their volume by the release or uptake of water which is necessary for growth and fission (replication). The great capability of lipid membranes was impressively demonstrated by Szostak and co-workers [379]. Two different populations of vesicles were prepared, one population contained encapsulated RNA whereas the other population consisted just of empty vesicles. Due to osmotic pressure, the filled vesicles had the tendency to take up water, which resulted in an increase of the surface tension of the vesicle's membrane. Due to the higher membrane tension, these vesicles had the ability for uptake of further lipids from outside. If the empty vesicles where brought into an aqueous environment with an osmolarity higher than that of the empty vesicle content, vesicles started to release water and membrane tension decreased. In consequence, these vesicles were likely to release lipid molecules to the aqueous environment. If both populations were now brought together in an aqueous environment, whose osmolarity was lower than that of the filled vesicles but higher than that of the empty vesicles, the empty vesicles started to release lipids whereas the filled vesicles started to gain lipids. Filled vesicles grew in size, whereas empty vesicles started to shrink. This system provided a very basic capability of competition: filled vesicles where evolutionarily superior to empty vesicles.

7.6 Biomembranes – starting point for engineering artificial cells?

When it comes to engineering synthetic biostructures, it is recommended to use a scaffold or platform. During evolution of the first cells, biomembranes have presumably taken a major role (see Sec. 7.5). The membrane is essential for the structural coherence of the cell. It defines the spatial boundary of the cell, provides the platform for many functional elements which guarantee the exchange of material and information with the outside, such as membrane channels and receptors. Additionally, there is accumulating evidence that the membrane is not just a passive material in which these functional elements are located: many cellular processes involving membrane proteins actually seem to be tightly regulated by the local membrane composition, which presumably forms functional sub-micron domains or "lipid raft" (see also Sec. 7.9). But the cell membrane plays not only an outstanding role in the cell's structure, but considering the cell's history, it was probably the starting point of everything. Therefore, it is recommendable to envisage artificial membranes also the starting point for building synthetic biostructures [386].

7.7 Lipid bilayers
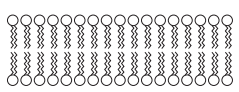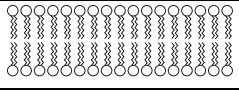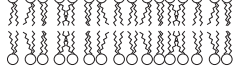
The basic building block of the cell membrane is the lipid molecule, an amphiphilic molecule consisting out of a hydrophilic head and a hydrophobic tail (Fig. 7.6). Lipids are capable of

Lipid	Critical packing parameter $v/a_0 l_c$	Critical packing shape	Structures formed
Single-chained lipids (surfactants) with large head-group areas: *SDS in low salt*	< 1/3	Cone	Spherical micelles
Single-chained lipids with small head-group areas: *SDS and CTAB in high salt, nonionic lipids*	1/3-1/2	Truncated cone	Cylindrical micelles
Double-chained lipids with large head-group areas, fluid chains: *Phosphatidyl choline (lecithin), phosphatidyl serine, phosphatidyl glycerol, phosphatidyl inositol, phosphatidic acid, sphingomyelin, DGDG[a], dihexadecyl phosphate, dialkyl dimethyl ammonium salts*	1/2-1	Truncated cone	Flexible bilayers, vesicles
Double-chained lipids with small head-group areas, anionic lipids in high salt, saturated frozen chains: *phosphatidyl ethanolamine, phosphatidyl serine + Ca^{2+}*	~1	Cylinder	Planar bilayers
Double-chained lipids with small head-group areas, nonionic lipids, poly *(cis)* unsaturated chains, high *T*: *unsat. phosphatidyl ethanolamine, cardiolipin + Ca^{2+} phosphatidic acid + Ca^{2+} cholesterol, MGDG[b]*	> 1	Inverted truncated cone or wedge	Inverted micelles

Figure 7.5: Lipids form different aggregate structures depending on their shape factor. v volume, a_0 head group area, l_c hydrocarbon chain length, SDS sodium dodecyl sulfate, CTAB cetrimonium bromide, DGDG digalactosyldiacylglycerol, MGDG monogalactosyldiacylglycerol. Figure is taken from Ref. [387].
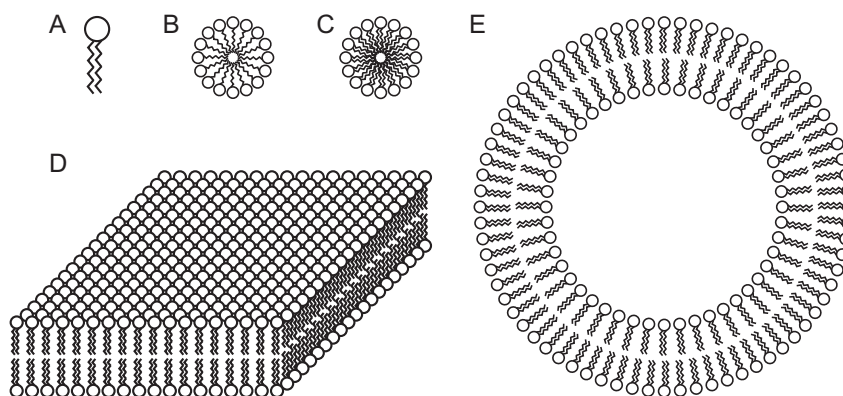
Figure 7.6: Different surfactant structures: A) single lipid molecule, B) micelles from single-chained lipids or detergents, C) micelles from lipids, E) bilayers and F) vesicles. Vesicle diameter can range from 30 nm (small unilamellar vesicles) up to several hundred micrometers (giant unilamellar vesicles).

	Name	Description	Top view	Side view
s_o	Solid-ordered phase	Ordered chains parallel to the membrane normal, chains packed in hexagonal lattice, low mobility		
l_o	Liquid-ordered phase	Ordered chains, high mobility of lipids		
l_d	Liquid-disordered phase	Disordered chains, high mobility of lipids		

Table 7.1: Phases of lipid bilayers.

self-assembly. Following the principles of self-assembly the resulting supramolecular structures are defined by the solvent's nature (hydrophilic or hydrophobic) and the molecule's structure. In other words, the basic structure of a cell, a hollow sphere, is already determined by the system water/lipids. When immersed into water, only the hydrophilic heads can build hydrogen bonds to the surrounding water molecules, whereas entropy forces the hydrophobic tails to get into contact to other hydrophobic particles (which are in general the hydrophobic tails of neighboring lipid molecules) [387]. Depending on the aspect ratio of the molecule, the so-called shape factor, given by the hydrophobic chain length and hydrophilic head group area, this entropy-driven mechanism can lead to different forms. Lipid molecules with a low shape factor (cone-shaped with a short chain and a large head group) tend to form micelles, whereas cylindrical shaped lipids with a large shape factor (long tail, small head group) form so-called bilayers (Table 7.5 and Fig. 7.6). Again, for entropic reasons, the open ends of such a bilayer close up to a hollow structure. Surface tension normally induces spheres but different forms are possible as well, either by external force or structural composition of the bilayer. The bilayer represents a two-dimensional fluid lattice rather than a rigid structure [388, 389]. For this reason, it is popular to compare lipid vesicles with soap bubbles. But it has to be pointed out that there is a crucial difference: a lipid vesicle represents in its basic version a two-component system (water and lipids), whereas soap bubbles require three components (water, soap molecules and a gas, normally air).

The two-dimensional fluid lattice of a lipid bilayer can exhibit different phases, defined by different order structures and mobility on the molecular level as depicted in Table 7.1 [390, 391, 392, 393]. Depending on the lipid composition and temperature, membranes can form three different phases (Table 7.1). The solid-ordered phase s_o is characterized by a high molecular structural order and low lateral mobility of lipids whereas the liquid-disordered phase l_d exhibits high lateral mobility and low order of acyl chains. The liquid-ordered phase l_o represents an intermediate state. This phase can be achieved upon addition of sterols to either one of the other two phases. In the case of the solid-ordered phase s_o the structural order is imposed onto the sterol molecules by neighboring molecules without reducing significantly the lateral mobility. If sterols are added to the liquid-disordered phase l_d it increases the structural order without reducing the lateral mobility. In the case of membranes with a composition of different lipids these phases can exist in parallel which results in phase-separating membranes [394, 395]. The biomembrane is a powerful tool to be used as a substrate and platform to integrate further functional elements.

7.7.1 Supported lipid bilayers

Certainly the most straightforward preparation of biomembranes is to make a continuous and flat film [396]. This can be obtained by adhesion of SUVs onto a hydrophilic support which creates

so-called supported lipid bilayers (SLB). A naturally hydrophilic surface (mica, glass etc.) is carefully cleaned and eventually plasma-treated in order to restore hydrophilicity of the surface. An aqueous suspension of SUVs is added to the clean (hydrophilic) surface and heated above the transition temperature of the lipids. Electrostatic double layer forces induced by virtual surface charges prevent vesicles from fusion to each other or to other hydrophilic surfaces. This surface charge can be shielded and the repulsion can be overcome by the addition of divalent cations such as Ca^{2+}. After incubation of some minutes, a continuous bilayer is formed on the support. For further analysis or treatment, it is necessary to remove the spare non-adhered vesicles in the buffer. They can be removed by simple washing off the fluid above the supported lipid bilayer.´

In general, the buffer above the membrane can be readily exchanged and additional components can be added to the reaction volume without limitations which makes manipulation of the reaction volume very easy. Whereas to other membrane assays, the reconstitution of membrane proteins to SLBs is rather uncomplicated and reconstituted membranes distinguish by stability [397].

Using transparent and flat, thin supports such as cover slides or the combination of cover-slides and transparent coatings makes observation of the membrane and the close space above extremely easy. First of all, the fact that the supported bilayer is in close proximity to the cover slide provides the accessibility by a microscope objective. Furthermore, the flatness of the support guarantees that focal plane and membrane are superimposed at all positions which makes it very easy to quickly scan the entire sample surface. The thin sandwich structure also allows the use of advanced fluorescence microscopy techniques such as total internal reflection fluorescence microscopy (TIRF) [398]. By using an open observation chamber, the membrane can be analyzed by atomic force microscopy (AFM) and can even be used simultaneously together with fluorescence microscopy [399, 400].

Supported lipid bilayers stand out due to simple preparation and long stability. However, one large drawback of supported lipid bilayers in respect to freestanding bilayers is the fact that the supported membrane almost adheres directly on the hydrophilic surface and swims only on a thin film of water of few nanometers. Despite this thin layer of water, the fluidity of the lipid bilayer is reduced due to interaction with the support surface [401]. This has even more effect for transmembrane proteins that penetrate the membrane completely and are in direct contact with the support. In addition, classical supported lipid bilayers can be accessed chemically only from one side. There are various ways to solve these problems of supported bilayers. One option is to assemble the lipid bilayer on a support that features a small aperture over which the lipid bilayer is suspended. In order to guarantee bilayer stability, this aperture must not be too large. Achieved pore diameters reach up to 600 nm but which is still very small in terms of observability by light microscopy [402, 403, 404, 405]. Another option is to spread the lipid bilayer not directly on the main support but to build sandwich structures with a layer between the main support and the lipid bilayers, which restores full lateral mobility and material and electronic access [406, 407, 408]. But these technologies are still under development, and possibilities of packaging of such bilayers with further functional elements has not been studied extensively yet.

Surface modifications of the support might not only help to solve the fluidity problem but also offer further potential by structuring of the artificial membrane. Binding affinity and physical properties of supported bilayers depend on the support material. An example of surface modification in order to change the binding affinity of the support for lipids using gold coating and microlithograpy is given in the materials & methods section and the principal technology applied in the research work presented here (Sec. 8.1.3). Through patterning the support, it is possible to obtained geometrically structured membranes. Structured membranes offer the possibility to mimic different cell membrane geometries and currently we investigate the influence of such structured membranes on the interaction with membrane proteins.

(a)   (b)
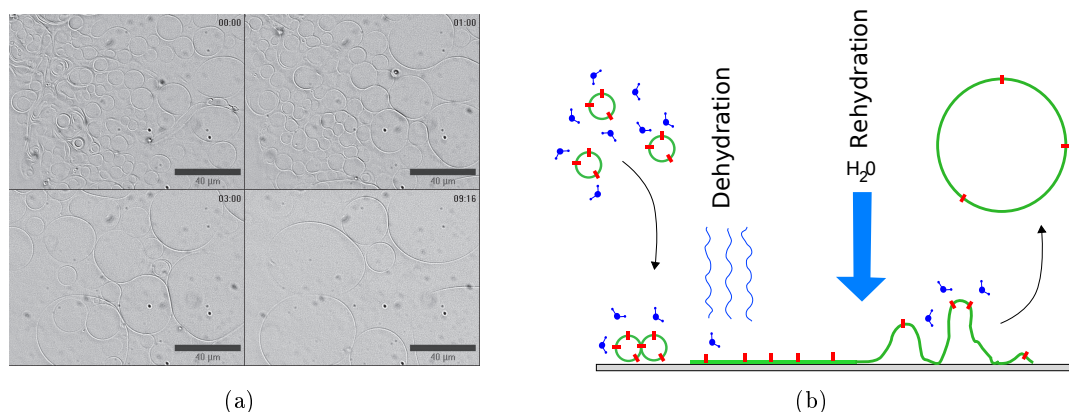
Figure 7.7: Lipid swelling of GUVs. (a) Growth of GUVs by electroformation during the period of 10 min. (b) GUVs reconstituted with transmembrane proteins can be obtained by performing the electroformation on lipid films that were obtained from previously dehydrated proteosomes.

7.7.2 Giant unilamellar vesicles

Fully freestanding and stable biomembranes, that can be functionalized, can be obtained by vesicles. Such vesicles are most readily obtained in form of small unilamellar vesicles which can be easily produced as described in Sec. 8.1.11. However, SUVs elude light microscopy which strongly restricts the analysis and manipulation. This problem can be overcome by expanding nanoscopic SUVs to the microscopic scale, to so-called giant unilamellar vesicles (GUV). So far, there are basically three methods known to create GUVs, which again are optimized by different means [409]. These three methods are:

- **Gentle hydration:** It is the most simple but does not produce very nice GUVs in terms of unilamellarity. In brief, SUVs are dehydrated or the organic solvent of dissolved lipids is evaporated to produce a thin lipid film on a support. The dried lipid film is then rehydrated for several hours without any further interaction (no shaking etc.). One of the advantages of gentle hydration is that GUVs can also be formed under high salt concentrations [410, 411].

- **Jetting:** It is a rather new method and still under development [412]. Similar to the creation of soap bubbles water or buffer is blown through a biomembrane suspended in a pore. This method features high monodispersity of GUVs in terms of size. One of major drawbacks of this technology is that GUVs produced by jetting contain significant amounts of oil (hexadecane for example) that is necessary for the creation of the suspension of the membrane in the aperture. Just like for black lipid membranes, these oils alter the bilayer properties and might interfere with experiments, especially when it comes to protein reconstitution.

- **Electroformation:** The most established method is that of electroformation of GUVs [413, 414]. SUVs are dehydrated or organic solvent is evaporated from dissolved lipids on electrical conducting (see Fig. 8.8). Theses electrodes can be two platinum wires or two glass slides coated with indium-titan oxide (ITO) for example. The dried lipid film is then rehydrated with water or the desired buffer. Normally, electrodes are integrated into a small reaction chamber or the glass slides are separated by a waterproof spacer of some millimeters in order to form a small volume. Then an alternating electric current is applied to the electrodes which induces lipid swelling. Depending on lipids, buffer and further parameters, giant unilamellar vesicles up to $500\,\mu$m grow within 10 min to 3 h. Frequency,

voltage and protocol details (such as time ramps and application of different voltages) vary from lab to lab and their influence is poorly investigated.

Electroformation works in buffers that are low in salt concentration (up to 5 mM). For this standard case, frequencies and voltages range around 10 Hz and 1 V (or $500\,V/m$ in terms of an electric field). GUV formation under physiological and therefore high salt concentration only works with much lower efficiency in terms of number, size and unilamellarity of GUVs. GUV formation under high salt concentrations can be obtained using high frequencies around 500 Hz and different voltage ramps [415]. GUVs can be either observed directly in transparent electroformation chambers (using glass sides with ITO-coating) or can be carefully harvested by using a small pipette or the like. See also the materials & methods section for a concrete example of GUV formation through the application of alternating electric currents (Sec. 8.1.13).

7.8 Functionalizing biomembranes

7.8.1 Proteins as functional elements

The function of proteins is defined by the task they perform and by their location within the cellular structure. Both, task performance and cellular location, are defined by the protein structure. The structure determines the solubility in aqueous environments and therefore whether the protein resides in the cytosol or in the membrane. Furthermore, the structure defines the binding affinity to other molecules and the catalytic function. In the following, the focus will lay on the packaging of biomembranes, and therefore to membrane proteins.

Membrane proteins can be classified according to their specific attachment or affinity to membranes. Biomembranes are characterized by the amphiphilic properties of their constituents (lipids). Some proteins simply adhere to the hydrophilic surface of membranes due to charged residues, whereas others penetrate partially into the hydrophobic layer of the biomembrane and a third class of proteins span completely through the hydrophilic-hydrophobic-hydrophilic sandwich structure (so-called transmembrane proteins) [416]. Whereas the first ones are very easy to reconstitute, the difficulty increases with the hydrophilic-hydrophobic structural complexity. Obviously, transmembrane proteins are hardest to functionally reconstitute.

Non-transmembrane proteins

Non-transmembrane proteins bind to the membrane through a specific membrane binding site or by binding to other membrane-associated proteins. For example, in case of MinD, the specific membrane binding site is given by the membrane targeting sequence MTS (see also Sec. 5.2.2). Often, the membrane binding ability of these proteins can be triggered through further signals and the membrane proteins show a dynamic binding behavior. In case of MinD, membrane binding is triggered through the binding of ATP to the protein. In contrast, MinE and MinC are examples of proteins binding to the membrane via other proteins (MinD).

Transmembrane proteins

Due to their structure, transmembrane proteins connect the volumes on both sides of the membrane, and often this structure already points to the protein function: transportation of ions and molecules from one side of the membrane to the other for metabolic and signaling issues. Transporters can, again, be classified into two categories: channels and active transporters.

Channels. Molecules and ions can pass the cell membrane by pores and endo- or exocytosis. But both processes transport matter non-specifically through the membrane. In contrast to
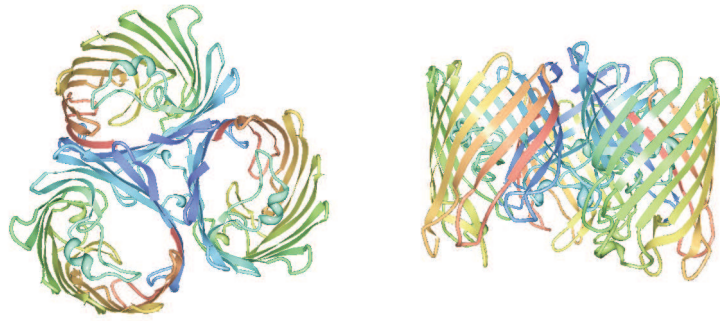
Figure 7.8: Top and side view of the structure of OmpF-trimer obtained by x-ray crystallography [417]. Images are taken from the RCSB PDB (www.pdb.org) of PDB ID 1OPF [417].

membrane pores and endo- or exocytosis, channels are only permeable for certain solutes. In general, these channels act as inactive transporters, e.g. they conduct ions and molecules along a chemical or electrical gradient. This specificity is given by the form of the inner channel. A potassium channel, for example, substitutes the hydrate-sheath of potassium by its form and charge distribution, whereas sodium is not mimicked well. Geometry can also adapt to non-charged molecules like sugars (e.g. OmpF, see below) or ATP (e.g. Voltage-dependent anion channels, VDAC) [418, 419]. In comparison to active transporters they allow fast translocation of solutes, which always follows an electrochemical potential. Channels can be closed and opened, for example by pH-value, electrical fields, ligands and/or temperature. Therefore, channels can be compared to adjustable conductances/resistances which discriminate between or sort solutes. The outer-membrane protein F (OmpF) is a good representative of such a channel protein [420] which can be found in the membranes of *E. coli*. OmpF belongs to the family of porins that form small aqueous channels through which small hydrophilic molecules and ions can diffuse. OmpF assembles into trimers as shown in Fig. 7.8.

Transporters. If molecules and ions shall be transported across the membrane against chemical and/or electrical gradients, this has to be achieved by active transporters. In the following, two examples of active transporters will be presented: the F1Fo-ATPase and bacteriorhodopsin.

- **F1Fo-ATP-Synthase:** This protein motor is a transmembrane protein with a large soluble part. It can be found in the plasma membrane of prokaryotes, in the mitochondrial membrane of eukaryotes and in chloroplasts, where it is responsible for the synthesis of adenine-triphosphate (ATP), the general energy currency of the biological cell. The F1Fo-ATP-synthase is a good example for protein function encoded by structure [421, 422]. The protein structure can again be decomposed in different structural elements which are built from amino-acid-chains. The F1Fo-ATP-synthase is a membrane protein that consists of two major units, the F1- and the Fo-unit as shown in Fig. 7.9. The part that resides in the membrane, Fo, represents the turbine and is built from an a-, b- and varying number of c-subunits. The c-subunits can be compared to the rotor sheets of a water or gas turbine whereas the a-unit has functions similar to an entry and exit-valve of a turbine. The membrane itself has the function of maintaining a potential that provides potential energy similar to a dam of a hydro-power plant. In the presence of a proton-gradient across the membrane, protons migrate across the membrane barrier by passing through the c-subunit-rotor which results in a rotation of the c-rotor. The F1-domain resides in the aqueous phase and is made up from five different Greek-letter denominated subunits. The rotation energy of the c-subunit rotor is transduced by an axle, the subunit γ, to the F1-domain. The α- and β-subunits catalyze the conversion of the energy-poor adenine-di-phosphate (ADP) into energy-enriched adenine-trip-phosophate (ATP). The structural completeness of the F1Fo-ATP-synthase can be verified by detection of the subunits in a
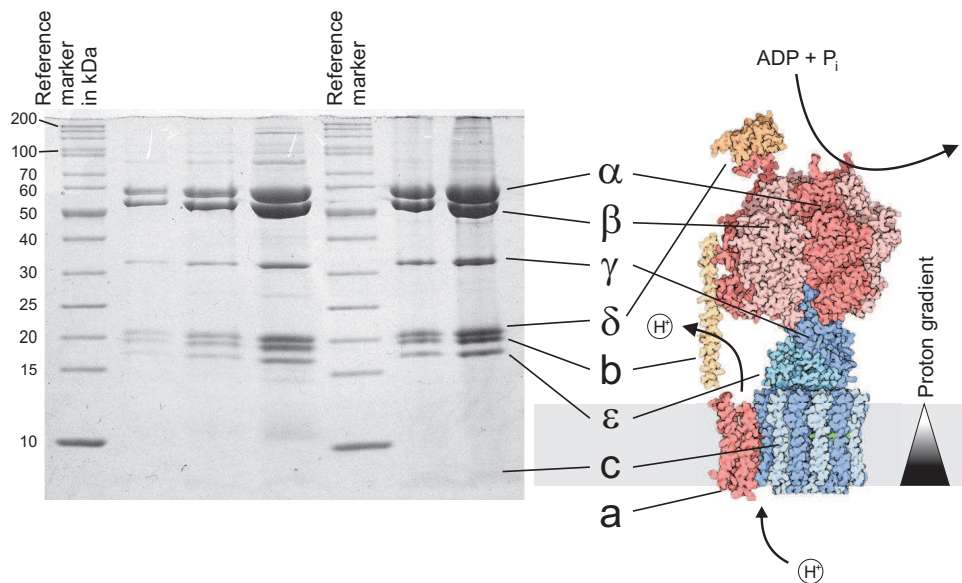
Figure 7.9: Protein motor ATP-synthase. Just like technical machines, protein motors also consist of different parts which can be separated and made visible by gel electrophoresis. The membrane-embedded Fo-domain decomposes into 3 structural elements (a to c) and the water-soluble Fo-domain into five subunits: (α to ϵ). As a control reference, markers with molecular weights from 10 to 200 kDa are added. One can clearly see that the c-subunits are the smallest parts whereas the α and β-subunits are the largest parts. In the presence of a proton gradient across the membrane, protons (H^+) can penetrate into the protein between the subunit a and the rotor. As the protons migrate through the rotor, the rotor and the axle γ are rotated by 360°/n whereas n is the number of c-subunits in the rotor. The rotational energy is transferred via the axle onto the F1-domain where it leads to conformational changes of the subunits α and β which catalyze in consequence the reaction of ADP and inorganic phosphate (P_i) into ATP.

SDS page. One can see clearly the bands of the different subunits in Fig. 7.9. The F1Fo ATP-synthase distinguishes itself also by an extraordinary flexible functionality, since its mechanism can be inverted. Instead of converting the potential energy of a chemical proton gradient into chemical energy (ATP), it can be used as a motor coupled to a proton pump. If no proton gradient is present, the F1Fo-ATP synthase hydrolyzes ATP into ADP, generating a torque on the γ-subunit which is transmitted onto the c-subunit-rotor which then can pump protons across the membrane. The capability of the ATP-synthase to produce a mechanical torque can be even decoupled from its original application of pumping protons and be used for other purposes. Kinosita, for example, immobilized the purified F1-domain on a support and supplied ATP to the protein, which resulted in a continuous rotation of the γ-subunit. This rotation was made visible by attaching a fluorescently labeled microtubulus [423]. This double function of the ATP-synthase can be controlled by other means than the proton gradient, which allows even higher functionality of the protein. In the case of the here studied example of the ATP-synthase, the F1Fo-ATP-synthase from the bacterium strain TA2.A1, the ability of hydrolyzing ATP is only activated upon addition of the detergent lauryldimethylamine-oxide (LDAO). This allows to control the functionality of the protein. So, the ATP-synthase could be, for example, used to produce ATP in a first step, and then to pump protons in order to generate a proton gradient in a second step by the addition of LDAO [424].

- **Bacteriorhodopsin:** Another protein with exemplary functionality is the membrane protein bacteriorhodopsin which can be compared to a photo-diode. Bacteriorhodopsin is a membrane protein that can be found densely packed in the outer membrane of certain archaebacteria such as the halobacteria that live in salt lakes [425, 426]. Bacteriorhodopsin absorbs light and uses the energy to pump protons through the core of the protein. If the protein is part of a membrane, separating two volumes, this mechanism can build up a proton gradient across the membrane and therefore store potential energy. In halobacteria, this mechanism supplies the organism with energy [427]. This feature could be exploited to use BR not only as a light sensor but also as a energy-generating powered by sun light [428, 429].

7.8.2 Reconstitution of proteins

Like the assembly of functional elements in packaging the reconstitution of proteins into biomembranes in synthetic biology is the crucial and most difficult step. General methods have been worked out in the past [430, 431, 432] but in fact suitable protocols have to be developed for each protein if not only the reconstitution but also the transfer of functionality shall be successful.

Reconstitution of membrane-associated proteins

In contrast to embedding of transmembrane proteins, the reconstitution of non-transmembrane proteins is relatively uncomplicated (see Sect. 7.8.1). Usually being water soluble in water, these proteins can easily dissolved into the reaction buffer. The family of Min-proteins in *E. coli* represent a nice example of membrane-associated proteins that can be reconstituted upon addition to the reaction buffer in the presence of lipid membrane. Though, membrane binding still has to be activated by the addition of ATP.

Reconstitution of transmembrane proteins

The reconstitution of transmembrane proteins is much more difficult, due to the amphiphilic structure of the protein. In general, for the reconstitution to any kind of bilayer (SLB, GUVs
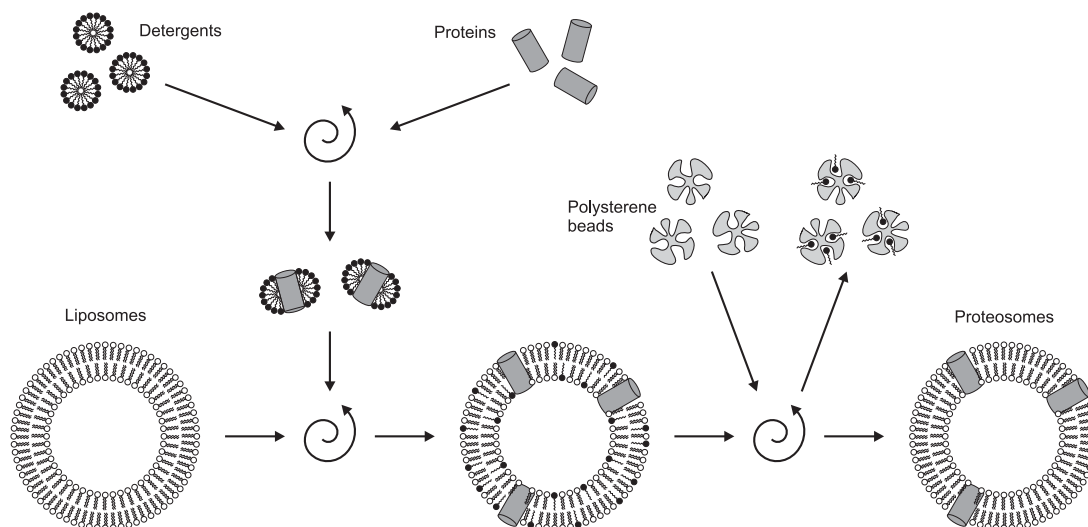
Figure 7.10: Principle of reconstitution of amphiphilic transmembrane proteins into vesicles. Proteins are dissolved in an aqueous solution by detergents forming protein-detergent aggregates. These binary micelles are mixed with preformed liposomes which results in vesicle built from lipids, detergents and proteins. Detergents can be removed by various methods, e.g. by polystyrene beads.

etc.), proteins have to be first reconstituted into SUVs. Once incorporated into liposomes, these so-called proteo-liposomes can be embedded in other bilayer structures.

Transmembrane proteins such as bacteriorhodopsin or the ATP-synthase will not integrate spontaneously into SUVs, but reconstitution has to be mediated by detergents [433, 434, 430]. The basic principle of reconstitution is sketched in Fig. 7.10. Proteins are dissolved in detergents, which produces binary micelles. In the ideal case, these binary micelles are monodisperse, i.e. one single protein is surrounded by several detergent molecules. The monodispersity can be monitored by measuring scattering losses by the suspension, which is easily performed by simple absorption measurement.

Proteins dissolved to binary micelles are then mixed with preformed SUVs. Insertion of binary micelles into vesicles occurs spontaneously which results in tertiary vesicles containing lipids, proteins and detergents. For most applications, the detergents have to be removed again. Different methods for the removal of detergents from vesicle suspensions have been described, including dilution, dialysis and gel filtration, but adsorption onto polystyrene beads (so-called biobeads) has become the method of choice nowadays [435, 436]. Reconstituted vesicles containing detergents are mixed together with fresh polystyrene beads for about an hour and this step is repeated at least three times by pipetting the vesicle suspension without the old beads to a fresh batch. The mass of beads should be tenfold the mass of detergents for each step. The resulting vesicles, proteo-liposomes, are nearly free of detergents. Proteoliposomes can be separated from non-reconstituted and free protein by ultracentrifugation.

Some protocols suggest to dissolve vesicles partially or completely by the addition of detergents prior to mixing with protein-detergent micelles [430]. This might enhance the efficiency of reconstitution. Again, solubilization of liposomes can be most easily monitored by measuring the turbidity of the liposome suspension.

Transmembrane proteins can not be reconstituted directly into GUVs as in SUVs, since detergents would destabilize the fragile GUV structure. Integration of transmembrane proteins therefore has to be performed by the detour of preparing SUVs first. There are basically two methods to obtain protein-reconstituted GUVs from preformed proteoliposomes. One way is to deliver proteins to GUVs by fusing proteoliposomes and preformed GUVs [432]. Although
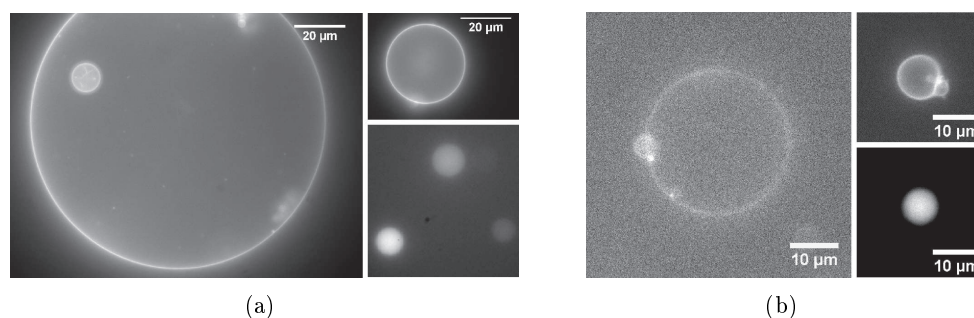
Figure 7.11: Giant unilamellar vesicles derived from proteosomes with proteins labeled by Alexa-488: (a) GUVs reconstituted with bacteriorhodopsin and (b) GUVs reconstituted with F1Fo-ATP-Synthases. The lower right images show control experiments for which only free dye and no proteins were used.

this is a very elegant method, it requires a complex lipid composition for the GUVs and further peptides for the SUVs which restricts its application to certain systems. Another method to obtain protein-reconstituted GUVs is the direct transformation of proteoliposomes into GUVs [431]. To do so, electroformation is performed using proteoliposomes as described in Sect. 7.7.2. The protocol of electroformation might be altered in order to meet requirements of the protein. For some proteins, it might be necessary to avoid complete dehydration of proteoliposomes in order to preserve protein integrity. This can be achieved by partial dehydration or dehydration under the atmosphere of a saturated salt solution.

Fig. 7.11 shows GUVs that were grown from proteoliposomes. Only proteins, bacteriorhodopsin and ATP-synthases, were fluorescently labeled. One can clearly see that the protein is attached to the membrane only. In order to verify that this is not fluorescence that is observed by the non-specific attachment for possible free dye, control experiments have been performed without labeled protein but with free dye (lower right images of each group in Fig. 7.11). In the control experiment, one can see that the free dye is only encapsulated into the vesicle but does not attach to the membrane.

Recently, it was reported that it is possible to deliver membrane proteins into GUVs neither by transformation of SUVs into GUVs nor by peptide-mediated fusion of SUVs and GUVs, but by spontaneous exchange of material between mixed GUVs and SUVs reconstituted with membrane proteins [437].

7.9 Unexpected but welcomed side effects of synthetic biology

Synthetic biology sometimes provides surprises which do not always have to be of negative nature. The following part explains, how synthetic biology helps observation in microscopy through magnification of the collective behavior of molecular structures. This section was published under the title in *Imaging & Microscopy* [438].

The history of cell and molecular biology displays an arms race between biological challenges and their technological solutions, regarding the detection and analysis of ever smaller structures and processes. For a long time, advancements in microscopy have kept pace with scientific motivations. But since fundamental physical laws cannot be simply overcome, appropriate instruments need to become more and more complex if modern biology does not simply want to stand still due to technical limitations. As a prominent example, the need to zoom further into biological matter in space and time recently sparked an explosion in sub-resolution techniques in microscopy. But is it actually always necessary to adapt our technology to the actual dimensions of biological matter if we want to understand fundamental processes? We know that biology

works on many scales. So why not just try and upscale biological phenomena?

In 1989, the movie *Honey, I shrunk the kids was released*, in which an unfortunate scientist develops a shrinking machine and accidentally shrinks his and the neighbor's children to the size of insects. In 1992, a sequel was released under the title *Honey, I Blew Up the Kid*. Justifiably, it eluded the success of the previous movie. Nevertheless, the idea behind the plot shall be of interest for us. This time, the unfortunate scientist - with the help of a new invention - inflates his 2-year old son to a 34 m-tall giant that starts to terrify Los Angeles in Godzilla manner.

Why not apply this concept to cell and molecular biology? If the structure or process of interest is too small to be observed with modern microscopy, why not just magnify the very phenomenon, instead of ever increasing optical magnification? Is this possible? Yes, under certain conditions, and the key to it seems to be an approach taken from synthetic biology.

Just to give an example: In the past ten years, membrane rafts have received much attention in the cell biology community. Until the mid-nineties, the cell membrane was generally viewed as a homogeneous fluid, in which membrane proteins are embedded. This view was challenged in 1997 by Simons and Ikonen [439], and by an avalanche of consecutive research work in the following years [103, 440]. According to this "raft hypothesis", lipids organize into domains within the plasma membrane, with physical properties that distinguishes the domains from the rest of the membrane. These physical properties can be, for example, lateral fluidity, surface tension, and thickness of the double layer structure. These domains, or rafts, are thought to play a major role in recruiting membrane proteins and controlling their function. The raft hypothesis is nowadays more or less accepted, with one blemish: no one has directly observed rafts in vivo so far. Many experiments point to their existence, but they could so far not be proven microscopically. Probably this will also not be possible for a long time, since rafts are assumed to organize on the nanoscale, and may have very fast turnover. Much effort is spent to make them "visible" by other means than optical microscopy, or just to indirectly prove their existence. An alternative to that would be to "blow up" these rafts so that they can be examined in a standard fluorescence microscope. This appears to be possible by leaving the *in vivo*-world and entering the field of synthetic biology of minimal systems [368]. When mimicking the cell membrane by artificial membranes containing specific raft-like lipid composition, phase separations of lipids appear as domains on the micrometer scale. These domains are supposed to be synthetic functional siblings of the assumed rafts in cells. Most importantly however, they distinguish themselves by their actual visibility in fluorescence microscopy. This, for example, has been achieved using supported lipid bilayers and giant unilamellar vesicles. The ability to make domains visible in minimal cell membrane-like systems yielded deeper insight into the features and functions of the hypothetical rafts [441, 394, 104, 400].

Is this application, blowing up molecular mechanisms from the nanoscopic to the microscopic scale by transformation of cellular processes into synthetic biology a singular example, or can this concept be transferred to other biological problems, e.g., fundamental ones such as structure and pattern formation? Here, we would like to present another demonstrative example of how membrane-related processes that elude quantitative fluorescence microscopy in vivo can be easily imaged and studied by subjecting the system to to a synthetic biology-like approach.The Min-system has proven to be another example of this unexpected but welcomed side effect of artificial membranes.

Loose et al. demonstrated that it is possible to transfer the self-organizing Min-protein system into an artificial environment [1]. Min-proteins did not only exhibit dynamic binding patterns represented as planar waves on supported membranes, but the scale of dynamics is increased about 10-fold compared to the cellular environment: on the artificial membranes, protein waves have a wavelength of about 50 to 100 µm, compared to about 5 to 8 µm in cells [188, 1]. This increase of the scale of the dynamics allowed us to study the cooperative behavior of Min-proteins

in much more detail than what could be achieved by in vivo studies.

A comfortable aspect of synthetic biology of minimal systems is that one can design systems with varying combinations of components. Loose et al. could prove, for example, that it needs only four components for the establishment of a dynamic protein pattern: a membrane, MinD, MinE and ATP. MinC itself is necessary for the inhibition of Z-Ring assembly at unwanted locations, but it is not necessary for the spatial positioning through the oscillation [1].

Another open question concerned the formation and nature of the MinE-ring that assembles close to the midcell position between the two polar caps in E.coli. In our in vitro measurements, we observe a linear gradient of MinE-concentration across a wave with a sharp peak at its rear. Different models have suggested dimerization of MinE-monomers or cooperative binding of MinE-dimers to the trailing edge. Dimerization of MinE-proteins upon binding to MinD could be excluded by FRET-measurements [92]. Cooperative binding of MinE-dimers from the bulk to the membrane was proven wrong, since freshly added MinE-proteins showed a homogeneous binding affinity to an existing Min-protein wave.

In summary, by combination of a synthetic "bottom up" approach of a biological phenomenon with single molecule techniques, we arrived at a better mechanistic understanding of the process. i.e., that the MinD-binding pattern is governed by a continuous migration of binding of MinD to the membrane, whereas MinE accumulates at the trailing edge by fast (quasi processive) re-binding of previously detached MinE-proteins. At the very end of the wave, the MinD-surface concentration on the membrane decreases, however, every MinD-dimer seems now to be occupied by a MinE-dimer. The addition of MinC to the system yielded further insight into the cooperativity of the system. Our minimal systems approach allowed, for the first time, the simultaneous observation of all three proteins in action. We could prove that MinE is required for the detachment of MinC. Analysis of wave profiles showed that MinC is actually not detached together with MinD and MinE, but that MinE actually displaces MinC from MinD.

Clearly, the concept of synthetic biology of minimal systems implies some negotiations with biological reality. After having resolved central molecular mechanisms in an extremely reduced system, the challenge is now to approach a more physiological situation again. In the reconstituted Min system, the main concern is now the spatial confinement of the Min-protein system in 2D and 3D, resembling the situation in a single cell. The goal is it not only to reproduce protein waves and determine their response to external constraints, but also to mimic true protein oscillations in closed volumes. The fact that the wavelength of Min-protein waves in our *in vitro* assay is about 10 times larger than their cellular counterparts allows us to use closed volumes that are still well in the range of microscopic imaging.

In conclusion, such a synthetic minimal systems approach can certainly not be generally applied for magnification of processes that elude optical microscopy in vivo. But synthetic biology indeed does open up new strategies for the quantitative study of biological processes, and among many other aspects, one should at least consider the possibility of rescaling of dynamical processes and structures.

7.10 Roadmap for bilayers in synthetic biology

Bottom-up synthetic biology always has been characterized by high goals in terms of mimicking biological cells as realistic as possible and at the same time by technical limitations. Whereas, in cell biology technical limitations nowadays are found rather in the field of observation, technical limitations in synthetic biology concern the production of cell-like structures. Supported lipid bilayers (SLBs) are one of the most reliable and reproducible artificial membrane models that it is currently at our hand. SLBs have definitely excelled in the past in terms of handling, reproducibility and flexibility. It can be obtained on nearly any hydrophilic surface with any
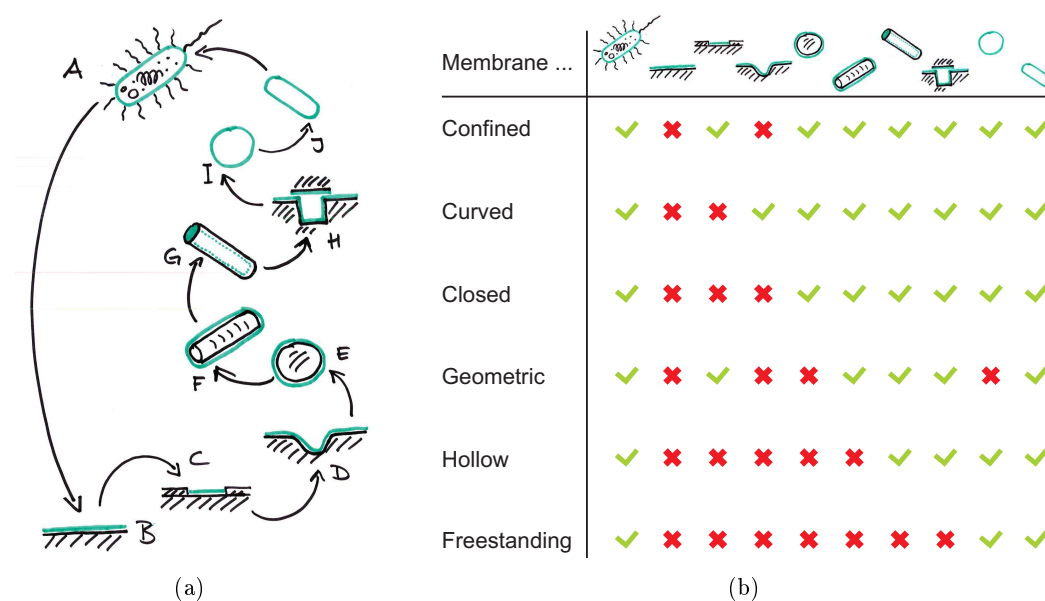
lipid composition that allows the formation of bilayers. Additionally, SLBs help the researcher by its convenient accessibility by microscopy: SLBs can be formed on transparent substrates and can be easily focused since only one single layer within the sample is of interest. Using purely lipid structures, also highly sophisticated structures up to complex networks of bubbles interconnected by lipid tubes can be built [442]. The difficulty starts, when it comes to protein reconstitution. Reconstitution of proteins is readily achieved using most basic representatives of artificial bilayers - supported lipid bilayers - but often fail in in more complex structures. These difficulties do not only concern the process of embedding the protein into the membrane itself but also more "trivial" steps. For example, if proteins shall be reconstituted on the inner leaflet of a GUV, how to deliver them to the inner volume without destroying the vesicle? Formation of GUVs in the presence of buffer already containing proteins often fail, either since the membrane proteins themselves require essential salts for protein function prevent formation of GUVs, or the GUV-formation requires a temperature gradient which would alter the structure and functionality of the proteins. Thus, although it is possible to build complex bilayer structures, when it comes to protein reconstitution, functionalization of biomembranes is often limited to supported lipid bilayers.

Therefore, we propose the roadmap described in the following in order to achieve complex lipid structures suitable for protein reconstitution. This approximation suggests a radical reduction of the biological cell to a simple bilayer structure from where to the bottom-up approach takes its start. Hereby, we propose supported lipid bilayers as the starting point in order to reach reconstruction of fully functional artificial membrane compartments. Then, after successful protein reconstitution protocols have been established, a slight modification of the bilayer shall be induced towards the desired direction, followed by readjustment of the protein reconstitution protocol. This strategy won't navigate us directly to our destination but we have to make stops in between. Fig. 7.12 illustrates such a roadmap starting at supported lipid bilayers and climbing the ladder of complexity up to vesicles with free-standing bilayers.

Thus, stops of the proposed road maps are the following. The most radical approximation of a cell membrane (7.12A) is a supported lipid bilayer (7.12B). Classical SLBs have no specific boundary and thus a more or less "infinite" surface area compared to the scale of cellular processes. However, cells have a limited membrane area. Therefore, the next step involves the confinement of the bilayer surface area (7.12C) which can be achieved surface modification of the support (see Sec. 8.1.3). In addition, this procedure allows the production of membrane patches of any two-dimensional geometry. Furthermore, cells do not have flat surface like SLBs but a curved membrane. Thus, next step is the integration of curvature into SLBs (7.12D). This step only requires high control of fabrication of the substrate and formation of supported lipid bilayers and though it is not very different from classical SLBs, the interaction of the membrane related biochemical system has to be carefully investigated. Though natural cell membranes have finite membrane area, they feature no lateral boundary which is achieved by complete closure of the membrane. Accordingly, the next step towards artificial membrane compartments would be the closure of the membrane accompanied by three-dimensional folding. This stage can be still achieved with the concept of supported lipid bilayers by formation of membranes on microscopic glass beads for example (7.12E). Geometry might play also a major role for many cellular processes; in consequence it is not only desirable to build artificial membranes in three-dimensional space but also to define the shape of these 3D-membrane structures. Thus, after having achieved spherical supported lipid bilayers, the next step would be to introduce various three-dimensional geometries (7.12F). All stages discussed so far are characterized by an open reaction volume above the membrane. Cells do not only feature a curved, confined and closed membrane but this membrane is also exposed to a nanoscopic reaction chamber, at least for intracellular processes. Thus, the next step requires not an inside-out but outside-in change of

perspective: closed bilayers with a hollow inner volume. Supports for bilayers can still be the key to such membrane compartments but require an ambitious process of microstructure fabrication. For example, a support with microscopic cavities could be combined with a lid whereat both are coated with an artificial membrane (7.12H). Completely closed reaction volumes might be a problem for the delivery of proteins and other essential components such as ATP. Thus, an intermediate step could be a semi-closed bilayer structure but with an open access. This can be for example achieved by membranes supported on the inner side of a glass capillary (7.12G). Next step is a big step: membrane compartments without supports but with free-standing bilayers (7.12I and J). As already pointed out, these can be obtained by the electroformation of lipid films to giant unilamellar vesicles.

This road map shall now be applied to the problem of oscillating Min-proteins. Previously, it was shown, that Min-proteins on unconfined supported lipid bilayers exhibit propagating wave patterns instead of oscillations observed in cells. In the following, we will show, how bilayers can be built according to our roadmap, how proteins are reconstituted and which resulting features can be observed. We will start by confining the available substrate area for wave propagation (7.12C), followed by the implementation of curvature into flat supports (7.12D). Curved supports mark the transition from two-dimensional to three-dimensional membranes. Finally, Min-protein waves on closed, curved membranes supported on spheres or elongated rods will be presented (7.12E and F). Unfortunately, internalization of Min-protein dynamics inside closed, hollow membrane structures (7.12 G to J) was not achieved but this aim was also outside the original scope of this PhD-project. However, we can show that such a roadmap of small steps is a promising strategy in order to develop protein reconstitution together with development of artificial membranes. On the other hand, the Min machinery has proven itself as a useful benchmarking system for testing bilayer structures.

Membrane ...	(A)	(B)	(D)	(E)	(F)	(G)	(H)	(C)	(I)	(J)
Confined	✓	✗	✓	✗	✓	✓	✓	✓	✓	✓
Curved	✓	✗	✗	✓	✓	✓	✓	✓	✓	✓
Closed	✓	✗	✗	✗	✓	✓	✓	✓	✓	✓
Geometric	✓	✗	✓	✗	✗	✓	✓	✓	✗	✓
Hollow	✓	✗	✗	✗	✗	✗	✓	✓	✓	✓
Freestanding	✓	✗	✗	✗	✗	✗	✗	✗	✓	✓

(a) (b)

Figure 7.12: Step-by-step roadmap from biological cells to artificial cells via low-aiming membrane structures. Concept of bottom-up approach using biomembranes (green). In the simplest approach, the principle of the uniquely shaped cell membrane of the biological system (A) is radically reduced to a flat supported lipid bilayer (B), the lipid bilayer can be laterally constricted by passivation of the support (C), or curvature can be introduced by three-dimensional structuring of the support (D). Closed supported bilayers can be achieved by coating beads (E) or rods (F). Hollow, closed biomembranes may be obtained by applying supported bilayers to cavities (G) whereas freestanding, hollow and closed biomembranes are realized with the help of the assay for GUV formation, as explained (H). Deformation of these may further be required to mimic spatial features of the original biosystem (I).

8 Materials and Methods

This section describes briefly general aspects of sample preparation and data acquisition. However, more specific sample preparation and data acquisition is described along with the results in the respective sections (see Chapter 9). Accordingly, data processing and analysis tools are also presented and explained directly on the basis of appropriate results.

8.1 Sample preparation

The principal components of a typical sample in this work consists out of the observation chamber, the lipid bilayer, a reaction buffer and the biochemical assay including the Min-proteins and ATP. In case of supported lipid bilayers, the support itself constitutes of course one of the decisive components. The description here covers the description of supports for SLBs, respective cleaning procedures, preparation of buffers, SUVs, SLBs, GUVs, oil-in-droplet emulsions and the protein reconstitution protocol.

8.1.1 Cover slides

Standard cover slides were obtained from Menzel (#1, 24 mm × 24 mm, Braunschweig, Germany) and from Corning (#1.5, 18 mm × 18 mm, Corning, USA). These had a specified thickness of 0.13-0.16 mm and 0.16-0.19 mm respectively.

8.1.2 Microcontact printing

The major interest of this work is to investigate the effect of lateral confinement of supported lipid bilayers and membrane geometries on the propagation of Min-protein waves. The basic idea in order to achieve laterally confined membranes of specified geometry was to passivate specifically the naked glass support in such a way that lipid can not form fluid membranes but in allowed regions. Upon addition of lipids, these adhere in consequence to the non-treated regions of the glass surface and only form a fluid membrane there. Various methods have been tested for specific passivation of glass supports against lipid adhesion. According to literature, such a passivation can be achieved by microcontact printing (µ CP)[445, 444, 446, 447]. This technology involves a surface modification with passivating molecules that adhere to the glass support but prevent lipids from binding. Different concepts of microcontact printing are presented in Fig. 8.1. Though different concepts were tested throughout this study, only the method shown in Fig. 8.1(a) (left) shall be discussed here.

In order to create a patterned surface modifications with passivated and non-passivated regions (for which lipid adhesion shall be allowed), the proposed way of application of passivating material is the transfer via a stamp. The stamp is incubated with the passivating material and this is transferred to the glass support by pressing the stamp to the support. By topological structuring of the stamp a patterned passivation can be achieved. Such structured stamps with topological features in the micrometer range can be achieved by creating PDMS templates from SU8-molds produced in standard photolithography. The stamping concepts covers several different protocols

(a)　　　　　　　　　　　　　　　　　(b)
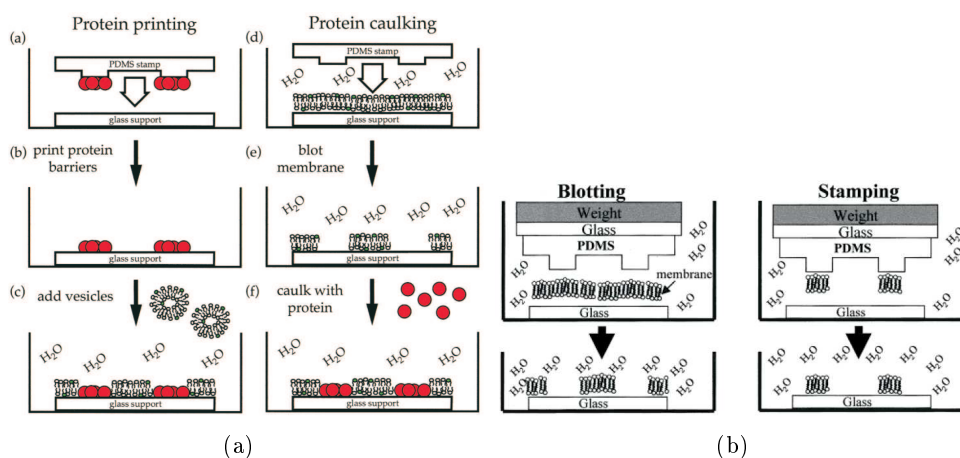
Figure 8.1: Four different concepts of structuring supported lipid bilayers through printing processes. All four concepts involve a template, usually made from PDMS, with a topologically structured surface whose pattern is then copied to a substrate. (a) Left: In classical microcontact printing, the template is incubated with a passivating material, for example BSA, and these are transferred onto a substrate by printing. Subsequently, lipid vesicles are added to the - originally hydrophilic - substrate. Lipids only adhere to regions without the passivating material which results in a negative copy of the template structure. (b) Right: Microstructured lipid bilayers can also printed directly to a hydrophilic support by incubation of the template with lipids yielding a positive copy of the template structure. Left: In blotting, a priorly formed supported lipid bilayer is patterned by partial removal of selective regions using a hydrophilic stamp which "catches´´ lipids like a magnet which gives a negative copy of the template structure. This method can be further extended by protein caulking (a, right). Stable barriers are built with proteins that are added to fill the blotted and empty regions. Image in (a) is taken from Ref. [443] an in (b) from Ref. [444].
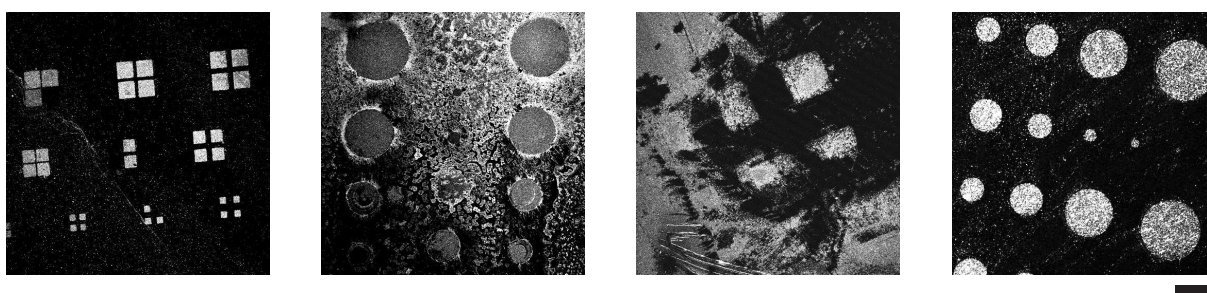
Figure 8.2: Microstructured supported lipid bilayers using microcontact printing with various passivating materials. From left to right: $50\,\mu gml$ BSA, $100\,\mu gml$, Biotin-BSA + Streptavidin + $1000\,\mu gml$ Biotin-BSA and APTS/GPTS + $1000\,\mu gml$ Biotin-BSA. All slides were cleaned with piranha solution (see Sec. 8.1.7). Scale bar is $200\,\mu$m.

with varying passivating material, stamps incubation methods and apparently mostly important stamping technologies ranging from hand stamping to stamping using specialized devices.

For the research project presented here, various passivating substances were tested including BSA and fibronectin. Printing procedure was also enhanced using mediating material such as biotin/streptavidin or APTS/GPTS as shown in Fig. 8.2. Respective protocols can be found in literature and shall not be further discussed at this point [448, 447, 449]. None of the tested materials could deliver any satisfying results. After transfer of the passivating material on the glass support and upon addition of lipids, either lipids bound everywhere, nowhere or binding was completely unspecific and unrelated to the printed pattern. In case that a printing procedure yielded successful membrane patterns, these were far from being reproducible. Further variation of the cleaning procedure of the stamp, concentrations of the passivating material, incubation time of the stamp in the passivating material, rinsing procedure of the stamp after incubation and rinsing procedure of the glass substrate after printing did not yield any improvement (data not shown). Solely, investigation of different cleaning methods of the glass substrate prior printing revealed that this step is crucial for best microcontact printing results. Among different cleaning procedure, the protocol involving the piranha solution seemed to provide the best results. However, "best" in these terms still has to be understood in a relative way. None of the procedure was appropriate for studies requiring high numbers of reproducible microstructured supported lipid bilayers. Thus, this method was abolished and the author strongly discourages further attempts of stamping passivating material in order to achieve patterned membranes. Alternatively, I suggest using microstructured metal surfaces. Next to the welcomed fact that they work, metal microstructures also excel by the fact that that they can be reused and samples are prepared in a simple and fast manner.

8.1.3 Gold microstructures

Protocols to use metal microstructures in combination with SLB technology were developed by Groves et al. [450, 451]. The idea is to coat substrates, which are intended for the use with supported lipid bilayers, with a pattern of a metal or metal oxide layer. The metals or metal oxide shall prevent lipids from forming a functional membrane and thus functional membranes are only obtained in regions which are free from metals or metal oxides. As passivation material we tested aluminum, chrome and gold. Since the first two did not withstand the cleaning procedures required for SLB formation, we finally chose gold as the passivating metal for microstructured supports.

Microstructure blueprints were designed using AutoCAD 2004. Examples are shown in the appendix. Gold microstructures were produced by Dr. Ingolf Mönch from the Leibniz Institute for Solid State and Materials Research Dresden (Germany) and carried out by standard photolithography in a class 100 clean room. Fused silica glass wafers ($3''$, two sides polished; by Semiconductor Wafer, Inc.) were cleaned in Piranha solution (see Sec. 8.1.7) for 30 min at 90°C, rinsed in water and dried. Subsequently, the glass was covered by a Cr(5nm)/Au(50nm)-layer using electron beam evaporation with condensation rates of 0.1 nm/sec (Cr) and 0.3 nm/sec (Au), respectively. This Cr/Au layer was spin-coated with photoresist (ARP 3510, Allresist GmbH, Straussberg, Germany, 3500/min, 35 sec), which was exposed to UV light through a Cr mask (mask aligner MA 56, Suss microtec, Garching, Germany; 365 nm, 275 W, 8 sec) and developed (AR 300-35, Allresist GmbH, Straussberg, Germany; diluted with water 1:1). Exposed regions of the Cr/Au layer were removed by ion-beam etching. The substrate was decollated using a dicing saw (Disco Corporation, Japan) into single square chips of 10 – 15 mm edge length. In order to protect the gold microstructures against swarfs, the surface was coated with a lacquer prior to that. Before usage this protective layer had to be removed by rinsing the gold structure chips with acetone.

(a)

(b)   (c)   (d)
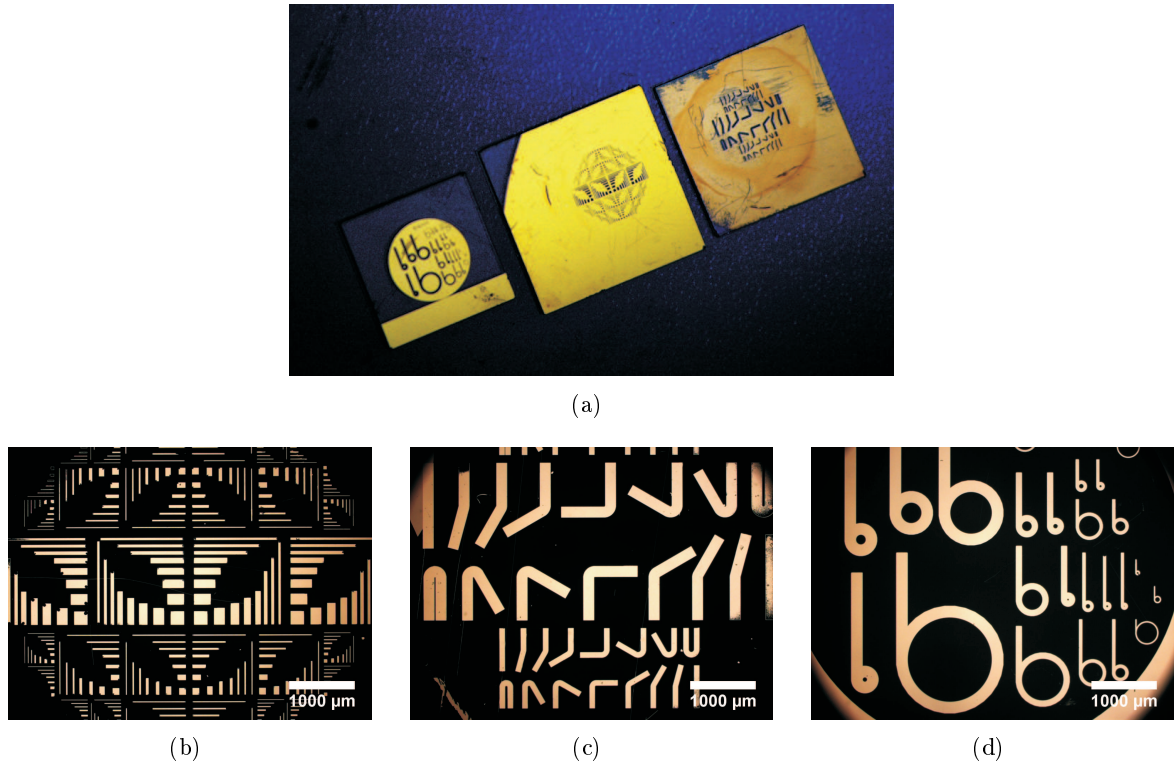
Figure 8.3: Gold micro structures. Photographs b) - d) were taken with a microscope using transmitted light. Therefore, gold areas appear as black.

8.1.4 Flat substrates with grooves

Macroscopic flat supports with three-dimensional, curved surfaces in the microscopic range were fabricated in various manners. Principally two different approaches were applied. Either the surface of glass substrates were directly modified. Alternatively, SU8-structures were brought of silicon-substrates which then served as molds to produce thin PDMS-films with carrying a copy of the microstructure. These PDMS-films were then transferred onto glass supports.

Glass substrates with troughs were obtained either from Dr. Ingo Mönch from the IFW Dresden or from Yaron Caspi from the Technical University of Delft.

Microstructures from the IFW were obtained by electron beam lithography as depicted in Fig. 8.4 and as described elsewhere [452]. In brief, a 70 nm layer of Tantalum was deposited on the surface of a glass substrates, followed by the deposition of a 100 nm layer of photoresist (AR N 7520.18, Allresist) through spin coating (8000 $1/\mathrm{min}$ for 35 s) and subsequent curing (85°C
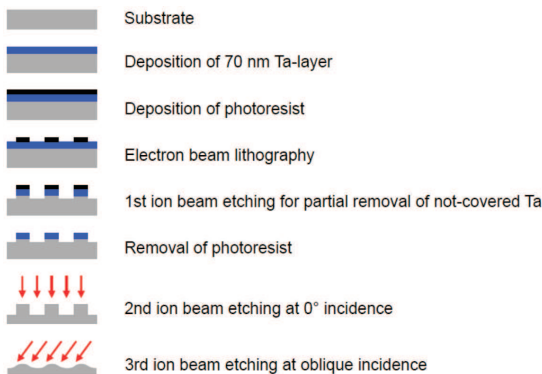
Figure 8.4: Fabrication of glass substrates with a trough topology using e-beam lithography. Image is taken from Ref. [452].

for 3 min). Structures were drawn into the photoresist by electron beam lithography using a scanning electron microscope (Hitachi S4500, Hitachi High-Technologies Corporation, Tokyo, Japan). Exposed regions of Tantalum were removed by ion beam etching. With this step, also glass material beneath the erased Tantalum regions were partially removed as well as shown in 8.4. Photoresist was removed and a second run of ion beam etching enhanced depth of the troughs created in the first run. The rectangular profile of the resulting structure was transformed into a curved topology by a third etching process with ion beams at various irradiation angles (IonSys500, Roth&Rau, Wüstenbrand, Germany).

The glass microstructures prepared by Yaron Caspi were also fabricated with electron beam lithography, however using a different protocol. A $2\,\mu m$ (expected value) layer of SiO_2 was brought onto previously cleaned cover slides by plasma-enhanced chemical vapor deposition (PECVD; Plasmalab 80 Plus by Oxford Instruments Plasma Technology with following parameters: 40 min at 300°C with a pressure of $p = 997\,mTorr$ under an atmosphere of $8.5\,sccm$ SiH_4, $710\,sccm$ N_2O, and $165\,sccm$ N_2) followed by a second layer of α-Si of 70 nm thickness (3.5 min at 250°C with a pressure of $p = 997\,mTorr$ under an atmosphere of $25\,sccm$ SiH_4 and $478\,sccm$ Ar). A 50 nm layer of Chromium was sputtered on top on the α-Si-layer (AC450, Alliance Concept; 2.5 min, 100 W, 20 μbar, 90-100 V). Photoresist was then spread over the surface (950K8A Poly(methyl methacrylate) (PMMA) in anzinol using a spin coater at 1000 rpm for 55 s) and cured at 180°C for 60 min. Structures were drawn into the the photoresist layer with an electron beam (EBPG5000Plus HR 100 by Vistec; dose of $1050\,\mu C/cm^2$, 20-150 nm resolution and 50-150 nm beam step size). The resulting mask was developed in a mixture of Methyl isobutyl ketone (MBIK) and isopropyl alcohol (1:3 v:v) for 3 min and subsequently rinsed in isopropyl alcohol for 30s. Residues were removed by a process known as descumming using a Tepla stripper (by Tepla; $50\,sccm$ O_2, 42 W, at 0.34 mbar for 20 s). Chromium was etched at regions where the photoresist had been removed using a Chromium etcher (application for 2.5 min). Chromium etching was then followed by etching of the exposed α-Si regions using a process called deep reactive ion etching (AMS 100 I-speeder by Adixen; $120\,sccm$ SF_6, $120\,sccm$ O_2 at 0.0023 mbar, 2 kW, bias 60 V, 10°C, at a distance of 200 mm for 40 s). Photoresist was removed by bathing the structure in acetone at room temperature for 15 min and the subjacent chromium layer was removed by action of a chromium etcher (5 min). The glass substrate was further etched again by the AMS 100 I-speeder by two subsequent runs (first run: $30\,sccm$ C_4F_8, $10\,sccm$ CH_4, $100\,sccm$ He at 0.0023 mbar, 2.5 kW, bias 300 V, 10°C, at a distance of 100 mm for 2.5 min; second run: $50\,sccm$ SF_6, $100\,sccm$ He at 0.0023 mbar, 2.5 kW, bias 20 V, 10°C, at a distance of 100 mm for 1 min;). In a final step, the α-Si, Chromium and photoresist layer was removed by bathing the substrate for 8 min in acetone at 45°C, for 5 min Chromium etchant and for 7 min in KOH at 70°C (all information about this process through personal communication by Yaron Caspi (TU Delft)).

8.1.5 PDMS wells

Membrane-coated compartments were achieved by the assembly of SLBs on microstructured PDMS. Microstructured PDMS were obtained from a mold composed of photoresist microstructures on silicon wafers. Optionally, micron-sized PDMS wells could be closed with a cover slip after SLB-formation and protein reconstitution.

8.1.6 Microbeads and microrods

Micron-sized glass beads were obtained by courtesy of Sophie Pautot (Biotechnological Center / TU Dresden, Germany) and purchased from Whitehouse Scientific, Ltd (USA). Glass rods were prepared from dismantled telecommunication glass fibers that were cut into little segments up

between 200 to 700 µm by a special cutter. The work was carried out by Jens Peupelmann from the Communications Laboratory of the TU Dresden, Germany.

8.1.7 Surface cleaning

Supported lipid bilayers can be obtained by fusion of SUVs (see Sec. 8.1.11) to hydrophilic surfaces, which have to be free from fatty or amphiphilic molecules. Such surfaces can be obtained by cleaving mica into sheets of µm-thickness which were then clued to a cover slip by UV-glue. Since mica has to be cleaved shortly before the formation of SLBs, it is not suitable in combination with metal microstructures.

Glass surfaces such as simple microscopy cover slides, glass substrates with structured surfaces, gold microstructures on glass slides, PDMS, glass micro beads and dismantled telecommunication fibers ("glass micro rods") can serve as supports for SLBs after intensive cleaning. Three different protocols were applied in this work:

Detergents/EtOH: Sonication of surfaces for 20 min in a detergent solution (for example 3 % mucasol), rinsed with dH_2O, followed by 20 min sonication in EtOH and final rinsing with ddH2O.

Alkaline washing: Sonication of surfaces for 20 min in a 0.5 % Extran solution, followed by two further sonication cycles in ddH2O (each 20 min). Extran solution had to be freshly prepared and could not be used longer than 3 days. Used solutions could be disposed directly to the sink.

Piranha solution: This cleaning protocol proved to be most effective but has several drawbacks concerning safety and environmental issues. The cleaning effect is provided by the oxidizing effect of peroxymonosulfuric acid which again is the reaction product of sulfuric acid and hydrogen peroxide:

$$H_2O_2 + H_2SO_4 => H_2SO_5 + H_2O \qquad (8.1)$$
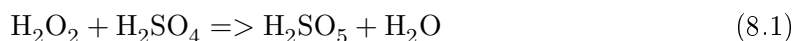
The piranha solution was prepared with 70 % sulfuric acid and 30 % hydrogen peroxide. Surfaces such as glass slides and gold microstructures were incubated in the piranha solution for 10 min and subsequently rinsed eight times in deionized water (ddH_2O). For disposal, used piranha solutions were diluted 1:10 in water and subsequently neutralized by the careful titration of 10 M KOH until a pH in the range of 5-8. Since the neutralization of the piranha solution takes place via an exothermic reaction with strong heat development, the beaker was placed in an ice bath. Since the solution boils up heavily upon addition of KOH, a beaker with a volume 5 times larger than the solution volume should be used. Before disposal, the neutralized solution was again diluted 1:5 by water.

For sonication a bath sonicator was used (USC100TH, 45 kHz, VWR International, Germany). The piranha solution was only used for glass slides and gold microstructures. In the case of micron-sized particles such as glass beads and rods, these were centrifuged to the bottom of a test tube before exchanging the aqueous media for rinsing. Cleaned surfaces were stored in ddH2O at 4°C.

SLBs formed on glass supports cleaned by detergents and EtOH showed a homogeneous structure and functional lateral fluidity. However, in combination with Min-proteins, the method using detergents and EtOH yielded non-reproducible results in terms of protein waves. Cover slides cleaned by piranha solution proved best quality of protein waves, characterized by parallelism and reproducibility. This advantage is thwarted by a high input of material and time

Figure 8.5: Reaction and observation chamber built from a Eppendorf tube. (A) cover slide or other glass support, (B) mica (optional), (C) UV-glue, (D) cut plastic test tube, (E) supported lipid membrane, (F) buffer and (G) schematic view of cutting the plastic test tube (Eppendorf, 05 ml).
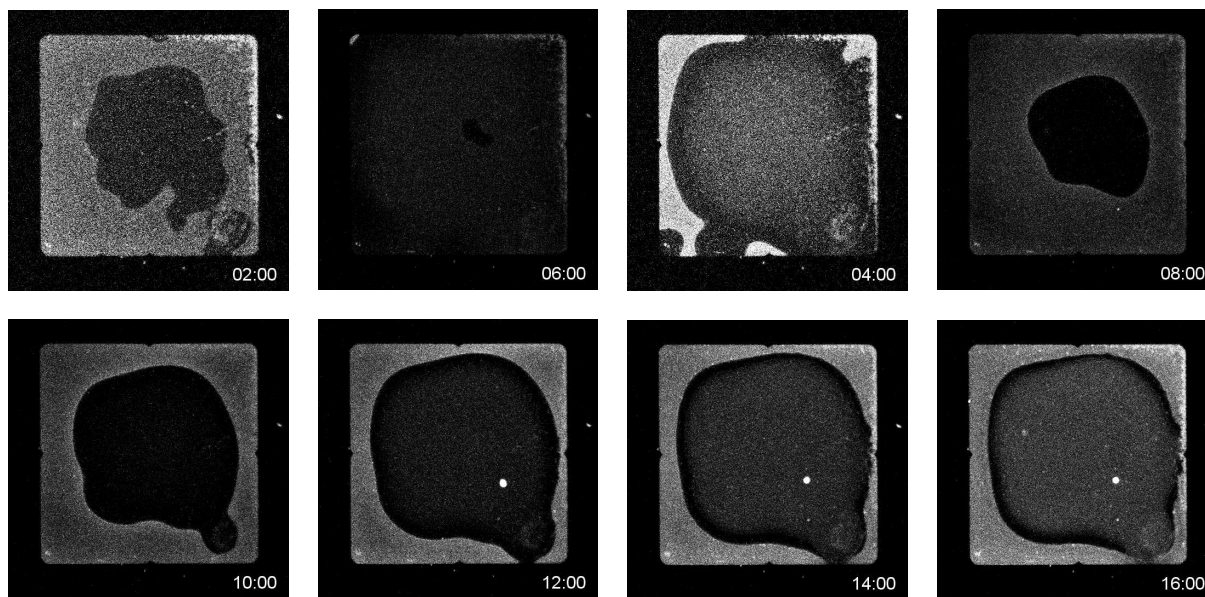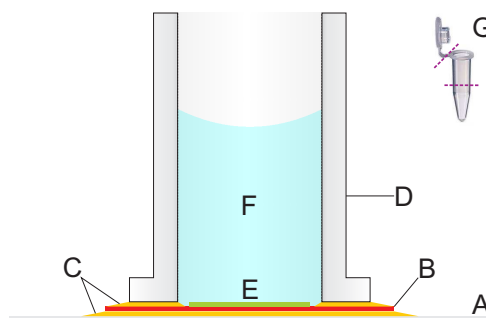
Figure 8.6: Freezing protein waves. Time counter indicates minutes and seconds (min:sec). Whereas Min-protein waves still propagate for the first minutes, they start to slow down after about 10 min of illumination with the LSM until they stall completely. Scale bar is 50 µm.

accompanied by high environmental impacts. The method using Extran is easy, cheap and can be executed at a high frequency. Quality of protein waves formed on supports cleaned by Extran is only slightly inferior to that using supports prepared by piranha solution. Thus, for the results presented here, glass supports, cover slides and gold microstructures, were cleaned by Extran.

8.1.8 Reaction and observation chamber

For protein reactions on and microscopy observation of glass microbeads or microrods in microscopy, GUVs and droplet-in-in-oil emulsions, these were given into a standard microscopy observation chambers (Lab-tek chambered cover glass, Nalge Nunc International, USA) containing the reaction solution (for example proteins and ATP). In the case of flat surfaces such as simple glass slides, mica, gold structures and PDMS, a small plastic tube was glued onto the support as shown in 8.5. When using mica sheets, gluing of the mica sheet and the plastic tube could be done in parallel. For gluing, a UV-glue was used (Norland Optical Adhesive, Cranbury, USA, Type 63, Lot 114). This glue solidifies upon irradiation with UV-light. For UV-irradiation, a UV-lamp (NU-6 KL, Benda, Wiesloch, Germany) with a 254 nm and a 366 line of 6 W power each was used for about 15 min. In case of SLB samples, it is absolutely necessary to guarantee complete solidification of the UV-glue which was achieved by irradiation for at least 10 min.
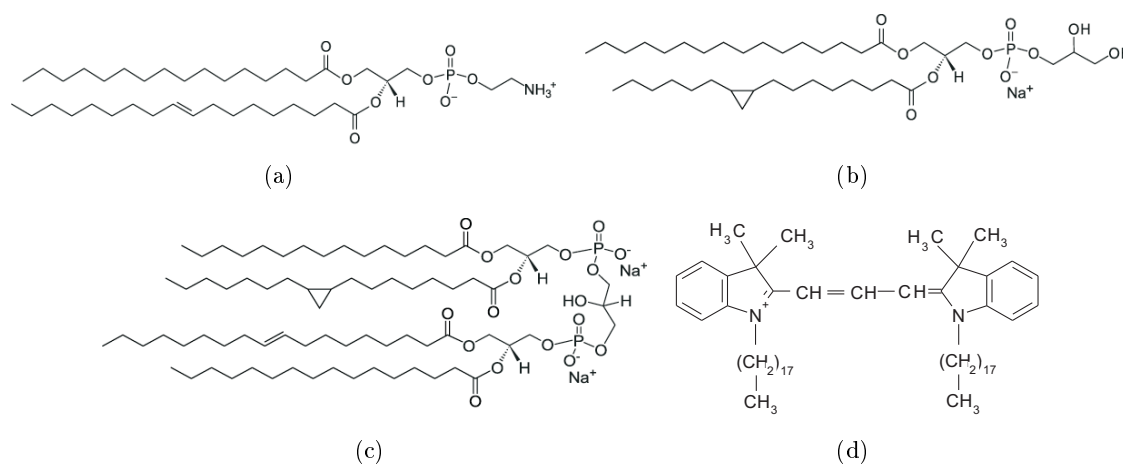
Figure 8.7: Lipids (a) -c)) and fluorescent membrane probes (d) used in this study. (a) Phosphatidylethanolamine (PE), MW = 719.3. (b) Phosphatidylglycerol (PG), MW = 757.0. (c) Cardiolipin (CA), MW = 1435.6. (d) 1,1'-dioctadecyl-3,3,3',3'- tetramethylindocarbocyanine perchlorate (DiI-C_{18}), MW = 1435.6. (MW = molecular weight). Lipid structures by Avanti Polar Lipids, Inc. DiI structure by Life Technologies Corp.

Shorter irradiation times down to 3 min seemed to be solidified on a macroscopic scale as well. For such a short irradiation duration, the plastic tube still seemed to be fixed in a stable manner to the support. However, for irradiation times less than 10 min it could happen that later on during experiments, the Min-protein waves showed abnormal behavior. Min-protein binding patterns "freeze" upon observation by laser scanning microscopy: wave propagation slowed down until it was completely stalled (Fig. 8.6). Apparently, due to insufficient irradiation duration, non-solidified glue migrates into or onto the bilayer. As long as no light is directed onto the bilayer, the membrane preserves its fluidity. But upon imaging using laser light the glue presumably solidifies and immobilizes the membrane which can be observed by Min-proteins that transform from propagating waves to immobilized patterns within minutes.

For the formation of SLBs the naked support should be exposed as shortly as possible to air. In our case, mica sheets or glass supports were mounted together with the plastic tube immediately after cleaving or cleaning respectively. After solidification of the UV-glue, lipid suspensions or other solutions were added without any delay to prevent dust to settle on the clean surfaces.

8.1.9 Liposome and reaction buffer

For the formation of liposomes, supported lipid bilayers and for the protein assay the same buffer was used and is referred as K-SLB buffer. This buffer contained 25 mM TRIS, 150 mM KCl and 5 mM $MgCl_2$. The pH was adjusted to 7.5 was regulated by the addition of hydrochloric acid (HCl). $MgCl_2$ is in fact only necessary for the ATP hydrolysis of MinD and therefore could be omitted for the formation of vesicles and the supported lipid bilayer. However, for reasons of convenience, the same buffer was used for all steps of sample preparation and experimentation.

8.1.10 Lipids

E. coli polar lipid extract was purchased in powder form from Avanti Polar Lipids Inc (Alabaster, USA) and contained 67 % Phosphatidylethanolamine (PE), 23.2 % Phosphatidylglycerol (PG) and 9.8 % Cardiolipin (CA). Molecular structures are shown in Fig. 8.7a) - c). Note that the percentages of the purchased lipid mixture differ from that found in literature (see Sec. 1.1.2).

(a)   (b)
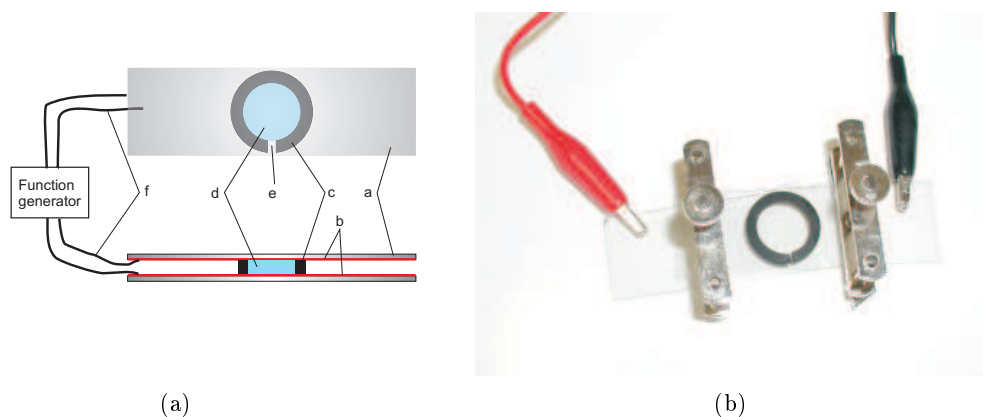
Figure 8.8: Chamber for the electroformation of giant unilamellar vesicles. (a) Principle: a) glass slide, b) ITO coating, c) rubber ring, d) buffer, e) opening, f) electrical connection. (b) Photograph.

8.1.11 Small unilamellar vesicles

Lipids were dissolved in $CHCl_3$ to a clear solution (reag. ISO, reag. Ph. Eur., 99.0-99.4 %, Sigma-Aldrich Chemie GmbH, Steinheim, Germany). A dried lipid film was obtained by evaporating the organic solvent mixture under a gentle N_2-stream while continuously rotating the lipid solution containing glass flask. Solvent evaporation was completed in vacuum for about 20 min with the help of a rotary vane vacuum pump (RZ 5, Vacuubrand, Wertheim, Germany). K-SLB-buffer was added to the lipid film to a final lipid density of 0.533 mg/ml. Heavy mixing of the lipid suspension yielded the formation of multilamellar vesicles, which were subsequently sonicated to a clear suspension which indicates the formation of small unilamellar vesicles (SUVs) with a bath sonicator (USC100TH, 45 kHz, VWR International, Germany). SUVs could either be used right away or were frozen in liquid nitrogen and subsequently stored at -20°C.

For fluorescent bilayers, 0.1 % DiI-C18 (Life Technologies Corp., Grand Island, USA) was added to the organic lipid solution.

8.1.12 Formation of SLBs

75 µl of a 0.533 mg/l vesicle suspension were shortly sonicated and applied to the supports as soon as possible after their surface treatment (see Sec.8.1.7). 2.3 µl of a 100 mM $CaCl_2$ solution was added in order to facilitate the fusion of the bilayers to the surface by shielding the double layer forces. The lipid suspension was incubated on the support for 15 min at 39°C to allow lipid rearrangement above the transition temperature of *E. coli* polar lipid extract.

After incubation, vesicles that have not fused with the supported were washed away by flushing and pipetting the chamber with 5× 400 µl of the K-SLB buffer. After washing, 200 µl of the same buffer were given to the chamber. Quality of the SLB, e.g. homogeneity and and fluidity was verified by LSM and FRAP (see Sec. 8.2.1 and 8.2.2).

For glass beads and rods, glass particles were mixed with 75 µl of the 0.533 mg/l vesicle suspension and 2.3 µl of a 100 mM $CaCl_2$ solution for 15 min at 39°C using a thermomixer followed by two washing cycles with K-SLB-buffer. Before exchanging the media, glass particles were centrifuged to the bottom of the test tube.

Once SLBs were formed, these could be used for several days. Between experiments they were stored at 4°C.

8.1.13 Formation of giant unilamellar vesicles

Giant unilamellar vesicles were obtained by electroformation in custom made electroformation chambers as shown in 8.8. Thin lipid films of about 1 cm^2 were applied onto two ITO-glass slides (indium tin oxide coating by Präzisions Glas & Optik, Iserlohn, Germany; 25 mm × 75 mm × 1.1 mm, $< 10\,\Omega\,\text{mm}^{-2}$) by pipetting small volumes onto the surface. Lipid films for electroformation can be either obtained from organic solutions or aqueous suspensions. In the first case, the lipid film was exposed to vacuum to guarantee complete evaporation of organic solvents. In the case of aqueous lipid suspensions, the lipid film was obtained by slow evaporation in an excicator.

8.1.14 Droplet-in-oil-emulsions

Aqueous droplets surrounded by a lipid monolayer were achieved as so-called droplet-in-oil emulsion [407, 453]. *E. coli* polar lipids were mixed into hexadecane to give a 10 mM oil/lipid mixture which was given into an observation chamber (see Sec. 8.1.8). Using a pipette, small droplets in the microliter-range containing the Min-protein assay (Sec. 8.1.16) were immersed into the mineral. Lipid molecules organized at the oil/water-interface and could be imaged in fluorescence microscopy (Sec. 9.4.3). Droplets were stable over days.

8.1.15 Protein purification and fluorescent labeling

Proteins were purified and fluorescently labeled as described elsewhere [1, 346]. The work was carried out by Martin Loose and Ariadna Martos.

8.1.16 Reconstitution of Min-proteins

Min-protein waves were initiated by the addition of Min-proteins to an existing bilayer built from *E. coli* lipid extract as described previously in the Sec. 8.1.12 and 7.7.2. The reaction volume was 200 µL and final standard protein concentrations were 0.8 µM MinD, 0.45 - 1 µM MinE and 0.25 µM MinE labeled with Cy5. Exact volumes of added protein had to be readjusted from time to time since aliquots obviously contained different protein concentrations. Proteins were well mixed by flushing the sample with a pipette in order to guarantee homogeneous distribution of proteins and to dissolve protein aggregates that have formed after purification as far as possible. Upon the addition of ATP (final concentration 2.5 mM) protein waves emerged. Within the same sample and under good conditions, protein waves could be observed for up to 5 days.

8.2 Data acquisition

Different technologies were applied for observation, however all base on fluorescence principles. These include basic imaging using LSM (laser scanning microscopy), FRAP (fluorescence recovery after photobleaching) and FCS (fluorescence correlation spectroscopy)

8.2.1 Imaging

Image data was acquired by confocal laser scanning microscopy using a confocal Zeiss LSM 510 Meta as shown in Fig. 8.9. Confocal laser scanning microscopy is an advancement of classical fluorescence microscopy. As in widefield fluorescence microscopy, excitation light is reflected by a dichroic mirror through an objective into the sample. Fluorescence is collected by the same objective, transmitted by the dichroic mirror and focused into the image plane. In widefield microscopy the fluorescence signal is recorded using an array-like charged coupled device (CCD).

(a)   (b)
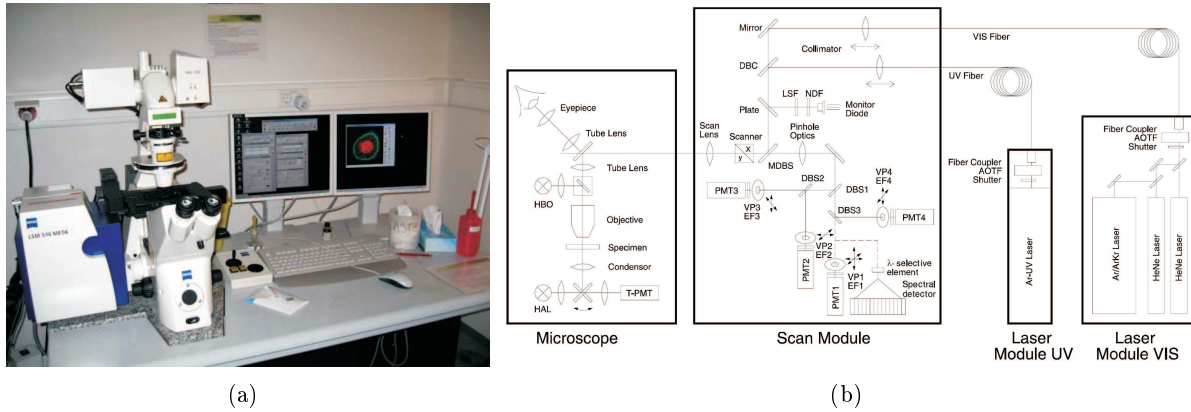
Figure 8.9: Photo (a) and sketch of the principle (b) of the confocal laser scanning microscope (Zeiss LSM 510 Meta). Photo by the courtesy of the Light Microscopy Facility of the Biotechnological Center of the TU Dresden. The sketch is taken from Ref. [454].

In classical wide-field fluorescence microscopy only the focal object plane is focused, from all other planes above and below no image information can be obtained. Nevertheless, since the sample volume is illuminated using a parallel beam with Gaussian intensity distribution in plane (the x/y-plane), all planes are excited with the same extent. In consequence, all planes contribute to a background fluorescent signal which reduces the signal-to-noise ratio (SNR). This disadvantage can be resolved by confocal laser scanning microscopy where the excitation light is focused into a small spot that is scanned across the plane of interest within the sample volume. By this, only the plane of interest gives rise to a fluorescence signal whereas the other remain dark. In addition, the focal depth (z) is determined by the diameter of a pinhole that restricts the image of the focal excitation volume in the image plane.

In order to scan the focal volume across the plane of interest in the sample volume, the laser beam has to be deflected in the excitation path before the objective. In practice, this achieved using two mirrors controlled by galvanometer. In contrast to widefield microscopy, the fluorescence signal is recorded by a point detector. In our system, this was a photo multiplier tube (PMT). The image information is then reconstructed using the coordinates from the scanning focal excitation volume.

In the case of the gold microstructures, magnification was limited to 10x and 20x objectives due to the restricted working distances of objectives with larger magnification (Zeiss EC Plan-Neofluar: 10x, NA 0.3 with a working distance of 5.2 mm, and 20x, NA 0.5 with a working distance of 2 mm). These objectives also allowed a relatively large field of view and therefore the ability to image several wave trains in one frame. Therefore, these objectives were also used for most micrograph acquisitions. For few experiments, a greater magnification was necessary, and thus, a 40x-objective was employed (Zeiss C-Apochromat, 40x, NA 1.2 with a working distance 0.28 mm) For greater magnification a MinE was labeled with Cy5 and therefore excited with a 633 nm helium-ion laser.

Images were obtained with varying resolutions up to 1024×1024 pixels (1 pixel = 0.11 to 2.54 µm). The standard frame number was 15 and the standard time interval was 20 s. For long time lapses up to hours the interval was set to durations from 1 min up to 10 min. For large overview micrographs covering several square millimeters multiple adjacent frames were acquired and subsequently stitched together.

Recorded data was stored and managed by the ZEISS AIM software.

(a)   (b)
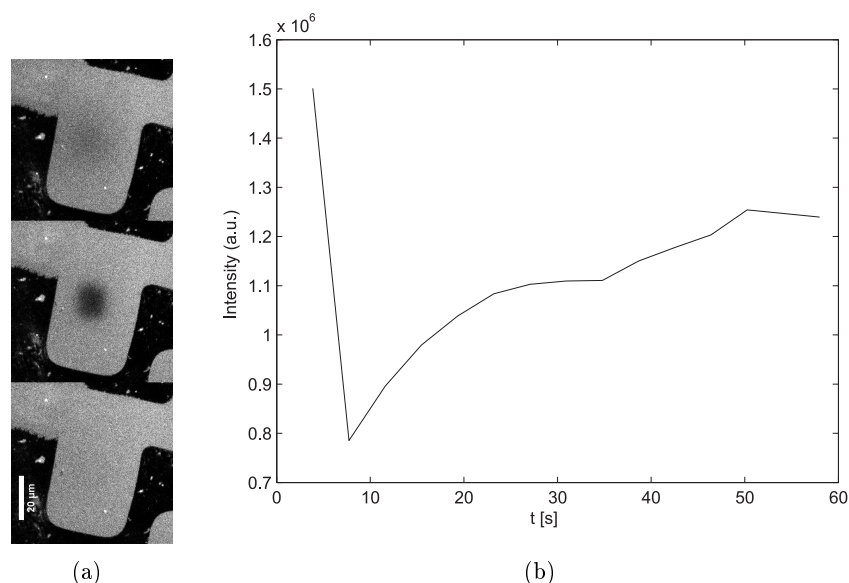
Figure 8.10: Photobleaching and fluorescent recovery of supported lipid bilayer. (a) Laser scanning micrographs before, shortly after and long after photo bleaching. A small region within in the bilayer is bleached which is observed by reduced fluorescence. Fluorescence recovers after some seconds. (b) Intensity of the bleached region versus time.

8.2.2 Fluorescence recovery after photobleaching

The fluidity of a membrane can be verified by a technique called fluorescence recovery after photobleaching (FRAP) [455]. The fluorescence capability of most molecular dyes can be destroyed by irradiation with high light intensity, which is known as photobleaching. A small region of the membrane is photobleached by scanning the laser of the LSM at high power across the membrane which results in decreased fluorescence signal within this specified region (Fig. 8.10(a)). If the membrane is in the fluid state, membrane probes that were outside the irradiated area diffuse laterally into the previously bleached region and the fluorescence signal increases again (Fig. 8.10(b)).

8.2.3 Fluorescence correlation spectroscopy

Classical fluorescence microscopy can reveal basic structural information and dynamics on the ensemble level and on a rather slow scale. If molecular dynamics and kinetics shall be investigated on the single molecule level and on fast timescales such as in the microsecond range or even faster, fluorescence correlation spectroscopy (FCS) is the method of choice [456, 457, 458, 393]. In fluorescence correlation spectroscopy, a small excitation volume is produced by focusing laser light with a microscope objective as depicted in Fig. 8.11 to a diffracted-limited spot. This focal excitation volume can be approximated by a Gaussian-Lorentzian intensity distribution and has an effective lateral diameter of 0.3 to 0.5 µm in classical FCS setups. When fluorescent particles diffuse into this excitation volume, they are excited and emit a burst of photons which is collected by the same objective and directed through a pinhole onto a sensitive point detector such as an avalanche photo diode (APD). The task of the pinhole is to crop the detection volume to an ellipsoid. In practice, the pinhole is often realized by a optical fiber that is attached to the detector. Due to this concept of double-focusing in excitation and detection, such a setup is called *confocal*. The time-resolved photon count rate F is auto-correlated by a time gap τ to
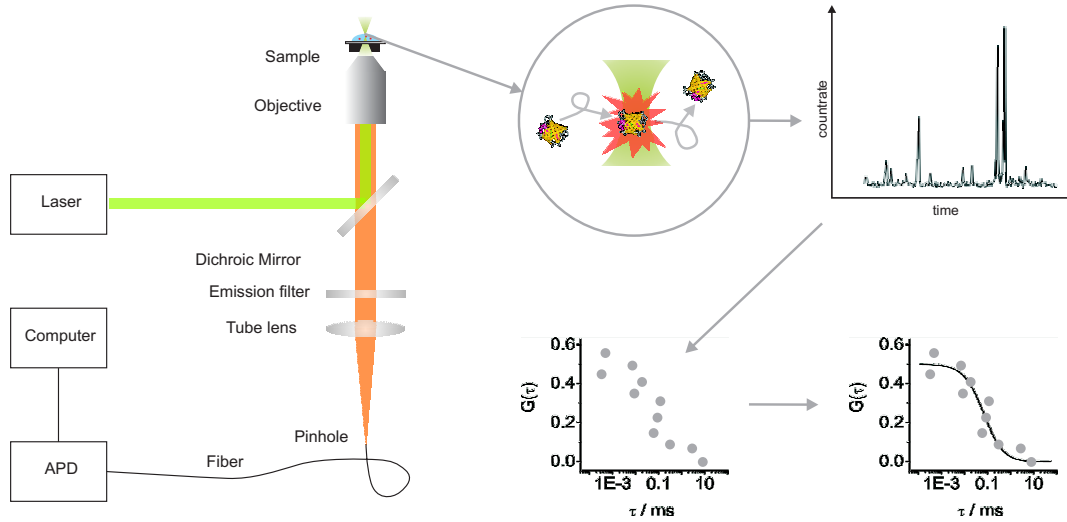
Figure 8.11: Principle of fluorescence correlation spectroscopy. Laser excitation is focused into a small focal volume. Fluorescent molecules diffusing into this excitation volume give rise to fluorescent bursts which can be detected by avalanche photo diodes (APD). Autocorrelation of the photon counts provides the autocorrelation curve which yields the concentration and diffusion coefficients of single molecules.

$$G(\tau) = \frac{\langle \delta F(t) \cdot \delta F(t+\tau) \rangle}{\langle \delta F(t) \rangle^2}. \tag{8.2}$$

The resulting auto-correlation data can be fitted to a very basic model describing the probability of diffusion within the focal excitation volume:

$$G(\tau) = \frac{1}{N} \cdot \frac{1}{1 + \frac{\tau}{\tau_D}} \cdot \frac{1}{\sqrt{1 + \frac{\omega_0^2}{z_0^2} \frac{\tau}{\tau_d}}}, \tag{8.3}$$

where N represents the mean number of particles in the confocal volume which corresponds to the local concentration. τ_D is the diffusion time within the confocal volume and is related to the general diffusion coefficient D by

$$\tau_D = \frac{\omega_0^2}{4D}. \tag{8.4}$$

z_0 and ω_0 are structural parameters of the detection volume that are determined by calibration measurements with fluorophores for which the diffusion coefficient is known.

9 Results

In this chapter, I present the experimental results which were obtained within the framework of this PhD-thesis. Previous *in vitro* experiments using Min-proteins were limited to self-organization and wave propagation on unconfined and flat artificial membranes, mostly supported lipid bilayers (SLB) (Sec. 4.9). The concept of artificial membranes is to mimic cellular membranes (Sec. 7.6). However, when comparing SLBs and cellular membranes, differences can still be found. Apart from the more complex lipid and protein composition and other structural components, SLBs distinguish on the first sight by its morphology. SLBs are flat and, in respect of cellular structures, "unconfined" in their planar extent whereas the cell membrane is curved and the surface area is limited on a dimension of cellular processes. Both, curvature and limitation of the membrane area might play a significant role for certain cellular processes. Thus, it was desired to study the comportment of Min-protein waves on artificial membranes whose extent is on the scale of the wavelength of Min-protein dynamics. Furthermore, curvature was introduced into artificial membranes by assembling *E. coli* polar lipid extract on curved objects such as glass beads or rods or on flat supports with a curved topology such as glass or PDMS with modified surfaces. Curved monolayers of lipids were also obtained by the droplet-in-oil technology, protein reconstitution to functional Min dynamics failed. Lateral confinement of artificial membranes was achieved by microstructures thin film technology. Though, artificial membranes of three-dimensional objects such as beads or rods have a closed and thus a confined membrane as well. All data presented here were acquired by myself, unless indicated otherwise. The sections are accompanied by sketches illustrating the different steps of the roadmap presented in Sec. 7.10.

Before presenting and discussing experiments with confined and curved artificial membranes, I would like to briefly introduce some general features of Min-protein waves.

9.1 General features of Min-protein waves

General features of propagating Min-protein waves were already described in detail by Martin Loose [1, 346, 10]. The following sections shall be understood as a small addendum or just as a confirmation.

9.1.1 Wave propagation on unconfined surfaces

On unconfined and isotropic artificial membranes such as supported lipid membranes, the emergence and direction of propagation of Min-protein waves is random [1]. Fig. 9.1(a) shows Min-proteins waves on an artificial membrane supported on mica. The actual image was obtained by LSM scanning 12 ×12 squares, each of 256 × 256 pixels and a scanned area of 650.24 μm × 650.24 μm (420 000 μm^2). The shown image was stitched together after acquisition and represents a total area of 7.8 mm × 7.8 mm (ca. 61 mm^2). This corresponds more or less to the entire surface of the observation chamber. No specific region of origins of spiral waves nor a preference for any direction of wave propagation can be observed. Min-protein waves emerge at various locations on the membrane and form parallel waves that propagate collectively away from
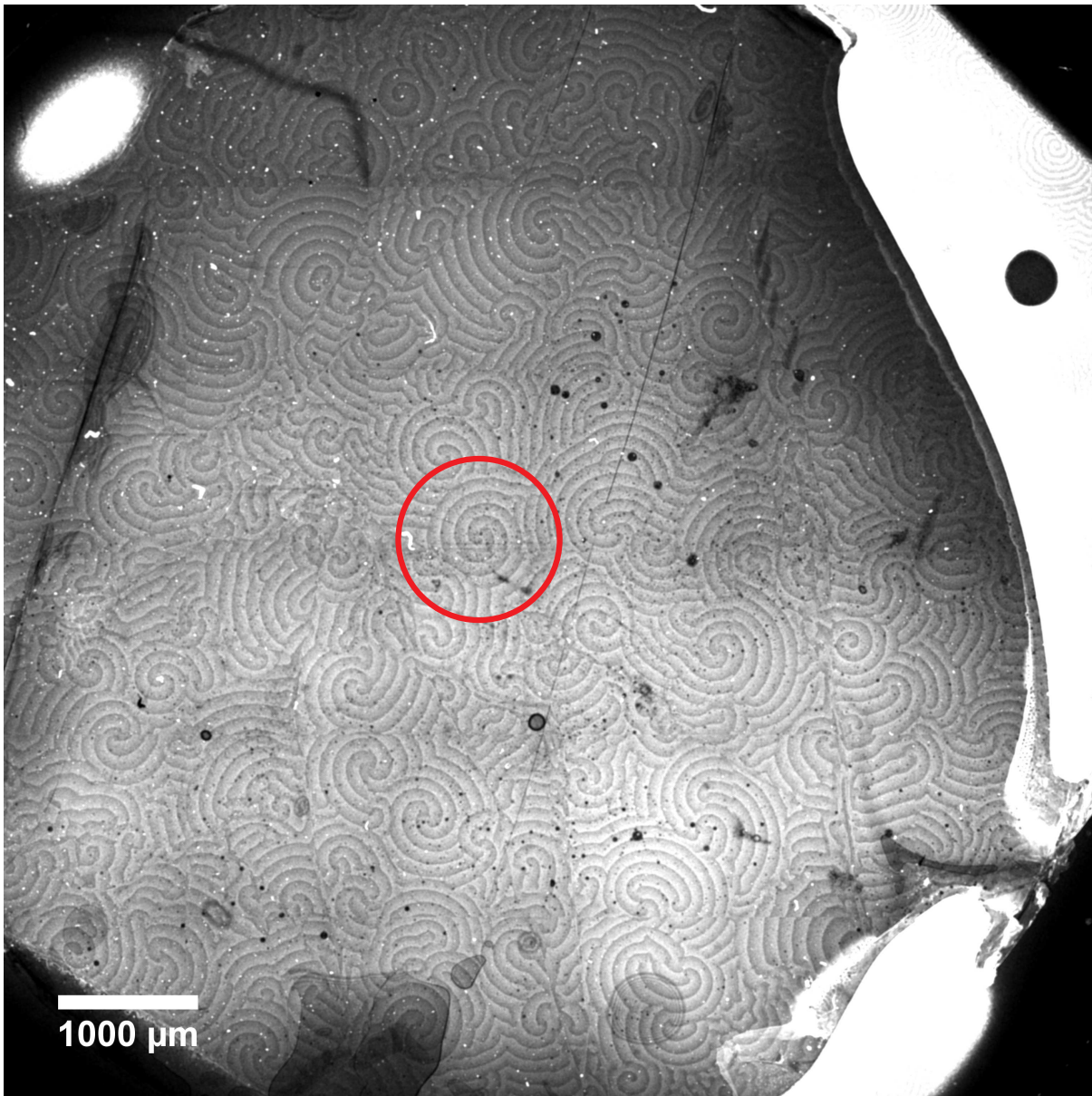
(a)
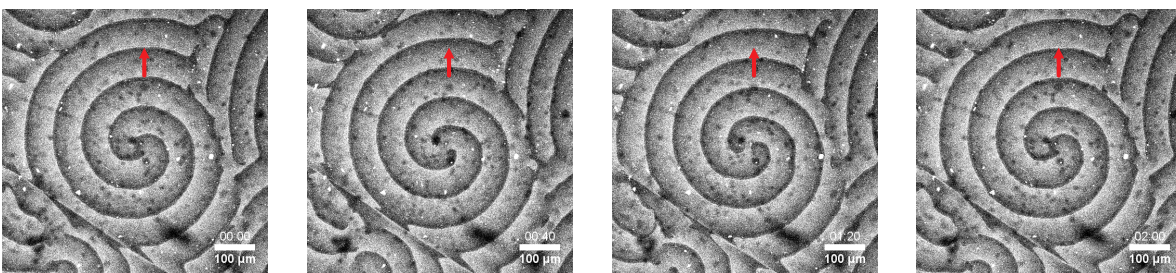
(b)

Figure 9.1: (a) Overview over almost the entire surface area of the observation chamber showing Min-protein waves propagating over the supported lipid membrane (only MinE is labeled fluorescently). The bright signal originates from regions covered with the UV-glue (see Sec. 8.1.8). The image is actually stitched together by 12 × 12 micrographs and covers an area of 7.8 mm × 7.8 mm. The red circle circumscribes a region which is further magnified below (b).

their source. The further away the waves are from the source, the straighter the wave front is. Sources were not identifiable for all waves. Min-protein waves can exist and propagate without any source on the membrane carpet. When waves meet coming from opposite directions, they annihilate each other. Likewise, Min-protein waves just vanish when the reach a wall or just the end of the membrane. Min-protein waves are not physical but chemical waves [459, 1]. Chemical waves do not show constructive oder destructive interference, nor reflections when they hit a barrier or the end of the substrate [460, 461].

The red circle in Fig. 9.1(a) marks a region which is shown more in detail in Fig. 9.1(b). Four consecutive images show the course of wave propagation with an interval of 40 s (however, timelapse images were acquired with a 20 s interval, for reasons of clarity only each second micrograph is shown).

Measured by hand, a wavelength of about 70 μm is estimated. During a period of 280 s the waves cover about 164 μm which makes a wave speed of 0.6 μm/s (red arrow). Both parameters can also calculated in a more sophisticated and automated manner.

9.1.2 Separating static and dynamic features

Although protein binding to membranes is characterized by dynamic behavior, acquired image data also show static features. These are probably due to vesicles that could not be removed by flushing (see Sec. 8.1.12) and that bind Min-proteins as well, or Min-protein aggregates. Normally these static features did not have any relevance for data analysis. But in some cases, these static features were removed by subtracting an average image of all movie frames from the movie. Fig. 9.2A shows the first frame of the timelapse in 9.1(b) as raw data. For us, only the dynamic features are of interest. If sufficient frames are collected and if the time interval between each frame is short enough, an average image of all frames can be produced. This average image only shows the features that are present in all frames and thus lack the dynamic signals (Fig. 9.2B). By subtraction of this average image from each frame of the timelapse, the static features are removed (Fig. 9.2C). In doing so, better results are obtained if each frame is processed by a mean filter prior to establishing the average image. After processing of the timelapse, adjustment of brightness and contrast improves the visualization. The respective MATLAB code can be found in the appendix (Sec. 11).

9.1.3 Velocity by kymographs

For the estimation of the wave speed, a kymograph is produced from the data from which static features had been removed. Fig. 9.2C shows a red line. This red line represents a cross section through the timelapse. The timelapse is represented in a xyt-stack. Thus, in the present case, this cross section represents a subset of the data in the yt-dimension and is shown in 9.2D. The height of the kymograph represents the length of the cross section and thus the entire path along which waves travel (which is about 304 μm in this example). For reasons of generalization, the spatial dimension is parametrized as the path p (the cross section could also be in x-direction or in any diagonal). The width of the kymograph represents the time (the "depth" of the xyt-stack) and is 280 s (which corresponds to 15 frames with an interval of 20 s). In the kymograph, the fluorescent signal "travels" through the one-dimensional space p and time t and thereby produces fluorescent curves. The slope of these curves, given as the differential equation of the traveled path p divided by the elapsed time t yields the velocity v with which the fluorescent signal propagates:

$$v = \frac{dp}{dt} \tag{9.1}$$

117
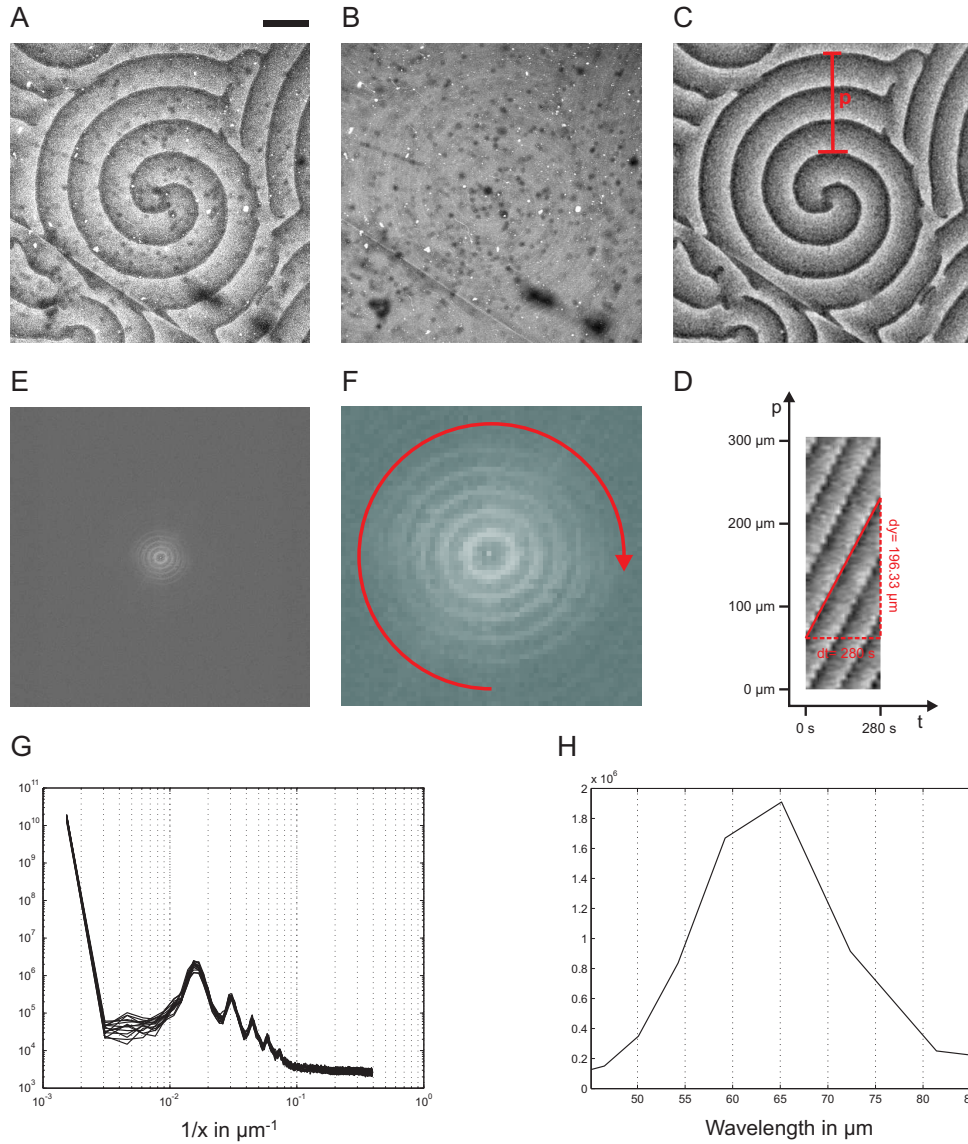
Figure 9.2: Basic image processing for analysis of Min-protein waves. (A) First frame of a 15-frame time lapse (source data). (B) Static features present in all frames. (C) Data corrected for static features. (D) Kymograph for the line in C. (E) Fourier transformation of the source data shown in A. (F) Zoom-in of E and polar averaging. (G) Power spectra for all 15 frames of the source data in reciprocal space. (H) Power spectrum averaged for all frames in the Cartesian space and zoomed onto the first order maximum. The distance between the first order maximum and the zero order corresponds to the dominating structure parameter in the source data, which is the wavelength. Scalebar is 100 μm.

As one can see, all the curves in Fig. 9.2D are linear. This means, that a Min-protein wave travels at a constant speed. Furthermore, all lines are parallel which means that all waves travel not only at constant but also at the same speed. With the curves in the kymograph being lines, calculation of wave speed becomes very easy: the slope of the lines corresponds to the wave velocity and can be directly calculated from the elapsed time and the entire length of a single line. During 280 s the signal travels for about 196 µm which makes about 0.7 µm/s. This value is good agreement with previously published data [1, 346].

9.1.4 Wavelength by Fourier transformation analysis

Fig. 9.2A is a very nice example for parallel Min-protein waves exhibiting one single wavelength. However, not all data show such a homogeneous picture of wavelength. Often, wavelengths differ largely within one sample. Nevertheless, though the distribution of wavelengths might be broad within one sample, the average wavelength might be characteristic for certain boundary conditions. In addition, the visual quality of waves is often also poor which makes manual determination of the wavelength impossible or at least highly inaccurate. Therefore, it is desirable to estimate an average wavelength from all visible waves. This can be achieved by Fourier transformation analysis which was realized using an automated Fourier transformation with a self-written code in MATLAB. The respective code can be found in the enclosed DVD at the end of this thesis and can be applied to any data in the .tiff- or .lsm-format, single images or image stacks (see Appendix, Sec. 11).

Fig. 9.2E-H show the principle of the Fourier transformation applied to Min-protein waves. The Fourier analysis can not be applied to filtered images since the application of the filter induces an additional artificial structural feature. Therefore it was processed on the raw data (Fig. 9.2A). Static features and random noise did not have major effects on the procedure. Fig. 9.2E shows the result of the Fourier transformation, the data in the reciprocal space. One can clearly identify the zero order maximum which is a feature of each Fourier transform, even for random noise data [462]. Fig. 9.2F represents a magnification of the central region. Several bright rings around the zero order central spot are visible. Each ring represents further maxima of higher order with the first ring being the maxima of the first order and so on. The distance between the different order maxima are in fact the reciprocal of the dominating structure length in the original data, which is the Min-protein wavelength in our case. This distance can be more easily and accurately estimated upon averaging the two-dimensional reciprocal space data by polar integration (indicated by the circular red arrows). This produces one-dimensional power spectra as shown in Fig. 9.2G. Each curve represents a frame of the short timelapse containing 15 frames. The zero order maximum is represented as the maximum to the left. Up to five higher order maxima can be distinguished. In fact, the distance between each maximum corresponds to the dominating structure length of the original data. Thus, the wavelength could be estimated from the reciprocal of the distance between zero and first order or between first and second order etc. However, since not all data produce power spectra with more than the zero and first order maxima, wavelength determination was limited to the position of the first order maximum. By further averaging of the power spectra for all 15 frames, the position of the maxima can be estimated with high precision. Fig. 9.2H shows a zoom-in in such an average power spectrum featuring the first order maximum. Here, the horizontal axis is already transformed back into the normal space. So, the position of the maximum directly corresponds to the characteristic structural length (in our case the wavelength). Since the distribution of values around the maximum is asymmetric, the position is not determined simply from the peak position but by weighing the entire curve. This produces a wavelength of 62 µm. This value is good agreement with previously published data [1, 346].

Figure 9.3: Horizontal and vertical cross section through a *xyz*-stack. Top: The *xy*-representation of the fluorescent signal at the level of the membrane shows parallel Min-protein waves that travel from left to right. Bottom: The *xz*-cross section shows distribution of Min-proteins along the path of propagation and in bulk. The distribution of Min-proteins in bulk clearly follows the Min-protein density on the membrane: a low concentration at the front of the wave which increases towards the trailing edge. Proteins do not diffuse far into the bulk after detachment but stay in the proximity of the membrane.

x = 318 μm

y = 163 μm

z = 23 μm

t = 702 s corresponds to 318 μm
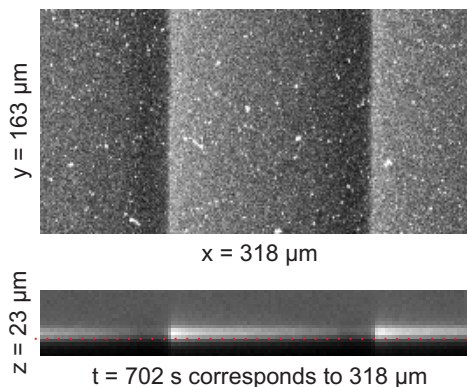
9.1.5 z-Profile

The wave pattern is formed on the membrane by Min-proteins attaching out of the bulk to the bilayer and detaching back into the aqueous buffer. Since the bulk also contains a high concentration of Min-proteins, thus also labeled particles, Min patterns on membranes can only obtained using sectioning imaging technologies such as LSM which allows signal collection solely from specific optical plane (Sec 8.2.1).

Throughout the solution, the concentration of Min-proteins is isotropic, however, close to the membrane, the distribution of Min-proteins in the bulk should reflect the surface density of the propagating waves on the membrane. Fig. 9.3 shows a close-up view of parallel propagating waves. The corresponding data was acquired as a *xyz*-stack and the upper image represents the frame at the level of the membrane in *xy*-dimension. The lower image was obtained by averaging all values in *y*-direction and thus collapsing the three-dimensional stack into a two-dimensional *xz*-image. The red dashed line represents the upper boundary of the mica sheet and thus the level of the membrane. This illustration is principally different from the profile shown in Fig. 5.4 which represents the Min-protein density *on* the membrane. The *xz*-image shows the distribution of proteins between the membrane and the bulk.

A bright thin fluorescent line is only visible close to the glass support (red dashed line) and thus to the membrane. Barely any fluorescence is visible in the bulk far above the membrane. From 9.3, it can be concluded that Min-proteins diffuse only few micrometers into the bulk before they reattach. This observation is in concordance with the results published by Loose et al. previously [10].

9.2 Min-protein waves on flat confined membranes

In order to test the effect of boundaries and lateral confinement of membranes on the comportment of wave propagation, microstructured artificial membranes were produced using photolithography technology in combination with supported lipid bilayers as described in Sec. 8.1.3 and 8.1.12.

9.2.1 Wave pattern is influenced by obstacles

It is the circumference which defines the geometry of an object or area. Therefore, in order to test whether Min-protein waves can sense membrane geometry, they must be able to recognize membrane boundaries. This capability of Min-proteins was tested using regular patterns of two-dimensional obstacles. Fig. 9.4 shows Min-protein waves on such checkerboard structures with varying obstacle size. For large membrane islands (and large obstacles) of about 90 μm in length, no coherent and common wave pattern evolved but each membrane island showed it's individual
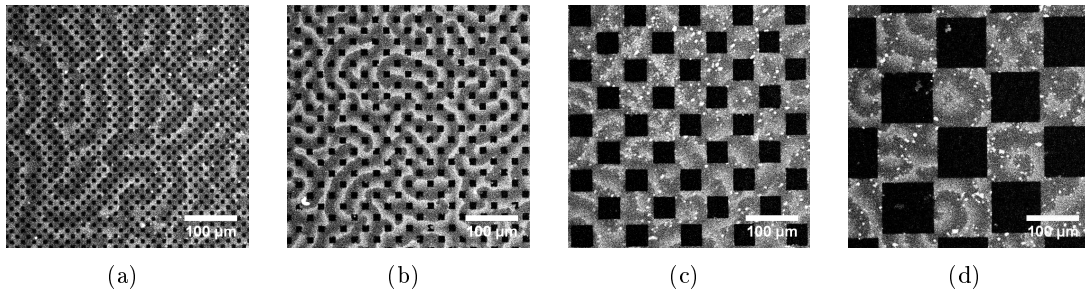
Figure 9.4: Min-protein wave propagation in dependence of obstacles. For small obstacles (images to the left) Min-protein wave propagation is not perturbed. However, when the obstacle size increases, the overall wave pattern becomes incoherent and individual wave pattern evolve.
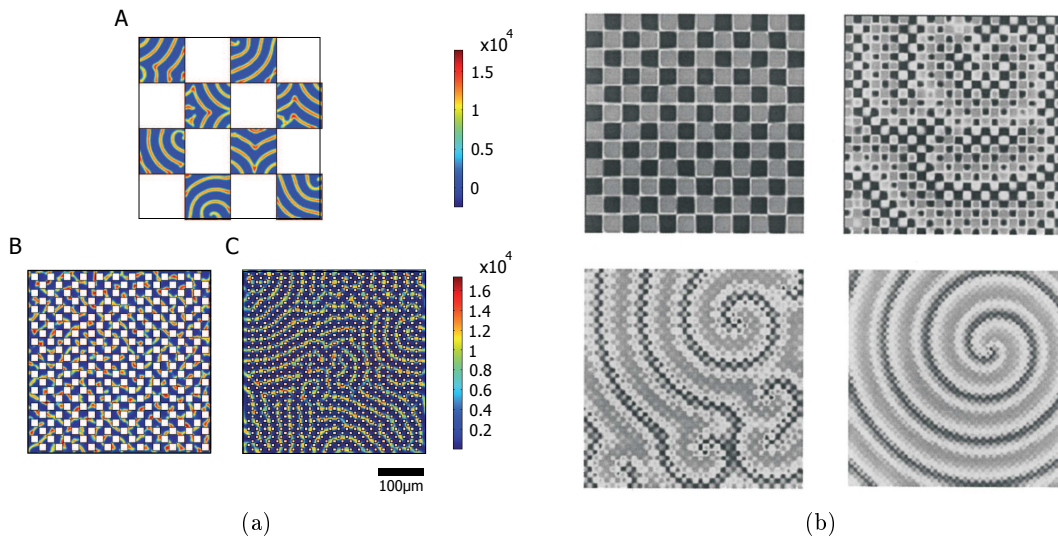
Figure 9.5: Wave propagation in heterogeneous media. (a) Numerical simulation of Min-protein waves on membranes with obstacles of varying size. Colors indicate the surface density of MinD (c_d) and of the MinDE-complex (c_{de}). Images by the courtesy of Mike Bonny and Karsten Kruse. (b) Simulation of chemical waves on an anisotropic substrate. Image is taken from Ref. [463].

wave pattern (Fig. 9.4(d)). For membrane islands and obstacles at the size of the wavelength (50 µm), only irregular patterns formed, with individual protein bands moving on the membrane patches (Fig. 9.4(c)). In the presence of smaller gold obstacles, which were about one third of the wavelength, we observed only a minor effect on the protein waves, which propagated almost unimpaired (Fig. 9.4(a) and 9.4(b)). This proved that Min-protein waves can detect membrane boundaries — which is an essential requirement for geometry sensing — if boundaries are on the length scale of the Min-protein wavelength. For obstacles much smaller or larger than the wavelength of Min-protein dynamics, boundaries have no influence on the wave pattern.

Theoretical calculations and simulations for other reaction-diffusion systems have predicted similar effects as shown in Fig. 9.5(b). Numerical simulations of Min-protein waves propagating around obstacles, carried out by Karsten Kruse and Mike Bonny, yield a similar picture (Fig. 9.5(a)).

9.2.2 Wave pattern is influenced by size of membranes

Using the checkerboard structures, the lengths of obstacles and membrane islands was always varied in both dimensions, x and y. What would happen if the boundary length was varied in

(a)　　　　　　　　　　　　　　　　(b)
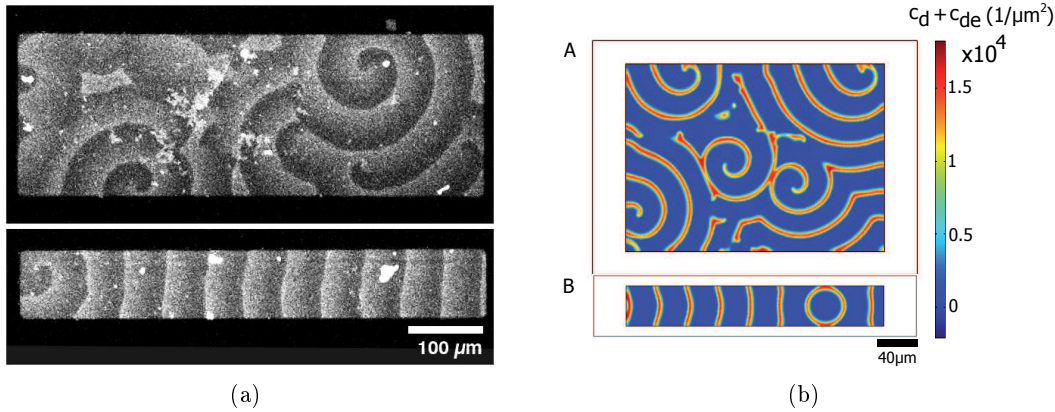
Figure 9.6: For large membrane patches, no influence of the boundary or of the geometry on the wave propagation is visible. However, if at least one dimension of the membrane patch is reduced to the scale of the wavelength, the geometry of the bilayer suddenly determines the wave propagation: waves travel along the elongation. (a) in vitro and (b) in silico. Colors indicate the surface density of MinD (c_d) and of the MinDE-complex (c_{de}). Images by the courtesy of Mike Bonny and Karsten Kruse.

only one dimension? Fig. 9.6(a) shows two rectangles of same length but different width. For both structures, the length of $617\,\mu m$ is well above the respective wavelength of about $52\,\mu m$. For the larger rectangle, the width of $216\,\mu m$ is also larger than the Min-protein wavelength. No influence of geometry on the wave propagation is visible, waves seem to propagate in a chaotic manner as on completely unconfined membranes (compare Sec. 9.1.1). However, if only one of the two dimensions of the rectangular membrane area is reduced to the scale of the length of Min-protein waves, the wave propagation is not longer of chaotic nature but determined by the membrane geometry: In the lower image of Fig. 9.6(a), the width is $90\,\mu m$ wide and thus in the regime of the Min-protein wavelength. Now, the Min-protein waves propagate along the elongation of the rectangular membrane patch.

Such a size-dependent behavior can also be observed for Min-protein waves *in silico* as shown in Fig. 9.6(b). As for the *in vitro* experiments, no influence on the propagation is observed for the Min-protein waves on the large membrane patch (Fig. 9.6(b)A). However, when one dimension (here, for example, the y-dimension is limited to the scale of the wavelength, the membrane geometry does determine the direction of wave propagation: waves travel along the elongation of the membrane patch (Fig. 9.6(b)B).

9.2.3 Min-protein waves follow the elongation

It was found that in rectangular membrane patches Min-protein waves follow the elongation if at least one dimension, the width, was reduced to the magnitude of the Min-protein wavelength (see Sec. 9.2.2). This effect was studied in more detail in rectangular structures and in rod-like but flat structures with round caps (in the following denominated as 2D-rods). For both measurement series, influence of geometric aspect ratio as well as the total surface area was investigated. The rectangular structures were especially interesting concerning the ability of Min-proteins to discriminate the diagonal as the longest axis from the longitudinal axis. 2D-rods were chosen since for these, the longitudinal axis also represents the longest axis and because of its geometric similarity to *E. coli* cells.

Rectangles of different aspect ratios were produced using standard microlithography (see Sec. 8.1.3). Often, aspect ratios are defined as the length divided by width (see Sec. 3.1 and Ref. [25]). However, for long structures, the aspect ratio becomes infinitely large which raises problems when displaying these in a graph. Thus, we define the aspect ratio ar in an inverse

Series	Square	Surface area	Number of acquired movies	Number of selected movies
a	200 µm × 200 µm	40 000 µm²	143	31
b	100 µm × 100 µm	10 000 µm²	121	30
c	50 µm × 50 µm	2500 µm²	111	33
		Total	375	94

Table 9.1: Data volume and parameters for rectangular microstructures.

manner as the ratio of width w to length l:

$$ar = \frac{w}{l} \tag{9.2}$$

Note, that this aspect ratio is the inverse of the aspect ratio a defined in Sec. 3.1. Consequently, the largest aspect ratio was given by square membrane structures with $ar = 1$ whereas long and thin rectangles were characterized by an aspect ratio close to zero. For 2D-rods, the aspect ratio was defined similarly with the short axis divided by the long axis. Thus, for a circular structure the aspect ratio was 1. In varying the aspect ratio, the total surface area of the microstructures was kept constant. However, influence of the absolute size of microstructures on wave propagation was also investigated by varying the total surface area as well. Tab. 9.1 and 9.2 list for both sample types, rectangles and 2D-rods, the different surface areas and volume of acquired data. Each surface area represents a proper measurement series with varying aspect ratios.

Determination of the propagation angles for Min-protein waves was the crucial analysis step in the work presented here. Priorly, several automated procedures programmed in MATLAB were tested but failed by producing too many artifacts. Finally, direction of wave propagation was determined manually using the Zeiss AIM software by drawing lines into the movie using the "Line Drawing Mode" together with the "Measure" tool which calculates directly the angle of the drawn line. Propagation angles were binned into bins of 5°. Propagation angles were plotted against the aspect ratio using a bubble diagram (Origin) with the bubble size indicating the occurrence of the respective propagation angle.

... in rectangles

Rectangular supported lipid bilayers of three different surface areas, namely 40 000, 10 000 and 2500 µm², were formed with varying aspect ratios (Tab. 9.1). For the largest structures (series a), squares measured 200 µm × 200 µm, for medium sized membrane patches (series b), squares were 100 µm × 100 µm and the smallest structures (series c) featured squares with dimensions of 50 µm × 50 µm. MinD and MinE was added and the formation of wave pattern was observed by LSM.

In total, 375 movies of Min-dynamics on rectangular membrane patches of different total surface areas and aspect ratios were acquired. Out of these, 94 movies were selected and the others were discarded due to bad sample quality or ambiguous direction of wave propagation. Samples showing spirals within the rectangle had to be omitted in order to exclude false positive results. In rectangles with a wave origin, waves always follow the long axis. For details on data volume and parameters see Tab. 9.1.

Fig. 9.7 shows examples of representative rectangles of various aspect ratios for all three sizes and respective bubble diagrams illustrating the distribution of wave propagation angles in respect of the aspect ratio. At first sight, waves seem to follow the longitudinal axis in rectangular membranes. For small aspect ratios (width/length) this is true for all three sizes (Fig. 9.7). For rectangles with a high aspect ratio (square-like), the difference between the longitudinal and

(a)

(b)

(c)
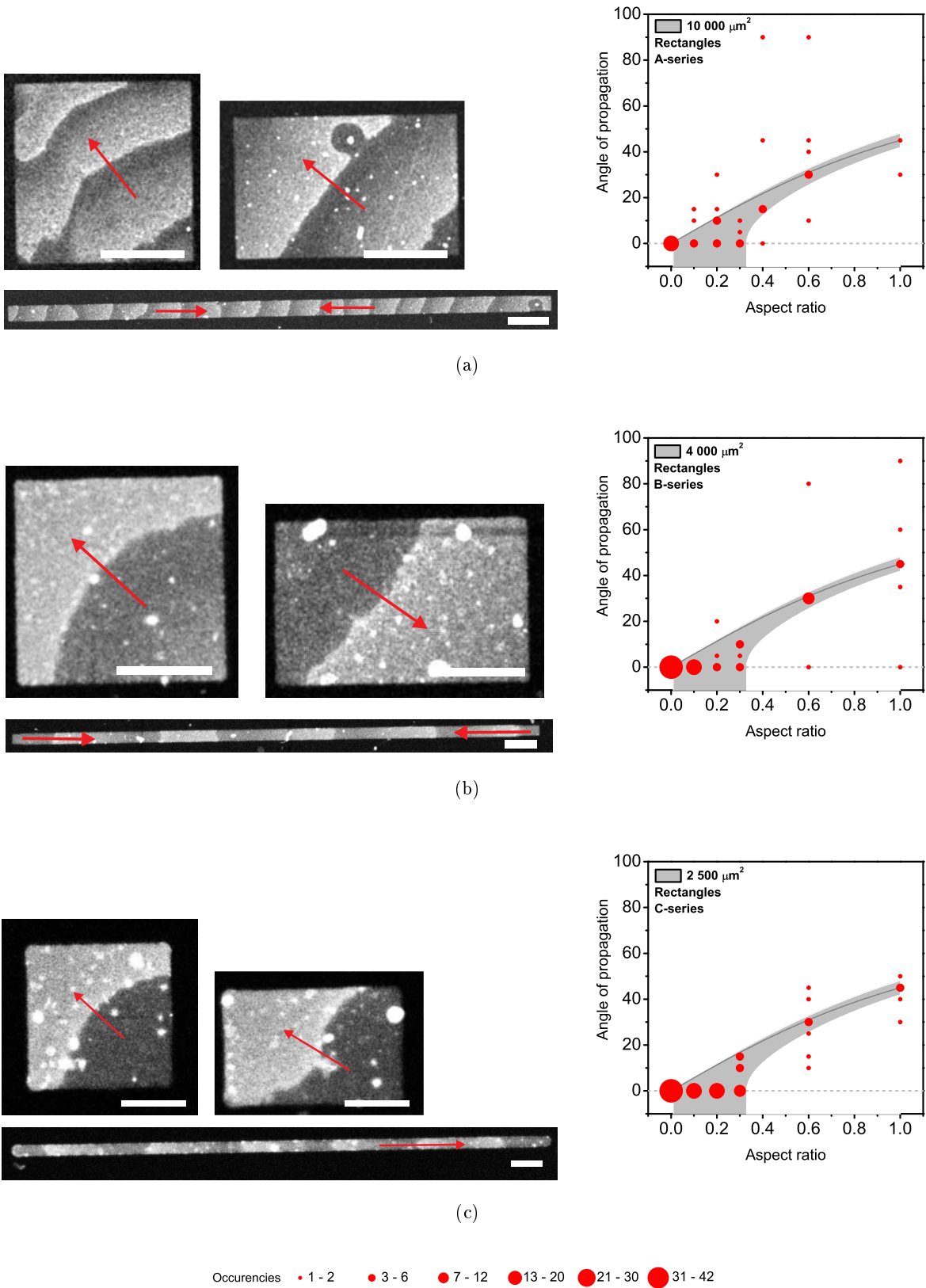
Figure 9.7: Examples of rectangular membrane patches and angle of propagation in dependence of the aspect ratio:. a) $40000\,\mu^2$, b) $10000\,\mu^2$ and c) $25000\,\mu^2$.

transverse axis is small, therefore a less clear alignment of wave propagation was expected. This assumption seemed to be justified when regarding the plots representing the two larger sets of rectangles (Fig. 9.7(a) and 9.7(b)). If Min-proteins can indeed sense geometry of membrane structures, then they have a certain sensitivity: The longest axis can only be determined if it distinguishes by a certain factor or threshold from possible other axes by length.

Strikingly, while recording wave propagation in square-like rectangles of the smallest set (series c), it was observed that waves did not propagate in arbitrary directions as expected but along the diagonal of the rectangle. This behavior is also reflected in the corresponding plot (see Fig. 9.7(c)). Again, for small aspect ratios, the wave propagation is small ($\alpha = 0$), for middle-sized aspect ratios, the distribution of propagation directions increases, but for high aspect ratios, the distribution narrows to around 45° which is the corresponding angle for a diagonal in a square. This makes sense, since in a rectangle, the diagonal (and not the longitudinal axis) represents the *longest* axis. For small aspect ratios, longitudinal and longest axes coincide, so no difference can be made at this point. The angle of a diagonal in a rectangle is calculated by the arctan of the aspect ratio, the corresponding curve is plotted in Fig. 9.7(c) as a dark gray line. In theory, Min-protein waves should follow this curve. For high aspect ratios the data points are well grouped around the curve representing the diagonal, for small aspect ratios data points are also in a good agreement with the theoretical prediction since the diagonal coincides with the longitudinal axis. However, there is a significant deviation to lower angles for aspect ratios between 0.1 and 0.3, but this aspect shall be explained later. For an aspect ratio of 0.6, there is a much broader distribution of propagation angles than for small and large aspect ratios. This behavior is a clear indication that direction of wave propagations is strongly linked to the sensitivity of the system to determine the longest axis.

The ratio r between diagonal d and longitudinal axis l is given by

$$r = \frac{l}{d} = \frac{l}{\sqrt{l^2 + w^2}} = \frac{1}{\sqrt{1 + ar^2}} \tag{9.3}$$

with w being the width and ar the aspect ratio of the rectangular structure.

Apparently, there is a certain threshold for this ratio below which the Min system can no longer determine the longer axis. For high aspect ratios, the difference between the diagonal and the longitudinal axis is sufficiently large to distinguish both. For small aspect ratios, it has to be assumed that the Min system can no longer distinguish between both, but this incapability can not be observed since diagonal and longitudinal axis coincide anyhow. The angular difference between diagonal and longitudinal axis is represented by the dark gray line. For medium-sized aspect ratios (0.6) the difference between diagonal and longitudinal axis is apparently too small for the Min system to clearly determine the longer axis of both, on the other hand, the angular difference between diagonal and longitudinal axis is large enough to observe the broad angular distribution.

In vivo, the Min-proteins were found to oscillate only along the longest axis of the cell [464]. Even in cells of aberrant shapes, e.g. cells lacking the gene for rodA, or when treated with A22, an inhibitor of the MreB cytoskeleton, the Min oscillations show a preference of orientation along the longest possible path. Only in almost perfectly round cells has the oscillation lost its preference for a certain axis (Fig. 9.8). The almost spherical shapes for which the Min system could not detect the longer axis anymore were thus characterized by an aspect ratio of 1.04 ± 0.04 which corresponds to a value of 0.96 in our system (In the cited work, the investigators used the inverse definition for the aspect ratio $\frac{1}{ar} = \frac{l}{w}$. The variation can not be directly converted since the distribution of measurement values was not given in the respective publication). Support for this high sensitivity of the Min system in detecting the cell geometry comes from numerical

Figure 9.8: In nearly round *E. coli* cells Min-proteins can still find the longest axis along which Min oscillations occur (closed circles and triangles). Plot axes designate the length of the short and long axes of the cell. Only when the relative difference between long and short axis falls below a certain threshold, Min-proteins oscillate in random directions (open circles and triangles). The diagonal represents perfectly round cells. One can see that the deviation from perfectly round cells and thus the relative difference is very small. Graphs are taken from [464].
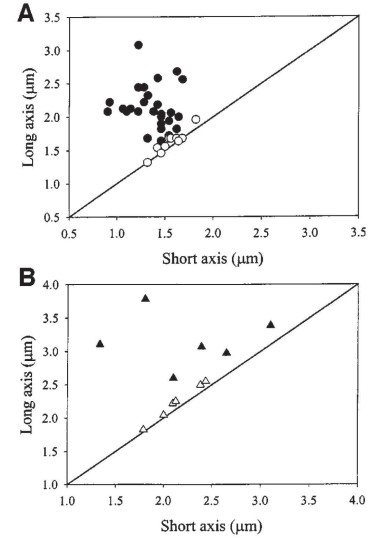
Figure 9.9: Numerical simulation of Min-protein waves on rectangular membrane patches with at least one dimension on the scale of the Min-protein wavelength. Colors indicate the surface density of MinD (c_d) and of the MinDE-complex (c_{de}). Images by the courtesy of Mike Bonny and Karsten Kruse.
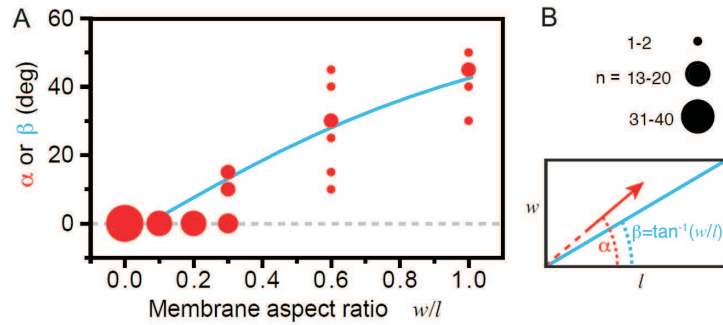
simulations, which propose that an aspect ratio as small as 0.95 is sufficient to give rise to a preferred oscillation axis [465].

Considering this 5 % difference between long and short axis as the possible threshold for the sensitivity, it can be stated vice versa that protein waves are allowed to oscillate along axes that are shorter than the longest axis but not more than 5 %. This consideration was applied to the rectangular membranes. Here, the diagonal represents the longest axis. Possible axes of wave propagation are those that deviate from the diagonal by a small angle but only to such an extent that the length of the alternative propagation axis is still at least 95 % of the diagonal. The angular range of these allowed propagation axes is shown as a gray shade for the entire range of aspect ratio in Fig. 9.7. Corresponding calculations can be found in the appendix (Sec. 11.1). These calculations explain especially well why the range of small aspect ratios deviate from the diagonal towards smaller angles (Fig. 9.7(c)).

Again, numerical simulations confirm our experimental results. Fig. 9.9A shows rectangles of various aspect ratios with simulated Min-protein waves. As in *in vitro* experiments, waves follow the longest possible axis which is represent by the diagonal. Fig. 9.9B shows the respective histogram of the angles of propagation in dependence of the aspect ratio. The blue line represents the angle of the diagonal for a rectangle with a given aspect ratio. For square-like rectangles, Min-protein waves clearly follow the diagonal. For smaller aspect ratios, waves tend to follow the longitudinal axis.
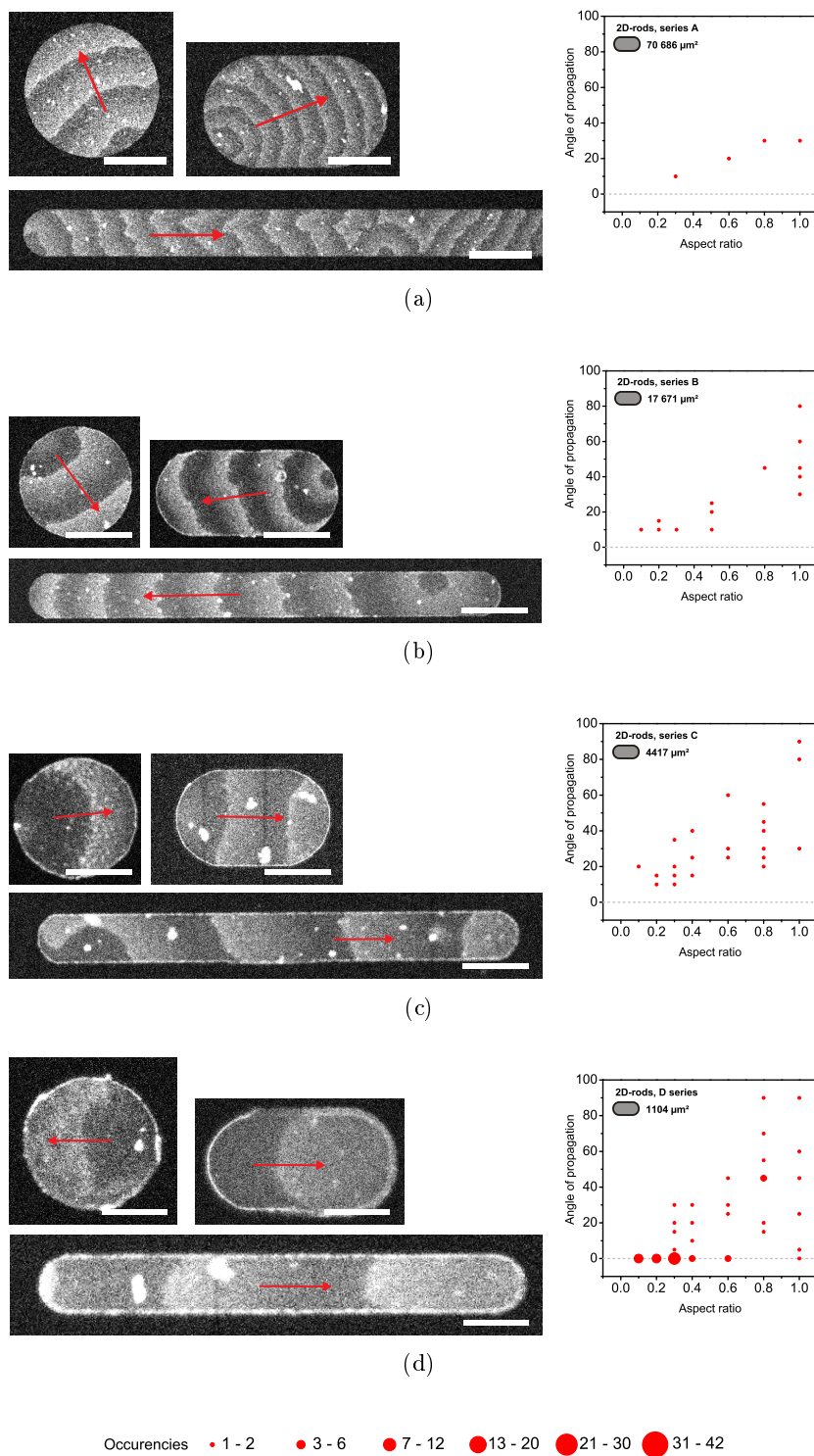
Figure 9.10: Angle of propagation in dependence of the aspect ratios for rod-like membranes of different sizes.

Series	Radius	Surface area	Number of acquired movies	Number of selected movies
a	150 μm	70 686 μm²	39	11
b	75 μm	17 671 μm²	70	35
c	37.5 μm	4417 μm²	68	63
d	18.75 μm	1104 μm²	73	73
		Total	250	182

Table 9.2: Data volume and parameters for 2D-rods.

... in 2D-rods

For rectangles, there is a difference between longitudinal and longest axes. Are there elongated geometries for which the longest axis coincides with the longitudinal axis for all aspect ratios? Ellipses or elongated structures with hemicircular caps fulfill this condition. The latter ones have been chosen because of their obvious visual similarity to the form of *E. coli* cells. In the following, such rod-like membranes shall be denominated as 2D-rods (2D for "two-dimensional"). For 2D-rods, the waves are expected to propagate along the longitudinal axis since it is the longest axis as well.

Again, 2D-rod-like membrane patches were obtained by assembling supported lipid bilayers on gold microstructures and Min-proteins were allowed to organize into propagating waves. Measurement series were performed for four different total sizes as listed in Tab. 9.2 and for different aspect ratios. In total, 250 movies of Min-dynamics on rectangular membrane stripes were obtained for different total surface areas and aspect ratios. Out of these, 182 movies were selected whereas the others were discarded due to bad sample quality or ambiguous direction of wave propagation. Fig. 9.10 shows some examples of propagating Min-protein waves in microstructured 2D-rods and the corresponding aspect ratio/propagation angle graphs. Again for long structures, e.g. small aspect ratios, waves propagate along the longitudinal axis ($\alpha = 0°$). But in contrast to rectangular membranes, direction of wave propagation is completely arbitrary for aspect ratios close to 1, i.e. nearly circular geometries. This is also true for small structures (Fig. 9.10(d)).

2D-rods are two-dimensional structures for which the longest axis coincides with the longitudinal axis of symmetry. In such membrane structures, Min-protein waves propagate along this axis of symmetry. This is in analogy to biology, in *E. coli* the Min-protein membrane binding pattern oscillates also along the longitudinal axis of symmetry.

9.2.4 Waveguiding...

Min-protein waves do not only follow the longest axis in straight but also in arcuate structures. Different geometries such as kinks, circles, synchrotron-like loops and slalom geometries were produced as gold microstructures and supported lipid bilayers were accordingly formed. When the Min-protein assay was added, Min-protein waves emerged whereas the waves apparently followed the path of the arcuate membrane stripes. Similar effects for other reaction-diffusion system have been reported in literature, examples are cited along with the results presented here for better comparison.

... in kinks

Kinks are a nice example to illustrate the waveguiding effect of membranes for Min-protein waves. Fig. 9.11 shows kinks of two different widths, namely 40 and 90 μm, and different angles

<table>
<tr><td>(a) 40 µm width.</td><td>(b) 90 µm width.</td></tr>
</table>
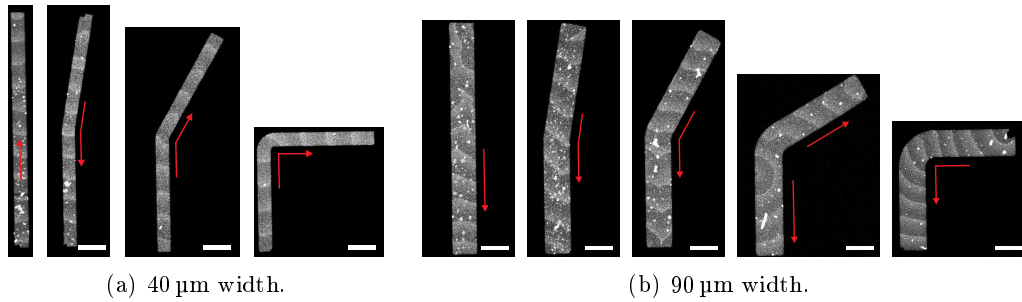
Figure 9.11: Waveguiding of Min-protein waves in kinks of different width and different angles. Angles range cover 0° (left), 10°, 30°, 60° (missing for 40 µm width) and 90° (right). Red arrows indicate the direction of wave propagation. The scalebar spans 100 µm.

from 0 to 90°. In most examples, the Min-protein waves enter the structure at either end of the elongated and arcuate structure (except for the 90 µm structure with a 60° angle, here the wave starts at the edge close to the kink). One can clearly see how the waves follow the elongation of the structure even around the kink, independent of the angle.

Delay of wave flanks

Wave propagation in arcuate membrane structures show a striking behavior which can be nicely seen in the 90°-kink of of 90 µm width in Fig. 9.11(b). The wave starts at the defect in the upper right corner of the microstructure and then propagates as discussed along the curved membrane structure towards the other end of the membrane. Although the wave enters the membrane at a corner, it aligns nicely perpendicular to the membrane elongation. Since the membrane path is curved, the outer flank of the wave has to to travel a longer way than the inner flank (inner path: 621 µm, outer path: 734 µm, which a makes a ratio of 0.846). Consequently, the outer wave flank is delayed in respect to the inner flank. However, when the wave reaches the end of the membrane, the wave is again nicely aligned perpendicular to the membrane boundary and both flanks are at the same "height". Although the outer flank is initially delayed due to the longer pathway, it catches up. Apparently, the wave at the outer edge of the structure propagates faster than the inner flank. This can also be seen in the structures with the 40 µm width (Fig. 9.11(a)). Here the different path lengths are 730 µm and 790 µm.

Fig. 9.12 investigates this change of wave propagation velocity further. In Fig. 9.12A two propagation paths are drawn: in blue at the outer boundary of the microstructured SLB and in yellow at the inner boundary. The origin of the one-dimensional path-axis p is set to the center of the knee (red dashed line). For both paths, kymographs were obtained from the timelapse data using ImageJ as described in Sec. 9.1.3. For this, the raw data was also processed using a procedure that removes static background features which also included mean filtering and brightness adjustment (Sec. 9.1.2). Both kymographs are displayed in Fig. 9.12B, with the kymograph of the outer boundary at top and for the inner boundary at the bottom. The path length is parametrized by the p-axis. This way, the path length differences are also nicely visualized. The region of curvature is marked with two red straight lines and a dashed line indicates the middle which splits the arcuate region into two halves in Fig. 9.12(a)B and C whereas the red-shaded area highlights the second half.
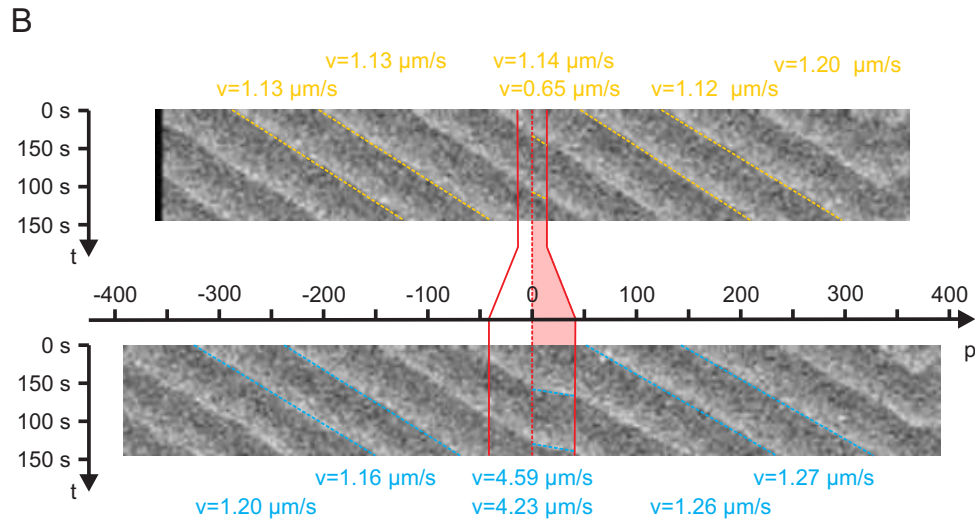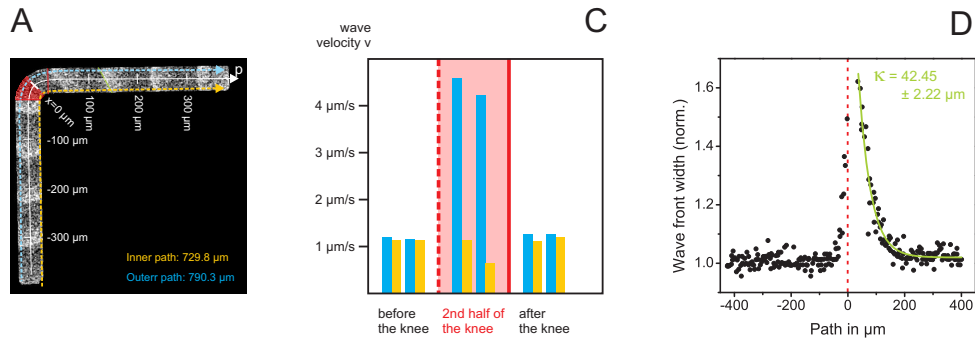
(a) L-shaped membrane of 40 µm width.
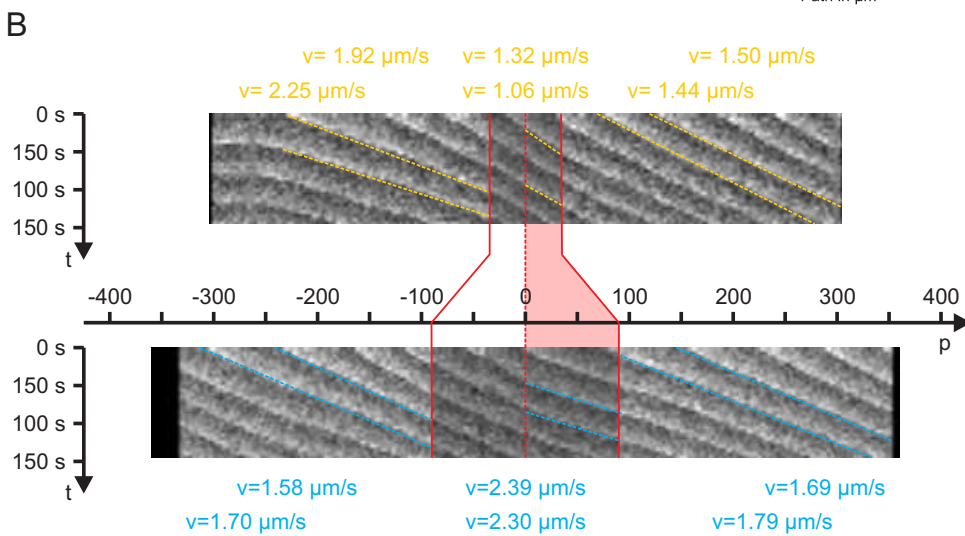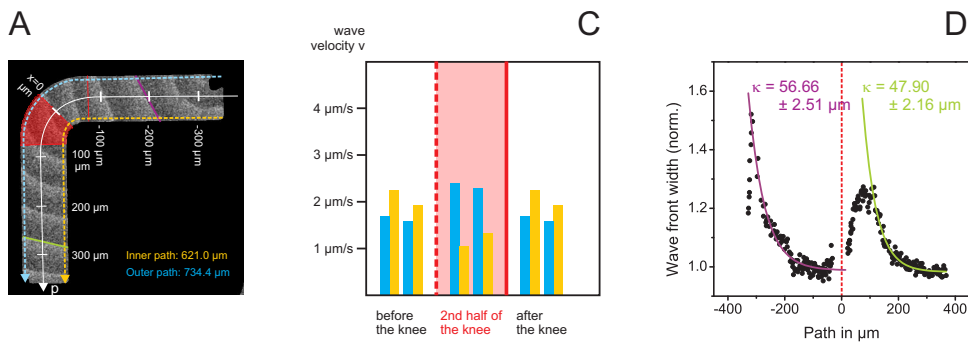
(b) L-shaped membrane of 90 µm width.

Figure 9.12: Analysis of wave velocity dispersion due to curved pathways for membrane stripes of different width. (a) Kink of 40 μm width. (b) Kink of 90 μm width. Following capital letter descriptions A-D apply to both figures. (A) The outer pathway of a curved membrane stripe is longer than the inner pathway. Consequently, the outer wave flank is delayed in respect to the wave flank at the inner edge of the knee. This delay is compensated by a transitory increase of propagation velocity of the wave at the outer edge. (B) The change of propagation velocity can be illustrated with the help of kymographs. Kymographs are extracted from the original data stack for a path on the inner (yellow, top kymograph in B) and on the outer (blue, bottom kymograph in B)) boundary. Original data and kymographs are subdivided into three regions indicated by two continuous red lines: before, during and after the knee. The red dashed line indicates the center of the curved region and splits it into two halves. The slope of the linear lines in the kymographs corresponds to the speed of propagation. Interestingly, the propagation speed is only increased during the second half of the arcuate region. Furthermore, no phase of acceleration or deceleration can be seen but the change of propagation speed seems to occur instantaneously. (C) compares the propagation speeds for the three regions and inner and outer path. Before and after the knee propagation speeds are of similar values. However, during the second half of the arcuate region, waves at the outer edge travel faster than at the inner edge (see especially the example for 40 μm).

First of all, it can be noted that both kymographs exhibit solely linear lines before, during and after the knee indicating that waves travel at constant speed (in blue for the path on the outer boundary and in yellow for the path on the inner boundary). However, in the second half of the arcuate region (red shaded area), the kymograph of the outer boundary, and this can especially nicely seen for the 40 μm example (Fig. 9.12(a)C top), exhibits lines that have a more horizontal orientation which means in this coordinate system that waves travel faster. No such change of slope can be seen in the kymograph for the inner boundary (Fig. 9.12(a)C bottom). This is apparently the moment when the waves at the outer boundary catch up with the waves at the inner boundary. Two observations are striking: First of all, this increase of wave propagation velocity only occurs during the second half of the curvature. Secondly, throughout this second half, the fluorescent signal also exhibits a linear course in the xt-space. This means that the wave speed is constant while catching up. No phase of acceleration or deceleration can be observed or at least takes place very fast. The lines of the fluorescent signal can be described as a function of three linear segments with with non-continuous transition.

Absolute values for the wave speed are extracted from the linear fluorescent signals in the kymographs for the paths at the outer and inner boundary of the microstructured membrane kink and are displayed in the bar plots Fig. 9.12C. The two lines before, within and after the knee were analyzed. The dashed central line marks the middle of the arcuate region and the single straight line the end. Thus, the horizontal axis represents the dimension of the traveled path p, however, it is not to scale. The vertical axis represents the wave velocity. Before and after the knee, wave velocities of the paths for the outer and inner boundary are equal. However, as already discussed qualitatively above, the wave velocity at the outer edge increases tremendously by a factor of four for the example of 40 μm width (9.12(a)C). On the contrary, at the inner edge, wave velocity does not change but even decreases slightly.

A similar behavior, though less evident, is observed for the 90°-kink of the 100 μm structure as shown in Fig. 9.12(b)A-C. Here, the effect is thwarted by the fact that the wave does not enter the structure already aligned to the elongation but emerges at a corner and takes some time to align perpendicularly to the boundary. Due to this asymmetric entrance of the wave, the kymograph exhibits also non-linear features at the beginning (Fig. 9.12(a)ii top and bottom, left part). Except this entrance and alignment phase, the kymographs display mainly linear lines. Though the effect of wave speed changes within the arcuate region is less emphasized, similar effects can be observed qualitatively. First of all, the change of wave speed only occurs in the second half of the knee. Secondly, the wave velocity at the outer boundary increases whereas it decreases at the inner boundary (Fig. 9.12(a)iii. Thirdly, this change occurs more or less abruptly without any visible phase of acceleration or deceleration.

The outer wave flank has a longer pathway to travel than the inner wave flank. First the outer wave flank experiences a delay and then catches up with the inner wave flank during the second half of the bended region. Due to this delay of catching up, the wave front should be stretched. Such an effect can be nicely seen again for the 90°-examples (Fig. 9.11 far right images and Fig. 9.12A respectively). This phenomenon was further investigated by analysis of the change of the wave front width. Wave front widths were extracted from each frame of the timelapses using a semi-automatized procedure in MATLAB. The respective code can be found in the enclosed DVD at the end of this thesis and can be applied to any data in the .tiff- or .lsm-format, single images or image stacks (see Appendix, Sec. 11). The stretching can be quantified as a wave front width w_w normalized to the width of the structure w:

$$W = \frac{w_w}{w} \tag{9.4}$$

This normalized width W is plotted against the path position in Fig. 9.12D. The red dashed line in the graph corresponds to the middle position of the knee. For both examples, shortly after the central region, there is a rapid increase and a slow decay of normalized wave front back to its original value. The example of the $90\,\mu$m structure features a second decay at the beginning of the structure because the wave enters the structure at a corner and thus is not aligned perpendicularly from the beginning on. The characteristics at the central region will be discussed first. The normalized wave front width increases rapidly within the first half of the arcuate region (left from the dashed red line) from where it decreases slowly to its original value (right from the dashed red line). This is in agreement with the observation, that the wave speed does not change during the first half of the knee but only during the second half the outer flank becomes faster whereas the inner flank slows down. If the wave speed would adapt already in the first half of the arcuate region, no stretching would be expected. However, since the wave speeds remain unchanged during the first half of the bound area, rapid stretching is the consequence of differences in the pathway length. Without an adaption of wave speed in the second half, stretching would increase further. However, due to the dramatic increase of the wave speed at the outer boundary, stretching is not only stalled but even reversed until the wave front has reached its original width. This decay of the normalized width $W(x)$ can be fitted with a simple exponential function

$$W(x) = W_0 e^{-\frac{x}{\kappa}} \tag{9.5}$$

whereas the W_0 is the initial and final value for the initial width (which is 1) and κ a characteristic decay length. Values for the decay length κ can be extracted from a fitting procedure which was performed using Origin. For the decay in the second half of the knee, a value of $\kappa = 42.45 \pm 2.22\,\mu$m is obtained for the thin kink and $\kappa = 47.91 \pm 2.16\,\mu$m for the wide kink. For the decay of normalized wave front width at the entry phase of the wide kink, a decay length of $\kappa = 56.66 \pm 2.51\,\mu$m is calculated. All three values are in the same range, apparently this decay length is of constant nature. Furthermore, the decay lengths are of striking similarity to the half of the wavelength of Min-protein waves. Experimental verification whether the decay length is a constant and whether it is coupled to the wavelength, is outside the scope of this PhD-project and has to be investigated in future work.

Nevertheless, these experiments showed, that Min-protein waves are able to rapidly adapt to changes in the membrane path and to sense geometry which encouraged us to further experiments.

Numerical simulations performed on Min-protein waves in membranes formed like the letter L produced similar effects. Fig. 9.13A shows first of all that the Min-protein waves are able to follow the path of the bended membrane patch. Furthermore, as in our *in vitro* experiments, the flank of the wave at the outer edge of the knee is delayed in respect to the flank at the inner side
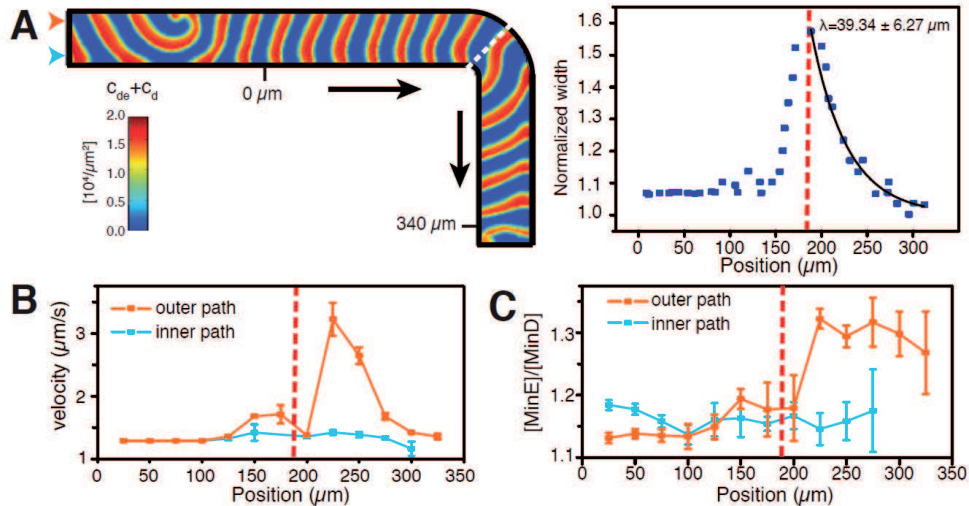
Figure 9.13: Numerical simulation of Min-protein waves on kink-like membrane patches. Image by the courtesy of Mike Bonny and Karsten Kruse.

of the knee. This delay is reflected in a stretching of the wave front width. When the outer flank catches up again, the wave front width again recovers its original length. This is analyzed in the graph depicted in Fig. 9.13A right: the normalized wave front width increases rapidly until the first half of the knee from where it decays slowly in an exponential manner. Again, the decay length is on the same scale as the wavelength of Min-protein waves.

9.2.5 Model for wave realignment and guiding

Despite the pending further proof of the correlation of decay length in kink realignment and wavelength, a model will be presented to explain the effect of wave alignment and wave guiding. Fig. 9.13C shows the surface density ratio of MinE to MinD for the outer path (orange) and inner path (blue). After the central position of the arcuate region (or in other words, after the first half of the knee), the MinE/MinD-ratio remains unchanged for the inner path, however, it increases for the outer path. Through the increase of MinE more MinD proteins are detached from the membrane which leads to an acceleration of the wave. Loose et al. have shown previously that an increase of the MinE fraction accelerates the wave propagation [1, 346]. This relationship is also shown in Fig. 9.14(a).

The question that remains to resolve is, why does the MinE/MinD-ratio increase at the outer boundary of an arcuate region? At a convex membrane edge, the available surface area in front of the propagating wave is limited. Or in other words, when the wave that travels straight forward reaches a curve, the substrate for either flank breaks away. From previous studies, it is known that MinD diffuses further into the bulk whereas MinE rebinds rapidly to neighboring membrane-bound MinD [10, 346]. If now in addition, MinD is missing due to the reduced membrane substrate, more MinE is available for less MinD. In consequence, the MinE/MinD-ratio increases and thus also the wave speed. Fig. 9.14(b) tries to illustrate this model.

... in loops and rings

In 1994, Graham et al. observed the CO-oxidation pattern on platinum surfaces and showed that it is possible that a chemical wave propagates in a circle as depicted in Fig. 9.15 A [466]. Using gold microstructures with similar geometries, Min-protein waves were allowed to organize in rings and synchrotron-like loops. As already observed by Graham et al. and expected from the

(a) (b)
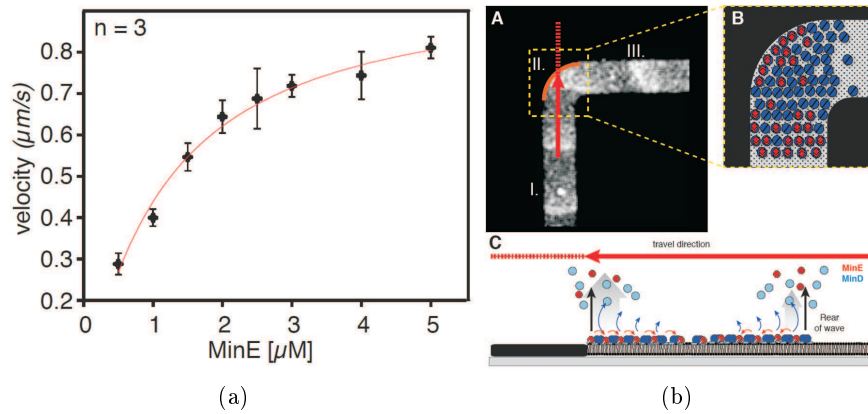
Figure 9.14: Model for the increase of wave velocity at arcuate regions and realignment of wave propagation. (a) Increasing the MinE/MinD-ratio increases the wave velocity. Image is taken from Ref. [1]. During normal wave propagation, MinE detaches MinD from the membrane, especially with an increased activity at the trailing edge. MinD diffuses into the bulk and rebinds relatively far from its point of detachment (presumably in a new wave). However, MinE quickly rebinds to neighboring membrane-bound MinD. Normally, free MinE finds membrane-bound MinD which is not already occupied by MinE just ahead through the course of the wave. By this mechanism, the wave advances. As long as sufficient membrane substrate is available for MinD, MinE will always also find sufficient free membrane-bound MinD. (b) However, when the membrane substrate is reduced, for example in an arcuate region, MinD just diffuses away, but local MinE density is enhance which leads to an increase of the MinE/MinD-ratio. Image is taken from Ref. [358].

Figure 9.15: Chemical waves spinning in circular structures. (A) Timelapse series of a CO-oxidation pulse (in white) traveling on a synchrotron-like Pt-surface. Each frame measures $150\,\mu\text{m} \times 150\,\mu\text{m}$ and the interval is 10s. Image is taken from Ref. [466]. (B) - (E) Min-protein waves spinning in circular structures such as rings and synchrotron-like loops. Red arrows indicate the direction of travel. All four micrographs with Min-protein waves are in scale to each other. Large scale bars are $200\,\mu\text{m}$, the small scalebar is $50\,\mu\text{m}$.

(a)

(b)
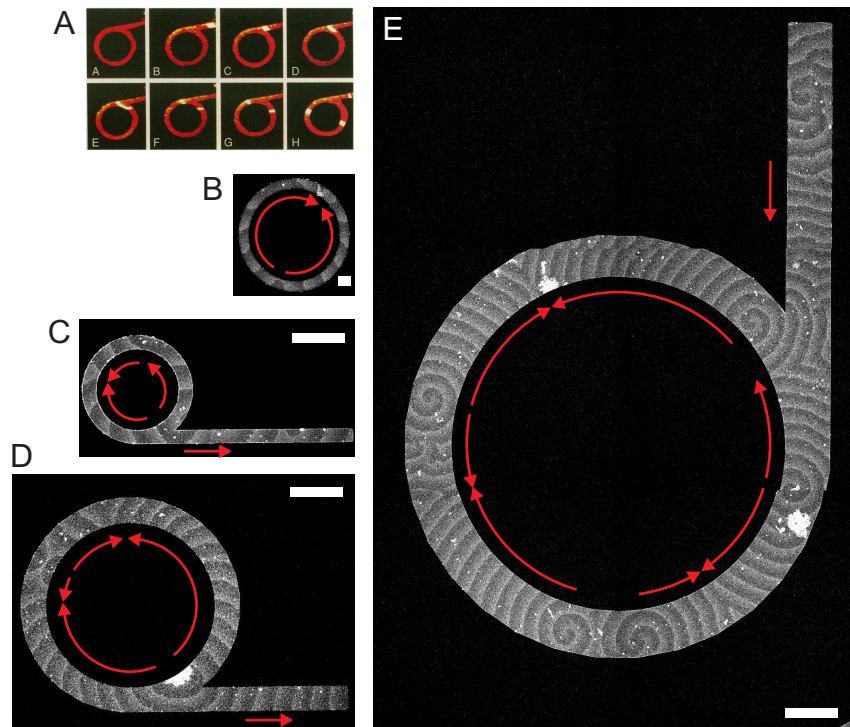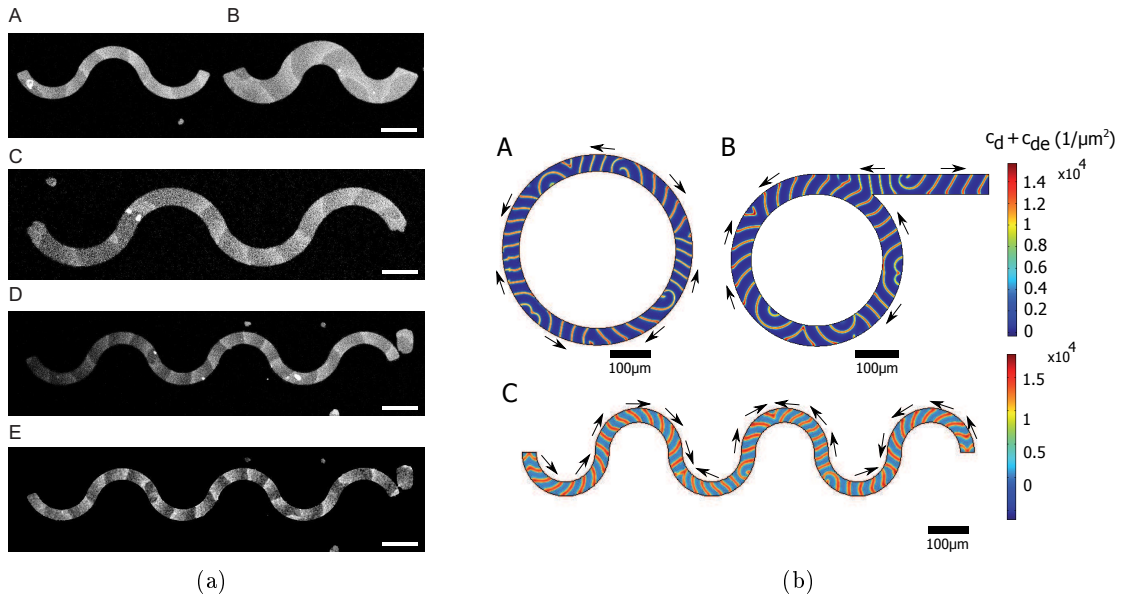
Figure 9.16: Min-protein waves in curved structures. (a) Fluorescence micrographs of Min-protein waves in slalom-like structures. For better visibility, the raw data was processed in such a way that the static features (for example bright immobile protein aggregates) were removed (see Sec. 9.1.2). Scale bars are 100 µm. (b) Numerical simulation of Min-protein waves on membrane patches formed like rings, loops and with a slalom path. Colors indicate the surface density of MinD (c_d) and of the MinDE-complex (c_{de}). Images by the courtesy of Mike Bonny and Karsten Kruse.

experiments with the kink structures, Min-protein waves followed the circular path. Inevitably, Min-protein waves originating from the same source can meet again within the same structure or collide with a wave from another origin. In any case, colliding waves vanish. As already pointed out, there is nothing like constructive or destructive interference for chemical waves as it is observed for physical waves.

... on a slalom path

The slalom example is especially interesting: Although the membrane structure continuously changes its path direction, the protein waves are able to follow these direction changes as depicted in Fig. 9.16(a). Again, numerical simulations could reproduce experimental results well as shown in Fig. 9.16(b).

9.2.6 Coupling across separated membrane patches

When Min-proteins detach from the membrane, they don't just disappear but they remain present in the buffer. MinE detaches only shortly before it rebinds, but MinD apparently diffuses further into the bulk (Sec. 5.2.5). As long as a membrane carpet is present below the free proteins, both rebind rapidly. However, when the wave reaches the end of a membrane patch, they presumably diffuse further into the bulk. Therefore, it has to be assumed that there is an increased level of proteins in the bulk in the proximity of a membrane boundary. If another membrane boundary is close-by, this local concentration of Min-proteins could affect wave formation in the neighboring membrane region. Therefore, when designing gold microstructures, it was an open question as to how far membrane patches would need to be so that wave formation on different membrane patches do no influence each other. Another question was: how close must membrane patches be so that waves on separated islands can communicate with each other?
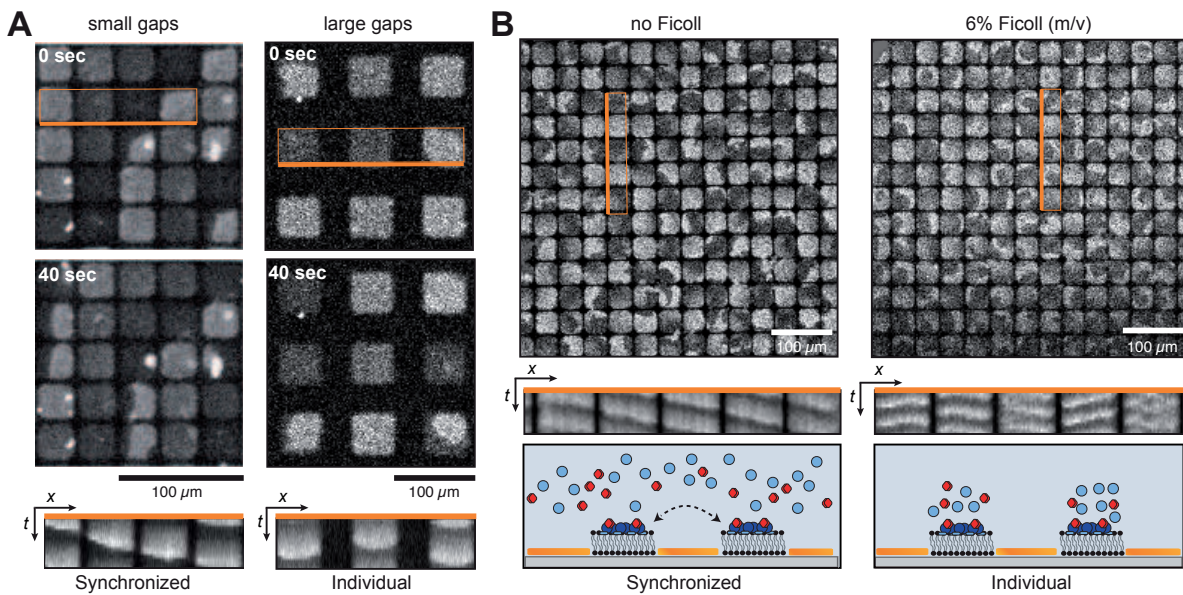
Figure 9.17: Protein waves "jumping" from one membrane patch to the other. (A) Detailed view of membrane grids. Left: Membrane patches with a separation inferior to 10 μm. A coherent wave propagates across several membrane patches. Right: For separations larger than 10 μm no wave coupling can be observed. Bottom: Kymographs of selected regions reveal wave coupling (left) and decoupled wave propagation (right). (B) Wave coupling across separated membrane is influenced by the mobility of proteins in bulk. For given grid and in standard buffer configuration, wave propagation is coherent across several membrane patches (left). For the same grid, but with decreased mobility due to molecular crowding in the buffer through the addition of Ficoll, wave propagation is decoupled which is also visible in respective kymographs (center). Bottom: Illustrative sketch of molecular interactions for the two cases, without (left) and with a molecular crowding agent (right).
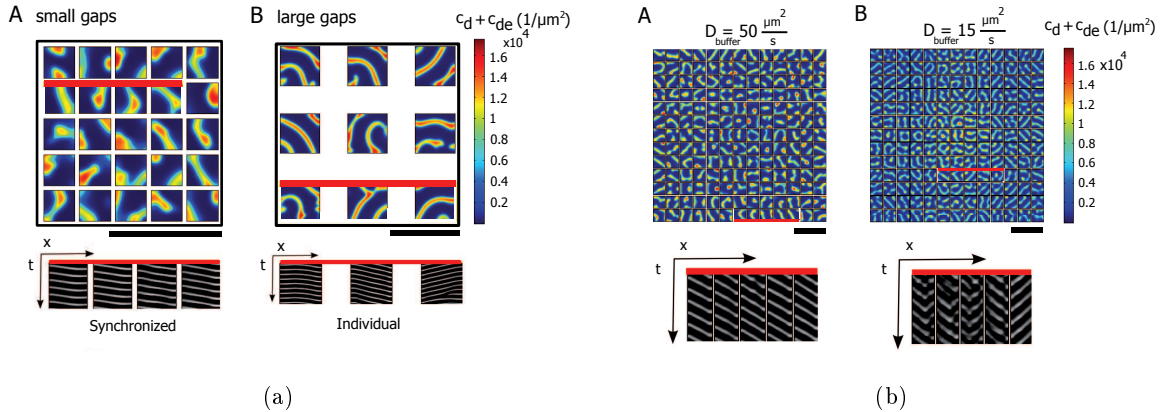
Figure 9.18: Numerical simulation of Min-protein waves on a grid of membrane patches. (a) Variation of the gap size and respective kymographs. (b) Variation of the diffusion mobility due to molecular crowding of Ficoll in the buffer. Scale bars are $100\,\mu m$. Colors indicate the surface density of MinD (c_d) and of the MinDE-complex (c_{de}). Images by the courtesy of Mike Bonny and Karsten Kruse.

This question is not only of technical but also of biological nature. As long an *E. coli* cell is not divided into two cell halves, the Min-protein oscillations occur within the entire cell. Upon fission the common oscillation splits up into two independent oscillations which are first in phase and eventually desynchronize [467, 468].

In order to investigate the capability of Min-protein waves to synchronize across a spatial barrier, grids of square membrane patches of different width with varying separations in between were designed using gold microstructures in combination with SLB technology (see Sec. 8.1.3).

Variation of gap size

Fig. 9.17 shows several grids with square membrane patches. For different grids, patch size and separation was varied. In some grids, a coherent and common wave pattern that couples across several membrane patches can be observed, whereas in other grids every individual membrane patch seems to exhibit its proper wave pattern. Independent from the patch size, coupled wave propagation can be observed for grids with a separation up to $10\,\mu m$.

For separations larger than $10\,\mu m$, two cases have to be distinguished: for large separations and small membrane islands ($<$?? μm) no wave pattern could be be observed at all, for large separations and large membrane islands, each membrane islands showed its own individual wave pattern, apparently decoupled from the wave pattern on neighboring patches. Fig. 9.17 A shows a detailed view of grids with separation smaller or larger than $10\,\mu m$. Here, for the example with the small gap size, it can be seen how the Min-protein membrane binding pattern propagates across several isolated islands as a single and common wave. In the example of the larger gap size no such coupling can be observed. This could be further verified analyzing kymographs.

Concerning our experimental results, it is conceivable that waves couple also for separations larger than $10\,\mu m$ but that this is not visible due to chaotic wave propagation in arbitrary directions. Thus, it has to be pointed out, that we can solely conclude that Min-protein waves are able to couple across gaps up to $10\,\mu m$. For larger separations no statements can be made except that no coupling could be observed (though coupling could exist).

Numerical simulations confirm our experimental observation as shown in Fig. 9.18(a) (top row). For small gap sizes, Min-protein waves can couple across several membrane patches, whereas if the gap size becomes significantly larger, each membrane island exhibits its own independent wave pattern. This effect can be further visualized using kymographs. The bottom row of

(a)   (b)
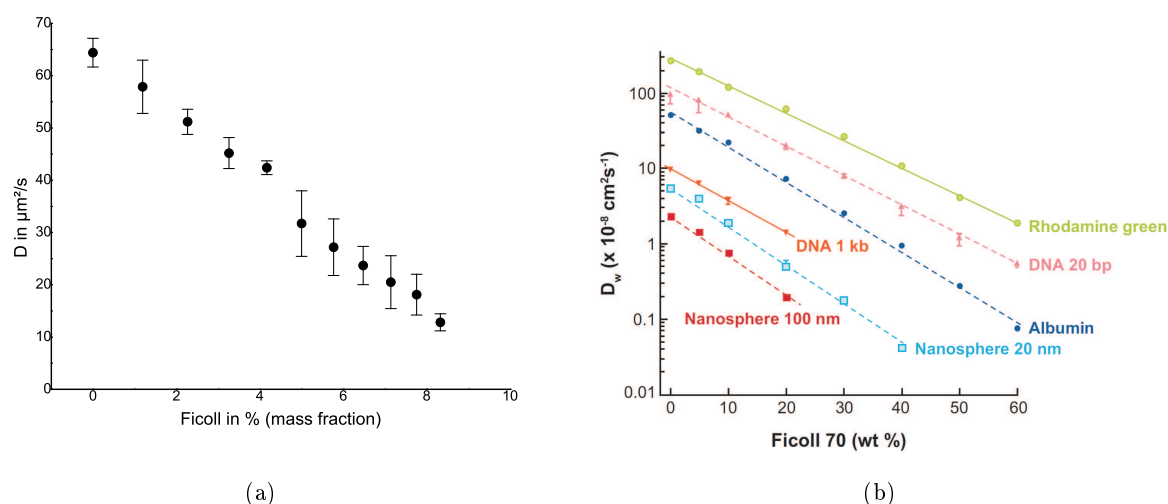
Figure 9.19: Mobility of particles in dependence of molecular crowding determined by FCS. (a) The diffusion coefficient of MinE-Alexa488 decreases linearly with increasing mass fraction of Ficoll 70. (b) For comparison this graph displays the decreasing diffusion coefficients of various biomolecules and further nanoparticles measured by Dix et al. The graph is taken from Ref. [469]. The Ficoll percentage is given as the mass fraction (wt/wt).

Fig. 9.18(a) shows the respective kymographs, the red bar marks the processed region. For small gaps (left), kymographs of all three patches show the same slope whereas for large gaps (right), the kymographs of each patch has an individual slope of the fluorescent signal in the xt-space.

Effect of molecular crowding

The wave is probably "transmitted" from one membrane patch to the other by a local increase in the buffer just above the membrane and therefore motivate the initiation of a protein wave on a close neighbor patch. If this is true, then such coupling behavior should be decreased if the mobility in the buffer is decreased. To test this hypothesis, SLBs were prepared on a grid structure and Min-proteins were allowed organize into waves. During observation of Min-protein binding dynamics, the molecular crowding was increased stepwise by addition of a highly concentrated solution of the crowding agent Ficoll. The Ficoll stock solution had a weight percentage of 25 % of Ficoll and volumes of 10 - 20 µL were added to the 200 µl K-SLB buffer in the observation chamber.

Molecular crowding was validated by measuring the diffusion coefficient of MinE labeled with Alexa 488 using FCS (see Sec. 8.2.3). Previously it was observed that in the presence of un-coated glass, Min-proteins adhere to the glass surface. In order to prevent adhesion of proteins to the cover slide and therefore constant removal of proteins from the aqueous volume, FCS measurements were performed in the presence of a SLB which does not allow adhesion or binding of MinE without MinD and ATP. 1 µL of a 100 µM MinE solution labeled with Alexa 488 was mixed with 200 µl K-SLB buffer and volumes of 10 µl of a 25 % Ficoll solution was added stepwise up to a final Ficoll mass fraction of percentage of 8.33 %. For 0 % Ficoll and after each addition, the diffusion time of MinE was measured recording the photoncount in ten runs, 10 s each. Autocorrelation curves of the photon count were fitted with a one-component model for three-dimensional diffusion (for further details see Sec. 8.2.3). From diffusion times, the diffusion coefficient was calculated and plotted against the Ficoll mass fraction. The corresponding graph is shown in Fig. 9.19(a). The diffusion coefficient of MinE decreases proportionally with

Characteristic	Cell	Artificial membrane
Wavelength	5 - 8 µm	50 - 100 µm
Wave velocity	~0.05 µm/s	~1 µm/s
Viscosity/Molecular crowding	High	Low
Membrane fixation	Free standing	Supported
Membrane crowding	Yes, transmembrane proteins	No, pure lipid membrane
Periodic pattern	Oscillations	Wave propagation
Reaction volume	Tiny	Large
Dimensions	3D	2D

Table 9.3: Differences between Min dynamics *in vitro* and *in vivo* and presumable reasons.

increasing Ficoll mass fraction.

For validation of the FCS data presented here, similar works are shown in Fig. 9.19(b). Dauty and Verkman have measured the diffusion coefficient of various particles in dependence of the FCS mass fraction as well [469].

For grids with a separation of 10 µm, wave coupling could be observed if no Ficoll was added. However, upon addition of Ficoll (final weight fraction 6%), membrane islands which shared common waves with neighboring membrane patches exhibited individual and decoupled wave pattern which can also be visualized in kymographs.

Numerical simulations on Min-protein waves in the presence of molecular crowding upon addition of Ficoll yield a similar picture. Fig. 9.18(b) shows two times the same microstructure grid. On the left side, Min-proteins diffuse through the standard buffer before and after binding to the membrane. On the left hand side, the aqueous buffer is characterized by an increased viscosity and thus a by a reduced mobility of Min-proteins. Mobility of Min-proteins in bulk is characterized by the diffusion coefficient D_{buffer} given in the graph. Whether waves couple or not, is difficult to distinguish looking at the pure images. But upon transfer of the data from the *xyt*- into the *xt*-space through kymographing (here indicated by the red bars), the coherence of wave propagation can be made visible. For the example with the high mobility (standard buffer without Ficoll), neighboring patches reveal the same pattern of the fluorescent signal. However, for a reduced mobility (buffer with the crowding agent Ficoll), neighboring membrane patches exhibit individual wave patterns although the gap between them would be sufficiently small.

9.3 Discrepancy between Min dynamics *in vitro* and *in vivo*

It was shown that Min-protein can be reconstituted *in vitro*. On supported lipid bilayers they self-organize into parallel propagating waves [1]. This is in stark contrast to previous observation of Min-protein dynamics *in vivo*. Here, an oscillatory pattern of the Min-protein membrane attachment pattern was observed, e.g. the alternating appearance of Min-proteins at the opposite poles of *E. coli* cells. In addition, the wavelength that was attributed to this oscillatory pattern in cells is 10-fold smaller than the wavelength observed *in vitro* [188, 189, 190, 358]. What is the origin of the difference of scale for the wavelength and for the different modes of periodic patterns? Tab. 9.3 lists the two main different phenomenologies (wavelength and periodic pattern) between the *in vivo*- and *in vitro*-World and the possible explanations and reasons. However, concerning the different modes of periodic patterns, it has to be questioned whether there is a difference between *in vivo* and *in vitro* at all.

9.3.1 Wavelength reduction by ...

One of the striking differences of Min dynamics between *in vivo* and *in vitro* systems is the magnitude of the wavelength. On artificial membranes, all observed Min-protein waves so far had wavelengths on the scale of 50 - 100 µm which is about 10-fold higher than the wavelength which is attributed to the oscillations observed in cells. In *E. coli* the wavelength of the Min oscillation is about 5 - 8 µm (see Sec. 4.8 and Ref. [188]). The reasons for this scaling effect still remains obscure. Solely, the ratio of MinD and MinE and molecular crowding of the bulk was found to influence the wavelength, however, wavelengths could only be reduced by about 50% and thus, these parameters were not considered to be responsible for this scaling effect. One possibility is that the diffusion and binding kinetics, notably the attachment and detachment rate of Min-proteins to the membrane, control the wavelength.

... by molecular crowding

In the artificial cell membrane assay, the cytoplasm and cytosol is represented by the buffer in the observation chamber above the supported lipid bilayer, thus a pure aqueous solution containing different salts (Sec. 8.1.9). However, in the biological cell, the cytoplasm and cytosol is characterized not only by a high density of proteins and other biological molecules but also by a dense meshwork. Altogether, these components reduce the mobility of particles in the inner space of the cell. This molecular crowding is lacking in a simple aqueous buffer and was thought to be responsible for the different scaling of wavelength *in vitro* and *in vivo*. Therefore we induced molecular crowding by addition of Ficoll (see also Sec. 9.2.6). Supported lipid bilayers were prepared according to the standard procedure on cleaved mica, subsequently different Ficoll densities (Ficoll 70 and 400) were adjusted in the different samples, Min-proteins were added and the system was allowed to organize into parallel and propagating waves. For the sample without Ficoll and for each addition, a timelapse of 15 frames with an interval of 20s was acquired. Fig. 9.20(a) and 9.20(e) show typical micrographs for samples without and with a fraction of Ficoll (12.5%, wt/wt), respectively. At first sight, the sample with Ficoll seems simply to show a more irregular pattern but no drastic change of the wavelength. If there is a change in wavelength, it is of rather subtle nature. Regarding the quality of the data, manual determination of the wavelength is impossible or at least highly inaccurate. Therefore, image data was analyzed using the automated Fourier transformation presented already in Sec. 9.1.4.

Two different measurement series were performed, one with Ficoll 70 and one with Ficoll 400, each with increasing fractions of Ficoll up to 12.5% (wt/wt). Of each sample, several timelapses at different positions on the membrane were acquired, the Fourier transformation was applied on the acquired images stacks and respective wavelengths were calculated. Determined wavelengths are plotted against Ficoll weight fractions in Fig. 9.21. Indeed, the Fourier transformation reveals that molecular crowding through the addition of Ficoll decreases the wavelength of Min-protein waves. Within the investigated regime of mass fraciotns, the decrease is of linear nature. However, only a reduction of the wavelength from roughly 70 µm to 45 µm was measured for Ficoll mass fractions up to 12.5%. The series was not extended further since the aqeuous media became quite viscous at this percentage of Ficoll content, and measurements became difficult.

... elevated temperature

Diffusion is definitely and binding could be influenced by the temperature. Therefore, a measurement series with increasing and decreasing temperature was performed using a heatable microscope stage. Fig. 9.22 shows the influence of temperature on the conduct of Min-protein waves. The temperature was raised from 24.8°C to 41.9°C. Afterwards the sample was allowed to cool down. At first glance, waves just seem to vanish with increasing temperature (Fig. 9.22(c))
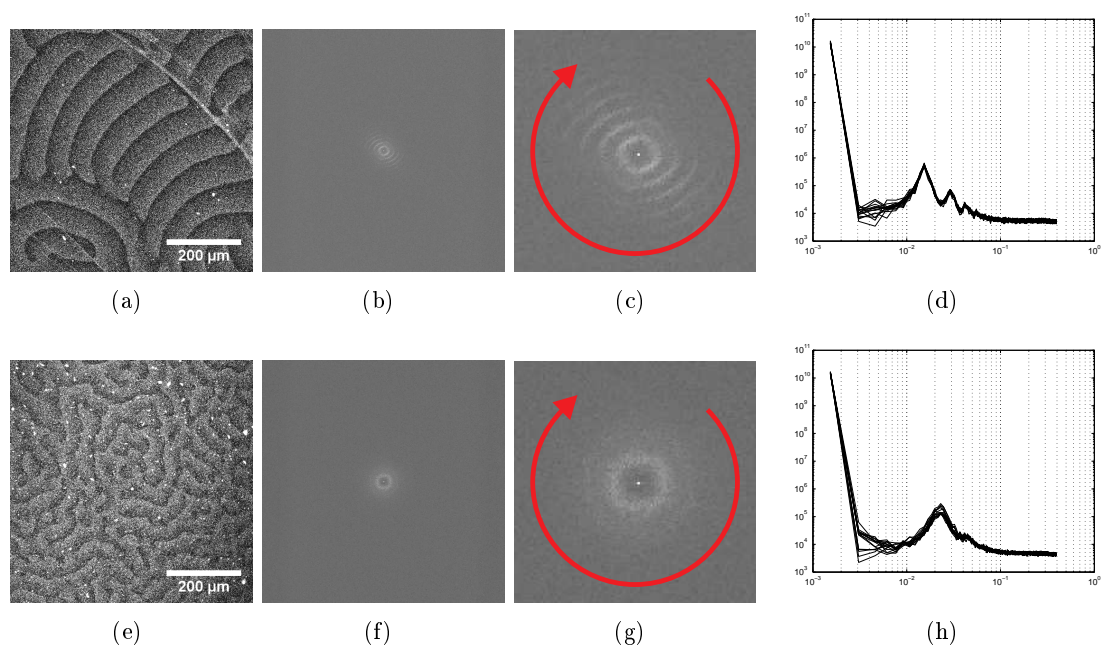
Figure 9.20: Fourier transformation of micrographs showing Min-protein waves using a custom MAT-LAB code (see Appendix, Sec. 11). (a)-(d) Min-protein waves without the crowding agent Ficoll. (e)-(h) with 12.5% Ficoll 400 (wt/wt). (a) and (e) Micrographs in real space. (b) and (f) Fourier transformation of (a) and (e). (c) and (g) Zoom-in of (b) and (f): The bright spot in the center marks the zero-order of the Fourier transformation and the rings the nth order. For the sample with Ficoll only the first order is visible (g) but for the sample without Ficoll up to four orders are visible (c). The distance between the maxima represent the length of the structure parameter dominating the original image, in our case this is the wavelength. The maxima of the different orders can estimated more easily and with higher precision when the two-dimensional reciproce space data is averaged by polar integration indicated by the circular red arrows. This produces one-dimensional power spectra shown in (d) and (h). Each line represents a frame of the timelapse containing 15 frames. By further averaging of these 15 frames, the position of the maxima can be estimated with higher precision.
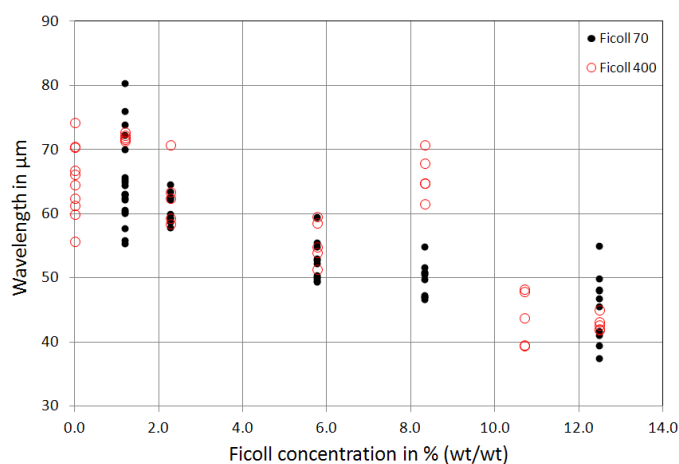
Figure 9.21: Addition of the molecular crowding agent Ficoll - here Ficoll 70 or 400 - reduces the wavelength by about 50%, probably by reduction of the mobility of Min-proteins in bulk.

 (a) 24.8°C   (b) 32.8°C   (c) 39.0°C   (d) 41.9°C   (e) 29.7°C to 28.7°C.
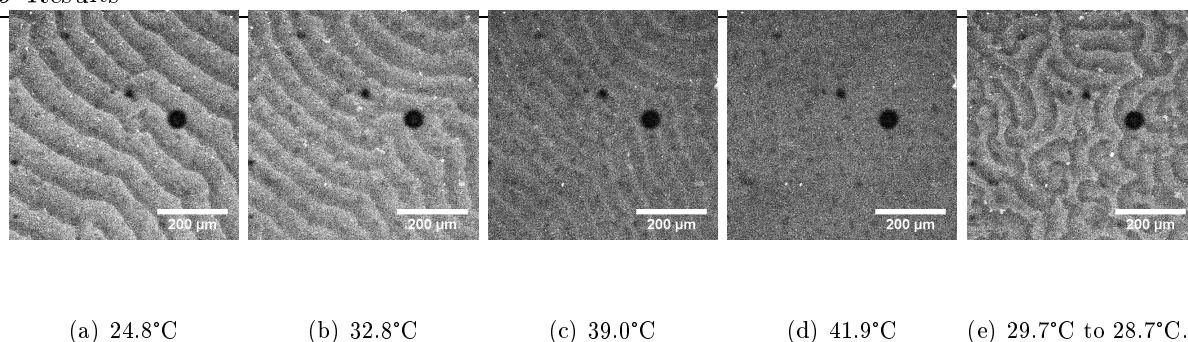
Figure 9.22: Influence of increasing temperature on the behavior of propagating Min-protein waves. At elevated temperatures the Min-protein waves start to vanish. After cooling down they reappear, however, waves are of poor quality.

(a)   (b)
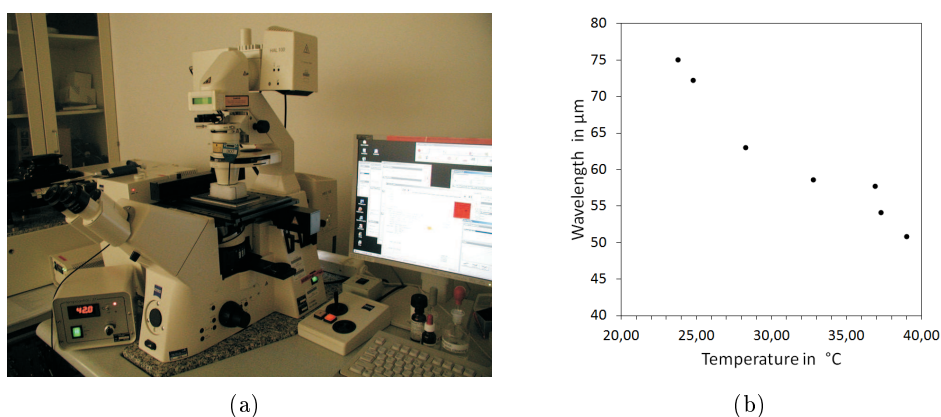
Figure 9.23: The temperature of the sample was controlled using a heatable microscope stage for petri-dishes. The observation chamber with the SLB was mounted into the petri dish which was filled with water as a heat transfer medium. In order to prevent heat dissipation, the petri dish was covered with a piece of plastic foam. The control unit of the heatable microscope stage features an actual temperature sensor, which, in fact represents the temperature of the stage but not that of the sample. The sample temperature was estimated using a separate thermometer immersed into the petri dish.

until they have completely disappeared (Fig. 9.22(d)). However, a Fourier transformation analysis (Sec. 9.1.4) reveals that the wavelength is decreased by about a third (from 75 to 50 µm) as shown in Fig. 9.23(b). The data point for 41.9°C had been omitted since the FFT analysis could not detect any wavelength in the respective data. When the sample was allowed to cool down again, waves reappeared (Fig. 9.22(e)), though waves were more crippled compared to before heating.

The reasons for this change of wavelength and decreasing contrast remained obscure. Either the properties of the Min-proteins were changed, or the lipid bilayer structure was changed by passing through the transition temperature of the lipid mixture. The origin for the disappearance of the Min-protein waves as well as the wavelength reduction remain to be clarified.

... by bulk height variation

Min-protein dynamics are not only confined laterally on the membrane by the short length and width of *E. coli* cells which are inferior to the wavelength that can be attributed to cellular Min-protein oscillations. Mobility of Min-proteins is additionally limited in the cytoplasm by two factors: molecular crowding and the confined bulk space which is reduced by the nucleoid which occupies the major part of the inner volume of the cell. In respect to the entire cell volume it occupies a relatively large space, about one fifth of the cytosolic volume which is about
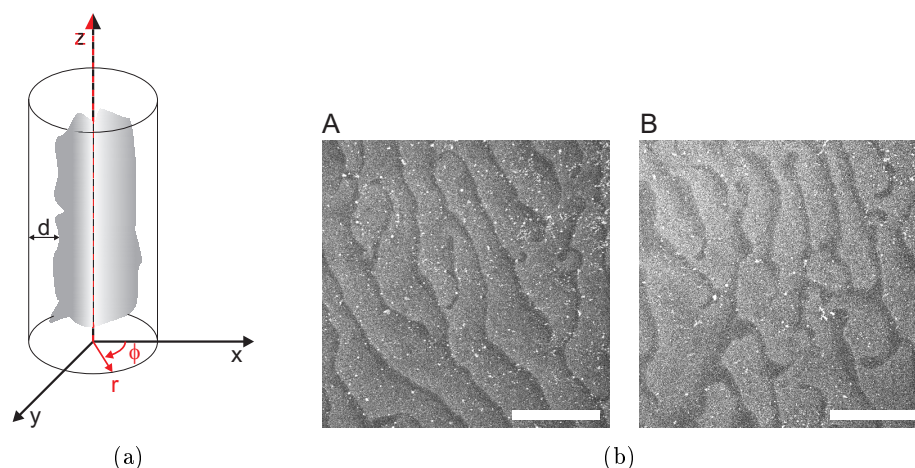
Figure 9.24: Influence of bulk diffusion space on Min-protein wave propagation. (a) A schematic view of the cell wall (cylinder) and the nucleoid (gray shaded area) in a Cartesian (black axes) and cylindrical (red axes) coordinate system. The z-axis is shared by both coordinate system. The nucleoid reduces the radial space d for diffusion of cytosolic particles, not only Min-proteins. (b) Reduction of the bulk height by applying a PDMS stamp on a SLB supporting Min-protein waves neither changes the wave pattern nor the wavelength. (A) Without stamp and (B) with stamp. Scale bars are 100 μm.
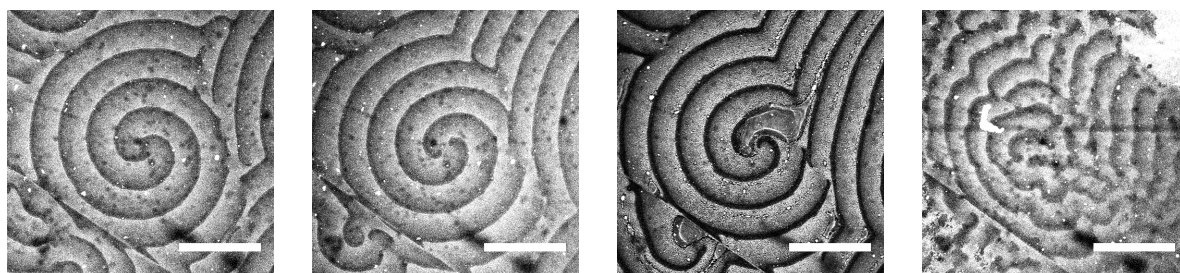
Figure 9.25: Removing of the buffer in order to reduce the bulk height. From left to right: full buffer volume (200 μL), 150 μL removed, all buffer removed and full buffer volume again. Scale bars are 200 μm.

$1\,\mu m^3$ [14, 15]. Consequently, regarding a cylindrical coordination system, the available space of Min-protein diffusion is reduced in radial direction by the nucleoid as shown in Fig. 9.24(a).

Numerical simulations suggest that variation of the bulk height modifies the wavelength of propagating Min-protein waves [470]. Narrowing the bulk height above the membrane reduces the available space for diffusion of Min-proteins away from the membrane which again is supposed to reduce the wavelength. On the other hand, it was shown within this work, that the protein density in bulk decreases rapidly above the membrane (see Sec. 9.1.5). Therefore, the influence of bulk height variation on Min-protein waves was also tested *in vitro* by different methods.

The most straightforward method to reduce the available space perpendicular to the membrane is by applying a stamp on a SLB. Fig. 9.24(b) shows Min-protein waves with an unconfined bulk space and the same region of interest after pressing a pure PDMS stamp on the membrane. Interestingly, no significant difference is observable between the sample with unconfined space and that with the drastically reduced bulk height. The wavelength has also not changed, nor any other influence of the naked PDMS on the lipid bilayer or protein pattern is observed.

In parallel, a different approach was tested to reduce the bulk height by simple removal of major quantities of the reaction buffer. Fig. 9.25 shows subsequent images of the same area of a supported lipid bilayer with Min-protein waves. Again, no influence of the bulk height is observed upon removal of the aqueous media. Only, when the membrane was completely cleared
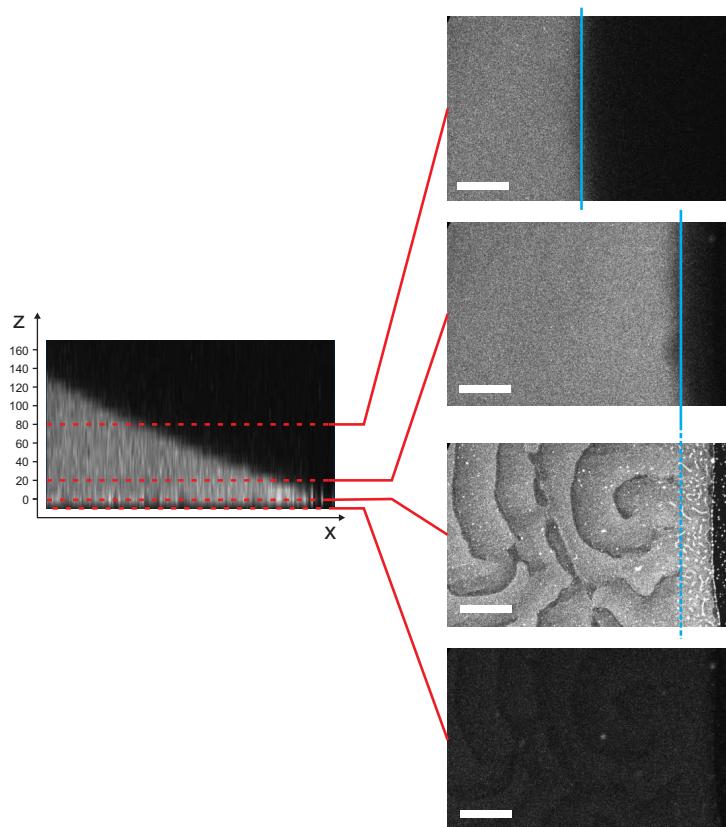
Figure 9.26: yxz-stack through a supported lipid bilayer with a buffer meniscus above. Left: xz-cross section, the meniscus (fluorescent triangle) is clearly visible. Right from bottom to top: xy-slices from below the bilayer (bottom), at the level of the bilayer

from the buffer, a change of Min-protein dynamics was observed: Without the reaction buffer, the dynamic Min-protein wave pattern stalled and froze in the current shape. When the removed buffer was added again, the dynamic wave behavior was resumed, however in a more irregular pattern.

The bulk height can be easily measured by scanning the focus in z-direction through the sample. This can be nicely demonstrated with a meniscus. Fig. 9.26 shows several cross sections of a simple SLB sample with Min-protein waves (right column of Fig. 9.26). The bottom displays the level just beneath the membrane which is occupied by the glass slide. The Min-protein pattern can only be guessed since it is out of focus. The second micrograph was acquired just at the level of the membrane and shows Min-protein waves as usual. The image stack was acquired at a region with a meniscus of the aqueous media just above. The meniscus was achieved by partial removal of the working buffer. On the right edge of the image at given height (second micrograph from below in the right column) a dark stripe is visible. This region has been cleared from the buffer, no Min-protein fluorescence can be observed. In the same micrograph, going from right to left, the change from dark to bright marks the edge of the meniscus. The rim of the membrane region that is covered by buffer shows bulk fluorescence with short bright, static and curved lines but no dynamic wave pattern. This region on the membrane without Min-protein waves is of interest here. Apparently the disappearance of waves is coupled to the narrow height of the meniscus above. This height shall be estimated. To the left, Min-protein waves appear. The border between the regions showing Min-protein waves and without waves, is marked with a blue dotted line. Further micrographs which were acquired at levels higher than the membrane are shown above. Note, that the bulk fluorescent withdraws from right to left as the microscope's focus rises. The blue line marks the meniscus interface between the fluorescent aqueous media and air. These micrographs are actually taken of an xyz-stack which is shown on the left hand side of Fig. 9.26. For better visuality, the stack is condensed to a xz-matrix by summing up

the y-dimension (Fig. 9.26, graph on the left). Several dotted red lines are drawn at different heights which correspond to the micrographs on the right side. The dark bottom line represents the space beneath the SLB which is the cover slide. The membrane itself is not visible in this view since its fluorescence disappears in the bulk fluorescence. The the blurred area represents the bulk containing fluorescently labeled Min-proteins. The dark area above is the air above the meniscus. Note that the xz-representation of the xyz-stack is not to scale. Scale bars are 100 µm and also apply to the x-axis of the xz-representation on the left. However, the scale of the z-axis is given on the axis (in µm). The level of the membrane is set to a height of 0 µm.

Now the focus is raised in such a way that the interface of the meniscus between aqueous media and air is at the same position as the border between the regions with and without Min-protein waves on the membrane (dotted blue line in the second and continuous blue line in the third micrograph in the right column counting from below). As it can be seen in the xz-representation, this level corresponds to a height of 20 µm above the membrane. This value is good agreement to the numerical simulations by Halatek et al. [470], however, in stark contrast to other experimental results presented in this work.

The origin of the discrepancy of wavelength *in vivo* and *in vitro* could not be fully elucidated. By molecular crowding in bulk, a decrease of the wavelength of about 40% was attained. Here, mass fractions of the crowding agent Ficoll up to 12.5% were applied. However, *in vivo*, the cytoplasm contains proteins and other molecules summing up to a mass fraction of 50% and other studies mimic the cytoplasm by applying Ficoll mass fractions of up to 60% [471]. If the linear decrease of the wavelength shown in Fig. 9.21 is extrapolated to a respective mass fraction of Ficoll, a further decrease of the wavelength is conceivable. However, higher concentrations of Ficoll became experimentally difficult because solutions were to viscous for pipetting and Min-proteins seemed to cluster as observed by FCS. Furthermore, molecular crowding by substances like Ficoll produce a mesh-like structure which solely decreases the potential diffusion path but not the diffusion coefficient itself. Diffusion itself can be decreased by increasing the viscosity of the sourrounding media. Elevating the temperature up to 42°C also decreased the wavelength by 33%. In addition, by the combination of mobility decrease and temperature elevation, cellular wavelengths could be attained. Another potential cause for different wavelengths in vitro and *in vivo* could be the molecular crowding within the membrane (see Sec. 10.2.2).

9.3.2 Oscillation vs. wave propagation?

Next to the discrepancy concerning wavelength, the other obvious difference between Min-protein dynamics *in vivo* and in *in vitro* is the appearance of different modi of dynamic and periodic pattern: oscillations in cells and propagating waves on supported lipid bilayers. What is the origin of this fundamental and qualitative discrepancy? It might seem absurd, but here it is questioned whether there is a difference at all.

Oscillatory pattern of Min-protein membrane binding is observed in wild type *E. coli* cells. Upon inhibition of cell division, cells grow to long tubular filaments. When the Min system itself is not changed (Filamentation of *E. coli* can be achieved by deletion of *minE* but also simply by deletion of *ftsZ*), periodic Min dynamics continue in those filaments. In such cells not only oscillations but also propagating Min-protein waves along the tubular structure are observed [188, 114, 193, 194]. Apparently, the emergence of wave pattern is linked to the length of the cell. Does the modus of periodic pattern formation switch from oscillation to waves upon increase of length? Another possibility is, that the periodic pattern that is observed in wild type cells is not an oscillation but also a wave whose propagation is stalled due to the lack of sufficient propagation path.

Thus, the periodic pattern in wild type cells have to be considered to be waves as well. The sole difference, concerning the appearance of waves, between *in vivo* and *in vitro* systems is the

space available for wave propagation. In wild type cells, the length of the membrane is short in respect to the wavelength, in addition the cytosolic space is closed and of tiny volume. Perhaps, similar Min-protein dynamics as *in vivo* can be reconstituted in artificial systems by stalling of Min-protein waves to an "oscillatory-like" pattern through reduction of membrane surface area and bulk volume. For example, an oscillatory-like pattern by volume confinement could evolve through the following mechanism: MinD and MinC bind to the membrane starting from the cell poles, and the membrane area coated by MinD and MinC expands towards the cell center. Expansion is stopped by MinE binding to MinD and detaching both, MinD and MinC from the membrane. Expansion of MinD binding is not only stalled but also pushed back to the cell pole where expansion originated. When the MinE-ring reaches the cell pole, almost all MinD and MinC proteins have detached from the membrane. These diffuse through the bulk until they bind again to the membrane. Binding to the membrane is thwarted by MinE and thus binding of MinD and MinC to the membrane is most successful at regions with a minimum of MinE which is naturally at the opposite cell pole. There, a new Min-protein wave can assemble. This oscillatory-like pattern would not be possible if the Min-proteins could diffuse somewhere else than to the opposite cell pole or even completely away.

Apparently, in order to provoke oscillations, it is not sufficient to reduce the surface area of the membrane, as it was shown by experiments with Min-protein waves on microstructured supported lipid bilayers (see Sec. 9.2.2) but rather the "cytosolic" volume has to be confined and sufficiently small. How small, this still has to be elucidated.

9.4 From supported lipid bilayers towards artificial cell structures

2D is not 3D. So far, only Min-protein waves on flat membranes have been investigated. But in *E. coli* the cell membrane is a curved, hollow and closed structure. Indeed, at this point, it is believed that the presence of a hollow and closed volume is an essential boundary condition in order to motivate protein oscillations instead of propagating waves (also see Sec. 9.3.2). Thus the first step towards closed and hollow artificial cells is the introduction of curvature into lipid bilayers.

Naturally, lipid bilayers form curved structures automatically in form of vesicles. But since vesicles come with several problems concerning control of curvature, protein reconstitution and especially imaging, a roadmap is suggested that starts with flat supported membranes with a certain curvature induced by the supporting substrate as described in Sec. 7.10. Supported lipid bilayers have an open surface in such a sense that the surface has a lateral boundary. Closed surfaces, such as surfaces found on spheres (solid or hollow) feature a surface without edges. Therefore, the next step is the closing up of open membranes to structures with closed surface. This is already achieved by vesicles. However, since vesicles can be very unstable and reconstitution of membrane proteins remains challenging on vesicles, especially in the micrometer range, it is suggested to use membranes supported on three-dimensional objects as an intermediate step. For this, any objects that are made out of (hydrophilic) material which allows the assembly of supported lipid bilayers is suitable such as glass, silica or plasma-cleaned PDMS (Sec. 8.1.7). Simplest three-dimensional structures are spheres, which are also readily available as glass beads in any desired size from the submicrometer range to centimeters. After successful reconstitution of the Min-protein assay, the next step would be test various geometries of closed, curved membranes supported on three-dimensional objects by variation of the object geometry. Here, the successful reconstitution of Min-protein waves on micrometer-sized glass cylinders is presented. Such systems are still distant from artificial cell by two characteristics: the solid support inside and the fact that the cell-mimicking reactions take place on the outside of the membrane and not on the inside. The possibility of reactions inside closed volumes is probably one the essential

features of biological cells Sec. 7.5. Thus, the next step on the road to an artificial cell supporting functional protein reconstitution is biased: The next level of complexity (and difficulty) could be achieved either by replacing the solid support by an aqueous media while keeping the reaction on the outside. This could be realized by GUVs to which the protein assay is added from the outside. Or, the previous system, protein reactions on the outside of membranes supported by three-dimensional objects, could be inverted: a cavity covered with a lipid bilayer on the inside. This could, for example be achieved by micrometer sized glass capillary coated with a membrane and flushed with the desired protein assay. However, both, GUVs with protein assay outside and glass capillaries with SLBs and open ends still lack the characteristic of a closed volume. In the case of the glass capillary this could achieved by closing the membrane coated glass tube on both ends after filling with the protein assay. Another option are microstructured compartments which are closed by a membrane-coated lid. In the case of vesicles, reactions inside a closed volume is achieved by inverting the previous system: the reaction must not take place on the outside of lipid vesicle but has to be introduced into the vesicle. This is nearly the last step on the roadmap from flat supported lipid bilayers to artificial cells concerning lipid bilayer manipulation. The last step would be the modification of the shape of the closed hollow membrane structure, for example to an *E. coli*-like rod (see also Fig. 7.12).

Again, it is important to point out why this road map was developed. Of course, "artificial cells" can be readily obtained by SUVs and if imaging is desired by GUVs. However, when it comes to protein reconstitution, researchers often have to recognize that protocols that work for supported lipid bilayers fail for vesicles for various technical reasons. This road map suggests a strategy of small steps: sidling up from a working membrane environment to a desired membrane environment by various intermediate steps. Each step should only involve minor modifications of the previous system successfully tested with the desired protein assay. This approach allows stepwise fine tuning of the biochemical system. Further steps using artificial cells concern pure biochemical issues. But the metamorphosis of biomembranes from supported lipid bilayers to artificial cells ends here.

9.4.1 Open curved membranes

Artificial membranes have perfectly excelled in terms of reproducibility and stability as flat supported lipid bilayers. But SLBs remain within the domain of two-dimensional membranes. Now, artificial membranes will be taken from two dimensions to the third dimension. Membranes in 3D implicate curvature of the bilayer.

In general, membrane curvature is thought to play a major role for cellular processes. The effect of membrane curvature on membrane and protein behavior can be nicely studied *in vitro* with supported lipid bilayers on substrates with a topological microstructure surface. For example, in the context of membrane phase separation, it has been shown that on microfabricated surfaces, imposing specific curvature patterns onto lipid bilayers, membrane geometry governs the spatial ordering of phase-separated domain structures in phase-separating membranes composed of cholesterol and phospholipids [472]. Here, the curvature-controlled phase separation is a consequence of the distinct mechanical properties of the lipid phases. With a similar substrate, it has been shown that periodically structured cationic membranes are capable of stretching DNA coils [473, 474].

In the Gram-positive bacterium *B. subtilis* the protein DivIVA takes a similar role as MinE in *E. coli* and limits the inhibitory activity of MinD to the cell poles [475, 476, 477]. For DivIVA it is known that it preferentially assembles to membranes with negative curvature [478, 479]. Thus, it is conceivable that the Min-system of *E. coli* is also influenced by membrane curvature.

The closest step from flat supported lipid bilayers to curved membranes is the introduction of
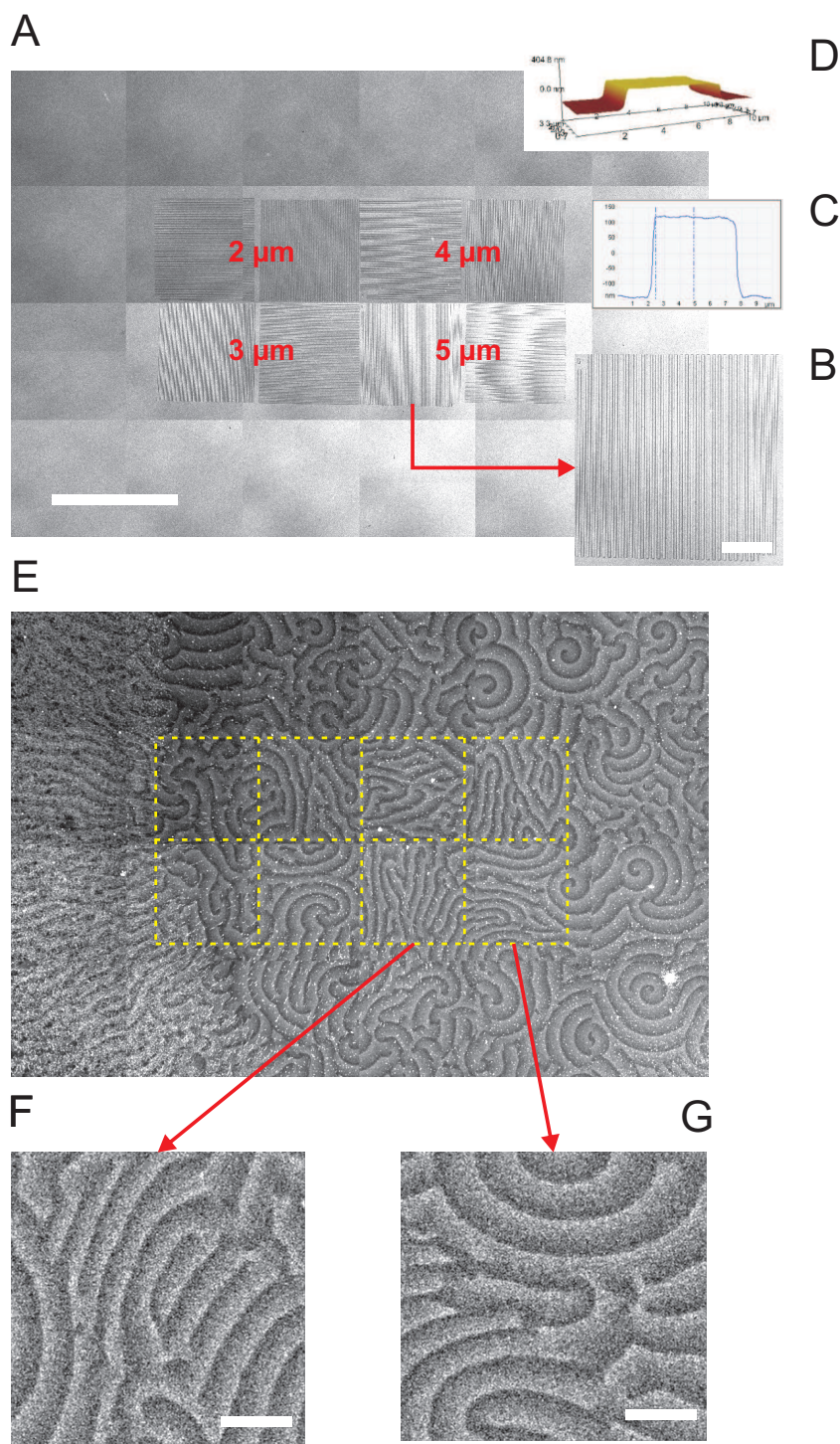
Figure 9.27: Guiding of protein waves (orientation of patterns) through microstructured surfaces. (A) Back reflection image of a glass substrate with horizontal and vertical trenches of varying width between 2-5 µm. (B) Zoom-in of vertical 5 µm-trenches. Height-profile (C) and AFM-representation (D). Min-protein waves organize into parallel and propagating waves on curved membranes (E). Interestingly, protein waves aligned parallel to trenches and propagated perpendicular to the trench orientation. Zoom of protein wave patterns for the 5 µm-trenches of vertical (F) and horizontal alignment (G).
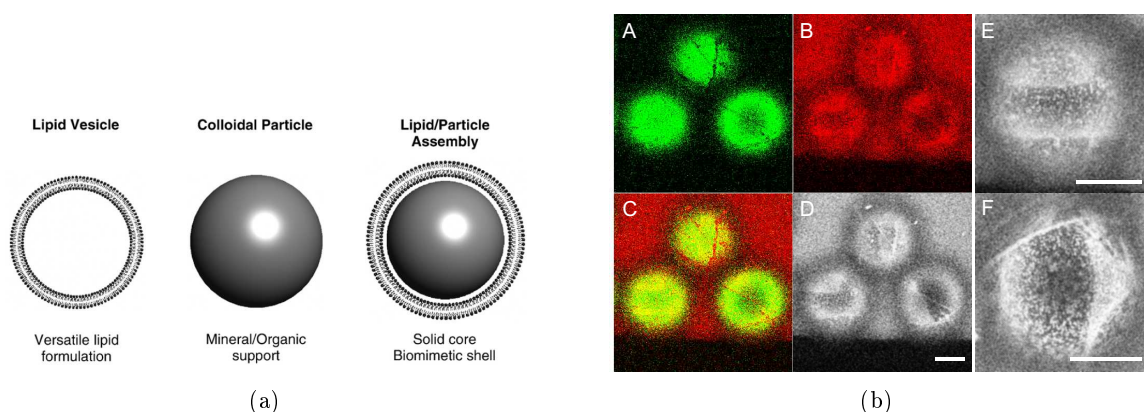
Figure 9.28: Artificial membranes on glass beads. (a) Concept three-dimensional objects coated with a membrane to mimic lipids with supported lipid bilayers. Graph is taken from Ref. [480]. (b) Protein waves on micron-sized glass beads. (A) Fluorescence channel for detection of the membrane (DiI). (B) Fluorescence channel of the MinE probe. (C) Merged image of the membrane and Min channel. (D) Min channel processed with a mean filter for better visibility of the waves. (E) and (F) Further examples of Min-protein waves on glass beads. Scale bars are 50 μm for all micrographs.

curvature into supported lipid bilayers by three-dimensional microstructuring of the substrate. This slight surface modification allows the retention of the sample preparation protocol and imaging procedure otherwise. Substrates with long parallel grooves of various width, depth and separation were produced as described in Sec. 8.1.4.

Supported lipid bilayers were prepared on such curved substrates using the standard protocol and Min-proteins were allowed to self-organize into waves. Fig. 9.27 shows the microstructured glass surface and the corresponding Min-protein wave pattern. In Fig. 9.27A, eight fields of parallel trenches of increasing width and separations ranging including 2, 3, 4 and 5 μm are visible. Width and separation are always equal. Each trench width is represented with a field of vertical lines and horizontal lines. Fig. 9.27B shows a further magnification of the field with 5 μm vertical trenches. Fig. 9.27C the corresponding height profile as obtained by AFM and Fig. 9.27D a 3D illustration. The trench depth is about 300 nm.

Fig. 9.27E depicts the respective pattern of Min-protein waves on the lipid bilayer supported on the curved glass substrate. The dotted line confines the structured region as shown in Fig. 9.27A. Surprisingly, the Min-protein waves seem to align parallelly to the trench orientation which is especially well visible for the fields with 5 μm trenches (zoom in in Fig. 9.27F and G). However, it has to be pointed out that these results could not be reproduced. The experiment was repeated several times, also using different microstructured substrates made from glass and PDMS but no alignment effects between parallel trenches and Min-protein wave propagation could be observed. Of course, these findings do not exclude an influence of membrane curvature on Min-protein wave pattern formation, but also does not proof it.

9.4.2 Min-proteins outside closed membranes

Cells are fully three-dimensional objects which provide the reaction chamber for biochemical processes. Synthetic systems mimicking cellular structures are given by lipid vesicles. However, reconstitution of Min-proteins inside liposomes has failed so far. A simplified lipid-based micron-sized reaction chamber are droplet-in-oil emulsions with a lipid-monolayer as an interface between the oil and water face. Unfortunately, reconstitution of Min-proteins into such systems could not be performed successfully (see Sec. 9.4.3). In the case of droplet-in-oil emulsions, the fact that the lipid interface is not a bilayer but a monolayer might be the crucial point for Min-protein
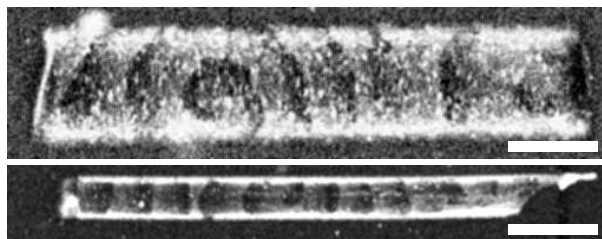
Figure 9.29: Protein waves on micron-sized glass rods obtained from telecommunication fibers. Micrographs are treated with a mean filter.

functionality, therefore reconstitution of the Min system might face principal feasibility issues that can not be overcome. However, reconstitution should be at least theoretically possible in lipid vesicles. In this case, problems are rather of technical than of fundamental nature. Therefore, research towards Min-protein systems in liposomes should be resumed.

Thus, the next step on the journey to fully functional membrane compartments is the closure of the membrane eliminating lateral boundaries and thus introducing a finite surface area of the reaction substrate for membrane-associated reactions. Still, this is most easily facilitated by the concept of supported lipid bilayers but now not with the help of flat or semi-flat substrates but with fully three-dimensional objects. Suitable, microscopic objects supporting lipid bilayers are glass or silica beads [480]. For the formation of lipid bilayers on the surface of mica or glass beads, these are simply incubated in the presence of lipid vesicles which thus adsorb to the objects. Glass beads covered with artificial membranes represent fully three-dimensional, closed membranes as depicted in Fig. 9.28(a). In addition, such membrane entities also feature area confinement of the lipid bilayer as obtained by gold microstructures.

Glass beads were prepared and SLBs were formed as described in Sec. 8.1.6 and 8.1.12, Min-proteins were added to the buffer containing the glass beads and beads were observed by LSM. The tricky part is that images of objects of different focus positions have to be acquired very fast in order to observe the wave propagation. Non-scanning sectioning microscopy systems such as spinning disk microscopes were available in our laboratory (for example Vt-Infinity III) but could not reach the signal quality attainable in LSM.

Naturally, these supported membrane systems facing open buffer solution did not support oscillatory behavior. However, Min-protein waves could still form on these membranes, where they propagated across the spherical bilayer. Fig. 9.28(b) shows several such glass beads covered with a lipid bilayers, *E. coli* polar lipid extract as usual, and propagating Min-protein waves spinning around the spherical structure. Fig. 9.28(b)(a) displays the membrane itself, Fig. 9.28(b)(b) the fluorescence of the labeled Min-proteins and Fig. 9.28(b)(c) both channels merged. Imaging is also made difficult since the bulk is filled with the protein probe as well and can not be excluded by sectioning. Therefore, Fig. 9.28(b)(d) depicts a copy of the Min channel processed with a mean filter. Fig. 9.28(b)(e) and (f) present two other examples of spinning protein waves on glass beads.

These experiments were a proof that Min-protein waves could emerge on curved and even closed SLBs. No characteristic effects were observed due to the fact the SLBs did not have open ends but formed closed structures. Furthermore, closed membranes successfully proved to be a rung on the ladder to artificial membrane compartments by supporting Min-protein dynamics.

The experiments with protein waves on glass beads encouraged the testing of the interaction of Min-proteins with SLBs on elongated glass rods. Many cells are not as isotropically spherical as a glass sphere. Furthermore, it was found out that propagation of Min-protein waves aligns with the longest axis of a flat membrane structure (Sec. 9.2.3). Would this also be the case for curved and closed membrane structures? Therefore anisotropic membrane structures have to

be considered and different geometries have to be tested while mimicking the cell membrane. Though this step is only a slight modification of membranes on glass beads, it is a technical challenge since anisotropic glass or silica objects in the microscopic range are not as readily available as microscopic spheres. In consequence, rod-like glass objects were produced from standard telecommunication glass fibers.

Telecommunication glass fibers of different diameters, chopped into short pieces, were used as supports for SLBs and Min-proteins were reconstituted as described previously (Sec. 8.1.6, 8.1.12 and 8.1.16). Particles were observed under LSM and protein dynamics were recorded in time-lapse z-stack. Protein waves were observed on most of the present microrods (Fig. 9.29). Interestingly, on these elongated glass rods, wave propagation always also occurred along the long axis of the rod, resembling the orientation of protein oscillations along the long axis of the *E. coli* cell. Unfortunately, the production of such microrods is very costly in terms of time and manpower (see Sec. 8.1.6), therefore the overall output of useful data was very small. Consequently, no correlation between direction of wave propagation and geometry or aspect ratio of microrods could be drawn.
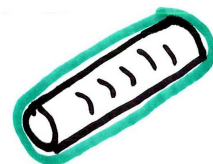
Furthermore, reconstitution of Min-proteins was also tested on the outside of giant unilamellar vesicles. GUVs were prepared by electroformation as described in Sec. 7.7.2. After formation of GUVs, the external media was exchanged in favor of K-SLB buffer for the Min-protein reactions (Sec. 8.1.9). In order to prevent membrane from bursting due to osmotic pressure, the internal osmolarity of the GUVs was adjusted to that of the K-SLB buffer by the usage of sucrose solutions instead of water during electroformation. Thus, after sample preparation, GUVs contained sucrose solution on the inside and the external media was K-SLB buffer. Min-proteins were added according to the standard protocol (Sec. 8.1.16). The limiting difficulty in this experiment was, that the external media, the K-SLB buffer, had to contain Magnesium ions for the ATPase by MinD. As discussed in Sec. 8.1.12 divalent ions facilitate the fusion of bilayers. In consequence, GUVs started to fuse and collapse rapidly within minutes. During this short time window no protein binding activities could be observed. For observation a spinning disk system was used. However, due to the fast bursting of the GUVs, no meaningful micrographs could be acquired.

9.4.3 Inside closed hollow structures

Because it is believed that oscillations can only be obtained inside hollow and closed compartments, there is a high motivation to find systems where Min-proteins can be reconstituted into closed membrane structures. The integration of Min-proteins into GUVs would be straightforward. This has been tested in the past using the GUV jetting method, unfortunately without success (unpublished data).

Droplets

The generation of curved and closed bilayers by droplets-in-oil emulsions was tested to reconstitute Min-proteins inside the droplets [407, 453]. Droplets were prepared as described in Sec. 8.1.14. The droplet media was K-SLB buffer containing the standard concentrations of Min-proteins and ATP. Droplets were observed by LSM. No protein binding dynamics were observed (Fig. 9.30). Min-proteins seem to be very sensitive to the bilayer structure, therefore it is highly probable that a remaining oil phase between the two leaflets of the lipid bilayer modified the bilayer in such a way that no protein waves could emerge. This is probably also the reason why no protein binding dynamics can be observed inside GUVS obtained by GUV jetting where also a small amount of oil remains between the leaflets of the vesicle bilayer.
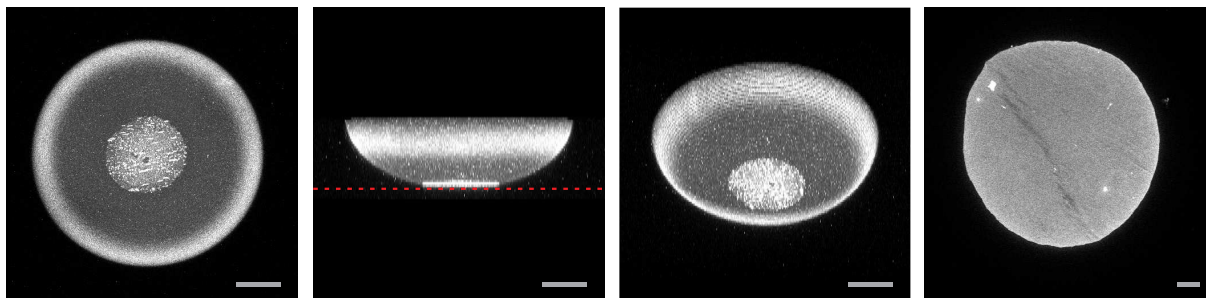
Figure 9.30: An droplet-in-oil containing Min-proteins and ATP. No protein binding dynamics but only static and homogeneous Min-protein binding could be observed. For reasons of better visuality, only the lower half of the droplet is shown. From left to right: Bottom view, side view with the red dotted line indicating the level of the cover slide, worm's-eye view and on the very far right side Min-proteins on a lipid monolayer of another droplet sitting on the cover slide. Scalebar is 100 µm for all micrographs.

Figure 9.31: Min-protein waves in a PDMS/glass chamber. The PDMS well is covered with a glass lid and both, PDMS and glass are covered by a supported lipid bilayer. Left: Min-protein waves on the SLB on the glass lid. Right: Min-protein waves at the "bottom" of the PDMS well.
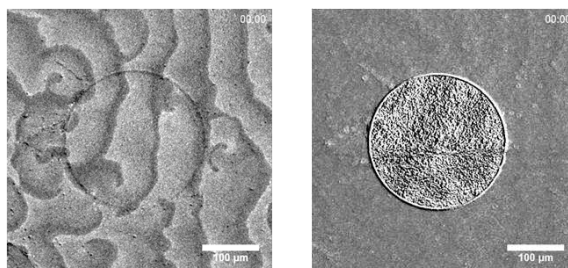
Closed wells

It is believed that one of the most important features of cells is the limited reaction volume (Sec. 7.5). So far, all membrane systems presented here were characterized by an open reaction volume which allowed diffusion away from the membrane and therefore loss of important reactants into the bulk and exchange between different membrane entities. It was wished to suppress both. How can one build microscopic and closed membrane compartments with a hollow inner volume that serves as the reaction chamber for biochemical processes? Of course, lipid vesicles seem to be the method of choice but acknowledging the difficulty of integration of membrane proteins inside liposomes, low-hanging fruits were aimed at first. Thus, the essential step was tried to be achieved without abscising too far from the established and working methods. Solid objects coated with a membrane in an open reaction volume flag the most distant position on our road map but still provide a safe base for the reconstitution of proteins. A nearby approach is therefore to simply invert the system, to turn inside-out: solid matter with a cavity providing a microscopic reaction volume and a membrane coating the inner wall of the cavity. It is possible to reconstitute Min-protein waves on supported lipid bilayers, in confined geometries and even on curved substrates. Therefore, it should be possible to encapsulate Min-proteins inside a compartment that is derived from a previously open configuration like a pot and a fitting lid. Micron-sized wells were achieved by PDMS microstructures obtained from SU8-molds produced photolithography (see Sec. 8.1.5) and coated with a lipid bilayer. Glass slides were covered with a membrane carpet and reconstituted with Min-protein. After successful formation of waves the lipid-coated PDMS substrate was pressed onto the glass slide.

Fig. 9.31 shows the pattern of Min-protein waves in such an inverted pot-lid system. Fig. 9.31(a) shows the lower level, the lid, which is represented by the glass slide. The circumference of the circular well is also clearly visible. The height of the chamber is in the range of 10 µm. Inter-

estingly, the Min-protein wave propagation is not influenced by a fact that a stamp is pressed onto the SLB. Fig. 9.31(b) shows the upper level, the bottom of the "pot". For better visuality, the micrograph is processed by an algorithm that removes the static background (see Sec. 9.1.2). Interestingly, the Min-protein waves propagate in the same direction as on the lower level. Apparently, wave propagation is coupled across the micron-sized bulk space between the two opposite sides of the compartment.

However, as Min-protein waves propagate unobstructed beneath the edge of the PDMS well, it has to be assumed that the PDMS cavity is not fully closed by the membrane coated cover slide. Apparently, a very narrow space above the membrane is sufficient for Min-protein wave propagation.

10 Conclusions

For the conclusions, first a brief summary of the scientific background and findings of this PhD-thesis will be given. Next, the most essential results will be discussed in the light of relevance for cell division in *E. coli*. Finally, the outlook suggests further steps in the research of Min-protein dynamics and chemical waves in general.

10.1 Summary

This section does not summarize the entire content of the PhD-thesis but compiles findings and results which are most important in the eyes of the author.

10.1.1 Cell cycle, cell division, Z-ring and Min-protein oscillation

Sec. 1, 2, 3 and 4

The process of cell division presumably represents the most drastic step of the cell cycle: out of one entity, two identical copies but individual entities emerge [13]. Cell division is essential for growth and replication of any biological matter. In the past, the process of cell division was extensively studied using different model organisms. In the model organism *Escherichia coli*, cell division is initiated by the assembly of FtsZ-proteins to the Z-ring at the membrane [30, 8]. For division into two equally halved cells, it is essential that the cell divides at its center. Assembly of the Z-ring is inhibited by the protein MinC, thus FtsZ-proteins only assemble at positions of the cell membrane low in MinC-concentration [178]. MinC binds to the protein MinD, and consequently, the topological distribution of MinC is directly coupled to the distribution of MinD. The localization of MinD is regulated by self-organizing oscillations in concert with MinE: MinD oscillates between the two cell poles whereas the third protein of the Min-family, MinE, forms a central ring which confines the distribution of MinD to the cell poles [188, 185, 183, 194]. Because of this, MinD and thus MinC have maximal residence probability at the cell poles and show minimal attachment at the cell center [194, 196, 92]. Since the inhibitory function of MinC, the Z-ring can only assemble at the cell center. In fact, *E. coli* has three potential division sites which are defined by the gap between the segregated chromosomes and by the DNA-free polar zones [97, 98]. This additional regulatory mechanism became known as the nucleoid occlusion model [83]. In case of mutations of *E. coli* at the genetic *min*-locus, the cells can also "divide" at these polar positions leading to so-called *minicells* [96]. The discovery of the minicells has triggered research of the division site selection mechanism in *E. coli* and the Min-proteins were named after the minicelling phenomenon [163, 164].

10.1.2 Min-protein waves *in vitro* and lateral confinement of membranes

To better study the mechanism behind the Min-oscillations, Loose transferred the involved components, MinC, MinD, MinE and ATP into an artificial membrane system [1]. On supported lipid bilayers, Min-proteins showed parallel and propagating waves and not oscillations. The lateral extension of the supported lipid membranes was infinitely large compared to the wavelength of the Min-protein waves. However, a cell membrane has a limited surface area. Thus, the

question arose, what would happen if the substrate for the Min-protein waves — the supported bilayer — would be confined to dimensions at the scale of the wavelength, and how boundaries and geometric structures would interact with the propagation of Min-protein waves?

Micro-structured bilayers by photolithography

Sec. 8.1.3

In order to obtain membrane patches of pre-defined geometry, supported lipid bilayers were combined with micro-photolithography [396, 397, 450]. Glass substrates were covered with a gold layer which was subsequently etched away to produce glass "windows" of defined geometry. Passivation of the glass substrate by metals is known to inhibit the formation of functional lipid bilayers. Thus, when lipids were added, fluid membranes were only formed in the glass areas free of gold. Upon reconstitution, Min-proteins self-organized into parallel and propagating waves.

Influence of boundaries on wave propagation

Sec. 9.2.1 and 9.2.2

The first open question was whether the propagation of Min-proteins is at all affected by passivation of the support. By the introduction of obstacles in form of passivated squares in a checkerboard fashion, it was shown that the Min-protein wave propagation indeed is affected by passivated areas (Sec. 9.2.1). For small obstacles, no influence could be observed. However, when the passivated squares were of the same dimension as the wavelength, wave propagation changed. For medium-sized obstacles, first the wave coherence suffered. For larger passivated squares, waves between the obstacles became decoupled. This behavior indicated that the Min-system could sense boundaries which is a prerequisite for the ability of geometry sensing.

Wave alignment in elongated structures

Sec. 9.2.3

From these findings, the question arose, how lateral confinement of the membrane substrate and thus reduction of the available surface area would affect wave propagation. For large structures, wave propagation seemed to be unaffected by the confinement of the membrane. However, when at least one dimension of the membrane extension was reduced to the scale of the wavelength, wave propagation adapted to the membrane geometry (Sec. 9.2.2). In the case of simple and very long structures, waves followed the long axis of the membrane extension (Sec. 9.2.3). In rectangular structures with an aspect ratio greater than 0.3, waves propagated along the diagonal which represents the longest extension in a rectangle. This effect underlines the capability of Min-protein waves to detect the extension of membrane structures.

For mutations of *E. coli* with round or nearly round cell shape, it was observed that Min-proteins oscillated along the longest axis if it is sufficiently longer than the shortest axis [464]. If the longest and shortest axis were of almost similar length, i.e. nearly spherical cells, direction of oscillations alternated in a random manner. Numerical simulations revealed that a minimal length difference of 5% would be necessary so that Min-protein oscillations can differentiate between longest and shortes axis [465]. Taking this tolerance into account, expected deviations of the angle of wave propagion from the diagonal in rectangular membrane patches were estimated theoretically. These calculations predicted that Min-protein waves can not differentiate between the longitudinal and the longest axis for rectangles with an aspect ratio lower than 0.3. This rough theoretical estimation is in good agreement with our experimental findings.

In elongated structures with round caps ("2D-rods"), the longitudinal axis is also the longest axis. For such structures, Min-protein waves always propagated along the longitudinal axis for

geometries of low aspect ratio (long structures), and became more and more random when the 2D-rod was of nearly circular form. Numerical simulations of our experiments in rectangular 2Drod-like membranes produced the same results.

Wave guiding in arcuate structures

Sec. 9.2.4

In kinked membrane stripes, for example in an L-shape, Min-protein waves followed the arcuate path (Sec. 9.2.4). Interestingly, in doing so, the outer flank of the wave front traveled at a significantly higher speed than the inner flank. This is presumably due to changing MinE/MinD-ratios at the edge of the kink. Min-protein waves can be guided through any kind of curved SLBS, including circles, loops and slalom-geometries.

Wave coupling

Sec. 9.2.6

The membrane exchanges Min-proteins with the bulk [182, 183]. In consequence, the bulk must reflect to some extent the protein density on the membrane. If two individual membrane patches are separated by only a small gap, then Min-protein dynamics on both membrane islands should be able to "communicate". This assumption was quantitatively investigated using grids of square membrane islands of various size with varying gaps (Sec. 9.2.6). First of all, it was shown that Min-protein waves can indeed couple across a separation. Coupling was observed for gap sizes up to $10\,\mu$m. However, due to the chaotic propagation of Min-protein waves, no conclusion could be drawn for gaps larger than $10\,\mu$m. The ability of waves to couple is apparently linked to the mobility of Min-proteins in solution. When diffusion was decreased by introduction of molecular crowding through Ficoll, waves lost the ability to couple across small gaps $< 10\,\mu$m (Sec. 9.2.6).

10.1.3 Parameters influencing the wavelength

Min-protein dynamics on a flat open geometry differ from those observed *in vivo* by two means. First of all, on supported lipid bilayers, Min-proteins form waves instead of oscillations and the respective wavelength is about 10-fold larger than in cells (Sec. 9.3).

Wavelength vs. molecular crowding

Sec. 9.3.1

The mobility of Min-proteins in bulk was suspected to be one of the crucial parameters for the emerging wavelength [92]. In order to study the effect of diffusion capability, the mobility was decreased using the crowding agent Ficoll [471]. Through the addition of Ficoll, the diffusion of Min-proteins could be decreased by a factor of 6 as measured with fluorescence correlation spectroscopy (FCS). Within the same regime, the wavelength decreased from about $70\,\mu$m to $45\,\mu$m.

Wavelength vs. temperature

Sec. 9.3.1

Another suspect as a determinative factor for the wavelength was the temperature. Temperature could influence wave formation by several means. First of all, an increase of temperature increases the mobility. Secondly, an increased temperature raises the rate of most biochemical

reactions [92]. An increase of the temperature from 25°C to 42°C made the waves look less coherent but also decreased the wavelength from about 75 μm to 50 μm.

Wavelength vs. bulk diffusion space

Sec. 9.3.1

As a third possible cause, the variation of the space in the solution above the membrane was investigated as suggested by Halatek and Frey [470]. First of all, the distribution of MinE-proteins in bulk in *z*-direction was studied (Sec. 9.1.5). *z*-stacks using laser scanning microscopy revealed that MinE-proteins accumulate few micrometers above the membrane and do not diffuse far into bulk. This finding is in good agreement with the model of transient binding of MinE developed by Loose et al. [10]. Next, diffusion of Min-proteins into the bulk was limited by applying a stamp on the membrane allowing only a thin, aqueous film between the membrane and the stamp. Surprisingly, this did not affect the wave propagation. Alternatively, the layer of the aqueous media was lowered. Here, wave propagation abruptly stopped upon removal of the buffer and froze into the current pattern or simply vanished. No change of wavelength was observed. However, this is certainly an aspect that should be investigated further (see 10.3).

Fourier-analysis of Min-protein waves

Sec. 9.1.4

In general, the wavelength represents a crucial parameter of Min-protein dynamics. The same Min-proteins lead to different length scales of periodic pattern in *in vitro* and *in vivo*. Thus, it is clear, that the wavelength difference can not be due to genetic mutations but must be under the control of external parameters. In this work, aspects of molecular crowding and temperature were tested and both clearly influenced the wavelength of Min-protein dynamics. However, *in vitro* experiments of this and previous studies show a high variation of the wavelength, even within the same sample. Other works analyzed wavelengths by hand [1, 10]. Considering the high variation of wavelength in one sample, this makes analysis by hand prone for errors. To minimize these, a high number of wavelength examples should be measured which makes analysis by hand time-consuming and inconvenient. By the introduction of an automated Fourier-analysis, wavelength analysis could be made fast, reliable and reproductive (Sec. 9.1.4). This method is also suggested for future studies on Min-protein waves. The respective code, written in MATLAB, can be found in the DVD enclosed with this PhD-thesis or downloaded from *www.qucosa.de*.

10.1.4 Min-protein waves on curved membranes and inside compartments

Flat supported lipid bilayers differ largely from cell membranes, not only in terms of lipid and protein composition but also in their supramolecular structure. In order to mimic cellular membranes better, different membrane geometries were tested together with the reconstitution of Min-proteins. For successful implementation of membrane curvature and three-dimensionality, a respective roadmap was developed (Sec. 7.10).

Waves on grooves

Sec. 9.4.1

Periodically curved membranes ("grooves") were obtained by assembly of supported lipid bilayers on glass substrates with a respective topology [452]. Upon reconstitution of Min-proteins, these self-organized into propagating waves (Sec. 9.4.1). Initially, a guiding effect of Min-protein waves perpendicular to the groove alignment was observed but could not be reproduced within this PhD-thesis.

Waves on three-dimensional objects

Sec. 9.4.2

Fully three-dimensional artificial membranes were obtained by coating glass beads with lipids [480]. When these were immersed into a buffer containing the Min-protein assay, Min-proteins attached to the membrane on the floating glass beads and formed waves which spun around the spheres (Sec. 9.4.2). Cylinder-like artificial membranes could be produced by the assembly of lipids on telecommunication glass fibers cut into short pieces. Min-protein waves also readily formed on these.

Waves in compartments

Sec. 9.4.3

In vivo, Min-proteins are enclosed into compartments, namely cells. In order to mimic a similar situation, Min-proteins were encapsulated into droplets immersed in an oil phase containing lipids which form a monolayer at the interface between the oil and the aqueous phase [407, 453]. Binding of Min-proteins to this lipid monolayer could be observed, but no apparent Min-dynamics emerged (Sec. 9.4.3). Alternatively, encapsulation of Min-proteins was tested by closing PDMS-wells — revetted with a membrane — with a glass lid carrying a supported lipid bilayer. However, closure was apparently not sufficient enough since Min-protein waves continued propagating on the membrane lid without being affected by the boundary of the PDMS-well.

10.2 Discussion

10.2.1 Role of the inner membrane

Cell division concerns the whole entity of the cell, therefore, a cell division mechanism must be able to capture the entire spatial extension of the cell. This is achieved by the Min-system which explores the full length of the cell through its oscillations. Here, the cell envelope represents the boundary and thus defines the spatial extension of the cell. In the case of gram-negative cells, the cell envelope consists of the inner membrane, the cell wall or sacculus and the outer membrane [16]. Furthermore, cell division is completed by synthesis of new cell wall material and closure of the septum between the dividing cells [29]. The two new daughter cells are separated from each other by their cell envelopes. Again, the cell envelope defines the identity of the two new-born cells.

Therefore, it is obvious that the cell envelope plays a major role in the cell division process. Through the closing septum, the cell envelope basically accomplishes the cell division in an active manner. On the other hand, the cell envelope is also essential for division-related processes that take place before the actual separation of the two daughter cells. Therefore, it is the inner or plasma membrane rather than the cell wall or the entire envelope that is important. Prior cell division, the inner membrane has two important functions, which are however - in contrast to the closing septum - of rather passive nature.

First of all, the inner membrane is the foundation on which the divisome is assembled [79, 80, 30]. It was discussed that specific lipid composition exist at the potential division sites (midcell and polar caps), particularly the enhanced accumulation of cardiolipin [99, 100]. However, these heterogenities of the plasma membrane presumably have no functional role for the cell division process but are rather themselves a consequence of the division process (Sec. 3.3.2 and 3.3.3). During division the membrane at the midcell position experiences a dramatic change in protein composition through the assembly of the divisome. Furthermore, the process of invagination introduces a local curvature to the membrane [8]. Both modifications, protein attachment and

curvature might positively regulate the localization of certain membrane components such as cardiolipin [101]. Thus, these membrane domains can not be seen as a marker for the assembly of the divisome. The role of the inner membrane for the assembly of the divisome is presumably of passive nature in terms of a scaffold for assembling proteins.

The second - passive - involvement of the inner membrane takes place before the actual assembly of the cell division machinery. The cell division machinery is localized to the central position of the cell with the help of the oscillations of the Min-system [481]. In a mutually and antagonistic mechanism between MinD and MinE, MinD oscillates between the two cell poles. Hereby, MinD experiences a time-averaged distribution with maximal accumulation at the cell poles and a minimal residence probability at the cell center. Since the distribution of MinC is directly coupled to that of MinD, the time-averaged MinC-distribution exhibits a minimum at the cell center as well. Furthermore, MinC acts as an inhibitor on the capability of FtsZ to assemble to the Z-ring. Therefore, FtsZ accumulates preferentially at a position with minimal MinC concentration on the membrane - which is at the cell center. These Min-oscillations require the inner membrane as a substrate. In a purely aqueous environment, Min-proteins would diffuse in isotropic manner, the emergence of inhomogeneities would be impossible. Only in the presence of a membrane to which Min-proteins can attach, inhomogeneous MinD — and thus MinC — distributions can emerge.

The cell division process is a nice example in order to understand the outstanding role of the membrane for the life of a cell.

10.2.2 Discrepancy between *in vivo* and *in vitro* phenomenology

Cells and *in vitro* assays differ largely in structure, size and number of different components. Thus, it is astonishing how well cellular mechanisms can be reconstituted in an artificial environment [382]. The prerequisite is that the respective mechanism involves only few components. This requirement is fulfilled by the Min-dynamics since they rely on only four components: MinD, MinE, ATP and the membrane. Yet, biochemical assays reconstituted in an artificial system still show different phenomenologies to their cellular counter parts. For example, it is assumed that the cell membrane features sub-micron lipid domains, so-called rafts [482, 395]. When respective lipid compositions are reconstituted into giant unilamellar vesicles, lipids phase-separate on the micrometer scale [394, 104]. Though this effect is welcomed by the researcher since it simplifies observation (see Sec. 7.9), it still represents a difference of the *in vitro* and *in vivo* phenomenology [438]. A similar discrepancy between cell and synthetic biology phenomenology is also observed for the Min-system: different scales of wavelengths and different modes of periodic patterns - oscillations and waves [1].

Though named oscillations, Min-proteins dynamics *in vivo* were also characterized by the attribution of a wavelength [188, 356, 345, 199, 189, 190, 358]. This wavelength and thus the oscillation period increases with length of the cell until the cell divides. However, if cell division is inhibited, for example through suppression of *ftsZ*, the cell continues to grow to filaments. In this case, the wavelength of the oscillation does not grow infinitely but at a certain threshold length, a second oscillation emerges. Normally, these oscillations are exactly in an anti-phase, i.e. both polar caps are populated by MinD at the same time. As MinD detaches from the cell poles, two new MinD accumulations appear at the cell center. As long as both oscillations are in exact anti-phase, every oscillation explores the same length share of the filament. The wavelength associated to the oscillation at the threshold between one and two oscillations in long cells can be seen as the asymptotic value which is independent from the actual cell length — and thus as the "natural" wavelength of the oscillation [188]. This characteristic wavelength is *in vivo* about 10-fold smaller than the observed wavelengths of parallel and propagating waves *in vitro* [188, 1, 349].

Thus, two essential questions arise:

- Why are dynamics *in vitro* magnified in respect to those observed *in vivo*?

- Why are there oscillations *in vivo* and parallel, propagating waves *in vitro*?

From large to small waves

Concerning the differences in wavelength, different parameters such as molecular crowding, bulk space and temperature were investigated within the present study. However, cell-like wavelengths could not be reproduced. When increasing the molecular crowding by addition of Ficoll, the maximal mass fraction of Ficoll was 12.5 % for technical reasons. Higher contents of Ficoll made the handling of the buffer media difficult since it became too sticky. Furthermore, Min-proteins seemed to aggregate as observed in FCS. In addition, Min-protein waves became more and more disintegrated which made analysis difficult. However, the cytoplasm contains about proteins and other molecules summing up to a mass fraction of 50 % and other studies mimic the cytoplasm by applying Ficoll mass fractions of up to 60 % [471]. Thus, a re-examination of the effect of molecular crowding with a higher crowding level should be considered. Furthermore, molecular crowding by substances like Ficoll produces a mesh-like structure which solely decreases the nanoscopic diffusion space but not the diffusion coefficient itself. Diffusion itself can be decreased by increasing the viscosity of the sourrounding media. Thus, next to further increase of molecular crowding, the effect of viscosity on the wave dynamics of Min-proteins needs to be elucidated as well.

E. coli normally lives in an environment of elevated temperature. Thus, for mimicking cellular conditions, the attempt of temperature increase seems to be more than justified. Yet, cell-like wavelengths could not be attained by this strategy. In contrast to molecular crowding, the maximal level of temperature increase was certainly reached with 42°C. The temperature increase did not decrease the wavelength sufficiently, yet by a significant factor of about 33 %. Therefore, combination of molecular crowding and elevated temperatures could be a possible route towards smaller wavelengths.

Another potential cause for different wavelengths in vitro and *in vivo* could be the molecular crowding within the membrane. The cell membrane is composed not only of phospholipids and other simple organic molecules such a sterols but also of membrane proteins. The artificial bilayers used in previous studies and the present thesis were purely of lipid nature. It is certainly also worth to investigate the effect of lateral membrane crowding on Min-protein wave characteristics.

From waves to oscillations

Interestingly, in the case of filaments, it is possible that oscillations shift out of phase and the Min-protein dynamics do not appear as oscillations but as waves which propagate along the tubular structure of the filaments [483]. Probably, the dynamics observed in wild-type cells are actually not "oscillations" but rather waves which are stalled due to the restricted extension of cells. After MinD-proteins have populated an entire cap of an *E. coli*-cell, MinD is processively detached from the membrane by the MinE-ring that progresses from a midcell-position towards the polar ends. Transport of MinD is purely diffusive in the cytoplasm (i.e. no active transport takes place) and thus free MinD tries to bind anywhere in the cell but succeeds to attach only to membrane positions which fulfill two conditions: membrane binding sites should be free (so that MinD can bind) and no MinE should be in the vicinity (otherwise MinD would be detached again). Naturally, such membrane regions can be found opposite to the previously populated cell pole. Now, the priorly free polar cap is populated by MinD. If no MinE would be present, this attachment would actually continue until the entire cell membrane is covered by MinD [188].

However, after the MinE-ring has successfully detached all MinD-proteins from the previous cell pole, MinE also detaches from the membrane and assembles at the boundary of the new polar cap of MinD and the oscillation cycle starts over again.

Now, let's consider that the cell is sufficiently long, so that the membrane region between the two cell poles already fulfills the two conditions for MinD-binding (free binding sites and no MinE in the vicinity). In this case, freshly detached MinD won't diffuse to the other cell pole but would populate the closer regions. Again, the MinE-ring would accumulate at the rear of this new MinD-accumulation. But this time, the MinD-region would be "pushed" forward until the end of the cell is reached where MinD has to detach from the membrane. Now, the "oscillation" behaves like a wave.

If the spatial confinement is the sole determining parameter, then it should be possible to transform *in vitro* waves into oscillations. How could this be achieved? As it was shown in the present study, lateral confinement of the two-dimensional supported lipid bilayer is not sufficient to convert waves into oscillations. From the description given above, it has to be considered that it is the bulk diffusion space which has to be finite. Therefore, by sufficient confinement of the bulk volume, oscillations of Min-proteins should be also possible in artificial membrane systems. In fact, a recent study in our laboratory has achieved *in vitro* oscillations of Min-proteins [484].

10.2.3 From flat bilayers towards artificial cells

The idea of synthetic biology is to mimic real biology in order to understand better basic mechanisms of life [485, 382]. The term *synthetic biology* covers two distinct approaches: top-down and bottom up. Whereas the top-down concept is based on the manipulation or restructuring of existing organisms, the bottom-up concept tries to imitate biological matter and processes by assembly of biomolecules from scratch[486, 487, 376, 368]. In the present work, a variation of the bottom-up approach was applied by using natural lipids and proteins derived from bacterial cells.

Bottom-up synthetic biology requires full control of all involved components. Therefore, it is recommended to reduce the number of different actors as much as possible. Min-protein dynamics excel for such a bottom-up *in vitro* assay since only four components are required: MinD, MinE, ATP and the membrane. Furthermore, previous studies by Loose also pursued a strategy of reduction of cellular structures: the cell membrane was mimicked using supported lipid bilayers [1, 10]. This artificial membrane can be seen as the most radical simplification of the cell membrane, maybe next to small unilamellar vesicles.

However, the far goal of the bottom-up approach is to approximate real cells as far as possible. Thus, a roadmap was developed as a proposition how to climb the ladder of complexity from a simple *in vitro* configuration towards an artificial cell. In our lab, the membrane is perceived as the principle structure that defines the cell. Therefore, any strategy to increase the complexity of an *in vitro* assay should address the lipid bilayer structure. Membranes of biological cells are confined in their surface area, furthermore they experience different degrees of curvature. The aspect of curvature also transfers artificial bilayers from a two-dimensional to a three-dimensional world. Cell membranes are closed, i.e. they don't expose any edges which produces an hollow inner volume. Finally, the membrane is free-standing and thus the cell can take and adapt to different forms. Therefore, the presented roadmap suggests a possible pathway from supported and unconfined lipid bilayers towards confined, curved, closed, hollow, fully free-standing and deformable artificial membranes. At the same time, the proposed steps of this roadmap shall be applied to the reconstitution of the Min-system. Here, several modifications of artificial bilayers have been presented in order to advance along this roadmap and each single step has been tested in combination with the Min-system. First, supported lipid bilayers were confined in their lateral extension by passivation of the support against lipid adhesion. Next, curvature was

introduced by topological modification of the substrate. Membranes were closed up by assembling lipid bilayers on spherical or rod-like objects which made these fully three-dimensional. Hollow membrane structures were achieved by inverting the approach of objects covered with bilayers by revetting the inner wall of compartments with lipids. For all these bilayer systems, the Min-system could be successfully reconstituted. The reconstitution of the Min-system on the outside of free-standing bilayers was recently achieved by Ariadna Martos [349]. Katja Zieske could establish full closure for the Min-system in bilayer structures in solid compartments [484]. Further steps — membrane configurations — of the proposed roadmap are already established, however awaiting the successful reconstitution of the Min-system. This especially concerns the reconstitution of the Min-assay inside droplets and giant unilamellar vesicles.

10.2.4 From geometry sensing to cell polarization

What is the significance of the capability of Min-proteins to sense membrane geometry *in vitro* for the cell?

Cell division in wild-type *E. coli* cells always divide at the cell center. Furthermore, the division plane is always perpendicular to the long axis. At first sight, this seems to be rather irrelevant. However, if the division plane would be flipped by 90° so that it would be no longer perpendicular but parallel to the long axis of the cellm, for example, then the division plane would intersect both chromosomes. In this case, cell division would be impossible or the distribution of replicated DNA would be incorrect. Recently, it was shown that in *urchin* eggs, the cell geometry determines the positioning of the cell division plane [11]. Min-protein waves can sense the geometry of artificial membranes. Thus, it is conceivable that the Min-proteins take a similar role in *E. coli*. A similar relationship between cell polarization and Min-protein oscillations was already considered by Huang [465]. Furthermore, the orientation of the division plane influences the supra-cellular structure (see Sec. 3.2).

10.2.5 The Min-system as temporal trigger for cell division

Nowadays, it is clear that division site localization is the principal function of the Min-system. Here, it is suggested that definition of the division plane could be an additional task. A third function of the Min-system was considered in the past but has drawn only little attention [188, 191, 92]. The Min-system could not only be decisive in where to divide but also *when*. When *E. coli* is full-grown, it divides at a position with a minimum in membrane-bound MinC and thus MinD. For wild-type cells, this minimum emerges at midcell. After division of the full-grown mother cell, two new daughter cells are generated which are naturally smaller than the mother cell. In each daughter cell, proper oscillations emerge. However, the respective minimum of MinD probably does not establish right away with the emergence of oscillations but only after the cell has grown to a specific length. An intrinsic wavelength can attributed to oscillations in *E. coli* [188, 356, 345, 199, 189, 190, 358]. This intrinsic wavelength is considered to be independent of the cell length and can be seen as a constant for given boundary conditions. Consequently, it is conceivable that the wavelength could serve as a cellular ruler which tells the cell when it has grown-up. For example, it is conceivable that the required minimum of MinD only emerges when the cell has reached a specific length in respect to the wavelength. For shorter cell lengths, polar cap accumulations of MinD could super-impose in such a way that the respective profile does not feature a minimum. Only when polar caps are far enough from each other, can a MinD gap emerge. Considering such a mechanism, the Min-system would not only be a detector of the cell center but also of the time point when to divide.

However, this function is speculative to this day. To my knowledge, no published research work has investigated the temporal development of the MinD-profile. In general, the existence of the

MinD-minimum was drawn in phenomenological manner from the observations of Min-protein oscillations *in vivo*. Only few publications have established respective MinD-profiles but did not perform further investigations on the temporal behavior [199, 92].

10.3 Outlook

10.3.1 Issues addressed in this study

The principal motivation for this PhD-thesis was the investigation of the comportment of Min-protein waves on confined supported lipid membranes. The principal finding from this study is that Min-protein waves can sense the geometry of a given membrane patch by aligning to its form and pathway. However, further issues are of interest.

In rectangular membranes with an aspect ratio higher than 0.3, Min-protein waves propagate along the diagonal. When a rectangle is split into two halves, the orientation of the diagonals of the two split rectangles has changed. Thus, the question arises, whether the direction of Min-protein wave propagation would adapt to the new diagonals and how fast would this occur.

It was shown that Min-protein waves can couple across gaps at least smaller than 10 µm. For larger gaps, no clear statement could be given. However, coupling between membrane islands could also be investigated by other means. For example, measuring the photon count of a confocal fluorescence spot, the momentary concentrations of Min-proteins between two patches could be measured. In the case of an coupled exchange, a periodic increase and decrease should be observable in the photon count.

Beyond the scope of membrane confinement, further issues of the Min-system were investigated. Yet, also here is an area for more research. As already pointed out, the influence of higher levels of molecular crowding as well as the effect of viscosity on the wavelength should be investigated. The effect of the combination, temperature increase and mobility reduction, could lead to an enhanced decrease of the wavelength and therefore should be also elucidated.

Bulk diffusion space above the membrane was also considered to be responsible for the wavelength. Prior to further attempts to narrow down the diffusion space, it would be helpful to establish a MinD-profile in z-direction as it was done for MinE in the present study.

10.3.2 Intrinsic wavelength

The Min-oscillation is probably in fact a propagating wave which is stalled due to the lack of propagation space. If cell division is inhibited in *E. coli* and filamentation of cells allowed, then multiple oscillations emerge [188]. The distance between these oscillations can be seen as the intrinsic wavelength of the Min-system [199, 189, 190, 358]. If oscillations shift out of phase, propagating waves emerge [483]. Most statements on the intrinsic wavelength base on the original observations of multiple oscillation in filaments by Raskin and de Boer in 1999 [188]. The respective publication shows a filamentous cell exhibiting four oscillations. The authors themselves do not consider any wavelength-like parameter, but other authors conclude an intrinsic wavelength from the observations made by Raskin and de Boer. Interestingly, though trivial, different values are established [189, 190, 358]. In the following time, the intrinsic wavelength has drawn only little attention. Touhami et al. have investigated the dependence of the intrinsic wavelength on the temperature and have observed that the intrinsic wavelength is independent from temperature [189]. A more systematic study and analysis of the intrinsic wavelength in *E. coli* would certainly help to complete our knowledge of the Min-system *in vivo*.

10.3.3 MinD- and MinE-profiles

Averaged over time, Min-protein oscillations result in a minimum of MinD at the cell center which is decisive for the assembly of the Z-ring and thus for the localization of the division site. However, only few studies have given a quantitative illustration of the MinD-minimum [199, 92]. Furthermore, the temporal evolution of the MinD-profile could trigger the time-point of cell division,. However, no respective investigation was presented thus far.

No description was found at all in literature for the MinE-profile based on experimental data. Yet, different considerations are made but which still await verification. For example, some authors consider a maximum for MinE at midcell whereas other consider a minimum like for MinD [356, 199].

Therefore, a systematic study of the MinD- and MinE-profiles, especially in terms of temporal evolution, would be helpful for the understanding of the Min-system.

10.3.4 Min-proteins, zebras and Mexican waves

Min-protein dynamics belong to the class of chemical waves. In contrast to physical waves, which can propagate without any energy consumption, chemical waves require energy to persist [461]. Furthermore, unlike physical waves, chemical waves can not be reflected at boundaries, they just vanish. When two chemical waves meet, they do not overlay and do not show constructive or destructive interferences [461]. This is also true for Min-protein waves, Min-protein waves require ATP and a wave disappears when it collides with another wave or when it reaches the end of the membrane substrate [92]. The first chemical wave, which was described in scientific terms was the Belousov-Zhabotinski-reaction (BZ) [461]. Other chemical waves are represented, for example, by prairie fires or by the famous Mexican wave in sport stadiums. Since the first description of chemical waves in 1959, they have been extensively studied in experiments and simulations. However, little attention was paid to the propagation of these chemical waves in confined and geometric substrates.

Maselko and Showalter have studied the comportment of BZ-waves on beads in the millimeter-range [488]. In 1994, Graham et al. observed guiding effects of catalytic oxidation waves of CO on geometric platinum surfaces [466]. Their observations are strikingly similar to the behavior of Min-protein waves on geometric membrane patches (Fig. 10.1(b) and 10.1(c)). One year later, Steinbock and Showalter used a substrate for BZ-reactions cut into a labyrinth and allowed BZ-waves to explore the maze [460]. BZ-waves propagated along all possible pathways but when two waves met, propagation was stopped. In consequence, each continuous path between two arbitrary points A and B in the maze always represents the shortest way between these two points. The respective maze geometry was adapted for a research work studying the directed growth by the slime *Physarum polycephalum* [489, 490, 491].

All these studies use chemical waves generated by the researcher and custom-made geometric structures. However, nature already provides us with a large range of chemical waves and geometric substrates. Especially in the world of animals, we can find many examples of pattern formation [492, 493]. When comparing pattern formation in fur of animals, striking similarities can be found to the observations of Min-protein waves on confined membranes. For example in zebras, black stripes are always oriented perpendicular to the elongation of the respective body parts: in case of a standing zebras, stripes are horizontal on legs but vertical on the torso (Fig. 10.1(a)). Together, the torso and the hind leg form a L-shaped-like structure with the thigh being the arcuate region. The "wave front" of the black stripes in this arcuate region shows a similar distortion like Min-protein waves in arcuate membrane patches with the outer flank being initially delayed.

Another example of chemical waves in constrained space is the so-called *Mexican wave* or *La*

(a)   (b)

(c)   (d)
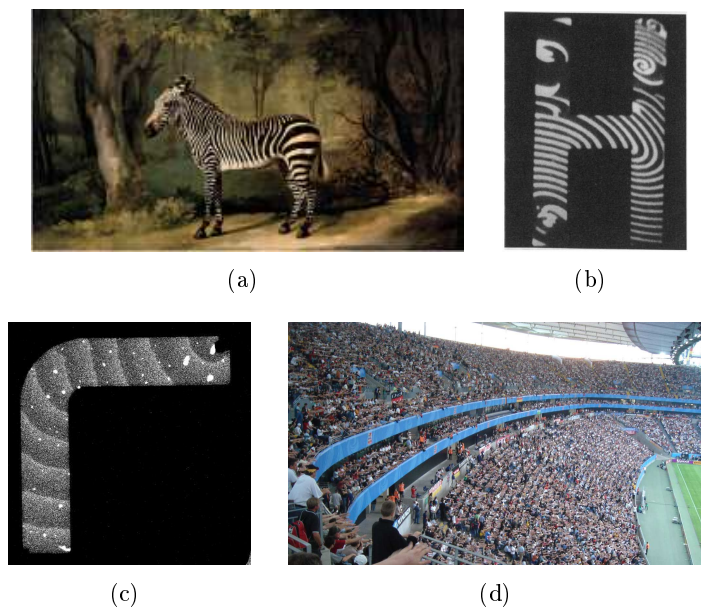
Figure 10.1: Different examples of chemical waves on confined substrates. (a) Zebra (Painting by George Stubbs, 1763). (b) CO-oxidations on a platinum surface (Image is taken from Ref. [466]). (c) Min-protein waves on a L-shaped membrane patch. (d) Mexican wave in the soccer stadium of Frankfurt (Image from Wikimedia Commons).

ola (Fig. 10.1(d)). A Mexican wave is the collective behavior of humans in an excited state expressing exultation by standing up or rising hands. Mexican waves can be observed in the audiences at soccer stadiums. However, Mexican waves have drawn only little attention. The sole investigation of Mexican waves in terms of a chemical wave did not elucidate the aspect of geometry [494]. It would be interesting to study the comportment of a Mexican wave within a group of people of a specific geometric form and the wave alignment in respect to the geometry. A first step could be the systematic investigation of the wave flank behavior of Mexican waves in the corners of rectangular stadiums.

11 Appendix

11.1 Calculation of the allowed deviation from the diagonal

The longest axis in a rectangle is represented by its two diagonals of length s_0 and with the angle δ_0 in respect to the longitudinal axes. Deviations from these axes are shorter than the diagonal (Fig. 11.1). There are two possibilities: one path representing a diagonal of a rectangle keeping the original width W but with a shortened length L' resulting in the path length s_W with an angle δ_W, and the other path representing a diagonal of a rectangle keeping the original length L and with a shortened width W', thus having a shorter path length s_L with an angle δ_L. The path lengths s_W and s_L shall represent the maximal deviation from the diagonal s_0 and they should BETRAGEN maximally the fraction p of the diagonal length s_0:

$$S_W \quad = p \cdot s_0 = p\sqrt{W^2 + L^2} = p\sqrt{W^2 + (W/ar)^2} = pW\sqrt{1 + (1/ar)^2} \tag{11.1}$$

$$S_L \quad = p \cdot s_0 = p\sqrt{W^2 + L^2} = p\sqrt{L^2 ar^2 + (W/ar)^2} = pW\sqrt{1 + (1/ar)^2} \tag{11.2}$$

The corresponding angles to the shortened path lengths can be thus calculated as

$$\sin\delta_W = \frac{W}{s_W} = \frac{a}{p\sqrt{ar^2 + 1}} \tag{11.3}$$

$$\delta_W = \arcsin\frac{a}{p\sqrt{a^2 + 1}} \tag{11.4}$$

$$\cos\delta_L = \frac{L}{s_L} = \frac{1}{p\sqrt{ar^2 + 1}} \tag{11.5}$$

$$\delta_W = \arccos\frac{1}{p\sqrt{ar^2 + 1}}. \tag{11.6}$$

$$\tag{11.7}$$

11.2 Supporting material

The enclosed DVD contains

- AutoCAD drawings of the gold microstructures

- Movies of acquired fluorescence microscopy data of Min-protein waves

- MATLAB codes for the determination of the wavelength and wave front distortion in arcuate paths
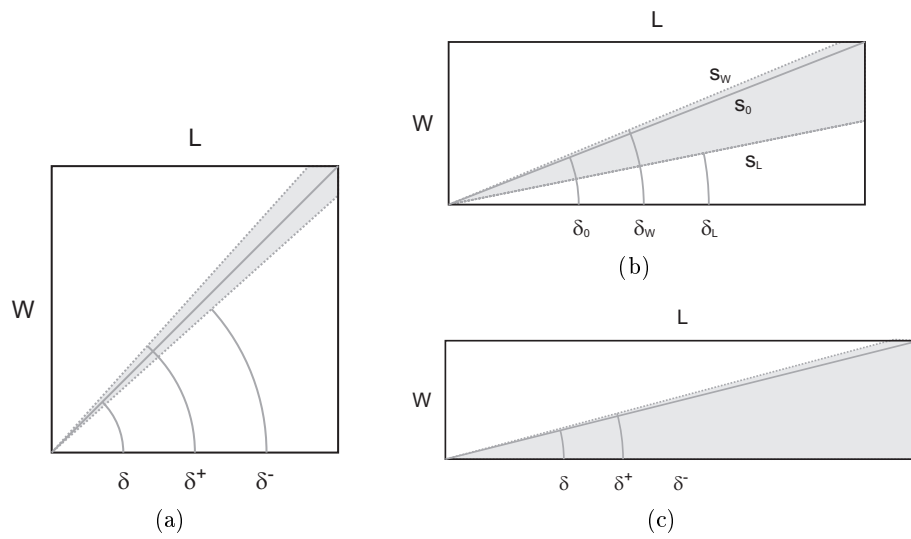
Figure 11.1: Angular deviation δ^+ and δ^- from the diagonal δ and corresponding paths that must not deviate more than 5 % from the longest axis which is the diagonal. Aspect ratios (a) $ar = 1$, (b) $ar = 0.39$ and (c) $ar = 0.25$.

Index of acronyms

Acronym	Full expression
AC	Aggregation current
bp	Base pair
CA	Cardiolipin
CA	Cooperative attachment
CAP	Covalently attached protein
DivIVA	Cell-division initiation protein in *B. subtilis*
DNA	Deoxyribonucleic acid
dnaA/DnaA	Gene/protein for DNA replication in *E. coli*
FCS	Flourescence correlation spectroscopy
FRAP	Fluorescence recovery after photobleaching
fts/Fts	Gene/protein-family: Filamentous growth is thermosensitive
GFP	Green fluorescent protein
GlcNAc	β-1,4-linked N-acetylglucosamine
GUV	Giant unilamellar vesicles
IM	Inner membrane
IMP	Integral membrane protein
IPTG	Isopropyl thiogalactoside
Lp	Lipoprotein
Lpp	Braun' lipoprotein
LPS	Lipopolysaccharides
LSM	Laser scanning microscopy
LTA	Lipteichoic acids
lts	Gene: temperature-sensitive lysis
min/Min	Gene/protein-family responsible for central cell division, mutation leads to the minicelling phenomenon
mreB	Gene controlling the width of *E. coli* cells
MukB	Cell division protein involved in chromosome partitioning
MurNAc	N-acteylmuramic acid
NO	Nucleoid occlusion (division selection model)
OM	Outer membrane
OMP	Family of Outer membrane proteins
Pbp	Family of penicillinbinding proteins
PE	Phosphatidyl ethanolamine
PG	Peptidoglycan
PG	Phosphatidyl glycerol
rodA	Gene responsible for maintaining the rod cell shape
sfiA/*sulA*	SOS cell division inhibitor
SLB	Supported lipid bilayer
slmA	DNA-associated division inhibitor that binds FtsZ and blocks septal rings, see NO model
SOS	Emergency cell division inhibition system
SUV	Small unilamellar vesicles
WTA	Wall teichoic acides
Zap	Family of Z-ring associated proteins
Zip	Family of Z-ring interacting proteins

Bibliography

[1] Martin Loose, Elisabeth Fischer-Friedrich, Jonas Ries, Karsten Kruse, and Petra Schwille. Spatial regulators for bacterial cell division self-organize into surface waves in vitro. *Science*, 320(5877):789–792, May 2008.

[2] Samuel Butler. *Life and Habit*. Jonathan Cape, 1910.

[3] Edmund Beecher Wilson. *The cell in development and heredity*. Macmillan, 1925.

[4] N. Nanninga, F. B. Wientjes, B. L. de Jonge, and C. L. Woldringh. Polar cap formation during cell division in escherichia coli. *Res Microbiol*, 141(1):103–118, Jan 1990.

[5] Bruno Müller and Ueli Grossniklaus. Model organisms–a historical perspective. *J Proteomics*, 73(11):2054–2063, Oct 2010.

[6] Theodor Escherich. Die darmbakterien des neugeborenen und säuglings. *Fortschr Med*, 3:515–528, 547–554, 1885.

[7] Heinz Flamm. The austrian pediatrician theodor escherich as bacteriologist and social hygienist: The 100th anniversary of his death on february 15th, 1911. *Wien Klin Wochenschr*, 123(5-6):157–171, Mar 2011.

[8] Piet A J de Boer. Advances in understanding e. coli cell fission. *Curr Opin Microbiol*, 13(6):730–737, Dec 2010.

[9] Joe Lutkenhaus. Assembly dynamics of the bacterial mincde system and spatial regulation of the z ring. *Annu Rev Biochem*, 76:539–562, 2007. x.

[10] Martin Loose, Elisabeth Fischer-Friedrich, Christoph Herold, Karsten Kruse, and Petra Schwille. Min protein patterns emerge from rapid rebinding and membrane interaction of mine. *Nat Struct Mol Biol*, 18(5):577–583, May 2011.

[11] Nicolas Minc, David Burgess, and Fred Chang. Influence of cell geometry on division-plane positioning. *Cell*, 144(3):414–426, Feb 2011.

[12] Mirjam E G. Aarsman, André Piette, Claudine Fraipont, Thessa M F. Vinkenvleugel, Martine Nguyen-Distèche, and Tanneke den Blaauwen. Maturation of the escherichia coli divisome occurs in two steps. *Mol Microbiol*, 55(6):1631–1645, Mar 2005.

[13] Daniel P. Haeusser and Petra Anne Levin. The great divide: coordinating cell cycle events during bacterial growth and division. *Curr Opin Microbiol*, 11(2):94–99, Apr 2008.

[14] A. Ryter. Association of the nucleus and the membrane of bacteria: a morphological study. *Bacteriol Rev*, 32(1):39–54, Mar 1968.

[15] David J. Sherratt. Bacterial chromosome dynamics. *Science*, 301(5634):780–785, Aug 2003.

[16] Thomas J. Silhavy, Daniel Kahne, and Suzanne Walker. The bacterial cell envelope. *Cold Spring Harb Perspect Biol*, 2(5):a000414, May 2010.

[17] Hans C. Gram. Ueber die isolirte färbung der schizomyceten in schnitt- und trockenpräparaten. *Fortschritte der Medizin*, 2:185–89, 1884.

[18] Kindal M Robertson and D. Peter Tieleman. Molecular basis of voltage gating of ompf porin. *Biochem Cell Biol*, 80(5):517–523, 2002.

[19] Waldemar Vollmer and Ute Bertsche. Murein (peptidoglycan) structure, architecture and biosynthesis in escherichia coli. *Biochim Biophys Acta*, 1778(9):1714–1734, Sep 2008.

[20] I. Takebe. Extent of cross linkage in the murein sacculus of escherichia coli b cell wall. *Biochim Biophys Acta*, 101:124–126, Mar 1965.

[21] U. Schwarz, A. Asmus, and H. Frank. Autolytic enzymes and cell division of escherichia coli. *J Mol Biol*, 41(3):419–429, May 1969.

[22] M.H. Saier. *Desk Encyclopedia of Microbiology*, chapter Cell Membrane, Prokaryotic, pages 251–265. Academic Press, 2009.

[23] Eugenia Mileykovskaya and William Dowhan. Role of membrane lipids in bacterial division-site selection. *Curr Opin Microbiol*, 8(2):135–142, Apr 2005.

[24] W. D. Donachie. The cell cycle of escherichia coli. *Annu Rev Microbiol*, 47:199–230, 1993.

[25] F. J. Trueba. On the precision and accuracy achieved by escherichia coli cells at fission about their middle. *Arch Microbiol*, 131(1):55–59, Feb 1982.

[26] W. D. Donachie and K. J. Begg. Growth of the bacterial cell. *Nature*, 227(5264):1220–1224, Sep 1970.

[27] W. Vollmer and J. V. Höltje. Morphogenesis of escherichia coli. *Curr Opin Microbiol*, 4(6):625–633, Dec 2001.

[28] J. V. Höltje. Growth of the stress-bearing and shape-maintaining murein sacculus of escherichia coli. *Microbiol Mol Biol Rev*, 62(1):181–203, Mar 1998.

[29] W. Margolin. Themes and variations in prokaryotic cell division. *FEMS Microbiol Rev*, 24(4):531–548, Oct 2000.

[30] Elizabeth Harry, Leigh Monahan, and Lyndal Thompson. Bacterial cell division: the mechanism and its precison. *Int Rev Cytol*, 253:27–94, 2006.

[31] Dirk-Jan Scheffers and Mariana G. Pinho. Bacterial cell wall synthesis: new insights from localization studies. *Microbiol Mol Biol Rev*, 69(4):585–607, Dec 2005.

[32] Mary J. Osborn and Lawrence Rothfield. Cell shape determination in escherichia coli. *Curr Opin Microbiol*, 10(6):606–610, Dec 2007.

[33] Nadège Philippe, Ludovic Pelosi, Richard E. Lenski, and Dominique Schneider. Evolution of penicillin-binding protein 2 concentration and cell shape during a long-term experiment with escherichia coli. *J Bacteriol*, 191(3):909–921, Feb 2009.

[34] Francois Jacob, Sydney Brenner, and Francois Cuzin. On the regulation of dna replication in bacteria. *Cold Spring Harbor Symposia on Quantitative Biology*, 28:329–348, 1963.

[35] K. von Meyenburg, F. G. Hansen, L. D. Nielsen, and P. Jørgensen. Origin of replication, oric, of the escherichia coli chromosome: mapping of genes relative to r.ecori cleavage sites in the oric region. *Mol Gen Genet*, 158(1):101–109, Dec 1977.

[36] Nicholas P. Robinson and Stephen D. Bell. Origins of dna replication in the three domains of life. *FEBS J*, 272(15):3757–3766, Aug 2005.

[37] W. D. Donachie. Relationship between cell size and time of initiation of dna replication. *Nature*, 219(5158):1077–1079, Sep 1968.

[38] C. E. Helmstetter. Dna synthesis during the division cycle of rapidly growing escherichia coli b/r. *J Mol Biol*, 31(3):507–518, Feb 1968.

[39] T. Den Blaauwen, N. Buddelmeijer, M. E. Aarsman, C. M. Hameete, and N. Nanninga. Timing of ftsz assembly in escherichia coli. *J Bacteriol*, 181(17):5167–5175, Sep 1999.

[40] Ole Michelsen, M Joost Teixeira de Mattos, Peter Ruhdal Jensen, and Flemming G. Hansen. Precise determinations of c and d periods by flow cytometry in escherichia coli k-12 and b/r. *Microbiology*, 149(Pt 4):1001–1010, Apr 2003.

[41] Ivy F. Lau, Sergio R. Filipe, Britta Søballe, Ole-Andreas Økstad, Francois-Xavier Barre, and David J. Sherratt. Spatial and temporal organization of replicating escherichia coli chromosomes. *Mol Microbiol*, 49(3):731–743, Aug 2003.

[42] David Bates and Nancy Kleckner. Chromosome and replisome dynamics in e. coli: loss of sister cohesion triggers global chromosome movement and mediates chromosome segregation. *Cell*, 121(6):899–911, Jun 2005.

[43] Xindan Wang, Christophe Possoz, and David J. Sherratt. Dancing around the divisome: asymmetric chromosome segregation in escherichia coli. *Genes Dev*, 19(19):2367–2377, Oct 2005.

[44] P. Steed and R. G. Murray. The cell wall and cell division of gram-negative bacteria. *Can J Microbiol*, 12(2):263–270, Apr 1966.

[45] E. W. Walker and W. Murray. Report lxxxvii: The effect of certain dyes upon the cultural characters of the bacillus typhosus and some other micro-organisms. *Br Med J*, 2(2270):16–18, Jul 1904.

[46] WJ Wilson. Pleomorphism, as exhibited by bacteria grown on media containing urea. *J Path Bact*, 11:394–U59, 1906.

[47] D. E. Lea, R. B. Haines, and C. A. Coulson. The action of radiations on bacteria. iii-γ -rays on growing and on non-proliferating bacteria. *Proc Royal Soc SerB*, 123(830):pp. 1–21, 1937.

[48] F. L. Gates. The reaction of individual bacteria to irradiation with ultraviolet light. *Science*, 77(1997):350, Apr 1933.

[49] P. van de Putte, C. Westenbroek, and A. Roersch. The relationship between gene controlled radiation resistance and filament formation in escherichia coli. *Biochim Biophys Acta*, 76:247–256, Oct 1963.

[50] Robert Jungk. *Heller als tausend Sonnen. Das Schicksal der Atomforscher*. Scherz & Goverts, Stuttgart, 1956.

[51] M. L. Morse and C. E. Carter. The synthesis of nucleic acids in cultures of escherichia coli, strains b and b/r. *J Bacteriol*, 58(3):317–326, Sep 1949.

[52] D. Billen and H. C. Lichstein. The effect of x radiation on the adaptive formation of formic hydrogenase in escherichia coli. *J Bacteriol*, 63(4):533–535, Apr 1952.

[53] W. L. Russell. Shortening of life in the offspring of male mice exposed to neutron radiation from an atomic bomb. *Proc Natl Acad Sci U S A*, 43(4):324–329, Apr 1957.

[54] H. I. Adler, H. An aftereffect of ionizing radiation on a mutant of escherichia coli. *Radiat Res*, 9(4):451–458, Oct 1958.

[55] H. I. Adler and A. A. Hardigree. Analysis of a gene controlling cell divsion and sensitivity to radiation in eschericha coli. *J Bacteriol*, 87:720–726, Mar 1964.

[56] E. M. Witkin. Inherited differences in sensitivity to radiation in escherichia coli. *Proc Natl Acad Sci U S A*, 32(3):59–68, Mar 1946.

[57] E. M. Witkin. Genetics of resistance to radiation in escherichia coli. *Genetics*, 32(3):221–248, May 1947.

[58] E. A. Grula and M. M. Grula. Cell division in a species of erwinia iii. reversal of inhibition of cell division caused by d-amino acids, penicillin, and ultraviolet light. *J Bacteriol*, 83:981–988, May 1962.

[59] H. I. Adler and A. A. Hardigree. Growth and division of filamentous forms of escherichia coli. *J Bacteriol*, 90(1):223–226, Jul 1965.

[60] Y Hirota, A Ryter, and F Jacob. Thermosensitive mutants of e. coli affected in the processes of dna synthesis and cellular division. *Cold Spring Harb Symp Quant Biol*, 33(0091-7451 (Linking)):677–93, 1968.

[61] P. Howard-Flanders, E. Simson, and L. Theriot. A locus that controls filament formation and sensitivity to radiation in escherichia coli k-12. *Genetics*, 49:237–246, Feb 1964.

[62] P. van de Putte, J. van Dillewijn, and A. Rorsch. The selection of mutants of escherichia coli with impaired cell division at elevated temperatures. *Mutat Res*, 106:121–128, Jul 1964.

[63] Y. Hirota, F. Jacob, A. Ryter, G. Buttin, and T. Nakai. On the process of cellular division in escherichia coli. i. asymmetrical cell division and production of deoxyribonucleic acid-less bacteria. *J Mol Biol*, 35(1):175–192, Jul 1968.

[64] J. R. Walker, A. Kovarik, J. S. Allen, and R. A. Gustafson. Regulation of bacterial cell division: temperature-sensitive mutants of escherichia coli that are defective in septum formation. *J Bacteriol*, 123(2):693–703, Aug 1975.

[65] H. J. Wijsman. A genetic map of several mutations affecting the mucopeptide layer of escherichia coli. *Genet Res*, 20(1):65–74, Aug 1972.

[66] S. Normark, H. G. Boman, and E. Matsson. Mutant of escherichia coli with anomalous cell division and ability to decrease episomally and chromosomally mediated resistance to ampicillin and several other antibiotics. *J Bacteriol*, 97(3):1334–1342, Mar 1969.

[67] M. Ricard and Y. Hirota. Process of cellular division in escherichia coli: physiological study on thermosensitive mutants defective in cell division. *J Bacteriol*, 116(1):314–322, Oct 1973.

[68] J. M. Pages, M. Piovant, A. Lazdunski, and C. Lazdunski. On the control of septation in escherichia coli. *Biochimie*, 57(3):303–313, 1975.

[69] J. F. Lutkenhaus, H. Wolf-Watz, and W. D. Donachie. Organization of genes in the ftsa-enva region of the escherichia coli genetic map and identification of a new fts locus (ftsz). *J Bacteriol*, 142(2):615–620, May 1980.

[70] J. E. Ward and J. Lutkenhaus. Overproduction of ftsz induces minicell formation in e. coli. *Cell*, 42(3):941–949, Oct 1985.

[71] E. Bi and J. Lutkenhaus. Ftsz regulates frequency of cell division in escherichia coli. *J Bacteriol*, 172(5):2765–2768, May 1990.

[72] J. Löwe and L. A. Amos. Crystal structure of the bacterial cell-division protein ftsz. *Nature*, 391(6663):203–206, Jan 1998.

[73] Q. M. Yi and J. Lutkenhaus. The nucleotide sequence of the essential cell-division gene ftsz of escherichia coli. *Gene*, 36(3):241–247, 1985.

[74] D. RayChaudhuri and J. T. Park. Escherichia coli cell-division gene ftsz encodes a novel gtp-binding protein. *Nature*, 359(6392):251–254, Sep 1992.

[75] P. de Boer, R. Crossley, and L. Rothfield. The essential bacterial cell-division protein ftsz is a gtpase. *Nature*, 359(6392):254–256, Sep 1992.

[76] A. Mukherjee, K. Dai, and J. Lutkenhaus. Escherichia coli cell division protein ftsz is a guanine nucleotide binding protein. *Proc Natl Acad Sci U S A*, 90(3):1053–1057, Feb 1993.

[77] A. Mukherjee and J. Lutkenhaus. Guanine nucleotide-dependent assembly of ftsz into filaments. *J Bacteriol*, 176(9):2754–2758, May 1994.

[78] S. G. Addinall, E. Bi, and J. Lutkenhaus. Ftsz ring formation in fts mutants. *J Bacteriol*, 178(13):3877–3884, Jul 1996.

[79] E. F. Bi and J. Lutkenhaus. Ftsz ring structure associated with division in escherichia coli. *Nature*, 354(6349):161–164, Nov 1991.

[80] X. Ma, D. W. Ehrhardt, and W. Margolin. Colocalization of cell division proteins ftsz and ftsa to cytoskeletal structures in living escherichia coli cells by using green fluorescent protein. *Proc Natl Acad Sci U S A*, 93(23):12998–13003, Nov 1996.

[81] H. P. Erickson, D. W. Taylor, K. A. Taylor, and D. Bramhill. Bacterial cell division protein ftsz assembles into protofilament sheets and minirings, structural homologs of tubulin polymers. *Proc Natl Acad Sci U S A*, 93(1):519–523, Jan 1996.

[82] C. L. Woldringh, J. A. Valkendurg, E. Pas, P. E. Taschner, P. Huls, and F. B. Wientjes. Physiological and geometrical conditions for cell division in escherichia coli. *Ann Inst Pasteur Microbiol*, 136A(1):131–138, 1985.

[83] Ling Juan Wu and Jeff Errington. Nucleoid occlusion and bacterial cell division. *Nat Rev Microbiol*, 10(1):8–12, Jan 2012.

[84] J Lutkenhaus and SG Addinall. Bacterial cell division and the z ring. *Annu Rev Biochem*, 66:93–116, 1997.

[85] M. Schaechter, J. P. Williamson, J. R. Hood, and A. L. Koch. Growth, cell and nuclear divisions in some bacteria. *J Gen Microbiol*, 29:421–434, Nov 1962.

[86] A. G. Marr, R. J. Harvey, and W. C. Trentini. Growth and division of escherichia coli. *J Bacteriol*, 91(6):2388–2389, Jun 1966.

[87] E. O. Powell. A note on koch and schaechter's hypothesis about growth and fission of bacteria. *J Gen Microbiol*, 37:231–249, Nov 1964.

[88] K. J. Begg and W. D. Donachie. Cell shape and division in escherichia coli: experiments with shape and division mutants. *J Bacteriol*, 163(2):615–622, Aug 1985.

[89] Qin Sun and William Margolin. Effects of perturbing nucleoid structure on nucleoid occlusion-mediated toporegulation of ftsz ring assembly. *J Bacteriol*, 186(12):3951–3959, Jun 2004.

[90] X. C. Yu and W. Margolin. Ftsz ring clusters in min and partition mutants: role of both the min system and the nucleoid in regulating ftsz ring localization. *Mol Microbiol*, 32(2):315–326, Apr 1999.

[91] Jonathan M. Guberman, Allison Fay, Jonathan Dworkin, Ned S. Wingreen, and Zemer Gitai. Psicic: Noise and asymmetry in bacterial division revealed by computational image analysis at sub-pixel resolution. *PLoS Comput Biol*, 4(11):e1000233, 11 2008.

[92] Martin Loose, Karsten Kruse, and Petra Schwille. Protein self-organization: lessons from the min system. *Annu Rev Biophys*, 40:315–336, Jun 2011.

[93] K. J. Begg and W. D. Donachie. Division planes alternate in spherical cells of escherichia coli. *J Bacteriol*, 180(9):2564–2567, May 1998.

[94] S. Normark, H. G. Boman, and G. D. Bloom. Cell division in a chain-forming enva mutant of escherichia coli k12. fine structure of division sites and effects of edta, lysozyme and ampicillin. *Acta Pathol Microbiol Scand B Microbiol Immunol*, 79(5):651–664, 1971.

[95] L. O. Ingram and H. C. Aldrich. Cell separation in blue-green bacteria. *J Bacteriol*, 118(2):708–716, May 1974.

[96] H. I. Adler, W. D. Fisher, A. Cohen, and A. A. Hardigree. Miniature escherichia coli cells deficient in dna. *ProcNatlAcadSciUSA*, 57(2):321–326, Feb 1967.

[97] R. M. Teather, J. F. Collins, and W. D. Donachie. Quantal behavior of a diffusible factor which initiates septum formation at potential division sites in escherichia coli. *J Bacteriol*, 118(2):407–413, May 1974.

[98] W. D. Donachie and K. J. Begg. "division potential" in escherichia coli. *J Bacteriol*, 178(20):5971–5976, Oct 1996.

[99] I. Fishov and C. L. Woldringh. Visualization of membrane domains in escherichia coli. *Mol Microbiol*, 32(6):1166–1172, Jun 1999.

[100] E. Mileykovskaya and W. Dowhan. Visualization of phospholipid domains in escherichia coli by using the cardiolipin-specific fluorescent dye 10-n-nonyl acridine orange. *J Bacteriol*, 182(4):1172–1175, Feb 2000.

[101] Lars D. Renner and Douglas B. Weibel. Cardiolipin microdomains localize to negatively curved regions of escherichia coli membranes. *Proc Natl Acad Sci U S A*, 108(15):6264–6269, Apr 2011.

[102] Céline Lafontaine, Jean-Marc Valleton, Nicole Orange, Vic Norris, Eugenia Mileykovskaya, and Stéphane Alexandre. Behaviour of bacterial division protein ftsz under a monolayer with phospholipid domains. *Biochim Biophys Acta*, 1768(11):2812–2821, Nov 2007.

[103] Daniel Lingwood and Kai Simons. Lipid rafts as a membrane-organizing principle. *Science*, 327(5961):46–50, Jan 2010.

[104] Kirsten Bacia, Dag Scherfeld, Nicoletta Kahya, and Petra Schwille. Fluorescence correlation spectroscopy relates rafts in model and native membranes. *Biophys J*, 87(2):1034–1043, Aug 2004.

[105] S. Brenner, F. A. Dark, P. Gerhardt, M. H. Jeynes, O. Kandler, E. Kellenberger, E. Klieneberger-Nobel, K. McQuillen, M. Rubio-Huertos, M. R. J. Salton, R. E. Strange, and J. Tomcsik & C. Weibull. Bacterial protoplasts. *Nature*, 181:1713–1715, 1958.

[106] Michael L. Higgins, Gerald D. Shockman, and Antoinette Ryter. Procaryotic cell division with respect to wall and membranes. *Critical Reviews in Microbiology*, 1(1):29–72, 1971.

[107] A. Ryter, Y. Hirota, and U. Schwarz. Process of cellular division in escherichia coli growth pattern of e. coli murein. *J Mol Biol*, 78(1):185–195, Jun 1973.

[108] P. Staugaard, F. M. van den Berg, C. L. Woldringh, and N. Nanninga. Localization of ampicillin-sensitive sites in escherichia coli by electron microscopy. *J Bacteriol*, 127(3):1376–1381, Sep 1976.

[109] A. Jaffé and R. D'ari. Growth of the escherichia coli cell envelope. *Biochimie*, 67(1):141–144, Jan 1985.

[110] D. Gally, K. Bray, and S. Cooper. Synthesis of peptidoglycan and membrane during the division cycle of rod-shaped, gram-negative bacteria. *J Bacteriol*, 175(10):3121–3130, May 1993.

[111] C. L. Woldringh, P. Huls, P., E. Pas, G. J. Brakenhoff, and N. Nanninga. Topography of peptidoglycan synthesis during elongation and polar cap formation in a cell division mutant of escherichia coli mc4100. *J Gen Microbiol*, 133(3):575–586, 1987.

[112] Thomas G. Bernhardt and Piet A J. de Boer. Slma, a nucleoid-associated, ftsz binding protein required for blocking septal ring assembly over chromosomes in e. coli. *Mol Cell*, 18(5):555–564, May 2005.

[113] K. Dai and J. Lutkenhaus. ftsz is an essential cell division gene in escherichia coli. *J Bacteriol*, 173(11):3500–3506, Jun 1991.

[114] D. M. Raskin and P. A. de Boer. Minde-dependent pole-to-pole oscillation of division inhibitor minc in escherichia coli. *J Bacteriol*, 181(20):6419–6424, Oct 1999.

[115] D. Bramhill. Bacterial cell division. *Annu Rev Cell Dev Biol*, 13:395–424, 1997.

[116] W. R. Cook and L. I. Rothfield. Nucleoid-independent identification of cell division sites in escherichia coli. *J Bacteriol*, 181(6):1900–1905, Mar 1999.

[117] Q. Sun, X. C. Yu, and W. Margolin. Assembly of the ftsz ring at the central division site in the absence of the chromosome. *Mol Microbiol*, 29(2):491–503, Jul 1998.

[118] M. Radman. Sos repair hypothesis: phenomenology of an inducible dna repair which is accompanied by mutagenesis. *Basic Life Sci*, 5A:355–367, 1975.

[119] E. Bi and J. Lutkenhaus. Cell division inhibitors sula and mincd prevent formation of the ftsz ring. *J Bacteriol*, 175(4):1118–1125, Feb 1993.

[120] A. Mukherjee, C. Cao, and J. Lutkenhaus. Inhibition of ftsz polymerization by sula, an inhibitor of septation in escherichia coli. *Proc Natl Acad Sci U S A*, 95(6):2885–2890, Mar 1998.

[121] D. Trusca, S. Scott, C. Thompson, and D. Bramhill. Bacterial sos checkpoint protein sula inhibits polymerization of purified ftsz cell division protein. *J Bacteriol*, 180(15):3946–3953, Aug 1998.

[122] A. Higashitani, N. Higashitani, and K. Horiuchi. A cell division inhibitor sula of escherichia coli directly interacts with ftsz through gtp hydrolysis. *Biochem Biophys Res Commun*, 209(1):198–204, Apr 1995.

[123] J. Huang, C. Cao, and J. Lutkenhaus. Interaction between ftsz and inhibitors of cell division. *J Bacteriol*, 178(17):5080–5085, Sep 1996.

[124] C. Jones and I. B. Holland. Role of the sulb (ftsz) protein in division inhibition during the sos response in escherichia coli: Ftsz stabilizes the inhibitor sula in maxicells. *Proc Natl Acad Sci U S A*, 82(18):6045–6049, Sep 1985.

[125] Suzanne C. Cordell, Elva J H. Robinson, and Jan Lowe. Crystal structure of the sos cell division inhibitor sula and in complex with ftsz. *Proc Natl Acad Sci U S A*, 100(13):7889–7894, Jun 2003.

[126] E. Mulder and C. L. Woldringh. Actively replicating nucleoids influence positioning of division sites in escherichia coli filaments forming cells lacking dna. *J Bacteriol*, 171(8):4303–4314, Aug 1989.

[127] C. L. Woldringh, E. Mulder, P. G. Huls, and N. Vischer. Toporegulation of bacterial division according to the nucleoid occlusion model. *Res Microbiol*, 142(2-3):309–320, 1991.

[128] Ling Juan Wu and Jeff Errington. Coordination of cell division and chromosome segregation by a nucleoid occlusion protein in bacillus subtilis. *Cell*, 117(7):915–925, Jun 2004.

[129] Lawrence Rothfield, Aziz Taghbalout, and Yu-Ling Shih. Spatial control of bacterial division-site placement. *Nat Rev Microbiol*, 3(12):959–968, Dec 2005.

[130] Shan Wang, S J Ryan Arends, David S. Weiss, and Elaine B. Newman. A deficiency in s-adenosylmethionine synthetase interrupts assembly of the septal ring in escherichia coli k-12. *Mol Microbiol*, 58(3):791–799, Nov 2005.

[131] A. Regamey, E. J. Harry, and R. G. Wake. Mid-cell z ring assembly in the absence of entry into the elongation phase of the round of replication in bacteria: co-ordinating chromosome replication with cell division. *Mol Microbiol*, 38(3):423–434, Nov 2000.

[132] B. Gullbrand and K. Nordström. Ftsz ring formation without subsequent cell division after replication runout in escherichia coli. *Mol Microbiol*, 36(6):1349–1359, Jun 2000.

[133] X. C. Yu, Q. Sun, and W. Margolin. Ftsz rings in mukb mutants with or without the min system. *Biochimie*, 83(1):125–129, Jan 2001.

[134] E. J. Harry. Bacterial cell division: regulating z-ring formation. *Mol Microbiol*, 40(4):795–803, May 2001.

[135] Jeffery Errington, Richard A. Daniel, and Dirk-Jan Scheffers. Cytokinesis in bacteria. *Microbiol Mol Biol Rev*, 67(1):52–65, table of contents, Mar 2003.

[136] Hongbaek Cho, Heather R. McManus, Simon L. Dove, and Thomas G. Bernhardt. Nucleoid occlusion factor slma is a dna-activated ftsz polymerization antagonist. *Proc Natl Acad Sci U S A*, 108(9):3773–3778, Mar 2011.

[137] Nam Ky Tonthat, Stefan T. Arold, Brian F. Pickering, Michael W. Van Dyke, Shoudan Liang, Yue Lu, Tushar K. Beuria, William Margolin, and Maria A. Schumacher. Molecular mechanism by which the nucleoid occlusion factor, slma, keeps cytokinesis in check. *EMBO J*, 30(1):154–164, Jan 2011.

[138] M. Schaechter, M., O. Maaloe, and N. O. Kjeldgaard. Dependency on medium and temperature of cell size and chemical composition during balanced grown of salmonella typhimurium. *J Gen Microbiol*, 19(3):592–606, Dec 1958.

[139] S. Cooper and C. E. Helmstetter. Chromosome replication and the division cycle of escherichia coli b/r. *J Mol Biol*, 31(3):519–540, Feb 1968.

[140] J. Herrick, M. Kohiyama, T. Atlung, and F. G. Hansen. The initiation mess? *Mol Microbiol*, 19(4):659–666, Feb 1996.

[141] William D. Donachie and Garry W. Blakely. Coupling the initiation of chromosome replication to cell size in escherichia coli. *Curr Opin Microbiol*, 6(2):146–150, Apr 2003.

[142] Martin Thanbichler. Synchronization of chromosome dynamics and cell division in bacteria. *Cold Spring Harb Perspect Biol*, 2(1):a000331, Jan 2010.

[143] E. J. Harry, J. Rodwell, and R. G. Wake. Co-ordinating dna replication with cell division in bacteria: a link between the early stages of a round of replication and mid-cell z ring assembly. *Mol Microbiol*, 33(1):33–40, Jul 1999.

[144] Margaret D. Migocki, Peter J. Lewis, R Gerry Wake, and Elizabeth J. Harry. The midcell replication factory in bacillus subtilis is highly mobile: implications for coordinating chromosome replication with other cell cycle events. *Mol Microbiol*, 54(2):452–463, Oct 2004.

[145] Jue D. Wang, Megan E. Rokop, Melanie M. Barker, Nathaniel R. Hanson, and Alan D. Grossman. Multicopy plasmids affect replisome positioning in bacillus subtilis. *J Bacteriol*, 186(21):7084–7090, Nov 2004.

[146] R. Bernander and K. Nordström. Chromosome replication does not trigger cell division in e. coli. *Cell*, 60(3):365–374, Feb 1990.

[147] L. J. Wu, A. H. Franks, and R. G. Wake. Replication through the terminus region of the bacillus subtilis chromosome is not essential for the formation of a division septum that partitions the dna. *J Bacteriol*, 177(19):5711–5715, Oct 1995.

[148] T. McGinness and R. G. Wake. Division septation in the absence of chromosome termination in bacillus subtilis. *J Mol Biol*, 134(2):251–264, Oct 1979.

[149] Laura Romberg and Petra Anne Levin. Assembly dynamics of the bacterial cell division protein ftsz: poised at the edge of stability. *Annu Rev Microbiol*, 57:125–154, 2003.

[150] A. J. Kelly, M. J. Sackett, N. Din, E. Quardokus, and Y. V. Brun. Cell cycle-dependent transcriptional and proteolytic regulation of ftsz in caulobacter. *Genes Dev*, 12(6):880–893, Mar 1998.

[151] E. Quardokus, N. Din, and Y. V. Brun. Cell cycle regulation and cell type-specific localization of the ftsz division initiation protein in caulobacter. *Proc Natl Acad Sci U S A*, 93(13):6314–6319, Jun 1996.

[152] E. M. Quardokus, N. Din, and Y. V. Brun. Cell cycle and positional constraints on ftsz localization and the initiation of cell division in caulobacter crescentus. *Mol Microbiol*, 39(4):949–959, Feb 2001.

[153] Richard B. Weart and Petra Anne Levin. Growth rate-dependent regulation of medial ftsz ring formation. *J Bacteriol*, 185(9):2826–2834, May 2003.

[154] Huaijin Zhou, Ryan Schulze, Sandra Cox, Cristian Saez, Zonglin Hu, and Joe Lutkenhaus. Analysis of mind mutations reveals residues required for mine stimulation of the mind atpase and residues required for minc interaction. *J Bacteriol*, 187(2):629–638, Jan 2005.

[155] P. Palacios, M. Vicente, and M. Sánchez. Dependency of escherichia coli cell-division size, and independency of nucleoid segregation on the mode and level of ftsz expression. *Mol Microbiol*, 20(5):1093–1098, Jun 1996.

[156] K. Dai and J. Lutkenhaus. The proper ratio of ftsz to ftsa is required for cell division to occur in escherichia coli. *J Bacteriol*, 174(19):6145–6151, Oct 1992.

[157] K. Begg, Y. Nikolaichik, N. Crossland, and W. D. Donachie. Roles of ftsa and ftsz in activation of division sites. *J Bacteriol*, 180(4):881–884, Feb 1998.

[158] A.D. Gardner. *A system of bacteriology in relation to medicine*, volume 95, pages 159–170. His Majesty's Stationery Office, London, 1930.

[159] P. Pease. The gonidial stages in spirillum spp. and vibrio spp. *J Gen Microbiol*, 14(3):672–675, Jul 1956.

[160] J. Vörös and R. N. Goodman. Filamentous forms of erwinia amylovora. *Phytopathology*, 55(8):876–879, Aug 1965.

[161] Y. Tanami and Y. Yamada. Miniature cell formation in chlamydia psittaci. *J Bacteriol*, 114(1):408–412, Apr 1973.

[162] M. Demerec, E. A. Adelberg, A. J. Clark, and P. E. Hartman. A proposal for a uniform nomenclature in bacterial genetics. *Genetics*, 54(1):61–76, Jul 1966.

[163] A. Cohen, D. P. Allison, H. I. Adler, and R. Curtiss III. Genetic transfer to minicells of escherichia coli k-12. *Genetics (Abstract)*, 56:550–551, 1967.

[164] A. L. Taylor and C. D. Trotter. Revised linkage map of escherichia coli. *Bacteriol Rev*, 31(4):332–353, Dec 1967.

[165] D. R. Stallions and R. Curtiss. Chromosome transfer and recombinant formation with deoxyribonucleic acid temperature-sensitive strains of escherichia coli. *J Bacteriol*, 105(3):886–895, Mar 1971.

[166] A. Cohen, W. D. Fisher, R. Curtiss, and H. I. Adler. The properties of dna transferred to minicells during conjugation. *Cold Spring Harb Symp Quant Biol*, 33:635–641, 1968.

[167] A. C. Frazer and R. Curtiss. Production, properties and utility of bacterial minicells. *Curr Top Microbiol Immunol*, 69:1–84, 1975.

[168] K. J. Roozen, R. G. Fenwick, and R. Curtiss. Synthesis of ribonucleic acid and protein in plasmid-containing minicells of escherichia coli k-12. *J Bacteriol*, 107(1):21–33, Jul 1971.

[169] B. J. Bachmann, K. B. Low, and A. L. Taylor. Recalibrated linkage map of escherichia coli k-12. *Bacteriol Rev*, 40(1):116–167, Mar 1976.

[170] B. J. Bachmann and K. B. Low. Linkage map of escherichia coli k-12, edition 6. *Microbiol Rev*, 44(1):1–56, Mar 1980.

[171] T. H. Schaumberg and P. L. Kuempel. Genetic mapping of the minb locus in escherichia coli k-12. *J Bacteriol*, 153(2):1063–1065, Feb 1983.

[172] B. J. Bachmann. Linkage map of escherichia coli k-12, edition 7. *Microbiol Rev*, 47(2):180–230, Jun 1983.

[173] E. Davie, K. Sydnor, and L. I. Rothfield. Genetic basis of minicell formation in escherichia coli k-12. *J Bacteriol*, 158(3):1202–1203, Jun 1984.

[174] J. N. Reeve, N. H. Mendelson, S. I. Coyne, L. L. Hallock, and R. M. Cole. Minicells of bacillus subtilis. *J Bacteriol*, 114(2):860–873, May 1973.

[175] P. A. de Boer, R. E. Crossley, and L. I. Rothfield. A division inhibitor and a topological specificity factor coded for by the minicell locus determine proper placement of the division septum in e. coli. *Cell*, 56(4):641–649, Feb 1989.

[176] P. A. de Boer, R. E. Crossley, and L. I. Rothfield. Isolation and properties of minb, a complex genetic locus involved in correct placement of the division site in escherichia coli. *J Bacteriol*, 170(5):2106–2112, May 1988.

[177] P. A. de Boer, R. E. Crossley, and L. I. Rothfield. Central role for the escherichia coli minc gene product in two different cell division-inhibition systems. *Proc Natl Acad Sci U S A*, 87(3):1129–1133, Feb 1990.

[178] P. A. de Boer, R. E. Crossley, and L. I. Rothfield. Roles of minc and mind in the site-specific septation block mediated by the mincde system of escherichia coli. *J Bacteriol*, 174(1):63–70, Jan 1992.

[179] D. M. Raskin and P. A. de Boer. The mine ring: an ftsz-independent cell structure required for selection of the correct division site in e. coli. *Cell*, 91(5):685–694, Nov 1997.

[180] C. R. Zhao, P. A. de Boer, and L. I. Rothfield. Proper placement of the escherichia coli division site requires two functions that are associated with different domains of the mine protein. *Proc Natl Acad Sci U S A*, 92(10):4313–4317, May 1995.

[181] S. Pichoff, B. Vollrath, C. Touriol, and J. P. Bouché. Deletion analysis of gene mine which encodes the topological specificity factor of cell division in escherichia coli. *Mol Microbiol*, 18(2):321–329, Oct 1995.

[182] P. A. de Boer, P.e Boer, R. E. Crossley, A. R. Hand, and L. I. Rothfield. The mind protein is a membrane atpase required for the correct placement of the escherichia coli division site. *EMBO J*, 10(13):4371–4380, Dec 1991.

[183] S. L. Rowland, X. Fu, M. A. Sayed, Y. Zhang, W. R. Cook, and L. I. Rothfield. Membrane redistribution of the escherichia coli mind protein induced by mine. *J Bacteriol*, 182(3):613–619, Feb 2000.

[184] E. Bi and J. Lutkenhaus. Interaction between the min locus and ftsz. *J Bacteriol*, 172(10):5610–5616, Oct 1990.

[185] Z. Hu and J. Lutkenhaus. Topological regulation of cell division in escherichia coli involves rapid pole to pole oscillation of the division inhibitor minc under the control of mind and mine. *Mol Microbiol*, 34(1):82–90, Oct 1999.

[186] Z. Hu and J. Lutkenhaus. Analysis of minc reveals two independent domains involved in interaction with mind and ftsz. *J Bacteriol*, 182(14):3965–3971, Jul 2000.

[187] L. I. Rothfield and C. R. Zhao. How do bacteria decide where to divide? *Cell*, 84(2):183–186, Jan 1996.

[188] D. M. Raskin and P. A. de Boer. Rapid pole-to-pole oscillation of a protein required for directing division to the middle of escherichia coli. *Proc Natl Acad Sci U S A*, 96(9):4971–4976, Apr 1999.

[189] Ahmed Touhami, Manfred Jericho, and Andrew D. Rutenberg. Temperature dependence of mind oscillation in escherichia coli: running hot and fast. *J Bacteriol*, 188(21):7661–7667, Nov 2006.

[190] Supratim Sengupta and Andrew Rutenberg. Modeling partitioning of min proteins between daughter cells after septation in escherichia coli. *Phys Biol*, 4(3):145–153, Sep 2007.

[191] Karsten Kruse. A dynamic model for determining the middle of escherichia coli. *Biophys J*, 82(2):618–627, Feb 2002. x.

[192] Jay E. Johnson, Laura L. Lackner, and Piet A J. de Boer. Targeting of (d)minc/mind and (d)minc/dicb complexes to septal rings in escherichia coli suggests a multistep mechanism for minc-mediated destruction of nascent ftsz rings. *J Bacteriol*, 184(11):2951–2962, Jun 2002.

[193] X. Fu, Y. L. Shih, Y. Zhang, and L. I. Rothfield. The mine ring required for proper placement of the division site is a mobile structure that changes its cellular location during the escherichia coli division cycle. *Proc Natl Acad Sci U S A*, 98(3):980–985, Jan 2001.

[194] C. A. Hale, H. Meinhardt, and P. A. de Boer. Dynamic localization cycle of the cell division regulator mine in escherichia coli. *EMBO J*, 20(7):1563–1572, Apr 2001.

[195] Yu-Ling Shih, Xiaoli Fu, Glenn F. King, Trung Le, and Lawrence Rothfield. Division site placement in e.coli: mutations that prevent formation of the mine ring lead to loss of the normal midcell arrest of growth of polar mind membrane domains. *EMBO J*, 21(13):3347–3357, Jul 2002.

[196] Laura L Lackner, David M Raskin, and Piet A J de Boer. Atp-dependent interactions between escherichia coli min proteins and the phospholipid membrane in vitro. *J Bacteriol*, 185(3):735–749, Feb 2003.

[197] Z. Hu and J. Lutkenhaus. Topological regulation of cell division in e. coli. *Mol Cell*, 7(6):1337–1343, Jun 2001.

[198] Zonglin Hu, Cristian Saez, and Joe Lutkenhaus. Recruitment of minc, an inhibitor of z-ring formation, to the membrane in escherichia coli: role of mind and mine. *J Bacteriol*, 185(1):196–203, Jan 2003.

[199] Giovanni Meacci and Karsten Kruse. Min-oscillations in escherichia coli induced by interactions of membrane-bound proteins. *Phys Biol*, 2(2):89–97, Jun 2005. x.

[200] Encyclopedia of escherichia coli k-12 genes and metabolism, Jun 2012.

[201] K. J. Begg, G. F. Hatfull, and W. D. Donachie. Identification of new genes in a cell envelope-cell division gene cluster of escherichia coli: cell division gene ftsq. *J Bacteriol*, 144(1):435–437, Oct 1980.

[202] William Margolin. Ftsz and the division of prokaryotic cells and organelles. *Nat Rev Mol Cell Biol*, 6(11):862–871, Nov 2005.

[203] David W Adams and Jeff Errington. Bacterial cell division: assembly, maintenance and disassembly of the z ring. *Nat Rev Microbiol*, 7(9):642–653, Sep 2009.

[204] P. E. Taschner, P. G. Huls, E. Pas, and C. L. Woldringh. Division behavior and shape changes in isogenic ftsz, ftsq, ftsa, pbpb, and ftse cell division mutants of escherichia coli during temperature shift experiments. *J Bacteriol*, 170(4):1533–1540, Apr 1988.

[205] J. Lutkenhaus. Ftsz ring in bacterial cytokinesis. *Mol Microbiol*, 9(3):403–409, Aug 1993.

[206] S. Vitha, R. S. McAndrew, and K. W. Osteryoung. Ftsz ring formation at the chloroplast division site in plants. *J Cell Biol*, 153(1):111–120, Apr 2001.

[207] H. P. Erickson. Ftsz, a prokaryotic homolog of tubulin? *Cell*, 80(3):367–370, Feb 1995.

[208] E. Nogales, S. G. Wolf, and K. H. Downing. Structure of the alpha beta tubulin dimer by electron crystallography. *Nature*, 391(6663):199–203, Jan 1998.

[209] E. Nogales, K. H. Downing, L. A. Amos, and J. Löwe. Tubulin and ftsz form a distinct family of gtpases. *Nat Struct Biol*, 5(6):451–458, Jun 1998.

[210] J. Pla, M. Sánchez, P. Palacios, M. Vicente, and M. Aldea. Preferential cytoplasmic location of ftsz, a protein essential for escherichia coli septation. *Mol Microbiol*, 5(7):1681–1686, Jul 1991.

[211] C. Lu, J. Stricker, and H. P. Erickson. Ftsz from escherichia coli, azotobacter vinelandii, and thermotoga maritima–quantitation, gtp hydrolysis, and assembly. *Cell Motil Cytoskeleton*, 40(1):71–86, 1998.

[212] Paola Bisicchia. *Personal Communication*, 2012.

[213] A. Tormo, A. Dopazo, A. G. de la Campa, M. Aldea, and M. Vicente. Coupling between dna replication and cell division mediated by the ftsa protein in escherichia coli: a pathway independent of the sos response, the "ter" pathway. *J Bacteriol*, 164(2):950–953, Nov 1985.

[214] J. Pla, A. Dopazo, and M. Vicente. The native form of ftsa, a septal protein of escherichia coli, is located in the cytoplasmic membrane. *J Bacteriol*, 172(9):5097–5102, Sep 1990.

[215] P. Bork, C. Sander, and A. Valencia. An atpase domain common to prokaryotic cell cycle proteins, sugar kinases, actin, and hsp70 heat shock proteins. *Proc Natl Acad Sci U S A*, 89(16):7290–7294, Aug 1992.

[216] W. Kabsch and K. C. Holmes. The actin fold. *FASEB J*, 9(2):167–174, Feb 1995.

[217] W. D. Donachie, K. J. Begg, J. F. Lutkenhaus, G. P. Salmond, E. Martinez-Salas, and M. Vincente. Role of the ftsa gene product in control of escherichia coli cell division. *J Bacteriol*, 140(2):388–394, Nov 1979.

[218] A. Tormo, E. Martínez-Salas, and M. Vicente. Involvement of the ftsa gene product in late stages of the escherichia coli cell cycle. *J Bacteriol*, 141(2):806–813, Feb 1980.

[219] A. Feucht, I. Lucet, M. D. Yudkin, and J. Errington. Cytological and biochemical characterization of the ftsa cell division protein of bacillus subtilis. *Mol Microbiol*, 40(1):115–125, Apr 2001.

[220] X. Wang, J. Huang, A. Mukherjee, C. Cao, and J. Lutkenhaus. Analysis of the interaction of ftsz with itself, gtp, and ftsa. *J Bacteriol*, 179(17):5551–5559, Sep 1997.

[221] N. Din, E. M. Quardokus, M. J. Sackett, and Y. V. Brun. Dominant c-terminal deletions of ftsz that affect its ability to localize in caulobacter and its interaction with ftsa. *Mol Microbiol*, 27(5):1051–1063, Mar 1998.

[222] G. Di Lallo, M. Fagioli, D. Barionovi, P. Ghelardini, and L. Paolozzi. Use of a two-hybrid assay to study the assembly of a complex multicomponent protein machinery: bacterial septosome differentiation. *Microbiology*, 149(Pt 12):3353–3359, Dec 2003.

[223] X. Ma and W. Margolin. Genetic and functional analyses of the conserved c-terminal core domain of escherichia coli ftsz. *J Bacteriol*, 181(24):7531–7544, Dec 1999.

[224] K. Yan, K. H. Pearce, and D. J. Payne. A conserved residue at the extreme c-terminus of ftsz is critical for the ftsa-ftsz interaction in staphylococcus aureus. *Biochem Biophys Res Commun*, 270(2):387–392, Apr 2000.

[225] Sebastien Pichoff and Joe Lutkenhaus. Unique and overlapping roles for zipa and ftsa in septal ring assembly in escherichia coli. *EMBO J*, 21(4):685–693, Feb 2002.

[226] Sebastien Pichoff and Joe Lutkenhaus. Tethering the z ring to the membrane through a conserved membrane targeting sequence in ftsa. *Mol Microbiol*, 55(6):1722–1734, Mar 2005.

[227] A. Mukherjee and W. D. Donachie. Differential translation of cell division proteins. *J Bacteriol*, 172(10):6106–6111, Oct 1990.

[228] S. J. Dewar, K. J. Begg, and W. D. Donachie. Inhibition of cell division initiation by an imbalance in the ratio of ftsa to ftsz. *J Bacteriol*, 174(19):6314–6316, Oct 1992.

[229] Sonsoles Rueda, Miguel Vicente, and Jesús Mingorance. Concentration and assembly of the division ring proteins ftsz, ftsa, and zipa during the escherichia coli cell cycle. *J Bacteriol*, 185(11):3344–3351, Jun 2003.

[230] H. C. Wang and R. C. Gayda. High-level expression of the ftsa protein inhibits cell septation in escherichia coli k-12. *J Bacteriol*, 172(8):4736–4740, Aug 1990.

[231] Brian D. Corbin, Brett Geissler, Mahalakshmi Sadasivam, and William Margolin. Z-ring-independent interaction between a subdomain of ftsa and late septation proteins as revealed by a polar recruitment assay. *J Bacteriol*, 186(22):7736–7744, Nov 2004.

[232] Ana Isabel Rico, Marta García-Ovalle, Jesús Mingorance, and Miguel Vicente. Role of two essential domains of escherichia coli ftsa in localization and progression of the division ring. *Mol Microbiol*, 53(5):1359–1371, Sep 2004.

[233] C. A. Hale and P. A. de Boer. Direct binding of ftsz to zipa, an essential component of the septal ring structure that mediates cell division in e. coli. *Cell*, 88(2):175–185, Jan 1997.

[234] Tomoo Ohashi, Cynthia A. Hale, Piet A J. de Boer, and Harold P. Erickson. Structural evidence that the p/q domain of zipa is an unstructured, flexible tether between the membrane and the c-terminal ftsz-binding domain. *J Bacteriol*, 184(15):4313–4315, Aug 2002.

[235] C. A. Hale, A. C. Rhee, and P. A. de Boer. Zipa-induced bundling of ftsz polymers mediated by an interaction between c-terminal domains. *J Bacteriol*, 182(18):5153–5166, Sep 2000.

[236] S. A. Haney, E. Glasfeld, C. Hale, D. Keeney, Z. He, and P. de Boer. Genetic analysis of the escherichia coli ftsz.zipa interaction in the yeast two-hybrid system. characterization of ftsz residues essential for the interactions with zipa and with ftsa. *J Biol Chem*, 276(15):11980–11987, Apr 2001.

[237] Z. Liu, A. Mukherjee, and J. Lutkenhaus. Recruitment of zipa to the division site by interaction with ftsz. *Mol Microbiol*, 31(6):1853–1861, Mar 1999.

[238] D. RayChaudhuri. Zipa is a map-tau homolog and is essential for structural integrity of the cytokinetic ftsz ring during bacterial cell division. *EMBO J*, 18(9):2372–2383, May 1999.

[239] C. A. Hale and P. A. de Boer. Recruitment of zipa to the septal ring of escherichia coli is dependent on ftsz and independent of ftsa. *J Bacteriol*, 181(1):167–176, Jan 1999.

[240] Cynthia A. Hale and Piet A J. de Boer. Zipa is required for recruitment of ftsk, ftsq, ftsl, and ftsn to the septal ring in escherichia coli. *J Bacteriol*, 184(9):2552–2556, May 2002.

[241] K. J. Begg, S. J. Dewar, and W. D. Donachie. A new escherichia coli cell division gene, ftsk. *J Bacteriol*, 177(21):6211–6222, Nov 1995.

[242] X. C. Yu, A. H. Tran, Q. Sun, and W. Margolin. Localization of cell division protein ftsk to the escherichia coli septum and identification of a potential n-terminal targeting domain. *J Bacteriol*, 180(5):1296–1304, Mar 1998.

[243] L. Wang and J. Lutkenhaus. Ftsk is an essential cell division protein that is localized to the septum and induced as part of the sos response. *Mol Microbiol*, 29(3):731–740, Aug 1998.

[244] Sean P. Kennedy, Fabien Chevalier, and François-Xavier Barre. Delayed activation of xer recombination at dif by ftsk during septum assembly in escherichia coli. *Mol Microbiol*, 68(4):1018–1028, May 2008.

[245] G. C. Draper, N. McLennan, K. Begg, M. Masters, and W. D. Donachie. Only the n-terminal domain of ftsk functions in cell division. *J Bacteriol*, 180(17):4621–4627, Sep 1998.

[246] G. Liu, G. C. Draper, and W. D. Donachie. Ftsk is a bifunctional protein involved in cell division and chromosome localization in escherichia coli. *Mol Microbiol*, 29(3):893–903, Aug 1998.

[247] W. Steiner, G. Liu, W. D. Donachie, and P. Kuempel. The cytoplasmic domain of ftsk protein is required for resolution of chromosome dimers. *Mol Microbiol*, 31(2):579–583, Jan 1999.

[248] Laurent Aussel, François Xavier Barre, Mira Aroyo, Andrzej Stasiak, Alicja Z. Stasiak, and David Sherratt. Ftsk is a dna motor protein that activates chromosome dimer resolution by switching the catalytic state of the xerc and xerd recombinases. *Cell*, 108(2):195–205, Jan 2002.

[249] Sarah Bigot, Jacqueline Corre, Jean-Michel Louarn, François Cornet, and François-Xavier Barre. Ftsk activities in xer recombination, dna mobilization and cell division involve overlapping and separate domains of the protein. *Mol Microbiol*, 54(4):876–886, Nov 2004.

[250] Thomas H. Massey, Christopher P. Mercogliano, James Yates, David J. Sherratt, and Jan Löwe. Double-stranded dna translocation: structure and mechanism of hexameric ftsk. *Mol Cell*, 23(4):457–469, Aug 2006.

[251] Omar A. Saleh, Corine Pérals, François-Xavier Barre, and Jean-François Allemand. Fast, dna-sequence independent translocation by ftsk in a single-molecule experiment. *EMBO J*, 23(12):2430–2439, Jun 2004.

[252] James E. Graham, David J. Sherratt, and Mark D. Szczelkun. Sequence-specific assembly of ftsk hexamers establishes directional translocation on dna. *Proc Natl Acad Sci U S A*, 107(47):20263–20268, Nov 2010.

[253] M. J. Carson, J. Barondess, and J. Beckwith. The ftsq protein of escherichia coli: membrane topology, abundance, and cell division phenotypes due to overproduction and insertion mutations. *J Bacteriol*, 173(7):2187–2195, Apr 1991.

[254] J. J. Barondess, M. Carson, L. M. Guzman Verduzco, and J. Beckwith. Alkaline phosphatase fusions in the study of cell division genes. *Res Microbiol*, 142(2-3):295–299, 1991.

[255] L. M. Guzman, J. J. Barondess, and J. Beckwith. Ftsl, an essential cytoplasmic membrane protein involved in cell division in escherichia coli. *J Bacteriol*, 174(23):7716–7728, Dec 1992.

[256] L. M. Guzman, D. S. Weiss, and J. Beckwith. Domain-swapping analysis of ftsi, ftsl, and ftsq, bitopic membrane proteins essential for cell division in escherichia coli. *J Bacteriol*, 179(16):5094–5103, Aug 1997.

[257] K. Dai, Y. Xu, and J. Lutkenhaus. Topological characterization of the essential escherichia coli cell division protein ftsn. *J Bacteriol*, 178(5):1328–1334, Mar 1996.

[258] Nienke Buddelmeijer and Jon Beckwith. Assembly of cell division proteins at the e. coli cell center. *Current Opinion in Microbiology*, 5(6):553 – 557, 2002.

[259] N. Buddelmeijer, M. E. Aarsman, A. H. Kolk, M. Vicente, and N. Nanninga. Localization of cell division protein ftsq by immunofluorescence microscopy in dividing and nondividing cells of escherichia coli. *J Bacteriol*, 180(23):6107–6116, Dec 1998.

[260] J. C. Chen, D. S. Weiss, J. M. Ghigo, and J. Beckwith. Septal localization of ftsq, an essential cell division protein in escherichia coli. *J Bacteriol*, 181(2):521–530, Jan 1999.

[261] J. C. Chen and J. Beckwith. Ftsq, ftsl and ftsi require ftsk, but not ftsn, for co-localization with ftsz during escherichia coli cell division. *Mol Microbiol*, 42(2):395–413, Oct 2001.

[262] J. M. Ghigo, D. S. Weiss, J. C. Chen, J. C. Yarrow, and J. Beckwith. Localization of ftsl to the escherichia coli septal ring. *Mol Microbiol*, 31(2):725–737, Jan 1999.

[263] Nienke Buddelmeijer and Jon Beckwith. A complex of the escherichia coli cell division proteins ftsl, ftsb and ftsq forms independently of its localization to the septal region. *Mol Microbiol*, 52(5):1315–1327, Jun 2004.

[264] Gouzel Karimova, Nathalie Dautin, and Daniel Ladant. Interaction network among escherichia coli membrane proteins involved in cell division as revealed by bacterial two-hybrid analysis. *J Bacteriol*, 187(7):2233–2243, Apr 2005.

[265] Nathan W. Goehring, Ivana Petrovska, Dana Boyd, and Jon Beckwith. Mutants, suppressors, and wrinkled colonies: mutant alleles of the cell division gene ftsq point to functional domains in ftsq and a role for domain 1c of ftsa in divisome assembly. *J Bacteriol*, 189(2):633–645, Jan 2007.

[266] J. M. Ghigo and J. Beckwith. Cell division in escherichia coli: role of ftsl domains in septal localization, function, and oligomerization. *J Bacteriol*, 182(1):116–129, Jan 2000.

[267] D. S. Weiss, J. C. Chen, J. M. Ghigo, D. Boyd, and J. Beckwith. Localization of ftsi (pbp3) to the septal ring requires its membrane anchor, the z ring, ftsa, ftsq, and ftsl. *J Bacteriol*, 181(2):508–520, Jan 1999.

[268] Nienke Buddelmeijer, Nicholas Judson, Dana Boyd, John J. Mekalanos, and Jonathan Beckwith. Ygbq, a cell division protein in escherichia coli and vibrio cholerae, localizes in codependent fashion with ftsl to the division site. *Proc Natl Acad Sci U S A*, 99(9):6316–6321, Apr 2002.

[269] Mark D. Gonzalez and Jon Beckwith. Divisome under construction: distinct domains of the small membrane protein ftsb are necessary for interaction with multiple cell division proteins. *J Bacteriol*, 191(8):2815–2825, Apr 2009.

[270] D. S. Boyle, M. M. Khattar, S. G. Addinall, J. Lutkenhaus, and W. D. Donachie. ftsw is an essential cell-division gene in escherichia coli. *Mol Microbiol*, 24(6):1263–1273, Jun 1997.

[271] A. O. Henriques, P. Glaser, P. J. Piggot, and CP Moran, Jr. Control of cell shape and elongation by the roda gene in bacillus subtilis. *Mol Microbiol*, 28(2):235–247, Apr 1998.

[272] H. Meinhardt and P. A. de Boer. Pattern formation in escherichia coli: a model for the pole-to-pole oscillations of min proteins and the localization of the division site. *ProcNatlAcadSciUSA*, 98(25):14202–14207, Dec 2001.

[273] Keri L N. Mercer and David S. Weiss. The escherichia coli cell division protein ftsw is required to recruit its cognate transpeptidase, ftsi (pbp3), to the division site. *J Bacteriol*, 184(4):904–912, Feb 2002.

[274] Nathan W. Goehring, Mark D. Gonzalez, and Jon Beckwith. Premature targeting of cell division proteins to midcell reveals hierarchies of protein interactions involved in divisome assembly. *Mol Microbiol*, 61(1):33–45, Jul 2006.

[275] Svetlana Alexeeva, Theodorus W J Gadella, Jr, Jolanda Verheul, Gertjan S. Verhoeven, and Tanneke den Blaauwen. Direct interactions of early and late assembling division proteins in escherichia coli cells resolved by fret. *Mol Microbiol*, 77(2):384–398, Jul 2010.

[276] Claudine Fraipont, Svetlana Alexeeva, Benoît Wolf, René van der Ploeg, Marie Schloesser, Tanneke den Blaauwen, and Martine Nguyen-Distèche. The integral membrane ftsw protein and peptidoglycan synthase pbp3 form a subcomplex in escherichia coli. *Microbiology*, 157(Pt 1):251–259, Jan 2011.

[277] Beatriz Lara and Juan A. Ayala. Topological characterization of the essential escherichia coli cell division protein ftsw. *FEMS Microbiol Lett*, 216(1):23–32, Oct 2002.

[278] Tamimount Mohammadi, Vincent van Dam, Robert Sijbrandi, Thierry Vernet, André Zapun, Ahmed Bouhss, Marlies Diepeveen-de Bruin, Martine Nguyen-Distèche, Ben de Kruijff, and Eefjan Breukink. Identification of ftsw as a transporter of lipid-linked cell wall precursors across the membrane. *EMBO J*, 30(8):1425–1432, Apr 2011.

[279] B. G. Spratt. Distinct penicillin binding proteins involved in the division, elongation, and shape of escherichia coli k12. *Proc Natl Acad Sci U S A*, 72(8):2999–3003, Aug 1975.

[280] C. Goffin and J. M. Ghuysen. Multimodular penicillin-binding proteins: an enigmatic family of orthologs and paralogs. *Microbiol Mol Biol Rev*, 62(4):1079–1093, Dec 1998.

[281] B. G. Spratt. Properties of the penicillin-binding proteins of escherichia coli k12,. *Eur J Biochem*, 72(2):341–352, Jan 1977.

[282] C. Fraipont, M. Adam, M. Nguyen-Distèche, W. Keck, J. Van Beeumen, J. A. Ayala, B. Granier, H. Hara, and J. M. Ghuysen. Engineering and overexpression of periplasmic forms of the penicillin-binding protein 3 of escherichia coli. *Biochem J*, 298 (Pt 1):189–195, Feb 1994.

[283] D. S. Weiss, K. Pogliano, M. Carson, L. M. Guzman, C. Fraipont, M. Nguyen-Distèche, R. Losick, and J. Beckwith. Localization of the escherichia coli cell division protein ftsl (pbp3) to the division site and cell pole. *Mol Microbiol*, 25(4):671–681, Aug 1997.

[284] T. J. Dougherty, K. Kennedy, R. E. Kessler, and M. J. Pucci. Direct quantitation of the number of individual penicillin-binding proteins per cell in escherichia coli. *J Bacteriol*, 178(21):6110–6115, Nov 1996.

[285] J. K. Broome-Smith, P. J. Hedge, and B. G. Spratt. Production of thiol-penicillin-binding protein 3 of escherichia coli using a two primer method of site-directed mutagenesis. *EMBO J*, 4(1):231–235, Jan 1985.

[286] L. D. Bowler and B. G. Spratt. Membrane topology of penicillin-binding protein 3 of escherichia coli. *Mol Microbiol*, 3(9):1277–1286, Sep 1989.

[287] M. Nguyen-Distèche, C. Fraipont, N. Buddelmeijer, and N. Nanninga. The structure and function of escherichia coli penicillin-binding protein 3. *Cell Mol Life Sci*, 54(4):309–316, Apr 1998.

[288] Mark C. Wissel and David S. Weiss. Genetic analysis of the cell division protein ftsi (pbp3): amino acid substitutions that impair septal localization of ftsi and recruitment of ftsn. *J Bacteriol*, 186(2):490–502, Jan 2004.

[289] G.A. Botta and Park J.T. Evidence for involvement of penicillin-binding protein 3 in murein synthesis during septation but not during cell elongation. *J Bacteriol*, 145(0021-9193 (Linking)):333–40, Jan 1981.

[290] A. G. Pisabarro, R. Prats, D. Váquez, and A. Rodríguez-Tébar. Activity of penicillin-binding protein 3 from escherichia coli. *J Bacteriol*, 168(1):199–206, Oct 1986.

[291] Mark C. Wissel, Jennifer L. Wendt, Calista J. Mitchell, and David S. Weiss. The transmembrane helix of the escherichia coli division protein ftsi localizes to the septal ring. *J Bacteriol*, 187(1):320–328, Jan 2005.

[292] L. Wang, M. K. Khattar, W. D. Donachie, and J. Lutkenhaus. Ftsi and ftsw are localized to the septum in escherichia coli. *J Bacteriol*, 180(11):2810–2816, Jun 1998.

[293] K. Dai, Y. Xu, and J. Lutkenhaus. Cloning and characterization of ftsn, an essential cell division gene in escherichia coli isolated as a multicopy suppressor of ftsa12(ts). *J Bacteriol*, 175(12):3790–3797, Jun 1993.

[294] S. G. Addinall, C. Cao, and J. Lutkenhaus. Ftsn, a late recruit to the septum in escherichia coli. *Mol Microbiol*, 25(2):303–309, Jul 1997.

[295] Matthew A. Gerding, Bing Liu, Felipe O. Bendezú, Cynthia A. Hale, Thomas G. Bernhardt, and Piet A J. de Boer. Self-enhanced accumulation of ftsn at division sites and roles for other proteins with a spor domain (damx, dedd, and rlpa) in escherichia coli cell constriction. *J Bacteriol*, 191(24):7383–7401, Dec 2009.

[296] Astrid Ursinus, Fusinita van den Ent, Sonja Brechtel, Miguel de Pedro, Joachim-Volker Höltje, Jan Löwe, and Waldemar Vollmer. Murein (peptidoglycan) binding property of the essential cell division protein ftsn from escherichia coli. *J Bacteriol*, 186(20):6728–6737, Oct 2004.

[297] Brett Geissler and William Margolin. Evidence for functional overlap among multiple bacterial cell division proteins: compensating for the loss of ftsk. *Mol Microbiol*, 58(2):596–612, Oct 2005.

[298] Ji Yang, Jung Shan Hwang, Helen Camakaris, Windy Irawaty, Akira Ishihama, and James Pittard. Mode of action of the tyrr protein: repression and activation of the tyrp promoter of escherichia coli. *Mol Microbiol*, 52(1):243–256, Apr 2004.

[299] Thomas G. Bernhardt and Piet A J. de Boer. The escherichia coli amidase amic is a periplasmic septal ring component exported via the twin-arginine transport pathway. *Mol Microbiol*, 48(5):1171–1182, Jun 2003.

[300] David S. Weiss. Bacterial cell division and the septal ring. *Mol Microbiol*, 54(3):588–597, Nov 2004.

[301] C. Heidrich, M. F. Templin, A. Ursinus, M. Merdanovic, J. Berger, H. Schwarz, M. A. de Pedro, and J. V. Höltje. Involvement of n-acetylmuramyl-l-alanine amidases in cell separation and antibiotic-induced autolysis of escherichia coli. *Mol Microbiol*, 41(1):167–178, Jul 2001.

[302] Frederico J. Gueiros-Filho and Richard Losick. A widely conserved bacterial cell division protein that promotes assembly of the tubulin-like protein ftsz. *Genes Dev*, 16(19):2544–2556, Oct 2002.

[303] Elaine Small, Rachel Marrington, Alison Rodger, David J. Scott, Katherine Sloan, David Roper, Timothy R. Dafforn, and Stephen G. Addinall. Ftsz polymer-bundling by the escherichia coli zapa orthologue, ygfe, involves a conformational change in bound gtp. *J Mol Biol*, 369(1):210–221, May 2007.

[304] Alex Dajkovic, Sebastien Pichoff, Joe Lutkenhaus, and Denis Wirtz. Cross-linking ftsz polymers into coherent z rings. *Mol Microbiol*, 78(3):651–668, Nov 2010.

[305] E Bi and Joe Lutkenhaus. *Prokaryotic Structure and Function: A New Perspective*, chapter Genetics of bacterial cell division, page 123–52. Cambridge Univ. Press, 1992.

[306] Zhuo Li, Michael J. Trimble, Yves V. Brun, and Grant J. Jensen. The structure of ftsz filaments in vivo suggests a force-generating role in cell division. *EMBO J*, 26(22):4694–4708, Nov 2007.

[307] Sigal Ben-Yehuda and Richard Losick. Asymmetric cell division in b. subtilis involves a spiral-like intermediate of the cytokinetic protein ftsz. *Cell*, 109(2):257 – 266, 2002.

[308] Phoebe C. Peters, Margaret D. Migocki, Carola Thoni, and Elizabeth J. Harry. A new assembly pathway for the cytokinetic z ring from a dynamic helical structure in vegetatively growing cells of bacillus subtilis. *Molecular Microbiology*, 64(2):487–499, 2007.

[309] Katherine A. Michie, Leigh G. Monahan, Peter L. Beech, and Elizabeth J. Harry. Trapping of a spiral-like intermediate of the bacterial cytokinetic protein ftsz. *J Bacteriol*, 188(5):1680–1690, Mar 2006.

[310] S. G. Addinall and J. Lutkenhaus. Ftsz-spirals and -arcs determine the shape of the invaginating septa in some mutants of escherichia coli. *Mol Microbiol*, 22(2):231–237, Oct 1996.

[311] Swapna Thanedar and William Margolin. Ftsz exhibits rapid movement and oscillation waves in helix-like patterns in escherichia coli. *Curr Biol*, 14(13):1167–1173, Jul 2004.

[312] Archana Varma and Kevin D. Young. Ftsz collaborates with penicillin binding proteins to generate bacterial cell shape in escherichia coli. *J Bacteriol*, 186(20):6768–6774, Oct 2004.

[313] Jesse Stricker, Paul Maddox, E. D. Salmon, and Harold P. Erickson. Rapid assembly dynamics of the escherichia coli ftsz-ring demonstrated by fluorescence recovery after photobleaching. *Proc Natl Acad Sci U S A*, 99(5):3171–3175, Mar 2002.

[314] Mark T. Anderson and Sandra K. Armstrong. The bfer regulator mediates enterobactin-inducible expression of bordetella enterobactin utilization genes. *J Bacteriol*, 186(21):7302–7311, Nov 2004.

[315] Kathleen R. Ryan and Lucy Shapiro. Temporal and spatial regulation in prokaryotic cell cycle progression and development. *Annu Rev Biochem*, 72:367–394, 2003.

[316] C. Lu, M. Reedy, and H. P. Erickson. Straight and curved conformations of ftsz are regulated by gtp hydrolysis. *J Bacteriol*, 182(1):164–170, Jan 2000.

[317] Biplab Ghosh and Anirban Sain. Origin of contractile force during cell division of bacteria. *Phys Rev Lett*, 101(17):178101, Oct 2008.

[318] Jun F. Allard and Eric N. Cytrynbaum. Force generation by a dynamic z-ring in escherichia coli cell division. *Proc Natl Acad Sci U S A*, 106(1):145–150, Jan 2009.

[319] Katharine A. Michie and Jan Löwe. Dynamic filaments of the bacterial cytoskeleton. *Annu Rev Biochem*, 75:467–492, 2006.

[320] Maria A. Oliva, Suzanne C. Cordell, and Jan Löwe. Structural insights into ftsz protofilament formation. *Nat Struct Mol Biol*, 11(12):1243–1250, Dec 2004.

[321] Phoebe C. Peters, Margaret D. Migocki, Carola Thoni, and Elizabeth J. Harry. A new assembly pathway for the cytokinetic z ring from a dynamic helical structure in vegetatively growing cells of bacillus subtilis. *Mol Microbiol*, 64(2):487–499, Apr 2007.

[322] R. A. Daniel, E. J. Harry, and J. Errington. Role of penicillin-binding protein pbp 2b in assembly and functioning of the division machinery of bacillus subtilis. *Mol Microbiol*, 35(2):299–311, Jan 2000.

[323] Christoph Heidrich, Astrid Ursinus, Jürgen Berger, Heinz Schwarz, and Joachim-Volker Höltje. Effects of multiple deletions of murein hydrolases on viability, septum cleavage, and sensitivity to large toxic molecules in escherichia coli. *J Bacteriol*, 184(22):6093–6099, Nov 2002.

[324] G. F. King, Y. L. Shih, M. W. Maciejewski, N. P. Bains, B. Pan, S. L. Rowland, G. P. Mullen, and L. I. Rothfield. Structural basis for the topological specificity function of mine. *Nat Struct Biol*, 7(11):1013–1017, Nov 2000.

[325] Wei Wu, Kyung-Tae Park, Todd Holyoak, and Joe Lutkenhaus. Determination of the structure of the mind-atp complex reveals the orientation of mind on the membrane and the relative location of the binding sites for mine and minc. *Mol Microbiol*, 79(6):1515–1528, Mar 2011.

[326] T. H. Szeto, S. L. Rowland, and G. F. King. The dimerization function of minc resides in a structurally autonomous c-terminal domain. *J Bacteriol*, 183(22):6684–6687, Nov 2001.

[327] Alex Dajkovic, Ganhui Lan, Sean X. Sun, Denis Wirtz, and Joe Lutkenhaus. Minc spatially controls bacterial cytokinesis by antagonizing the scaffolding function of ftsz. *Curr Biol*, 18(4):235–244, Feb 2008.

[328] Z. Hu, A. Mukherjee, S. Pichoff, and J. Lutkenhaus. The minc component of the division site selection system in escherichia coli interacts with ftsz to prevent polymerization. *ProcNatlAcadSciUSA*, 96(26):14819–14824, Dec 1999.

[329] S. Ramirez-Arcos, V. Greco, H. Douglas, D. Tessier, D. Fan, J. Szeto, J. Wang, and J. R. Dillon. Conserved glycines in the c terminus of minc proteins are implicated in their functionality as cell division inhibitors. *J Bacteriol*, 186(9):2841–2855, May 2004.

[330] Luyan Ma, Glenn F. King, and Lawrence Rothfield. Positioning of the mine binding site on the mind surface suggests a plausible mechanism for activation of the escherichia coli mind atpase during division site selection. *Mol Microbiol*, 54(1):99–108, Oct 2004.

[331] Zonglin Hu and Joe Lutkenhaus. A conserved sequence at the c-terminus of mind is required for binding to the membrane and targeting minc to the septum. *Mol Microbiol*, 47(2):345–355, Jan 2003.

[332] S. C. Cordell, R. E. Anderson, and J. Löwe. Crystal structure of the bacterial cell division inhibitor minc. *EMBO J*, 20(10):2454–2461, May 2001.

[333] Gilbert Di Paolo and Pietro De Camilli. Phosphoinositides in cell regulation and membrane dynamics. *Nature*, 443(7112):651–657, Oct 2006.

[334] Joe Lutkenhaus and M. Sundaramoorthy. Mind and role of the deviant walker a motif, dimerization and membrane binding in oscillation. *Mol Microbiol*, 48(2):295–303, Apr 2003.

[335] Tim H. Szeto, Susan L. Rowland, Lawrence I. Rothfield, and Glenn F. King. Membrane localization of mind is mediated by a c-terminal motif that is conserved across eubacteria, archaea, and chloroplasts. *Proc Natl Acad Sci U S A*, 99(24):15693–15698, Nov 2002.

[336] J. Szeto, S. Ramirez-Arcos, C. Raymond, L. D. Hicks, C. M. Kay, and J. A. Dillon. Gonococcal mind affects cell division in neisseria gonorrhoeae and escherichia coli and exhibits a novel self-interaction. *J Bacteriol*, 183(21):6253–6264, Nov 2001.

[337] Eugenia Mileykovskaya, Itzhak Fishov, Xueyao Fu, Brian D Corbin, William Margolin, and William Dowhan. Effects of phospholipid composition on mind-membrane interactions in vitro and in vivo. *J Biol Chem*, 278(25):22193–22198, Jun 2003.

[338] Laura Lackner. *Investigating the mechanism of Escherichia coli Min protein dynamics.* PhD thesis, Case Western Reserve University, 2006.

[339] G. F. King, S. L. Rowland, B. Pan, J. P. Mackay, G. P. Mullen, and L. I. Rothfield. The dimerization and topological specificity functions of mine reside in a structurally autonomous c-terminal domain. *Mol Microbiol*, 31(4):1161–1169, Feb 1999.

[340] Y. Zhang, S. Rowland, G. King, E. Braswell, and L. Rothfield. The relationship between hetero-oligomer formation and function of the topological specificity domain of the escherichia coli mine protein. *Mol Microbiol*, 30(2):265–273, Oct 1998.

[341] Lu-Yan Ma, Glenn King, and Lawrence Rothfield. Mapping the mine site involved in interaction with the mind division site selection protein of escherichia coli. *J Bacteriol*, 185(16):4948–4955, Aug 2003.

[342] Houman Ghasriani, Thierry Ducat, Chris T. Hart, Fatima Hafizi, Nina Chang, Ali Al-Baldawi, Saud H. Ayed, Patrik Lundström, Jo-Anne R. Dillon, and Natalie K. Goto. Appropriation of the mind protein-interaction motif by the dimeric interface of the bacterial cell division regulator mine. *Proc Natl Acad Sci U S A*, 107(43):18416–18421, Oct 2010.

[343] Dennis Ramos, Thierry Ducat, Jenny Cheng, Nelson F. Eng, Jo-Anne R. Dillon, and Natalie K. Goto. Conformation of the cell division regulator mine: evidence for interactions between the topological specificity and anti-mincd domains. *Biochemistry*, 45(14):4593–4601, Apr 2006.

[344] Yu-Ling Shih, Trung Le, and Lawrence Rothfield. Division site selection in escherichia coli involves dynamic redistribution of min proteins within coiled structures that extend between the two cell poles. *Proc Natl Acad Sci U S A*, 100(13):7865–7870, Jun 2003.

[345] Kerwyn Casey Huang, Yigal Meir, and Ned S Wingreen. Dynamic structures in escherichia coli: spontaneous formation of mine rings and mind polar zones. *Proc Natl Acad Sci USA*, 100(22):12724–12728, Oct 2003. x.

[346] Martin Loose. *Self-organization of Min proteins in vitro.* PhD thesis, Technische Universität Dresden, 2010.

[347] Q. Sun and W. Margolin. Influence of the nucleoid on placement of ftsz and mine rings in escherichia coli. *J Bacteriol*, 183(4):1413–1422, Feb 2001.

[348] Kyoko Suefuji, Regina Valluzzi, and Debabrata RayChaudhuri. Dynamic assembly of mind into filament bundles modulated by atp, phospholipids, and mine. *Proc Natl Acad Sci U S A*, 99(26):16776–16781, Dec 2002.

[349] Ariadna Martos, Mercedes Jiménez, Germán Rivas, and Petra Schwille. Towards a bottom-up reconstitution of bacterial cell division. *Trends Cell Biol*, Oct 2012.

[350] D. Axelrod. Cell-substrate contacts illuminated by total internal reflection fluorescence. *J Cell Biol*, 89(1):141–145, Apr 1981.

[351] Bryan A. Millis. Evanescent-wave field imaging: an introduction to total internal reflection fluorescence microscopy. *Methods Mol Biol*, 823:295–309, 2012.

[352] Satya Nanda Vel Arjunan and Masaru Tomita. A new multicompartmental reaction-diffusion modeling method links transient membrane attachment of e. coli mine to e-ring formation. *Syst Synth Biol*, 4(1):35–53, Mar 2010.

[353] Cheng-Wei Hsieh, Ti-Yu Lin, Hsin-Mei Lai, Chu-Chi Lin, Ting-Sung Hsieh, and Yu-Ling Shih. Direct mine-membrane interaction contributes to the proper localization of minde in e. coli. *Mol Microbiol*, 75(2):499–512, Jan 2010.

[354] Julien Derr, Jason T. Hopper, Anirban Sain, and Andrew D. Rutenberg. Self-organization of the mine protein ring in subcellular min oscillations. *Phys Rev E Stat Nonlin Soft Matter Phys*, 80(1 Pt 1):011922, Jul 2009.

[355] Karsten Kruse, Martin Howard, and William Margolin. An experimentalist's guide to computational modelling of the min system. *Mol Microbiol*, 63(5):1279–1284, Mar 2007. x.

[356] M. Howard, A. D. Rutenberg, and S. de Vet. Dynamic compartmentalization of bacteria: accurate division in e. coli. *Phys Rev Lett*, 87(27 Pt 1):278102, Dec 2001.

[357] Elisabeth Fischer-Friedrich. *Pattern formation by the Min system of Escherichia coli*. PhD thesis, Universität des Saarlandes, 2008.

[358] Jakob Schweizer, Martin Loose, Mike Bonny, Karsten Kruse, Ingolf Mönch, and Petra Schwille. Geometry sensing by self-organized protein patterns. *Proc Natl Acad Sci U S A*, 109(38):15283–15288, Sep 2012.

[359] Elisabeth Fischer-Friedrich, Giovanni Meacci, Joe Lutkenhaus, Hugues Chaté, and Karsten Kruse. Intra- and intercellular fluctuations in min-protein dynamics decrease with cell length. *Proc Natl Acad Sci USA*, 107(14):6134–6139, Apr 2010.

[360] Zonglin Hu, Edward P Gogol, and Joe Lutkenhaus. Dynamic assembly of mind on phospholipid vesicles regulated by atp and mine. *Proc Natl Acad Sci USA*, 99(10):6761–6766, May 2002.

[361] Aziz Taghbalout, Luyan Ma, and Lawrence Rothfield. Role of mind-membrane association in min protein interactions. *J Bacteriol*, 188(8):2993–3001, Apr 2006.

[362] Martin Loose and Petra Schwille. Biomimetic membrane systems to study cellular organization. *J Struct Biol*, 168(1):143–151, Oct 2009.

[363] Elisabeth Fischer-Friedrich, Romain Nguyen van yen, and Karsten Kruse. Surface waves of min-proteins. *Phys Biol*, 4(1):38–47, Mar 2007.

[364] Jakob Schweizer. *Bio and Nano Packaging Techniques for Electron Devices: Advances in Electronic Device Packaging*, chapter Packaging in Synthetic Biology, pages 383–418. Springer Verlag, 2012.

[365] Y. Lazebnik. Can a biologist fix a radio? – or, what i learned while studying apoptosis, (cancer cell. 2002 sep;2(3):179-82). *Biochemistry*, 69(12):1403–1406, Dec 2004.

[366] Mark A Bedau, John S McCaskill, Norman H Packard, and Steen Rasmussen. Living technology: exploiting life's principles in technology. *Artif Life*, 16(1):89–97, 2010.

[367] Drew Endy. Foundations for engineering biology. *Nature*, 438(7067):449–453, Nov 2005.

[368] Petra Schwille and Stefan Diez. Synthetic biology of minimal systems. *Crit Rev Biochem Mol Biol*, 44(4):223–242, 00 2009.

[369] David Loakes and Philipp Holliger. Darwinian chemistry: towards the synthesis of a simple cell. *Mol Biosyst*, 5(7):686–694, Jul 2009.

[370] P. L. Luisi. About various definitions of life. *Orig Life Evol Biosph*, 28(4-6):613–22, Oct 1998.

[371] Steen Rasmussen, Liaohai Chen, David Deamer, David C Krakauer, Norman H Packard, Peter F Stadler, and Mark A Bedau. Evolution. Transitions from nonliving to living matter. *Science*, 303(5660):963–5, Feb 2004.

[372] J. I. Glass, N. Assad-Garcia, N. Alperovich, S. Yooseph, M. R. Lewis, M. Maruf, C. A. Hutchison, H. O. Smith, and J. C. Venter. Essential genes of a minimal bacterium. *ProcNatlAcadSciUSA*, 103(2):425–430, January 2006.

[373] Daniel G Gibson, Gwynedd A Benders, Cynthia Andrews-Pfannkoch, Evgeniya A Denisova, Holly Baden-Tillson, Jayshree Zaveri, Timothy B Stockwell, Anushka Brownley, David W Thomas, Mikkel A Algire, Chuck Merryman, Lei Young, Vladimir N Noskov, John I Glass, J. Craig Venter, Clyde A Hutchison, and Hamilton O Smith. Complete chemical synthesis, assembly, and cloning of a mycoplasma genitalium genome. *Science*, 319(5867):1215–1220, Feb 2008.

[374] Dae-Kyun Ro, Eric M Paradise, Mario Ouellet, Karl J Fisher, Karyn L Newman, John M Ndungu, Kimberly A Ho, Rachel A Eachus, Timothy S Ham, James Kirby, Michelle C Y Chang, Sydnor T Withers, Yoichiro Shiba, Richmond Sarpong, and Jay D Keasling. Production of the antimalarial drug precursor artemisinic acid in engineered yeast. *Nature*, 440(7086):940–943, Apr 2006.

[375] Stephen W. Hawking. *The universe in a nutshell.* Bantam Books, New York, 2001.

[376] J. W. Szostak, D. P. Bartel, and P. L. Luisi. Synthesizing life. *Nature*, 409(6818):387–90, Jan 2001.

[377] Pier Luigi Luisi. Toward the engineering of minimal living cells. *Anat Rec*, 268(3):208–214, Nov 2002.

[378] Pier Luigi Luisi and Pasquale Stano. Synthetic biology: minimal cell mimicry. *Nat Chem*, 3(10):755–756, Oct 2011.

[379] Irene A Chen, Richard W Roberts, and Jack W Szostak. The emergence of competition between model protocells. *Science*, 305(5689):1474–6, Sep 2004.

[380] Jason P. Schrum, Ting F. Zhu, and Jack W. Szostak. The origins of cellular life. *Cold Spring Harb Perspect Biol*, 2(9):a002212, Sep 2010.

[381] Gerald Karp, editor. *Cell and molecular biology, 7e.* Wiley-VCH, 2013.

[382] Petra Schwille. Bottom-up synthetic biology: Engineering in a tinkerer's world. *Science*, 333(6047):1252–1254, 2011.

[383] S. L. Miller. A production of amino acids under possible primitive earth conditions. *Science*, 117(3046):528–529, May 1953.

[384] Walter Gilbert. Origin of life: The rna world. *Nature*, 319(6055):618–618, February 1986.

[385] D. Segré, D. Ben-Eli, D. W. Deamer, and D. Lancet. The lipid world. *Orig Life Evol Biosph*, 31(1-2):119–145, 2001.

[386] T. Oberholzer and P. L. Luisi. The use of liposomes for constructing cell models. *J Bio Phys*, 28(4):733–744, 2002.

[387] Jacob Israelachvili. *Intermolecular & Surface Forces.* Academic Press, 1991.

[388] S.J. Singer and G.L. Nicolson. The fluid mosaic model of the structure of cell membranes. *Science*, 175(23):720–31, Feb 1972.

[389] G. Vereb, J. Szöllosi, J. Matkó, P. Nagy, T. Farkas, L. Vigh, L. Mátyus, T. A. Waldmann, and S. Damjanovich. Dynamic, yet structured: The cell membrane three decades after the singer-nicolson model. *Proc Natl Acad Sci USA*, 100(14):8053–8058, Jul 2003.

[390] E. Sackmann and H. Träuble. Studies of the crystalline-liquid crystalline phase transition of lipid model membranes. I. Use of spin labels and optical probes as indicators of the phase transition. *J Am Chem Soc*, 94(13):4482–91, Jun 1972.

[391] Salvatore Chiantia, Jonas Ries, and Petra Schwille. Fluorescence correlation spectroscopy in membrane structure elucidation. *Biochim Biophys Acta*, 1788(1):225–233, Jan 2009.

[392] Kai Simons and Winchil L C Vaz. Model systems, lipid rafts, and cell membranes. *Annu Rev Biophys Biomol Struct*, 33:269–295, 2004.

[393] Ana J García-Sáez, Dolores C Carrer, and Petra Schwille. Fluorescence correlation spectroscopy for the study of membrane dynamics and organization in giant unilamellar vesicles. *Methods Mol Biol*, 606:493–508, 2010.

[394] Nicoletta Kahya, Dag Scherfeld, Kirsten Bacia, Bert Poolman, and Petra Schwille. Probing lipid mobility of raft-exhibiting model membranes by fluorescence correlation spectroscopy. *J Biol Chem*, 278(30):28109–28115, Jul 2003.

[395] Lawrence Rajendran and Kai Simons. Lipid rafts and membrane dynamics. *J Cell Sci*, 118(Pt 6):1099–1102, Mar 2005.

[396] L. K. Tamm and H. M. McConnell. Supported phospholipid bilayers. *Biophys J*, 47(1):105–113, Jan 1985.

[397] E. Sackmann. Supported membranes: scientific and practical applications. *Science*, 271(5245):43–8, Jan 1996.

[398] T. Dewa, R. Sugiura, Y. Suemori, M. Sugimoto, T. Takeuchi, A. Hiro, K. Iida, A. T. Gardiner, R. J. Cogdell, and M. Nango. Lateral organization of a membrane protein in a supported binary lipid domain: Direct observation of the organization of bacterial light-harvesting complex 2 by total internal reflection fluorescence microscopy. *Langmuir*, 22(12):5412–5418, June 2006.

[399] Salvatore Chiantia, Nicoletta Kahya, and Petra Schwille. Dehydration damage of domain-exhibiting supported bilayers: an afm study on the protective effects of disaccharides and other stabilizing substances. *Langmuir*, 21(14):6317–6323, Jul 2005.

[400] Salvatore Chiantia, Jonas Ries, Nicoletta Kahya, and Petra Schwille. Combined afm and two-focus sfcs study of raft-exhibiting model membranes. *Chemphyschem*, 7(11):2409–2418, Nov 2006.

[401] Martin Benes, Didier Billy, Ales Benda, Han Speijer, Martin Hof, and Wim Th Hermens. Surface-dependent transitions during self-assembly of phospholipid membranes on mica, silica, and glass. *Langmuir*, 20(23):10129–10137, Nov 2004.

[402] Ingo Mey, Milena Stephan, Eva K Schmitt, Martin Michael Müller, Martine Ben Amar, Claudia Steinem, and Andreas Janshoff. Local membrane mechanics of pore-spanning bilayers. *J Am Chem Soc*, 131(20):7031–7039, May 2009.

[403] C Hennesthal and C Steinem. Pore-spanning lipid bilayers visualized by scanning force microscopy. *J Am Chem Soc*, 122(33):8085–8086, AUG 23 2000.

[404] Christian Hennesthal, Janine Drexler, and Claudia Steinem. Membrane-suspended nanocompartments based on ordered pores in alumina. *Chemphyschem*, 3(10):885–889, Oct 2002.

[405] C Schmidt, M Mayer, and H Vogel. A chip-based biosensor for the functional analysis of single ion channels. *Angew Chem Int Ed Engl*, 39(17):3137–3140, Sep 2000.

[406] Mikhail Merzlyakov, Edwin Li, Ivan Gitsov, and Kalina Hristova. Surface-supported bilayers with transmembrane proteins: role of the polymer cushion revisited. *Langmuir*, 22(24):10145–10151, Nov 2006.

[407] Hagan Bayley, Brid Cronin, Andrew Heron, Matthew A. Holden, William L. Hwang, Ruhma Syeda, James Thompson, and Mark Wallace. Droplet interface bilayers. *Mol Biosys*, 4:1191–1208, 2009.

[408] Tivadar Mach, Catalin Chimerel, Jürgen Fritz, Niels Fertig, Mathias Winterhalter, and Claus Fütterer. Miniaturized planar lipid bilayer: increased stability, low electric noise and fast fluid perfusion. *Anal Bioanal Chem*, 390(3):841–846, Feb 2008.

[409] Peter Walde, Katia Cosentino, Helen Engel, and Pasquale Stano. Giant vesicles: preparations and applications. *Chembiochem*, 11(7):848–865, May 2010.

[410] K. Akashi, H. Miyata, H. Itoh, and K. Kinosita. Preparation of giant liposomes in physiological conditions and their characterization under an optical microscope. *Biophys J*, 71(6):3242–50, Dec 1996.

[411] P. Mueller, T. F. Chien, and B. Rudy. Formation and properties of cell-size lipid bilayer vesicles. *Biophys J*, 44(3):375–381, Dec 1983.

[412] Jeanne C Stachowiak, David L Richmond, Thomas H Li, Allen P Liu, Sapun H Parekh, and Daniel A Fletcher. Unilamellar vesicle formation and encapsulation by microfluidic jetting. *Proc Natl Acad Sci USA*, 105(12):4697–4702, Mar 2008.

[413] M. I. Angelova and D. S. Dimitrov. Liposome electroformation. *Faraday DiscussChem Soc*, 81(81):303–311, 1986.

[414] Nicoletta Kahya, Dag Scherfeld, Kirsten Bacia, and Petra Schwille. Lipid domain formation and dynamics in giant unilamellar vesicles explored by fluorescence correlation spectroscopy. *J Struct Biol*, 147(1):77–89, Jul 2004.

[415] L-Ruth Montes, Alicia Alonso, Felix M Go ni, and Luis A Bagatolli. Giant unilamellar vesicles electroformed from native membranes and organic lipid mixtures under physiological conditions. *Biophys J*, 93(10):3548–3554, Nov 2007.

[416] Sindy Neumann, Angelika Fuchs, Armen Mulkidjanian, and Dmitrij Frishman. Current status of membrane protein structure classification. *Proteins*, Jan 2010.

[417] S. W. Cowan, R. M. Garavito, J. N. Jansonius, J. A. Jenkins, R. Karlsson, N. König, E. F. Pai, R. A. Pauptit, P. J. Rizkallah, and J. P. Rosenbusch. The structure of ompf porin in a tetragonal crystal form. *Structure*, 3(10):1041–1050, Oct 1995.

[418] S. M. Bezrukov, L. Kullman, and M. Winterhalter. Probing sugar translocation through maltoporin at the single channel level. *FEBS Lett*, 476(3):224–228, Jul 2000.

[419] T. K. Rostovtseva and S. M. Bezrukov. Atp transport through a single mitochondrial channel, vdac, studied by current fluctuation analysis. *Biophys J*, 74(5):2365–2373, May 1998.

[420] S. W. Cowan, T. Schirmer, G. Rummel, M. Steiert, R. Ghosh, R. A. Pauptit, J. N. Jansonius, and J. P. Rosenbusch. Crystal structures explain functional properties of two e. coli porins. *Nature*, 358(6389):727–733, Aug 1992.

[421] J. P. Abrahams, A. G. Leslie, R. Lutter, and J. E. Walker. Structure at 2.8 a resolution of f1-atpase from bovine heart mitochondria. *Nature*, 370(6491):621–628, Aug 1994.

[422] D. Stock, A. G. Leslie, and J. E. Walker. Molecular architecture of the rotary motor in atp synthase. *Science*, 286(5445):1700–1705, Nov 1999.

[423] H. Noji, R. Yasuda, M. Yoshida, and K. Kinosita. Direct observation of the rotation of f1-atpase. *Nature*, 386(6622):299–302, Mar 1997.

[424] Gregory M Cook, Stefanie Keis, Hugh W Morgan, Christoph von Ballmoos, Ulrich Matthey, Georg Kaim, and Peter Dimroth. Purification and biochemical characterization of the f1fo-atp synthase from thermoalkaliphilic bacillus sp. strain ta2.a1. *J Bacteriol*, 185(15):4442–4449, Aug 2003.

[425] D. Oesterhelt and W. Stoeckenius. Rhodopsin-like protein from the purple membrane of halobacterium halobium. *Nat New Biol*, 233(39):149–152, Sep 1971.

[426] S. C. Kushwaha and M. Kates. Isolation and identification of "bacteriorhodopsin" and minor c40-carotenoids in halobacterium cutirubrum. *Biochim Biophys Acta*, 316(2):235–243, Aug 1973.

[427] Stefan Streif, Wilfried Franz Staudinger, Wolfgang Marwan, and Dieter Oesterhelt. Flagellar rotation in the archaeon halobacterium salinarum depends on atp. *J Mol Biol*, 384(1):1–8, Dec 2008.

[428] GW Rayfield. Photodiodes based on bacteriorhodopsin. In RR Birge, editor, *Molecular and Biomolecular Electronics*, volume 240 of *Advances in Chemistry Series*, pages 561–575, 1994.

[429] Paolo Bertoncello, Davide Nicolini, Cristina Paternolli, Valter Bavastrello, and Claudio Nicolini. Bacteriorhodopsin-based langmuir-schaefer films for solar energy capture. *IEEE Trans Nanobioscience*, 2(2):124–132, Jun 2003.

[430] Jean-Louis Rigaud and Daniel Lévy. Reconstitution of membrane proteins into liposomes. *Methods Enzymol*, 372:65–86, 2003.

[431] Philippe Girard, Jacques Pécréaux, Guillaume Lenoir, Pierre Falson, Jean-Louis Rigaud, and Patricia Bassereau. A new method for the reconstitution of membrane proteins into giant unilamellar vesicles. *Biophys J*, 87(1):419–429, Jul 2004.

[432] N. Kahya, E. I. Pécheur, W. P. de Boeij, D. A. Wiersma, and D. Hoekstra. Reconstitution of membrane proteins into giant unilamellar vesicles via peptide-induced fusion. *Biophys J*, 81(3):1464–74, Sep 2001.

[433] M. T. Paternostre, M. Roux, and J. L. Rigaud. Mechanisms of membrane protein insertion into liposomes during reconstitution procedures involving the use of detergents. 1. Solubilization of large unilamellar liposomes (prepared by reverse-phase evaporation) by triton X-100, octyl glucoside, and sodium cholate. *Biochemistry*, 27(8):2668–2677, Apr 1988.

[434] J. L. Rigaud, M. T. Paternostre, and A. Bluzat. Mechanisms of membrane protein insertion into liposomes during reconstitution procedures involving the use of detergents. 2. Incorporation of the light-driven proton pump bacteriorhodopsin. *Biochemistry*, 27(8):2677–2688, Apr 1988.

[435] P. W. Holloway. A simple procedure for removal of Triton X-100 from protein samples. *Anal Biochem*, 53(1):304–308, May 1973.

[436] J.-L-Rigaud and D. Levy. Detergent removal by non-polar polystyrene beads: Applications to membrane protein reconstitution and two-dimensional crystallization. *Eur Biophys*, 27:2677–2688, 1998.

[437] Armelle Varnier, Frédérique Kermarrec, Iulia Blesneac, Christophe Moreau, Lavinia Liguori, Jean Luc Lenormand, and Nathalie Picollet-D'hahan. A simple method for the reconstitution of membrane proteins into giant unilamellar vesicles. *J Membr Biol*, 233(1-3):85–92, Feb 2010.

[438] Jakob Schweizer. Synthetic biology - a new way to access biological phenomena. *Imaging & Microscopy*, 2011/3:36 − 39, 2011.

[439] K. Simons and E. Ikonen. Functional rafts in cell membranes. *Nature*, 387(6633):569–572, Jun 1997.

[440] Elliot L Elson, Eliot Fried, John E Dolbow, and Guy M Genin. Phase separation in biological membranes: integration of theory and experiment. *Annu Rev Biophys*, 39:207–226, Jun 2010.

[441] L. A. Bagatolli and E. Gratton. Two photon fluorescence microscopy of coexisting lipid domains in giant unilamellar vesicles of binary phospholipid mixtures. *Biophys J*, 78(1):290–305, Jan 2000.

[442] Aurélien Roux, Giovanni Cappello, Jean Cartaud, Jacques Prost, Bruno Goud, and Patricia Bassereau. A minimal system allowing tubulation with molecular motors pulling on giant liposomes. *Proc Natl Acad Sci U S A*, 99(8):5394–5399, Apr 2002.

[443] Li A. Kung, Lance Kam, Jennifer S. Hovis, and Steven G. Boxer. Patterning hybrid surfaces of proteins and supported lipid bilayers. *Langmuir*, 16:6773–6776, 2000.

[444] Jennifer S. Hovis and Steven G. Boxer. Patterning barriers to lateral diffusion in supported lipid bilayer membranes by blotting and stamping. *Langmuir*, 16:894–897, 2000.

[445] CD James, RC Davis, L Kam, HG Craighead, M Isaacson, JN Turner, and W Shain. Patterned protein layers on solid substrates by thin stamp microcontact printing. *Langmuir*, 14(4):741–744, FEB 17 1998.

[446] Jennifer S. Hovis and Steven G. Boxer. Patterning and composition arrays of supported lipid bilayers by microcontact printing. *Langmuir*, 17:3400–3405, 2001.

[447] L. Kam and S. G. Boxer. Cell adhesion to protein-micropatterned-supported lipid bilayer membranes. *J Biomed Mater Res*, 55(4):487–495, Jun 2001.

[448] Pilnam Kim, Sang Eun Lee, Ho Sup Jung, Hea Yeon Lee, Tomoji Kawai, and Kahp Y. Suh. Soft lithographic patterning of supported lipid bilayers onto a surface and inside microfluidic channels. *Lab Chip*, 6(1):54–59, Jan 2006.

[449] Xuexin Duan, Veera B. Sadhu, Andras Perl, Maria Péter, David N. Reinhoudt, and Jurriaan Huskens. Bifunctional, chemically patterned flat stamps for microcontact printing of polar inks. *Langmuir*, 24(7):3621–3627, Apr 2008.

[450] J. T. Groves, N. Ulman, and S. G. Boxer. Micropatterning fluid lipid bilayers on solid supports. *Science*, 275(5300):651–653, Jan 1997.

[451] JT Groves, N Ulman, PS Cremer, and SG Boxer. Substrate-membrane interactions: Mechanisms for imposing patterns on a fluid bilayer membrane. *Langmuir*, 14(12):3347–3350, 06 1998.

[452] Senthil Arumugam, Grzegorz Chwastek, Elisabeth Fischer-Friedrich, Carina Ehrig, Ingolf Mönch, and Petra Schwille. Surface topology engineering of membranes for the mechanical investigation of the tubulin homologue ftsz. *Angew Chem Int Ed Engl*, Aug 2012.

[453] Ralf Seemann, Martin Brinkmann, Thomas Pfohl, and Stephan Herminghaus. Droplet based microfluidics. *Rep Prog Phys*, 75(1):016601, Jan 2012.

[454] Carl Zeiss AG. *LSM 510 and LSM 510 META Laser Scanning Microscopes*, 3.2 edition, 10 2002.

[455] D. Axelrod, D.E. Koppel, J. Schlessinger, E. Elson, and W.W. Webb. Mobility measurement by analysis of fluorescence photobleaching recovery kinetics. *Biophys J*, 16(9):1055–69, Sep 1976.

[456] D Magde, WW Webb, and E Elson. Thermodynamic fluctuations in a reacting system - measurement by fluorescence correlation spectroscopy. *Phys Rev Lett*, 29(11):705–&, 1972.

[457] M. Eigen and R. Rigler. Sorting single molecules: application to diagnostics and evolutionary biotechnology. *Proc Natl Acad Sci USA*, 91(13):5740–5747, Jun 1994.

[458] P. Schwille, F. Oehlenschläger, and N. G. Walter. Quantitative hybridization kinetics of dna probes to rna in solution followed by diffusional fluorescence correlation analysis. *Biochemistry*, 35(31):10182–10193, Aug 1996.

[459] Karsten Kruse and Frank Jülicher. Oscillations in cell biology. *Curr Opin Cell Biol*, 17(1):20–26, Feb 2005.

[460] O. Steinbock, A. Tóth, and K. Showalter. Navigating complex labyrinths: optimal paths from chemical waves. *Science*, 267(5199):868–871, Feb 1995.

[461] Alexander S. Mikhailov and Kenneth Showalter. Control of waves, patterns and turbulence in chemical systems. *Physics Reports*, 425(2-3):79 − 194, 2006.

[462] Rafael C. Gonzalez and Richard E. Woods (Autor). *Digital Image Processing*. Prentice Hall International, 2002.

[463] Markus Bar, Ehud Meron, and Clemens Utzny. Pattern formation on anisotropic and heterogeneous catalytic surfaces. *Chaos*, 12(1):204–214, Mar 2002.

[464] Brian D Corbin, Xuan-Chuan Yu, and William Margolin. Exploring intracellular space: function of the min system in round-shaped escherichia coli. *EMBO J*, 21(8):1998–2008, Apr 2002.

[465] Kerwyn Casey Huang and Ned S Wingreen. Min-protein oscillations in round bacteria. *Phys Biol*, 1(3-4):229–235, Dec 2004.

[466] M. D. Graham, I. G. Kevrekidis, K. Asakura, J. Lauterbach, K. Krischer, H. H. Rotermund, and G. Ertl. Effects of boundaries on pattern formation: Catalytic oxidation of co on platinum. *Science*, 264(5155):80–82, Apr 1994.

[467] Filipe Tostevin and Martin Howard. A stochastic model of min oscillations in escherichia coli and min protein segregation during cell division. *Phys Biol*, 3(1):1–12, Mar 2006.

[468] Barbara Di Ventura and Victor Sourjik. Self-organized partitioning of dynamically localized proteins in bacterial cell division. *Mol Syst Biol*, 7:457, Jan 2011.

[469] James A. Dix and A. S. Verkman. Crowding effects on diffusion in solutions and cells. *Annu Rev Biophys*, 37:247–263, 2008.

[470] Jacob Halatek and Erwin Frey. Highly canalized mind transfer and mine sequestration explain the origin of robust mincde-protein dynamics. *Cell Rep*, 1(6):741–752, Jun 2012.

[471] Emmanuel Dauty and A. S. Verkman. Molecular crowding reduces to a similar extent the diffusion of small solutes and macromolecules: measurement by fluorescence correlation spectroscopy. *J Mol Recognit*, 17(5):441–447, 2004.

[472] Raghuveer Parthasarathy, Cheng-han Yu, and Jay T. Groves. Curvature-modulated phase separation in lipid bilayer membranes. *Langmuir*, 22(11):5095–5099, May 2006.

[473] Marion B. Hochrein, Judith A. Leierseder, Leonardo Golubovi?, and Joachim O. Rädler. Dna localization and stretching on periodically microstructured lipid membranes. *Phys Rev Lett*, 96(3):038103, Jan 2006.

[474] Marion B. Hochrein, Judith A. Leierseder, Leonardo Golubovi?, and Joachim O. Rädler. Dna molecules on periodically microstructured lipid membranes: localization and coil stretching. *Phys Rev E Stat Nonlin Soft Matter Phys*, 75(2 Pt 1):021901, Feb 2007.

[475] J. H. Cha and G. C. Stewart. The diviva minicell locus of bacillus subtilis. *J Bacteriol*, 179(5):1671–1683, Mar 1997.

[476] D. H. Edwards and J. Errington. The bacillus subtilis diviva protein targets to the division septum and controls the site specificity of cell division. *Mol Microbiol*, 24(5):905–915, Jun 1997.

[477] Marc Bramkamp, Robyn Emmins, Louise Weston, Catriona Donovan, Richard A. Daniel, and Jeff Errington. A novel component of the division-site selection system of bacillus subtilis and a new mode of action for the division inhibitor mincd. *Mol Microbiol*, 70(6):1556–1569, Dec 2008.

[478] Rok Lenarcic, Sven Halbedel, Loek Visser, Michael Shaw, Ling Juan Wu, Jeff Errington, Davide Marenduzzo, and Leendert W. Hamoen. Localisation of diviva by targeting to negatively curved membranes. *EMBO J*, 28(15):2272–2282, Aug 2009.

[479] Prahathees Eswaramoorthy, Marcella L. Erb, James A. Gregory, Jared Silverman, Kit Pogliano, Joe Pogliano, and Kumaran S. Ramamurthi. Cellular architecture mediates diviva ultrastructure and regulates min activity in bacillus subtilis. *MBio*, 2(6), 2011.

[480] Anne-Lise Troutier and Catherine Ladavière. An overview of lipid membrane supported by colloidal particles. *Adv Colloid Interface Sci*, 133(1):1–21, 05 2007.

[481] Joe Lutkenhaus. Min oscillation in bacteria. *Adv Exp Med Biol*, 641:49–61, 2008.

[482] K. Simons and D. Toomre. Lipid rafts and signal transduction. *Nat Rev Mol Cell Biol*, 1(1):31–9, Oct 2000.

[483] Elisabeth Fischer-Friedrich. *Personal Communication*, 2007.

[484] Katja Zieske and Petra Schwille. Reconstitution of pole-to-pole oscillations of min proteins in micro-engineered pdms compartments. *Angewandte Chemie*, 2012.

[485] Brian R. Fritz, Laura E. Timmerman, Nichole M. Daringer, Joshua N. Leonard, and Michael C. Jewett. Biology by design: from top to bottom and back. *J Biomed Biotechnol*, 2010:232016, 2010.

[486] Michael C. Jewett and Anthony C. Forster. Update on designing and building minimal cells. *Curr Opin Biotechnol*, 21(5):697–703, Oct 2010.

[487] Hamilton O Smith, Clyde A Hutchison, Cynthia Pfannkoch, and J. Craig Venter. Generating a synthetic genome by whole genome assembly: phiX174 bacteriophage from synthetic oligonucleotides. *Proc Natl Acad Sci*, 100(26):15440–5, Dec 2003.

[488] Jerzy Maselko and Kenneth Showalter. Chemical waves on spherical surfaces. *Nature*, 339(6226):609–611, June 1989.

[489] T. Nakagaki, H. Yamada, and A. Tóth. Maze-solving by an amoeboid organism. *Nature*, 407(6803):470, Sep 2000.

[490] T. Nakagaki. Smart behavior of true slime mold in a labyrinth. *Res Microbiol*, 152(9):767–770, Nov 2001.

[491] Atsushi Tero, Ryo Kobayashi, and Toshiyuki Nakagaki. A mathematical model for adaptive transport network in path finding by true slime mold. *J Theor Biol*, 244(4):553–564, Feb 2007.

[492] J. B. Bard. A model for generating aspects of zebra and other mammalian coat patterns. *J Theor Biol*, 93(2):363–385, Nov 1981.

[493] J. D. Murray. On pattern formation mechanisms for lepidopteran wing patterns and mammalian coat markings. *Philos Trans R Soc Lond B Biol Sci*, 295(1078):473–496, Oct 1981.

[494] I. Farkas, D. Helbing, and T. Vicsek. Mexican waves in an excitable medium. *Nature*, 419(6903):131–132, Sep 2002.

List of publications

Jakob Schweizer and Petra Schwille Synthetic Biology.
A New Way to Access Biological Phenomena.
Imaging & Microscopy, 2011, vol. 3, pp. 36–39

Jakob Schweizer, Matthias Garten and Petra Schwille.
Packaging in Synthetic Biology.
in *Bio and Nano Packaging Techniques for Electron Devices: Advances in Electronic Device Packaging*, Gerald Gerlach and Klaus-Jürgen Wolter (Eds.)
Springer Verlag, 2012, pp. 383–418

Jakob Schweizer, Martin Loose, Mike Bonny, Karsten Kruse, Ingolf Mönch and Petra Schwille.
Geometry sensing by self-organized protein patterns.
Proc. Natl. Acad. Sci. USA, 2012, vol. 109, pp. 15283–15288

Acknowledgments

Erklärung

Erklärung gemäß §5(5) der Promotionsordnung der Fakultät Mathematik und Naturwissenschaften der Technischen Universität Dresden

(Declaration required according to §5(5) of the regulations for obtaining a doctoral degree of the Faculty of Science of the TU Dresden)

Hiermit versichere ich, dass ich die vorliegende Arbeit ohne unzulässige Hilfe Dritter und ohne Benutzung anderer als der angegebenen Hilfsmittel angefertigt habe; die aus fremden Quellen direkt oder indirekt übernommenen Gedanken sind als solche kenntlich gemacht. Die Arbeit wurde bisher weder im Inland noch im Ausland in gleicher oder ähnlicher Form einer anderen Prüfungsbehörde vorgelegt.

Diese Dissertation wurde unter der Betreuung von Prof. Dr. Petra Schwille am Biotechnologischen Zentrum der Technischen Universität Dresden angefertig.

Ich erkenne die Promotionsordnung der Fakultät Mathematik und Naturwissenschaften der Technischen Universität Dresden an.

Dresden, 16. November 2012   Jakob Schweizer

Table comparing reaction-diffusion models of the Min system.

		Aggregation current				Cooperative attachment						
References	Authors	Kruse	Meacci and Kruse	Fischer-Friedrich and Kruse		Meinhardt and de Boer	Howard	Huang	Huang (Fischer-Friedrich)	Fischer-Friedrich and Kruse		Bonny and Kruse
	Year	2002	2005	2007	2008	2001	2001	2003	2008	2008		2012
	Publications	[191]	[199]	[363]	[357]	[272]	[356]	[345]	[357]	[357]		[358]
Conditions	Membrane geometry	Cell	Cell	Cell	SLB	Cell	Cell	Cell	SLB	Cell	SLB	SLB
	Dimensionality	1	1	3	2	1	1	1	3	3	2	2
	Length, Radius or area	1 (au)	2 µm	3.2 µm, 0.68 µm	250 µm × 250 µm	3 µm	2 µm	4/10 µm, 0.5 µm	450 µm × 450 µm	2 µm	900 µm × 900 µm	various
	Replacements in equations	—	$\delta=1,\ \nabla=\partial_x,\ \Delta=\partial_x^2$	$\delta=\delta(\mathcal{S})$	—	—	—	$\delta=\delta(r-R)$	$\delta=\delta(\mathcal{S})$	—	—	—

Differential equations

MinD cytosolic $\partial_t c_D=$
- Kruse: $+D_d\partial_x^2 c_D$ $-\omega_1(1-c_d)c_D$ $+\omega_2 c_e c_d$
- Meacci / Fischer-Friedrich and Kruse (aggregation): $+D_D\Delta c_D$ $-\omega_D(c_{max}-c_d-c_{de})c_D\delta$ $+\omega_{de}c_{de}\delta$
- Meinhardt and de Boer: $+D_D\partial_x^2 c_D$ $-\rho_d(c_d^2+\sigma_d)-\rho_D c_D$ $+\sigma_D$
- Howard: $+D_D\partial_x^2 c_D$ $-\dfrac{\sigma_1 c_D}{1+\sigma_1' c_e}$ $+\sigma_2 c_e c_d$
- Huang:
$$\partial_t c_{D:ADP}=+D_D\Delta c_{D:ADP}-\sigma_D^{ATP}c_{D:ADP}+\delta\sigma_{de}c_{de}$$
$$\partial_t c_{D:ATP}=+D_D\Delta c_{D:ATP}+\sigma_D^{ATP}c_{D:ADP}-\delta[\sigma_D+\sigma_{dD}(c_d+c_{de})]c_{D:ATP}$$
- Huang (Fischer-Friedrich): $+D_D\Delta c_D$ $-c_D(\omega_D+\omega_{dD}c_d)$ $+\omega_{de}c_{de}c_d$
- Bonny and Kruse: $+D_D\Delta c_D$ $-c_d(\omega_D+\omega_{dD}c_d)(c_{max}-c_d-c_{de})/c_{max}$ $+(\omega_{de,m}+\omega_{de,c})c_{de}$

MinE cytosolic $\partial_t c_E=$
- Kruse: $+D_e\partial_x^2 c_E$ $-\omega_3(1-c_e)c_E$ $+\omega_4 c_e$
- Fischer-Friedrich and Kruse (aggregation): $+D_E\Delta c_E$ $-\omega_E c_d c_E\delta$ $+\omega_{de}c_{de}\delta$
- Meinhardt and de Boer: $+D_E\partial_x^2 c_E$ $-\rho_e c_E\dfrac{c_d}{1+\omega_{de}c_d^2}\dfrac{(c_e^2+\sigma_e)}{1+\sigma_{de}c_e^2}-\mu_E c_E$ $+\sigma_E$
- Howard: $+D_E\partial_x^2 c_E$ $-\sigma_2 c_D c_E$ $+\dfrac{\sigma_4 c_e}{1+\sigma_4' c_D}$
- Huang (Fischer-Friedrich): $+D_E\Delta c_E$ $-\omega_E c_d c_E$ $+\delta\sigma_{de}c_{de}$
- Fischer-Friedrich and Kruse (cooperative): $+D_E\Delta c_E$ $-c_E c_d(\omega_E+\omega_e c_{de}^2)$ $+\omega_{de}c_{de}$
- Bonny and Kruse: $+D_E\Delta c_E$ $-\omega_E c_E c_d$ $+\omega_{de,c}c_{de}+\omega_e c_e$

MinD on membrane $\partial_t c_d=$
- Kruse: $+\omega_1(1-c_d)c_D$ $-\omega_2 c_e c_d$ $-\partial_x j_d$
- Meacci / FF and Kruse (aggregation): $+\omega_D(c_{max}-c_d-c_{de})c_D$ $-\omega_E c_d c_E$ $-\nabla\cdot j_d$
- Meinhardt and de Boer: $+D_d\partial_x^2 c_d$ $+\rho_d c_D(c_d^2+\sigma_d)$ $-\mu_d-\mu_{de}c_d c_e$
- Howard: $+\dfrac{\sigma_1 c_D}{1+\sigma_1' c_e}$ $-\sigma_2 c_D c_E$
- Huang (Fischer-Friedrich): $+[\sigma_D+\sigma_{dD}(c_d+c_{de})]c_{D:ATP}$ $-\sigma_E c_d c_E$
- Fischer-Friedrich and Kruse (cooperative): $+D_d\Delta c_d$ $+c_D(\omega_D+\omega_{dD}c_d)$ $-c_E c_d(\omega_E+\omega_e c_{de}^2)$
- Bonny and Kruse: $+D_d\Delta c_d$ $+c_d(\omega_D+\omega_{dD}c_d)(c_{max}-c_d-c_{de})/c_{max}$ $-\omega_E c_E c_d$

MinE c_e or MinDE c_{de} on membrane
- Kruse: $\partial_t c_e=+\omega_3(1-c_e)c_E$ $-\omega_4 c_e$
- Meacci: $\partial_t c_{de}=+\omega_E c_d c_E$ $-\omega_{de}c_{de}$ $-\partial_x j_{de}$
- FF and Kruse 2007: $\partial_t c_{de}=+\omega_E c_E c_d$ $-\omega_{de}c_{de}$
- Meinhardt and de Boer: $\partial_t c_e=+D_e\partial_x^2 c_e$ $+\rho_e c_E\dfrac{c_d}{1+\omega_{de}c_d^2}\dfrac{c_e^2+\sigma_e}{1+\sigma_{de}c_e^2}$ $-\mu_e c_e$
- Howard: $\partial_t c_e=+\sigma_2 c_D c_E$ $-\dfrac{\sigma_4 c_e}{1+\sigma_4' c_D}$
- Huang (Fischer-Friedrich): $\partial_t c_{de}=+\sigma_E c_d c_E$ $-\sigma_{de}c_{de}$
- Fischer-Friedrich and Kruse (cooperative): $\partial_t c_{de}=+D_{de}\Delta c_{de}$ $+c_E c_d(\omega_E+\omega_e c_{de}^2)$ $-\omega_{de}c_{de}$
- Bonny and Kruse:
$$\partial_t c_{de}=+D_{de}\Delta c_{de}+\omega_E c_E c_d+\omega_{dD}c_d c_{de}-(\omega_{de,m}+\omega_{de,c})c_{de}$$
$$\partial_t c_e=+D_e\Delta c_e+\omega_{de,m}c_{de}-\omega_e c_e$$

Diffusion coefficients

	Kruse	Meacci	FF 2007	FF 2008	Meinhardt	Howard	Huang	Huang (FF)	FF cell	FF SLB	Bonny
Diffusion of cytosolic MinD $D_D=$	100 (au)	2.5 µm²/s	15.4 µm²/s	63 µm²/s	0.2 (≙7.3 µm²/s)	0.28 µm²/s	2.5 µm²/s	63 µm²/s	12.5 µm²/s	60 µm²/s	50 µm²/s
Diffusion of cytosolic MinE $D_E=$	100 (au)	2.5 µm²/s	15.4 µm²/s	63 µm²/s	0.2 (≙7.3 µm²/s)	0.6 µm²/s	2.5 µm²/s	63 µm²/s	12.5 µm²/s	60 µm²/s	50 µm²/s
Diffusion of MinD D_d on membrane	3.25 (au)	0.06 µm²/s	0.2 µm²/s	1.5 µm²/s	0.02	—	—	—	0.013 µm²/s	1.2 µm²/s	0.24 µm²/s
Diffusion of MinE D_e on membrane	—	—	—	—	0.0004	—	—	—	0.013 µm²/s	0.4 µm²/s	$D_{de}=0.24$ µm²/s (MinDE-complex), $D_e=0.48$ µm²/s (MinE without MinD)

Parameters

	Kruse	Meacci	FF 2007	FF 2008	Meinhardt	Howard	Huang	Huang (FF)	FF cell	FF SLB	Bonny
MinD membrane attachment	$\omega_1=1$	$\omega_D=4\times10^{-5}$ µm/s	$\omega_D=8.4\times10^{-5}$ µm³/s	$\omega_D=0.0004\ s^{-1}$	Constant synthesis of MinD: $\sigma_D=0.0035$, $\sigma_d=0.05$	Spontaneous MinD attachment to membrane: $\sigma_1=20\ s^{-1}$	$\sigma_D=0.025$ µm/s	$\sigma_D=0.98\ s^{-1}$	$\omega_D=0.0013/s$	$\omega_D=0.00029/s$	$\omega_D=0.045/s$
MinD-MinD interaction on membrane	—	$k_1=2.1\times10^{-6}$ µm⁴/s, $k_2=2.5\times10^{-7}$ µm⁵/s	$k_1=16.6\times10^{-6}$ µm⁶/s, $k_2=26.6\times10^{-7}$ µm⁸/s	$k_1=7.2\times10^{-12}$ µm⁶/s, $k_2=1.8\times10^{-10}$ µm⁸/s	Catalytic synthesis of MinD: $\rho_d=0.002$	Cooperative MinD attachment to membrane: —	$\sigma_{dD}=0.0015$ µm³/s	$\sigma_{dD}=6.6\times10^{-7}$ µm²/s	$\omega_{dD}=9.3\times10^{-4}$ µm²/s	$\omega_{dD}=4.8\times10^{-8}$ µm²/s	$\omega_{dD}=9\times10^{-4}$ µm²/s
MinE attachment to MinD	$\omega_3=1$	$\omega_E=3\times10^{-4}$ µm/s	$\omega_E=3.4\times10^{-4}$ µm³/s	$\omega_E=3.3\times10^{-9}$ µm²/s	Constant synthesis of MinE: $\sigma_E=0.002$, $\sigma_e=0.1$	MinE recruitment by MinD: $\sigma_3=0.04$ µm/s (by cytosolic MinD)	$\sigma_E=0.093$ µm³/s	$\sigma_E=4\times10^{-5}$ µm²/s	$\omega_E=3.8\times10^{-5}$ µm/s	$\omega_E=1.9\times10^{-9}$ µm²/s	$\omega_E=5\times10^{-4}$ µm²/s
MinD-MinDE interaction on membrane	—	$\bar{k}_1=-1.2\times10^{-6}$ µm⁴/s, $\bar{k}_2=1.2\times10^{-10}$ µm⁶/s	$\bar{k}_1=-k_1$, $\bar{k}_2=-10^{-4}k_2$		Catalytic synthesis of MinE: $\rho_e=0.005$	Cooperative MinE attachment to membrane: —	—	—	$\omega_{eE}=8\times10^{-9}$ µm⁶/s	$\omega_{eE}=2.1\times10^{-20}$ µm⁶/s	$\omega_{eD}=2.5\times10^{-3}$ µm²/s
MinD detachment from membrane by MinD	$\omega_2=10$	$\omega_{de}=0.04\ s^{-1}$	$\omega_{de}=0.04\ s^{-1}$	$\omega_{de}=0.002\ s^{-1}$	MinD detachment by MinE: $\mu_{de}=0.0004$	MinD detachment by MinE: $\sigma_2=0.0063$ µm/s	$\sigma_{de}=0.7/s$	$\sigma_{de}=0.7/s$	$\omega_{de}=0.125/s$	$\omega_{de}=0.029/s$	MinE remains on membrane $\omega_{de,m}=0.8/s$; MinE leaves membrane $\omega_{de,c}=0.8/s$
MinE detachment from membrane	$\omega_4=0.1$				Saturation and mutual interference: $\kappa_{DE}=0.5$, $\kappa_D=0.02$	MinE detachment: $\sigma_4=0.8\ s$					$\omega_e=0.8/s$
Aggregation current $j_d=$	$-D_d\partial_x c_d+p\partial_x\cdot\Big[(1-c_d)c_d^2+\big(\tfrac{7}{6}-\tfrac{15}{12}c_D\big)\cdot c_d\partial_x^2 c_d g^2-\big(\tfrac{5}{6}-\tfrac{1}{2}c_D\big)(\partial_d c_d)^2 g^2\Big]$	$-D_d\nabla c_d+c_d(c_{max}-c_d-c_{de})\cdot\big[k_1\nabla c_d+k_2\nabla\triangle c_d\,\bar{k}_1\nabla c_{de}+\bar{k}_2\nabla\triangle c_{de}\big]$; For Meacci j_{de} equivalent j_d			MinD decay rates $\mu_d=\rho_d=0.002$, $\mu_D=0$; MinE decay rates $\mu_e=\rho_e=0.005$, $\mu_E=0.0002$	Membrane-bound MinE suppresses MinD attachment: $\sigma_1'=0.028$ µm; Cytoplasmic MinD suppresses MinE detachment: $\sigma_1'=0.027$ µm	ATP exchange rate $\sigma_D^{ATP}=1/s$	—	—	—
Maximal density of MinD on membrane $c_{max}=$	—	1000/µm	500/µm²	6×10^6/µm²	—	—	—	18.75×10^6/µm²	—	—	2×10^4/µm²
Total MinD density $\mathcal{D}=$	—	900/µm	1300/µm	1 µM	—	1500/µm	1000/µm	1 µM	1000/µm	1 µM	2.9×10^3/µm²
Total MinE density $\mathcal{E}=$	—	350/µm	500/µm	1 µM	—	85/µm	350/µm	0.35 µM	400/µm	1 µM	1.9×10^3/µm²
Spatial discretization	0.05				20 × 0.15 µm	0.008 µm	0.05 µm		0.2 µm	7.5 µm	
Temporal discretization					0.6 ms	0.05 ms			0.03 ms	10 ms	

Model	Aggregation current				Cooperative attachment						
Authors	Kruse	Meacci and Kruse	Fischer-Friedrich and Kruse		Meinhardt and de Boer	Howard	Huang	Huang (Fischer-Friedrich)	Fischer-Friedrich and Kruse		Bonny and Kruse
Year	2002	2005	2007	2008	2001	2001	2003	2008	2008	2008	2012
Publications	[191]	[199]	[363]	[357]	[272]	[356]	[345]	[357]	[357]		[358]
Membrane geometry	Cell	Cell	Cell	SLB	Cell	Cell	Cell	SLB	Cell	SLB	SLB
Oscillation graph		MinD: MinE:	MinD: MinE:	MinD + MinE:	Min (green), MinE (red), FtsZ (blue):	MinD: MinE:		MinD (green), MinE (red):	MinD (green), MinE (red):	MinD (green), MinE (red):	MinE:
Oscillation period	35 (au)	40 – 120 s	—	—	50 s	max. 145 s for $\lambda = 4.2\,\mu m$	$33 - \infty$ s	—	67 s	—	—
MinD and MinE maxima			—	—			MinD: MinE:		—	—	—
Phase diagram MinE/MinD			—	—	—			—	—	—	—
Oscillation period MinE/MinD			—	—			—	—	—		—
Oscillation period vs. length	—		—	—	But: 1000 s (!) for 10 µm	120 s for 10 µm	—	—	—	—	—
Multiple oscillations in filaments		MinD:	—	—		—		—	—	—	—